Enhanced Design and Operation of Small High-Speed Craft

Federico Prini

Submitted for the degree of Doctor of Philosophy

June 2019

Marine, Offshore and Subsea Technology Group
School of Engineering
Faculty of Science, Agriculture and Engineering
Newcastle University
Newcastle upon Tyne, UK

"No one believes simulation results,
except for the person who has run the simulations.
Everyone believes experiment results,
except for the person who has run the experiments."

Bob Dow

Abstract

This thesis presents a functional approach to improve the structural design and operation of small high-speed craft through the direct calculation of seakeeping loads and structural response. A novel procedure, combining computational and experimental methods, is developed to superimpose static, slowly varying and transient loads on a structural model of the craft. The approach is validated on a 17-metre search and rescue vessel with a maximum operating speed of 25 knots.

Current structural design methods for small craft follow a relatively simplistic process and do not explicitly calculate the loads sustained and the response of the structure. To better inform the level of structural adequacy in different possible operating conditions of the craft, both loads and structural response need to be explicitly analysed. In this thesis, hydrostatic and wave loads are determined with hydrodynamic simulations, validated against towing tank tests and seakeeping trials. Slamming loads are estimated by matching strain measurements, taken during the seakeeping trials, to local finite element models of the structure. The single load components are superimposed in the generation of a load case, which represents the extreme loads expected to be sustained within a given return period. The structural response is computed using a global finite element model of the vessel and results are presented as graphs showing the structural response as a function of vessel speed and sea state severity. These graphs contribute to defining the 'operational envelope' of the craft, which informs designers and crews on the limits to speed for the safe operation in waves.

The study finds broad applicability in the design of small high-speed craft. The approach has the potential to provide designers with better control over the structural design and maintainers with a vessel-specific understanding of the lifetime load patterns and of the structural behaviour, hence aiding targeted inspections. It also increases the awareness of the implications of high speed to the structural integrity of the vessel, enabling coxswains to make informed decisions on the risks being taken and enhance the safety of the on-board crew.

Acknowledgements

I would like to acknowledge Newcastle University for providing me with a supportive environment, which allowed me to successfully complete my doctoral studies. I also thank the Royal National Lifeboat Institution for funding this project and for the value they gave to my work. Furthermore, I am grateful to Lloyd's Register that 'came aboard', brought their class expertise to the table and ensured high standards of research.

This work could have not been done without the guidance and constant support of many individuals. Special thanks go to those who closely followed or supervised it:

To Bob Dow, an unequalled expert of marine structures who, leading me through this research, grew me as a naval architect. Working under his guidance has been an honour.

To Richard Birmingham, a true leader from whom I learnt how to handle a long and complex project. Richard has been an inspirational line manager and a mentor in life.

To Simon Benson, a skilled naval architect who always pointed me in the right direction. Simon has been my teacher and my constant reference for all technical aspects of my research.

To Holly Phillips and Pete Sheppard, first-rate naval architects who enabled me to focus on the authentic needs of the industry and supported me with their far-reaching practical experience.

To Jesus Mediavilla Varas, Michael Johnson and Spyros Hirdaris, invaluable experts in the field, who filled me with motivation and precious technical support.

The work presented in Chapter 5 was conducted with the following contributions:

> The hull models were manufactured by Hobson Design Ltd. Their outstanding construction standards certainly contributed to the accuracy of the results.
>
> The towing arrangement was an original idea of Mehmet Atlar, who I thank for his technical advice at the early design stages of the hull models.

The tests were possible thanks to the technician team at Newcastle University's hydrodynamics laboratory: Peter Bowes, Bob Hindhaugh, Ian Howard-Row and Phil Letouze. A special thanks to Kieron Fallows for standing next to me throughout the testing and for coping well with my tendency to perfection.

The work presented in Chapter 6 was conducted with the following contributions:

The tests were possible thanks to the support of the RNLI and of many staff from within the Engineering Office that worked towards their planning and execution. The specifications for the data acquisition system were developed by Luke Ferguson. The sensors installation work was supervised by Iain Wallbridge, Owain Hughes and Ben Thomas.

A special thanks also to the coxswain Michael Nugent and the RNLI crews of the Tynemouth lifeboat station. *"Tranquillo quilibet gubernator est"* ("when it is calm, anybody can be the helmsman" by Lucius Annaeus Seneca in his work "Epistulae Morales ad Lucilium"). They took up the task with extreme rigour, employing their experience to translate into practice rather unusual requests of a scientific character. They also welcomed me on board and made me feel part of the crew.

Lastly, I thank all those who, as part of my personal life, made my work easier. To my friends, who made Newcastle my hometown ("home is where the heart is"). To Duygu, with whom I shared these years. To my parents, for always believing in me.

Contents

Abstract V

Acknowledgements VI

Contents VIII

List of Figures XIV

List of Tables XXI

Nomenclature & Sign Conventions XXII

Chapter 1 Introduction 1

1.1 Research Context 1

1.1.1 Definition of Small High-Speed Craft 1

1.1.2 Small High-Speed Craft Operating Principles 3

1.1.3 Operational Envelopes 5

1.2 Research Rationale 7

1.2.1 The Severn Life Extension Project 7

1.2.2 The Structural Response of the Severn 8

1.3 Research Aim and Objectives 9

1.4 Outline of the Chapters 9

Chapter 2 Background 13

2.1 Loads on Ships 13

2.2 Seakeeping Load Prediction Methods 15

2.2.1 Semi-Empirical Methods 15

2.2.2 The RNLI Load Prediction Method 17

2.2.3 Computational Methods 19

2.2.4 Experimental Methods 22

2.2.5 Slamming 24

2.2.6 Experimental Pressure Measurements 26

2.2.7 Response Amplitude Operators 27

2.3 Structural Response Analysis 28
2.3.1 Analytical Methods 28
2.3.2 The Finite Element Method 29
2.3.3 Experimental Methods 31
2.4 Summary 31
Chapter 3 Overview of the Approach 33
3.1 Introduction 33
3.2 The RNLI and the Severn Class Lifeboat 34
3.3 Calculation of Seakeeping Loads and Response 40
3.3.1 Foundations of the Work 40
3.3.2 General Outline 41
3.3.3 Validation 43
Chapter 4 Numerical Simulations 47
4.1 Framework 47
4.2 The Marine Design Package MAESTRO 48
4.2.1 Finite Element Modelling 48
4.2.2 Loading Definition 50
4.2.3 Restraints and Static Equilibrium Balance 51
4.2.4 The Hydrodynamic Solver MAESTRO-Wave 51
4.2.5 Extreme Load Analysis 52
4.2.6 Structural Response Analysis 52
4.3 The MAESTRO Model of the Severn Class 53
4.3.1 Finite Element Modelling 53
4.3.2 Loading Condition and Hydrostatic Balance 55
4.4 Hydrodynamic Analysis 56
4.5 Seakeeping Results 60
4.6 Discussion 66
4.7 Summary 67
Chapter 5 Small-Scale Tests 69

5.1 Framework 69
5.2 The Small-Scale Tests of the Severn Class 70
5.3 Description of the Tests 71
5.3.1 The Facility 71
5.3.2 Scaling and Construction 72
5.3.3 Towing Point 74
5.3.4 Turbulence Stimulation 75
5.3.5 Setup and Ballasting 76
5.3.6 Segmented Model – Strength Bar 77
5.3.7 Segmented Model – Global Load Measurement 78
5.3.8 Segmented Model – Segmentation and Sealing 82
5.3.9 Test Apparatus and Procedure 84
5.3.10 Data Acquisition and Analysis 85
5.4 Results 87
5.4.1 Data Series 87
5.4.2 Resistance 88
5.4.3 Seakeeping 88
5.5 Discussion 102
5.5.1 Accuracy of the Measurement System 102
5.5.2 Similarity between the Hull Models 103
5.5.3 Comparison with Numerical Simulations 105
5.6 Practical Considerations 107
5.7 Summary 108
Chapter 6 Full-Scale Tests 109
6.1 Framework 109
6.2 Testing Procedure 110
6.2.1 Description of the Trials 110
6.2.2 Test Matrix 110
6.2.3 Trial Area and Trajectory 112
6.3 Data Acquisition 117

6.3.1 Sea State Measurement 117
6.3.2 On-Board Instrumentation 119
6.3.3 Manually Recorded Data 124
6.4 Data Analysis Basics 124
6.5 Analysis of Wave Data 125
6.5.1 Visual Estimates 125
6.5.2 Wave Buoy Data 126
6.5.3 Displacement Time Histories 127
6.5.4 Wave Spectrum 127
6.5.5 Wave Encounter Spectrum 128
6.6 Analysis of Global loads 131
6.6.1 Data De-Trending 131
6.6.2 Strain to Bending Moment Conversion 131
6.6.3 Wave-Induced Bending Moment 133
6.6.4 Slamming-Induced Bending Moment 134
6.6.5 Descriptive Statistics 136
6.6.6 Spectral Analysis 137
6.7 Analysis of Local Loads 139
6.7.1 Data De-Trending 139
6.7.2 Wave-Induced Strain 140
6.7.3 Slamming-Induced Strain 140
6.7.4 Strain-to-Pressure Conversion 142
6.8 Results 144
6.9 Discussion 164
6.9.1 Accuracy of the Measurements 164
6.9.2 Wave Period 165
6.9.3 Wave Direction and Spread 165
6.9.4 Response at Different Headings 170
6.9.5 Sagging-to-Hogging Ratio 170
6.9.6 Wave Load RAOs 171
6.9.7 Comparison with Numerical Simulations 172

6.10 Summary 173

Chapter 7 Structural Response 175

7.1 Framework 175

7.2 Definition of Extreme Loads 175

7.3 Construction of a Structural Response Curve 177

7.4 Extreme Values of Linear Responses 178

7.4.1 Prediction of Wave Loads 179

7.4.2 Prediction of Hydrostatic Loads 180

7.5 Extreme Values of Nonlinear Responses 180

7.5.1 Prediction of Global Slamming Loads 185

7.5.2 Prediction of Local Slamming Loads 188

7.6 Load Case Definition 193

7.7 Structural Response Analysis 194

7.8 Results 194

7.9 Discussion 197

7.10 Summary 198

Chapter 8 Conclusions 201

8.1 Direct Calculation of Seakeeping Loads and Structural Response 201

8.1.1 General View 201

8.1.2 Numerical simulations 203

8.1.3 Small-Scale Tests 204

8.1.4 Full-Scale Tests 204

8.1.5 Structural Response Analysis 206

8.2 Applicability of the Research 207

8.3 Guidance for Practical Design 208

8.3.1 General Remarks 208

8.3.2 Validation of Numerical Simulations without Full-Scale Tests 209

8.3.3 Determination of Slamming Loads without Full-Scale Tests 210

8.4 Guidance for Future Work 211
8.5 Original Contribution to Knowledge 212
8.6 Potential Beneficiaries 213
8.7 Conclusions and Future Directions 214
References 215
Appendices 223
Appendix 1 Publications and other Outputs 225
Appendix 2 Specifications for the Construction of the Severn Class Hull Models 227
Appendix 4 Trial Trajectories 249
Appendix 5 Instrumentation Plan 255
Appendix 6 Trial Record Sheet 261
Appendix 7 Strain to Pressure Conversion 265

List of Figures

Figure 1.1. Operational envelope for a small planing craft 6
Figure 1.2. Operational envelope for an RNLI all-weather lifeboat 8
Figure 1.3. Outline of the methodology chapters. 11
Figure 2.1. RNLI's design pressure prediction method. 18
Figure 2.2. RNLI's design pressure longitudinal distribution factor. 18
Figure 3.1. The Severn Class lifeboat. 35
Figure 3.2. Overview of the approach. 43
Figure 4.1. MAESTRO model of the Severn class. 54
Figure 4.2. 'Top-hat' cross-section and equivalent 'T' cross-section 55
Figure 4.3. Longitudinal weight and buoyancy distribution. 56
Figure 4.4. Transverse weight and buoyancy distribution. 56
Figure 4.5. Heave in head waves at 10kts. 57
Figure 4.6. Heave in head waves at 20kts. 57
Figure 4.7. VBM at 0.50LWL in head waves at 10kts. 57
Figure 4.8. VBM at 0.50LWL in head waves at 20kts. 57
Figure 4.9. Panel pressure output from MAESTRO-Wave. 59
Figure 4.10. Motion and load output from MAESTRO-Wave. 59
Figure 4.11. Heave in head waves. Varying speed. 61
Figure 4.12. Pitch in head waves. Varying speed. 61
Figure 4.13. Roll in head waves. Varying speed. 61
Figure 4.14. Heave in bow quartering waves. Varying speed. 61
Figure 4.15. Pitch in bow quartering waves. Varying speed. 61
Figure 4.16. Roll in bow quartering waves. Varying speed. 61
Figure 4.17. Heave in beam waves. Varying speed. 62
Figure 4.18. Pitch in beam waves. Varying speed. 62
Figure 4.19. Roll in beam waves. Varying speed. 62
Figure 4.20. Heave in stern quartering waves. Varying speed. 62
Figure 4.21. Pitch in stern quartering waves. Varying speed. 62
Figure 4.22. Roll in stern quartering waves. Varying speed. 62

Figure 4.23. Heave in following waves. Varying speed. 63
Figure 4.24. Pitch in following waves. Varying speed. 63
Figure 4.25. Roll in following waves. Varying speed..... 63
Figure 4.26. VBM at 0.50LOA in head waves. Varying speed..... 63
Figure 4.27. HBM at 0.50LOA in head waves. Varying speed. 63
Figure 4.28. VSF at 0.50LOA in head waves. Varying speed. 63
Figure 4.29. VBM at 0.50LOA in bow quartering waves. Varying speed. 64
Figure 4.30. HBM at 0.50LOA in bow quartering waves. Varying speed..... 64
Figure 4.31. VSF at 0.50LOA in bow quartering waves. Varying speed. 64
Figure 4.32. VBM at 0.50LOA in beam waves. Varying speed. 64
Figure 4.33. HBM at 0.50LOA in beam waves. Varying speed..... 64
Figure 4.34. VSF at 0.50LOA in beam waves. Varying speed..... 64
Figure 4.35. VBM at 0.50LOA in stern quartering waves. Varying speed. 65
Figure 4.36. HBM at 0.50LOA in stern quartering waves. Varying speed. 65
Figure 4.37. VSF at 0.50LOA in stern quartering waves. Varying speed. 65
Figure 4.38. VBM at 0.50LOA in following waves. Varying speed. 65
Figure 4.39. HBM at 0.50LOA in following waves. Varying speed. 65
Figure 4.40. VSF at 0.50LOA in following waves. Varying speed..... 65
Figure 4.41. Direct calculation approach – CFD simulations. 67
Figure 5.1. Severn class scaled hull models..... 71
Figure 5.2. Internal structure of the solid model. 74
Figure 5.3. Internal structure of the segmented model. 74
Figure 5.4. Structural details of the segmented model. 74
Figure 5.5. Towing rig on the segmented model (left) and solid model (right)..... 75
Figure 5.6. Strength bar layout. 78
Figure 5.7. Strength bar. Longitudinal section taken at the hull centreline..... 78
Figure 5.8. Strain gauge layout..... 79
Figure 5.9. Backbone beam calibration. 81
Figure 5.10. Calibration of the strain gauges measuring VBM at 0.50LWL. 83
Figure 5.11. Calibration of the strain gauges measuring HBM at 0.50LWL. 83
Figure 5.12. Calibration of the strain gauges measuring VSF at 0.50LWL. 83
Figure 5.13. Calibration of the strain gauges measuring VSF 0.50LWL..... 83

Figure 5.14. Hull model segmentation and sealing. 83
Figure 5.15. Test at forward speed 85
Figure 5.16. Test at zero speed 85
Figure 5.17. Data analysis for heave motions. 87
Figure 5.18. Resistance in calm water. 90
Figure 5.19. Sinkage in calm water. 90
Figure 5.20. Running trim in calm water. 90
Figure 5.21. Heave in head waves at 0kts. 91
Figure 5.22. Pitch in head waves at 0kts. 91
Figure 5.23. Roll in head waves at 0kts. 91
Figure 5.24. Heave in bow quartering waves at 0kts. 91
Figure 5.25. Pitch in bow quartering waves at 0kts. 91
Figure 5.26. Roll in bow quartering waves at 0kts. 91
Figure 5.27. Heave in beam waves at 0kts. 92
Figure 5.28. Pitch in beam waves at 0kts. 92
Figure 5.29. Roll in beam waves at 0kts. 92
Figure 5.30. Heave in stern quartering waves at 0kts. 92
Figure 5.31. Pitch in stern quartering waves at 0kts. 92
Figure 5.32. Roll in stern quartering waves at 0kts. 92
Figure 5.33. Heave in following waves at 0kts 93
Figure 5.34. Pitch in following waves at 0kts. 93
Figure 5.35. Roll in following waves at 0kts. 93
Figure 5.36. VBM at 0.25LWL in head waves at 0kts. 93
Figure 5.37. VBM at 0.50LWL in head waves at 0kts. 93
Figure 5.38. VBM at 0.75LWL in head waves at 0kts. 93
Figure 5.39. VBM at 0.25LWL in bow quartering waves at 0kts. 94
Figure 5.40. VBM at 0.50LWL in bow quartering waves at 0kts. 94
Figure 5.41. VBM at 0.75LWL in bow quartering waves at 0kts. 94
Figure 5.42. VBM at 0.25LWL in beam waves at 0kts. 94
Figure 5.43. VBM at 0.50LWL in beam waves at 0kts. 94
Figure 5.44. VBM at 0.75LWL in beam waves at 0kts. 94
Figure 5.45. VBM at 0.25LWL in stern quartering waves at 0kts. 95

Figure 5.46. VBM at 0.50LWL in stern quartering waves at 0kts. 95
Figure 5.47. VBM at 0.75LWL in stern quartering waves at 0kts. 95
Figure 5.48. VBM at 0.25LWL in following waves at 0kts. 95
Figure 5.49. VBM at 0.50LWL in following waves at 0kts. 95
Figure 5.50. VBM at 0.75LWL in following waves at 0kts. 95
Figure 5.51. VBM longitudinal distribution in head waves at 0kts. 96
Figure 5.52. VBM longitudinal distribution in bow quartering waves at 0kts. 96
Figure 5.53. VBM longitudinal distribution in beam waves at 0kts. 96
Figure 5.54. VBM longitudinal distribution in stern quartering waves at 0kts 97
Figure 5.55. VBM longitudinal distribution in following waves at 0 kts. 97
Figure 5.56. Heave in head waves at 5kts. 98
Figure 5.57. Pitch in head waves at 5kts. 98
Figure 5.58. Heave in head waves at 10kts. 98
Figure 5.59. Pitch in head waves at 10kts. 98
Figure 5.60. Heave in head waves at 15kts. 99
Figure 5.61. Pitch in head waves at 15kts. 99
Figure 5.62. Heave in head waves at 20kts. 99
Figure 5.63. Pitch in head waves at 20kts. 99
Figure 5.64. VBM at 0.25LWL in head waves at 5kts. 100
Figure 5.65. VBM at 0.50LWL in head waves at 5kts. 100
Figure 5.66. VBM at 0.75LWL in head waves at 5kts. 100
Figure 5.67. VBM at 0.25LWL in head waves at 10kts. 100
Figure 5.68. VBM at 0.50LWL in head waves at 10kts. 100
Figure 5.69. VBM at 0.75LWL in head waves at 10kts. 100
Figure 5.70. VBM at 0.25LWL in head waves at 15kts. 101
Figure 5.71. VBM at 0.50LWL in head waves at 15kts. 101
Figure 5.72. VBM at 0.75LWL in head waves at 15kts. 101
Figure 5.73. VBM at 0.25LWL in head waves at 20kts. 101
Figure 5.74. VBM at 0.50LWL in head waves at 20kts 101
Figure 5.75. VBM at 0.75LWL in head waves at 20kts. 101
Figure 5.76. Direct calculation approach. Small-scale tests. 108
Figure 6.1. Trial trajectory. Symmetric ‘star’ pattern 115

Figure 6.2. Trial trajectory. Asymmetric 'star' pattern..... 115
Figure 6.3. Trial trajectory. Asymmetric 'star' pattern modified..... 115
Figure 6.4. Cable routing..... 121
Figure 6.5. HF antenna cable routing..... 121
Figure 6.6. Data acquisition unit secured to a survivor seat. 121
Figure 6.7. HF link receiver and laptops secured to the stretcher. 121
Figure 6.8. Strain gauge bonded to a primary longitudinal structural member. 123
Figure 6.9. Strain gauge bonded on the deck in way of the hull-to-deck joint. 123
Figure 6.10. Strain gauges bonded to a hull bottom panel. 123
Figure 6.11. Strain gauges bonded to two bow panels 123
Figure 6.12. Wave height PSD transformation 130
Figure 6.13. Raw strain signal de-trended. 131
Figure 6.14. Wave-induced vertical bending moment signal filtered. 134
Figure 6.15. Slamming-induced vertical bending moment signal filtered. 136
Figure 6.16. Detection of sagging and hogging bending moment peaks. 137
Figure 6.17. Calculation of the VBM transfer function. 139
Figure 6.18. Slamming-induced strain signal filtered. 141
Figure 6.19. Hull bottom panel. Geometrical model.....143
Figure 6.20. Hull bottom panel. Meshed model.....143
Figure 6.21. Hull bottom panel. Boundary conditions and loads.....143
Figure 6.22. Hull bottom panel. Surface strain in the strain gauges' active direction ..143
Figure 6.23. Wave-induced VBM. Highest 1/3rd and maximum values..... 146
Figure 6.24. Wave-induced VBM. Highest 1/3rd and maximum values. 147
Figure 6.25. Wave-induced VBM. Highest 1/3rd and maximum values. 148
Figure 6.26. Wave-induced VBM. Highest 1/3rd and maximum values. 149
Figure 6.27. Wave-induced VBM. Highest 1/3rd and maximum values. 150
Figure 6.28. Wave-induced VBM. Highest 1/3rd and maximum values. 151
Figure 6.29. Wave-induced VBM. Highest 1/3rd and maximum values. 152
Figure 6.30. Wave-induced VBM. Highest 1/3rd and maximum values. 153
Figure 6.31. Wave-induced VBM. Highest 1/3rd and maximum values. 154
Figure 6.32. Wave-induced VBM RAOs. Head sea, 5kts, Hs=0.6m. 155
Figure 6.33. Wave-induced VBM RAOs. Head sea, 5kts, Hs=1.6m. 156

Figure 6.34. Wave-induced VBM RAOs. Head sea, 5kts, Hs=3.0m. 157
Figure 6.35. Wave-induced VBM RAOs. Head sea, 10kts, Hs=4.5m. 158
Figure 6.36. Wave-induced VBM RAOs. Head sea, 15kts, Hs=0.4m. 159
Figure 6.37. Wave-induced VBM RAOs. Head sea, 15kts, Hs=1.7m. 160
Figure 6.38. Wave-induced VBM RAOs. Head sea, 20kts, Hs=3.1m. 161
Figure 6.39. Wave-induced VBM RAOs. Head sea, 25kts, Hs=1.3m. 162
Figure 6.40. Wave-induced VBM RAOs. Head sea, 25kts, Hs=1.5m. 163
Figure 6.41. Wave scatter diagram for the North Sea 166
Figure 6.42. Wave scatter diagram for the North Sea 166
Figure 6.43. Estimated and actual wave direction. Trial at 10kts in Hs=4.5m. 168
Figure 6.44. Estimated and actual wave direction. Trial at 20kts in Hs=3.1m. 168
Figure 6.45. Estimated and actual wave direction. Trial at 15kts in Hs=0.4m. 169
Figure 6.46. Estimated and actual wave direction. Trial at 25kts in Hs=1.3m. 169
Figure 6.47. Wave-induced VBM RAOs near amidships (FR08). 172
Figure 6.48. Wave-induced VBM RAOs near amidships (FR08). 172
Figure 6.49. Direct calculation approach. Full-scale tests. 174
Figure 7.1. Wave scatter diagram for the North Sea showing the wave periods considered for the construction of the structural response curve 178
Figure 7.2. Extreme wave pressures in sagging (left) and hogging (right). 179
Figure 7.3. Hydrostatic pressures. 180
Figure 7.4. Sagging and hogging VBM maximum values 182
Figure 7.5. Positive and negative strain maximum values 182
Figure 7.6. Probability histograms of sagging and hogging VBM values. 183
Figure 7.7. Probability histograms of positive and negative strain values. 183
Figure 7.8. Gumbel plots of VBM (left) and panel strains (right). 184
Figure 7.9. Slamming-induced VBM. Extreme values 186
Figure 7.10. Longitudinal distribution of slamming-induced VBM. 187
Figure 7.11. Speed effect on the slamming-induced VBM 187
Figure 7.12. Wave height effect on the slamming-induced VBM 187
Figure 7.13. Speed and wave height effect on the slamming-induced VBM 187
Figure 7.14. Slamming pressure distribution at V≤15kts. 189
Figure 7.15. Slamming pressure distribution at V>15kts. 189

Figure 7.16. Slamming pressures. Extreme values 190
Figure 7.17. Longitudinal distribution of slamming pressures at V≤15kts. 191
Figure 7.18. Speed effect on slamming pressures 191
Figure 7.19. Speed and wave height effect on slamming pressures 191
Figure 7.20. Longitudinal distribution of slamming pressures at V>15kts. 192
Figure 7.21. Speed effect on slamming pressures 192
Figure 7.22. Wave height effect on slamming pressures 192
Figure 7.23. Speed and wave height effect on slamming pressures 192
Figure 7.24. Structural analysis results. 194
Figure 7.25. Example of a high stress area. 195
Figure 7.26. Example of an artificial stress area. 195
Figure 7.27. Structural response of the hull to global seakeeping loads. 196
Figure 7.28. Structural response of the hull to local seakeeping loads. 196
Figure 7.29. Direct calculation approach. Structural response. 199
Figure 8.1. Direct calculation of seakeeping loads and structural response. 202

List of Tables

Table 3.1. Severn Class main particulars. 35
Table 3.2. Severn Class speed conversion from knots to Froude numbers. 35
Table 3.3. Sample hull laminates of the Severn Class. 37
Table 3.4. Sample wheelhouse laminates of the Severn Class. 38
Table 3.5. Sample laminae's mechanical properties (1 of 2). 38
Table 3.6. Sample laminae's mechanical properties (2 of 2). 39
Table 3.7. Sample foams' mechanical properties 40
Table 4.1. MAESTRO model main particulars. 54
Table 4.2. MAESTRO model loading condition. 56
Table 5.1. Towing tank main particulars. 72
Table 5.2. Severn Class main particulars at real and model scale. 73
Table 5.3. Hull model loading condition. Small-scale values. 77
Table 5.4. Hull model loading condition. Full-scale values. 77
Table 6.1. Target sea trial matrix. 111
Table 6.2. Achieved sea trial matrix. 111
Table 6.3. Sea trial trajectory at 5kts. Leg breakdown. 115
Table 6.4. Sea trial trajectory at 10kts. Leg breakdown. 116
Table 6.5. Sea trial trajectory at 15kts. Leg breakdown. 116
Table 6.6. Sea trial trajectory at 20kts. Leg breakdown. 116
Table 6.7. Sea trial trajectory at 25kts. Leg breakdown. 117
Table 6.8. On-board instrumentation. 121
Table 6.9. Measurements and sampling frequencies. 123
Table 6.10. Sea state visual observations and wave buoy measurements. 126
Table 6.11. Strain to pressure conversion. 144
Table 6.12. MAESTRO model loading condition tuned to sea trial vessel. 145
Table 7.1. Loading condition for extreme load prediction. 178

Nomenclature & Sign Conventions

Terminology

CFD	Computational Fluid Dynamics
FE, FEA, FEM	Finite Element, Finite Element Analysis, Finite Element Method
FRP	Fibre Reinforced Plastic
ITTC	International Towing Tank Conference
JONSWAP	Joint North Sea Wave Project
Lifeboat	In this thesis, it refers to the RNLI's lifeboats, which are dedicated search and rescue vessels.
RANSE	Reynolds-Averaged Navier-Stokes Equations (also RANS equations)
RAO	Response Amplitude Operator (In this thesis the convention is followed whereby the RAO is taken to be the same as its transfer function and used in its unsquared form)
RIB	Rigid Inflatable Boat
RNLI	Royal National Lifeboat Institution
SAR	Search And Rescue
SG	Strain Gauge

Roman Symbols

AP	Aft perpendicular
B_{ij}	ith damping force or moment on the jth velocity [e.g.B_{44}]
BL	Baseline
BOA	Overall beam
BWL	Waterline beam
CG	Centre of gravity
Dir_{obs}	Wave direction estimated through visual observations
$Dirp$	Wave spectrum peak direction
E	Young's modulus

F	1) Frequency characteristics of a filter [e.g. F_{Pass}]
	2) In statistics, cumulative distribution function [e.g. $F_X(x)$]
Fn	Froude number
Fn_∇	Volumetric Froude number
FP	Forward perpendicular
fs	Sampling frequency
G	Shear modulus
g	Gravitational acceleration
HBM	Horizontal bending moment
H_{obs}	Wave height estimated through visual observations
Hs	Significant wave height
I	Second moment of area of the cross-section about the neutral axis
k	Critical damping ratio
k_i	ith radius of gyration [e.g. k_4]
L	Overall submerged hull length
LCG	Longitudinal centre of gravity position
LOA	Overall ship length
LWL	Waterline hull length
M	Bending moment
N	Number of samples in a record
n	In statistics, number of observations
∇	Volume of displacement
PSD	Power spectral density
P_i	In statistics, cumulative frequency of the ith term within a dataset with values ranked in ascending order
Pt	Port (side)
Q	First moment of area of the cross-section about the neutral axis
S	Spectral ordinate [e.g. $S_\zeta(\omega_e)$, $S_{VBM}(\omega_e)$]
SLR	Speed-to-length ratio
SOG	Speed over ground
Stb	Starboard (side)

T	1) Ship draught
	2) Shear force
	3) In statistics, return period
TCG	Transverse centre of gravity position
T_{obs}	Wave period estimated through visual observations
Tp	Wave spectrum peak period
Tz	Wave spectrum zero-crossing period
t	Thickness
V	Speed
VBM	Vertical bending moment
VCG	Vertical centre of gravity position
VSF	Vertical shear force
WSA	Wet hull surface area
X	In statistics, random variable
x	In statistics, value assumed by the variable X
y	1) In general, value on the y-axis
	2) Vertical distance from the neutral axis
	3) Vertical distance between two measuring points (e.g. y_{BD})
	4) In statistics, reduced variate

Greek Symbols

β	Vessel heading, as detailed hereunder
γ	Shear strain
Δ	Ship displacement
ε	Strain
ζ	Instantaneous wave elevation relative to the mean level
η_i	ith ship motion (e.g. η_4)
λ	Wavelength
μ	In statistics, location parameter
σ	1) Bending stress
	2) In statistics, scale parameter

τ	Shear stress
ω	Wave frequency

Subscripts

0	Amplitude [e.g. y_0, η_{30}, ζ_0, VBM_0]
$crit$	Critical value, as defined in the text [e.g. $B_{44,crit}$]
e	Wave encounter [e.g. ω_e]
i, j	1) Ship motion or radius of gyration, as detailed hereunder
	2) In statistics, order of the observations within a sorted dataset
v	Viscous [e.g. $B_{44,v}$]
Φ	Potential flow [e.g. $B_{44,\Phi}$]
obs	Observed (visually) [e.g. $H_{obs}, T_{obs}, Dir_{obs}$]
$pass$	Passband [e.g. F_{pass}]
p	Peak of a signal [e.g. y_p]
t	Trough of a signal [e.g. y_t]
M	Model scale (e.g. V_M)
S	Ship (real) scale (e.g. V_S)
$stop$	Stopband (e.g. F_{stop})

Coordinate Systems and Sign Conventions

Heading Convention

The definition of vessel's heading follows the convention whereby the vessel is assumed to maintain a straight course and the heading is the angle β between the intended track of the vessel and the direction of wave propagation. The heading angle, therefore, assumes the values β=0° in following waves, β=90° in beam waves encountering the vessel on the starboard side, β=180° in head waves and β=270° in beam waves encountering the vessel on the port side.

Ship Motion Coordinate System

Ship motions are defined according to a right-handed coordinate system fixed in the vessel and with origin at its (moving) centre of gravity. This reference system has the x-axis positive forward, the y-axis positive starboard and the z-axis positive downward.

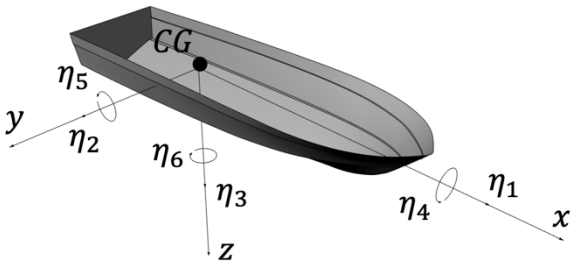

Motion	Symbol	Units	Positive
Surge	η_1	m	forward
Sway	η_2	m	starboard
Heave	η_3	m	down
Roll	η_4	deg	starboard down
Pitch	η_5	deg	bow up
Yaw	η_6	deg	bow to starboard

Ship motion coordinate system.

Ship Structure Coordinate System

To define structural global loads, the vessel is idealised as a beam (hull girder). The coordinate system is right-handed, fixed in the vessel and with origin at the intersection of the design aft perpendicular and the design base line. The x-axis is positive forward, the y-axis is positive upward and the z-axis is positive starboard.

The sign of internal forces and moments follows the normal convention used in most structural engineering applications: axial forces are positive when generate tension in the structure; vertical bending moment is positive when produces compression in the deck and tension in the hull bottom (sagging); horizontal bending moment is positive when produces compression in the port side and tension in the starboard side; vertical shear force is positive when produces a clockwise rotation of the hull girder section.

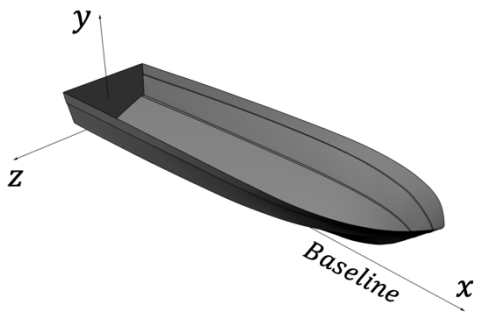

Ship structure coordinate system.

Chapter 1

Introduction

1.1 Research Context

1.1.1 Definition of Small High-Speed Craft

What is meant by 'high speed' and what is meant by 'small' craft'? Both terms are widely used for boats that span from a length of a few metres and with maximum speeds in excess of 60 knots to larger vessels of tens of metres in length and speeds of up 25-30 knots.

If the field is restricted to monohulls, a practical rule to classify vessels according to their length and speed has been, for a long time, the speed-to-length ratio (SLR):

$$SLR = \frac{V}{\sqrt{LWL}} \tag{1.1}$$

where V is the vessel speed and LWL is the waterline hull length. Although the metric system would be preferred, in the past the SLR used to be expressed as a dimensional number, with the speed in knots and the length in feet. This custom is kept here and SLRs are presented with units $kts/\sqrt{ft}$.

As summarised by Savitsky (2003), because a vessel moving through the water generates waves of celerity and length proportional to the vessel speed, as the speed increases the length of the generated waves also increases. At SLR≈1.3 the wavelength approaches the hull length with a consequent dramatic increase of the hull resistance, which becomes a practical barrier to further increases of speed. This tends to determine the limit of application of displacement hull forms. To operate at higher SLR values, different hull forms, compatible with the hydrodynamics of higher speeds, are required. This leads to semi-planing hulls, which show best performance in the region of approximately 1.3<SLR<3.0, and to planing hulls, which are suitable for operation at SLR>3.0. A high-speed craft could therefore be considered one with SLR>1.3.

As stated by Faltinsen (2006), amongst hydrodynamicists, it is the Froude number (Fn) that is the most popular:

$$Fn = \frac{V}{\sqrt{gL}} \tag{1.2}$$

where V is the ship speed, L is the overall submerged length of the ship and g is acceleration of gravity.

If the Froude number is used in place of the SLR, displacement hulls operate at approximately Fn<0.4, semi-planing hulls operate at 0.4<Fn<1.0-1.2 and planing hulls at Fn>1.0-1.2. The Froude number is also used to characterise the transition from displacement to planing regime, which is accompanied by an increasing hydrodynamic lift. At Fn<0.4, buoyancy forces are dominant and the weight of the vessel is mainly supported by the hydrostatic pressures, which give a buoyancy force proportional to the submerged hull volume (displacement). As the Froude number increases, a portion of the weight becomes supported by the lift provided by the hydrodynamic pressures. At Fn>1.0-1.2 the weight is mainly carried by the hydrodynamic lift (Faltinsen 2006). This means that a high-speed craft could be considered one capable of Fn>0.4.

Other formulations of the Froude number, which emphasize the lightweight aspect of high-speed craft, are also used. An example is the volumetric Froude number Fn_{∇}, defined as:

$$Fn_{\nabla} = \frac{V}{\sqrt{g\nabla^{1/3}}} \tag{1.3}$$

where ∇ is the volume of displacement. This seems to be the formulation adopted by many regulatory bodies. The High Speed Craft Code adopted by the IMO (2000), for example, states that a "*high-speed craft is a craft capable of maximum speed V, in metres per second (m/s)":*

$$V \geq 3.7\ \nabla^{0.1667} \tag{1.4}$$

where ∇ is the volume of displacement, in m^3, corresponding to the design waterline. This means a volumetric Froude number Fn_{∇}≈1.2.

This thesis presents the work conducted on a 17-metre search and rescue vessel with a maximum design speed of 25 knots. This corresponds to SLR=3.5 and Fn=1.0. The volumetric Froude number Fn_{∇}=2.2 makes this vessel subject to the design criteria adopted for high-speed craft.

1.1.2 Small High-Speed Craft Operating Principles

Small high-speed craft normally operate at a wide range of speeds and in different sea conditions. Even craft that possess adequate static stability may exhibit unstable characteristics at semi-planing and planing speeds, which are referred to as dynamic instabilities. A review of typical dynamic instabilities relevant to high-speed craft can be found in Savitsky and Brown (1976), Codega and Lewis (1987), Blount and Codega (1992) and Müller-Graf (1997). Phenomena such as loss of running trim, bow steering, progressive heeling, porpoising (heave-pitch oscillations), chine-walking (roll oscillations), cork-screwing (pitch-roll-yaw oscillations) are all speed related and occur when the hydrodynamic forces are large compared to the buoyancy forces. Directional instabilities become of concern during operation in following and stern quartering seas, where broaching can even lead to capsize. At these headings, also the quasi-static stability of roll can be of concern (Faltinsen 2006). Propulsion system, rudders, stabilisation devices, cavitation and ventilation can also play a role (Faltinsen 2006). Dynamic instability can result in structural damage, loss of control, or even crew injury, which may impose limits on the maximum operating speed of the craft. Methods to

estimate the stability characteristics of a high-speed craft and criteria of dynamic stability have been developed and can be found, amongst others, in Savitsky and Brown (1976), Codega and Lewis (1987), Blount and Codega (1992) and Müller-Graf (1997).

For a dynamically stable craft, the maximum achievable speed in calm water is determined by the installed propulsive power. When travelling in waves, this decreases due to the added wave resistance, but the speed that is reached in practice also largely depends on the sea-keeping of the vessel (the effect of the added wind resistance should also be accounted for). If the field is restricted to monohulls, and assuming operation at a given displacement and in given sea conditions, it is generally accepted that motion and load responses tend to worsen as the speed increases. This is particularly true in waves from between the fore and the beam, rather than for waves from abaft the beam. The increased motions and loads experienced at high speed in waves, make the crew's comfort and safety, the functionality of the on-board equipment and the structural integrity often of concern, even before the maximum achievable speed is reached.

As suggested by Ryley and Marshall (2013), the maximum allowable speed is often limited by either accelerations, which have a negative effect on personnel and equipment, or by large loads that lead to excessive structural stresses. Faltinsen (2006) reports an example of engine load fluctuations experienced on a craft fitted with a waterjet propulsion system. These load fluctuations, attributed to the effects of ventilation, penetration of air and flow separation at the waterjet inlet, induced high thermal loads, which may have led to engine breakdowns. Hence, also the machinery and the propulsion system may impose operational limits in a seaway. Which of these limits is reached first, and whether instability problems arise even before, partially depends on the success of the design, on the size and weight of the craft, on the hull form, on the propulsion apparatus and on the vibration damping systems installed for the crew and the equipment. This makes operational limits very much vessel-specific.

The literature on criteria for the prediction of operational limits is large (Lloyd 1989, Faltinsen 2006, Riley and Marshall 2013). These criteria are usually related to slamming, deck wetness, roll motions and vertical and lateral accelerations. If the limit values are met, action is usually taken by adapting the speed and/or the heading.

1.1.3 Operational Envelopes

Depending on the craft type and on the mission requirements, different operational limits can be identified. By combining what stated by Faltinsen (2006) and Riley and Marshall (2013), operational limits are, in general, set by:

- Stability
- Crew safety, comfort and workability
- Structural loads and response
- Installed propulsive power
- Machinery and propulsion loads and response
- Equipment functionality

These are all factors that set boundaries to the safe operation of the vessel, defining its 'operational envelope', 'operating envelope' or 'safe operating envelope'. Not all limits are necessarily relevant to all craft and there might be others, not included here, that are relevant to some craft, depending on their mission requirements. Some limits could also be grouped together. For example, the stability issues could be considered as part of the crew's safety; the equipment functionality, which largely depends on the motions and accelerations experienced, could be considered together with the crew's comfort and workability; and the installed propulsive power could be looked at together with the machinery and propulsion loads and response.

There are also several possible representations of an operational envelope. Faltinsen (2006) reports the operational limits calculated for two vessels on a significant wave height versus mean wave period graph. The limits are computed for head sea and at given speeds. Razola (2013) reports an example of speed versus sea state graph, originally produced by Gupta *et al.* (2003). Here the sea state is in terms of the highest $1/10^{th}$ waves and the speed is in knots. Riley and Marshall (2013) present a similar speed versus sea state graph, but based on the significant wave height. This is shown in Figure 1.1 and includes:

- Operating & Survival Limit. These are a function of the sea state only and are established by the maximum operating wave height and survival wave height for those craft whose operation is limited by the sea conditions.
- Power Limit. This represents the maximum speed that is achieved, for any given wave height, based on the installed propulsive power.
- Ride Quality Limit. This shows how, as the wave height increases, the severity of wave impacts tends to limit the craft speed because of stability concerns or because of the shocks experienced by the personnel, which can compromise their performance and safety.
- Structural Design Limit. This concerns the craft structure and represents where the seakeeping loads induce excessive stresses that may lead to structural failures.

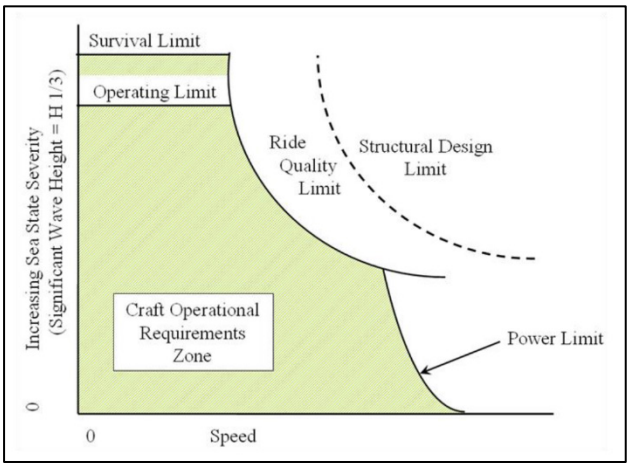

Figure 1.1. Operational envelope for a small planing craft (from Riley and Marshall (2013)). Curves are notional.

As stated by the authors, the curves are only notional and are meant to convey how different criteria establish limit lines for a specific craft. In practice, the graph shows the operation transition from low risk to higher risk, as speed and wave height increase. This means that lines should not be taken as hard limits, but rather as best estimates of where a transition occurs.

The authors also suggest that the separation between the Ride Quality and the Structural Design Limit typically depends on the size of the craft as well as on its mission requirements. In the operation of a small light craft, the large peak accelerations experienced tend to negatively affect the crew's comfort and safety, and the equipment operability, well before the structural limit is reached. On larger craft, instead, the

weight of the craft may result in lower accelerations that are not of concern for the crew and the equipment, but could impart large loads to the structure and lead to structural failures. This explains why operational limits can vary from one craft design to another.

1.2 Research Rationale

1.2.1 The Severn Life Extension Project

The Royal National Lifeboat Institution (RNLI) operates a number of lifeboat classes, all designed with a specified service life. The Severn Class (Hudson *et al.* 1993), consisting of a fleet of 45 vessels, first entered service in 1995. These lifeboats are now approaching the end of their original operational life of 25 years. However, due to their exceptional in-service performance, the RNLI has started a life extension programme to extend the operational life of the fleet to 50 years (Roberton 2015).

For the Severn Class, as for the other lifeboats designed and operated by the RNLI, crew's endurance has traditionally been one of the main limitations to speed during operation in rough seas. Excessive motions and accelerations can reduce the crew's operational effectiveness and raise the risk of personal injury. In those situations, the coxswain in command of the lifeboat, and aware of the shocks experienced, would usually adapt the speed, and/or the heading, with respect to the prevailing sea conditions. Since structural failures have proved to be extremely rare, although do occasionally occur (Phillips *et al.* 2009), the structural limit of the lifeboat has been traditionally assumed to be far beyond the crew's safety limit.

Many lifeboats in the Severn fleet have already been fitted with more modern replacement engines (Johns 2018). New technologies to improve the ride quality, such as seats with improved suspension systems, are also available (Cripps, Cain, *et al.* 2004) and, if adopted, would reduce the crew's exposure to the effects of extreme wave impacts, thereby reducing the risk of injury. Whilst this would be beneficial for the response to emergency call-outs, for which speed may be a critical factor, it would also provide the possibility to operate the lifeboat closer to its structural limit. Furthermore, improved seats, and thus an improved ride quality, could limit the ability of the coxswain to appreciate the loads being sustained by the structure. This has the potential to push

the operation of the vessel close to or even beyond the structural limit. Such a scenario is graphically illustrated in Figure 1.2, an adaptation of the original plot presented by Riley & Marshall (2013).

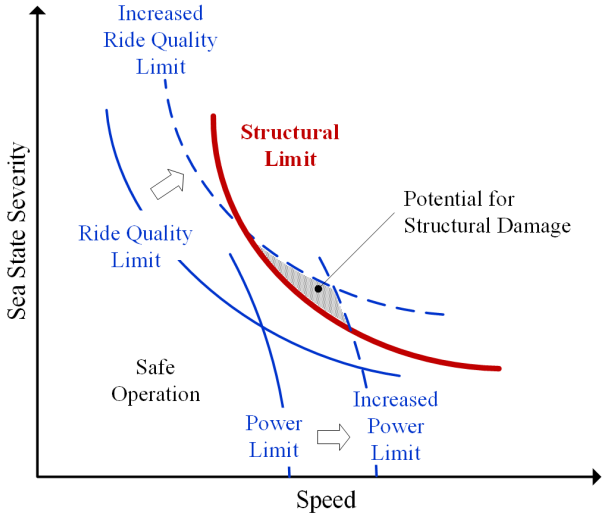

Figure 1.2. Operational envelope for an RNLI all-weather lifeboat (adapted from Riley and Marshall (2013)). Curves are notional.

1.2.2 The Structural Response of the Severn

The original operational requirements of the Severn Class, as well as of other RNLI's all-weather lifeboats, were *"to be capable of not less than 25 knots in best trials conditions (Beaufort 2), a mean speed of 15-17 knots in Beaufort 7 and safe operation in wave heights of 11-15 metres and 60 knots winds"* (Hudson *et al.* 1993). It was recognised that these requirements can be a subjective measure for the operators. Moreover, the proven track record of the Severn suggests that the structural design broadly exceeded the minimum requirements, leaving an uncertainty over the actual design margins embedded into it.

The Severn life extension programme highlighted the need to gain a better understanding of the structural performance of the RNLI's all-weather lifeboats in terms of strength and stiffness. This could only be achieved by predicting with confidence the loads sustained during operation and the behaviour of the structure. A study undertaken by Newcastle University, the RNLI and Lloyd's Register set out to develop a procedure for the direct calculation of the seakeeping loads sustained by small high-speed craft and the consequential structural response. This was exploited to produce a set of structural

response curves to provide the RNLI's design, maintenance, operation and training teams with an enhanced insight into the operational envelope of the Severn Class.

1.3 Research Aim and Objectives

The aim of this research is to enhance the structural design of small high-speed craft, thus improving design and operational practice.

This goal is accomplished through achievement of the following objectives:

- Review the state of the art for the prediction of seakeeping loads and structural response for small high-speed craft.
- Develop a procedure for the explicit calculation of seakeeping loads and response.
- Include validation of results (numerical vs small scale vs full scale).
- Produce load and structural response results in a form suitable for the identification of the 'structural limit' of the vessel.

1.4 Outline of the Chapters

Relevant background information is provided at the beginning of the thesis, which then advances systematically through the numerical and experimental tasks that form the core of the study (Figure 1.3). Overarching conclusions are drawn at the end.

Chapter 1 sets the scene for the study and presents the concept of operational limits and operational envelope of a small high-speed craft. It also presents the inspiration for the work and justifies the need for an approach that enables designers and operators to identify the structural limit of a vessel.

Chapter 2 provides relevant background information. It presents the state-of-the-art knowledge on the prediction of seakeeping loads and structural response. This includes a brief introduction to the finite element method and to the use of response amplitude operators to assess the seakeeping responses, both instrumental to the study.

Chapter 3 provides the details of the vessel used as case study. It gives an overview of the approach developed and outlines how numerical and experimental methods are

combined to produce an integrated procedure for the direct calculation of seakeeping loads and structural response. The chapter is based on work previously published in Prini, Birmingham, *et al.* (2018).

Chapter 4 describes the theory underpinning the hydrodynamic and structural simulations that form the basis of the study and provides the details of the global structural model developed. It also presents seakeeping simulation results and includes preliminary comments on the accuracy and range of applicability of the simulations. This chapter is based on work previously published in Prini *et al.* (2015) and Prini, Birmingham *et al.* (2018).

Chapter 5 describes the small-scale tests conducted in a towing tank. Details of the hull models, test apparatus, data collection and data analysis are given together with practical recommendations as guidance for future tests. Small-scale data is compared against numerical results and differences are discussed. This chapter is based on work previously published in Prini *et al.* (2016) and Prini, Birmingham *et al.* (2018).

Chapter 6 describes the full-scale tests conducted on an instrumented vessel. Details of the trial plan, instrumentation, data collection and data analysis are given as guidance for future tests. Full-scale data is compared against numerical results and differences are discussed. This chapter is based on work previously published in Prini, Benson, *et al.* (2018) and Prini, Birmingham *et al.* (2018).

Chapter 7 discusses the concepts of 'extreme loads' and 'structural limit'. It describes how extreme values of linear and nonlinear loads are estimated, and how these are used to formulate loading scenarios, representative of the loads sustained in different operating conditions. It presents the results of structural response analyses and shows how the structural limit of the vessel can be identified. This chapter is based on work previously published in Prini, Birmingham *et al.* (2018).

Chapter 8 draws the main conclusions from the work and provides guidance for possible future developments. It defines the types of vessel for which the research finds application. Lastly, it reviews the original contribution to knowledge and outlines the beneficiaries of the research.

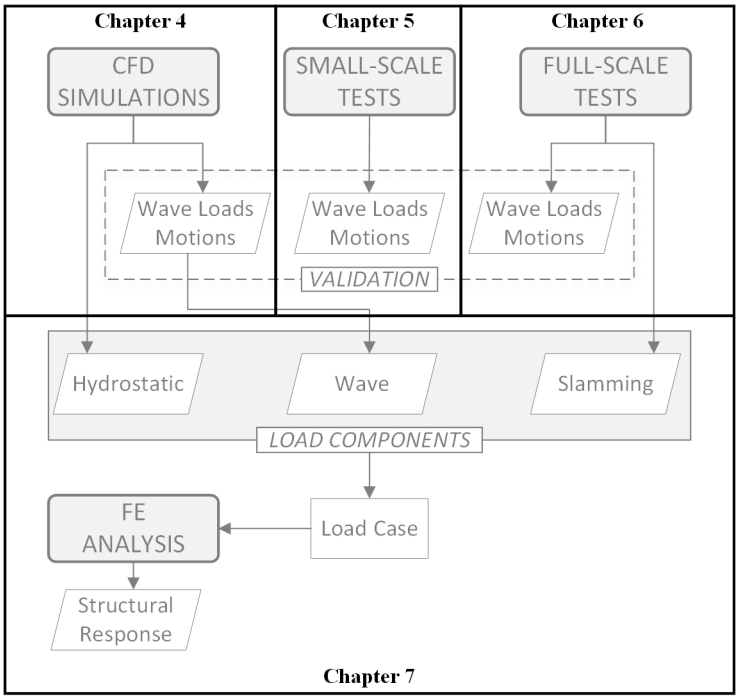

Figure 1.3. Outline of the methodology chapters.

Chapter 2

Background

2.1 Loads on Ships

Operation in a seaway subjects the vessel's structure to a variety of loads. These can be classified into categories to facilitate their analysis and, depending on the determinant used, several classifications can be made. A common way is according to how the loads, and the load responses, vary with time. This is the approach taken, for example, in Principles of Naval Architecture (Lewis 1988a), where four timescales are used:

- **Static loads** do not vary with time or vary within an irrelevant timeframe. These loads include:
    - Static buoyancy pressures of the ship at rest or moving.
    - Pressures and forces from self-weight, contents and cargo.
    - Drydocking and grounding loads.
    - Thermal loads.
- **Low frequency dynamic loads** vary with time at frequencies that are low compared to the natural frequency of the hull and its parts. Consequently, there is no resonant amplification of the structural responses induced. These loads are:

  - Wave-induced pressures from the combination of the passing waves and the resulting oscillatory ship motions.
  - Inertial reactions of the ship and its contents resulting from the accelerations of the ship in waves.
- **High-frequency dynamic loads** also vary with time but at frequencies sufficiently high to induce a vibratory response of the ship structure, as a whole or parts of it, with potential resonant amplification. Examples are:
  - Forced (hydrodynamic) vibrations induced by propulsive devices.
  - Forced (mechanical) vibrations induced by reciprocating and rotating machinery.
  - Wave-induced loads due to waves encountered at a frequency near the fundamental natural frequency of the hull girder, which may, therefore, excite a resonant response (springing).
  - Transient hull girder vibrations (whipping) induced by impact loads.
- **Impact loads** include shocks and suddenly applied loads such as:
  - Slamming pressures from wave impacts.
  - Green water impacts on deck.
  - Internal tank sloshing impacts.
  - Explosions and weapon effects.

The list is not comprehensive and, in addition to the items mentioned, there are special loads (e.g. ice loads, landing of aircraft and helicopters, collision and accidental grounding) that are relevant to some vessels only. This way of classifying loads (according to their timescale) is reflected in the different types of structural analysis, mainly: static, quasi-static and dynamic (Hughes 1983). In a static analysis, loads are modelled as independent of time. This includes static loads and is often extended to slowly varying loads, whose frequency is much lower than the fundamental natural frequency of the structure. A quasi-static analysis is still effectively a static analysis, as it assumes that the problem is static at a given instant in time. Some dynamic aspects, however, are accounted for by including inertial forces. In a dynamic analysis the time dependency of the loads is fully accounted for, which is usually required to study the effect of rapidly varying loads with sufficient accuracy.

Another useful method (Hughes 1983, Lewis 1988a) to classify loads is according to the level at which they act on the structure: hull girder, hull module, principal member or local. Some loads generate a response at just one level, whilst other have an influence at more than one or even at all levels. The external pressure on the hull, for example, generates loads at all levels. This classification reflects the approach adopted for the design and assessment of ship structures, which consist of different strength analyses, from a global down to a local level. Global analysis concerns the design of the hull girder, which must be capable of sustaining bending moments, shear forces and torsion, while local analysis focuses on a particular part of the ship's structure or a single structural member. Very local analyses can be conducted to assess stress concentrations within relatively small areas of the structure.

The following sections deal with the available methods for calculating and measuring seakeeping loads on vessels, with a focus on small high-speed craft. Since static buoyancy and weight forces can be estimated numerically with a high degree of confidence, the treatment focuses on wave and slamming loads and relative effects on the structure.

2.2 Seakeeping Load Prediction Methods

2.2.1 Semi-Empirical Methods

Although a high-speed craft travelling in waves is an inherently dynamic problem, the structural design is considerably simplified if it can be treated as nearly static. The fundamental assumption underlying semi-empirical methods is that a transient non-uniform pressure distribution can be modelled as static and uniform. Pressures for the structural design are modelled as equivalent static pressures that, if applied to the structural member, will produce the same maximum deflection and same peak stress as those produced by the actual loading.

The development of the first semi-empirical method for the structural design of high-speed craft is attributed to Heller and Jasper (1960). The method is based on rough water sea trials conducted with a 23-metre motor torpedo boat (Jasper 1949). The pressure, acceleration and strain measurements taken during the trials were used, together with

theoretical calculations, to formulate load factors that allow to convert dynamic loads to equivalent static loads. The work was extended to a design methodology, based on global and local strength calculations, where the pressures for design are determined from the vertical accelerations taken at the centre of gravity. Following Heller and Jasper, several re-elaborations were presented. According to Razola (2013), Allen and Jones' method (1978) largely superseded that of Heller and Jasper and, as of today, represents the most widely used design method. A revision of Allen and Jones' method, based on modern numerical and experimental analyses, was presented by Razola *et al*. (2014a), together with a valuable review of the original authors' work. Semi-empirical methods have been implemented in most classification societies' basic rules for the design of high-speed craft and, even as of today, appear to be the state-of-the-art for practical work. An overview of these methods, as implemented by major classification societies, can be found in Stone (2005).

Semi-empirical loads used together with structural engineering formulae to determine the scantlings represent a practical option. Further improvements in the structural design can be achieved by using these loads as an input for finite element structural analyses (e.g. Ojeda *et al.* (2004)). As stated by Razola (2013), however, finite element analysis based on semi-empirical pressures makes little sense because the pressures are formulated according to assumptions on the load carrying area of the structural member considered and on the degree of fixity of its framing edges.

The main argument over semi-empirical formulations is in the simplification of the hydro-structural problem, particularly in the modelling of slamming pressures. Less important for traditional thin-plated structures, it becomes substantial for composite sandwich panels, for which it has been shown (Hayman *et al.* 1991, Razola *et al.* 2014b) that calculations based on a uniformly distributed static pressure give less conservative estimates of the maximum core shear stress than of the maximum skin bending stress. The impossibility to formulate a uniform static pressure that truly resembles the actual pressure field, in terms of both bending and shear stresses generated, often results in an underestimation of the shear stresses. This explains why core shear failure is predominant in sandwich structures subject to extreme slamming loads (Hayman *et al.* 1991).

2.2.2 The RNLI Load Prediction Method

Due to the extreme conditions in which the RNLI lifeboats operate, and their challenging structural requirements, the RNLI developed an in-house semi-empirical design method for the determination of the design pressures (Clark *et al.* 1997, Cripps, Phillips, *et al.* 2004, Cripps 2005, Cripps *et al.* 2005). Initially formulated based on experimental measurements coupled with theoretical formulations, this approach treats the design loads in terms of equivalent static ultimate pressures.

The hull pressures for the design of a new lifeboat are determined as a function of the vessel load displacement Δ_T in tonnes and the maximum operational speed V_k in knots, using the semi-empirical lines shown in Figure 2.1. Line 'A' is a lower limit that corresponds to the design pressures adopted for earlier lifeboat classes, whilst line 'B' is an upper limit based on in-service experience and known cases of structural damage on later lifeboat classes. The Severn Class (previously denoted Fast Afloat Boat 3 (FAB3)), for example, was designed with a vessel numeral $\Delta_T \times V_k = 36t \times 25kts = 900$, which calls for a design panel pressure between 72 and 120 psi (lb/in^2), these values being the intersections with the lines 'A' and 'B' respectively. For the final structural design, a hull bottom pressure of 120psi was adopted.

The pressure value found from Figure 2.1 is then modified according to the longitudinal position of the structural member under consideration and for the topsides, which carry only a percentage of the pressure applied over the hull bottom. The original Severn structural design was based on the longitudinal distribution curve developed by Heller and Jasper (denoted H&J). The RNLI later modified (extended further aft and forward) this distribution to better account for the severe loads experienced by more modern lifeboats, which were capable of maintaining moderate/high speed in severe weather conditions. The current longitudinal distribution, superimposed onto the original, is shown in Figure 2.2. The pressure values obtained through this method are maximum static ultimate pressures to be applied as a uniformly distributed load over the whole of the respective hull panel.

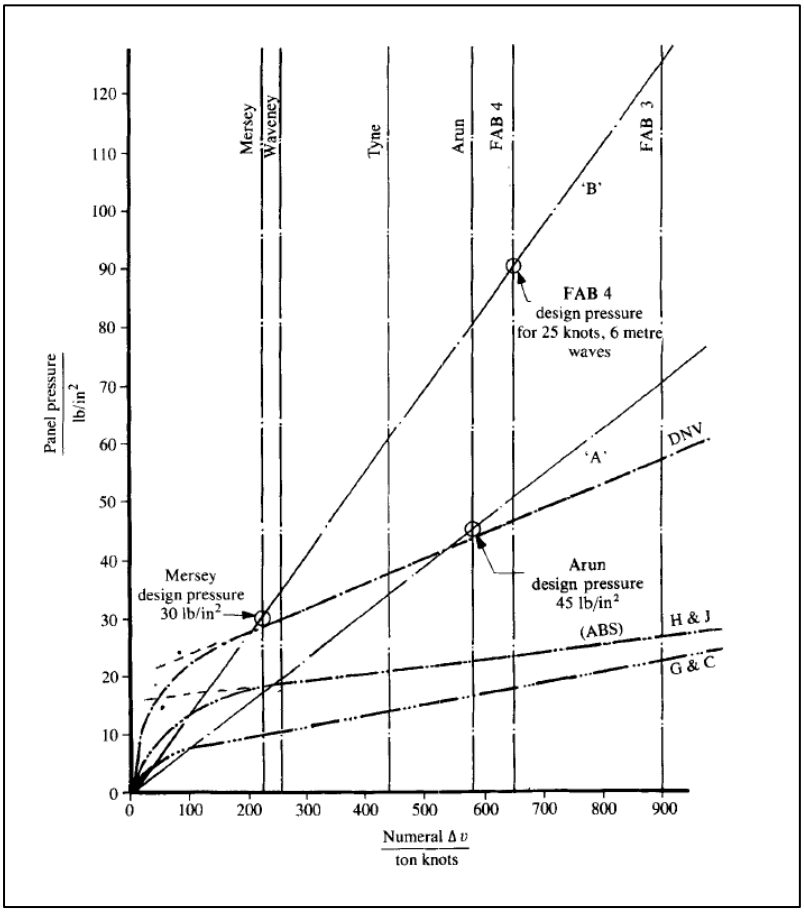

Figure 2.1. RNLI's design pressure prediction method.

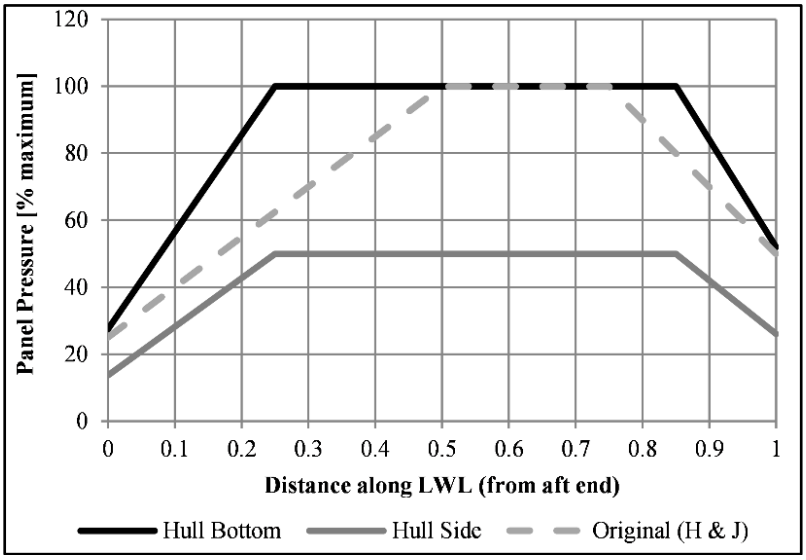

Figure 2.2. RNLI's design pressure longitudinal distribution factor.

2.2.3 Computational Methods

Computational Fluid Dynamics (CFD) comprises different descriptions of the fluid flow and different techniques of computation to solve its field equations. A thorough description of the basic principles and numerical formulations can be found in many textbooks. The following review (after Faltinsen (2006), Hughes and Kee Paik (2010) and Bertram (2012)) is limited to computational tools suitable to predict seakeeping motions and loads on ships.

The seakeeping of a ship has been tackled for a long time assuming that the ship-wave system is linear with respect to the wave height and that the sea surface can be modelled as a linear superposition of regular harmonic waves of various amplitudes and frequencies. The useful consequence is that motions and wave-induced loads can be studied in elementary harmonic waves and the principle of superposition applied to determine the overall response in an irregular seaway.

The majority of seakeeping predictions are based on potential flow theory, modelling the fluid as incompressible, inviscid and irrotational. These assumptions reduce a system of four nonlinear partial differential governing equations that describe the fluid flow, down to one linear differential equation. Potential flows find application in boundary element methods, which discretize only the boundaries of the domain instead of the whole fluid domain, therefore simplifying the grid generation task. Both these aspects make potential flow solvers computationally efficient and a convenient option for practical work. Under the assumptions of linearity, seakeeping predictions can be made even more efficient by solving the problem in the frequency domain.

A common boundary element method is the so-called panel method, which consists of dividing the hull surface and the surrounding water surface into a number of finite elements, or panels, and calculating the solution from a set of linear equations equal, in number, to the number of panels. Further simplifications can be made within the framework of the slender body theory, applicable to hull forms that have the longitudinal dimension much larger than the transverse dimensions and the cross-section that varies smoothly along the length. The ‘slender body’ assumption allows to reduce the potential flow problem from three to two dimensions, using the so-called

strip theory. This method consists of dividing the underwater part of the hull into a number of transverse sections, or strips, and computing the hydrodynamic forces at each strip independently. The three-dimensional problem is therefore broken down into a series of two-dimensional problems in the transverse plane, which are easier to solve. The forces computed at each strip are then combined, through integration along the hull length, to provide the response for the whole vessel.

Strip theory is the most conventional tool for ship seakeeping simulations. Different formulations can be found in the literature and implemented into commercially available software packages. In general, linear strip theory codes have the following limitations:

- The slender body theory is applicable to conventional hull forms with length much greater than beam and draught and with smooth variations of the cross-section.
- The variation of the flow in the transverse plane is assumed much larger than the variation along the hull, so that the flow around each strip does not affect the flow on adjacent strips. This implies that three-dimensional interactions in the longitudinal direction should be negligible, as they are not properly accounted for.
- From the above it follows that the frequency of oscillation is assumed high, which makes strip theory methods more applicable in head, bow quartering and beam waves than in following and stern quartering waves, where the encounter frequency reduces significantly as the ship speed increases.
- In the formulation of the boundary conditions at the free surface, linear theory assumes that the velocity potential and the fluid velocity are constant from the mean free surface to the instantaneous free surface. This implies that all the hydrodynamic forces are calculated only on the calm-water wetted surface and that the hull is considered wall-sided. The assumption of 'wall-sidedness' means that predictions of the wave-induced vertical bending moment and vertical shear force have the same magnitude for both sagging and hogging condition.
- From the above it also follows that linear theory is no longer accurate when the instantaneous wetted surface departs significantly from the mean wetted surface, which is the case for: large amplitude motions; and speeds that generate appreciable planing lift, with consequent changes of sinkage and trim. According to Bertram

(2012), the difficulty associated with the modelling of the dynamic sinkage and trim is likely to be the reason why classical strip theory methods are generally deemed accurate for Froude numbers up to 0.4.

- Linear theory would only be suitable for seakeeping predictions in light to moderate seas, as the assumption of linearity becomes questionable in severe seas. In fact, linear theory is still applied to find extreme wave-induced motion and load values for design calculations. In these cases, the predictions can either be used directly to give only rough estimates or can be corrected for small nonlinearities to enhance their accuracy.
- Potential flow theory assumes that the fluid is inviscid, hence the effects of viscous damping have to be implemented artificially.
- Potential flow theory also requires a continuous water surface and is not appropriate for problems that involve complex free surface shapes with spray, air trapping or flow around sharp edges. This makes it unsuitable for studying and predicting loads from slamming impacts, sloshing in partially filled tanks, green water on deck or breaking waves.

In many applications, linear theory predictions can be corrected for small nonlinearities and used to obtain large amplitude responses for design calculations. However, if the vessel responses are strongly nonlinear, there is little sense in seakeeping simulations with regular waves. These waves do not occur in nature, hence they are not usually of interest, and the vessel responses in a natural seaway cannot be deducted from the responses in regular waves. In these cases, time-domain solvers that facilitate the modelling of nonlinear effects are the appropriate tool, but it should be accepted that the computations become considerably more expensive.

For fully nonlinear computations, the viscosity of the fluid must be included in the solution of the governing equations, precluding the use of potential flows. This implies solving all the four nonlinear partial differential equations with four unknowns, which is computationally impractical. Approximations are made by computing a time-averaged solution of the equations of motions of the fluid flow. The common approach is to solve the Reynolds-Averaged Navier-Stokes Equations (RANSE) in the time domain. The RANS equations are derived by assuming that the instantaneous velocity

components can be decomposed into a time-averaged quantity and a fluctuating quantity that represents the turbulence of the mean flow. As opposed to potential flow solvers that discretize only the boundary of fluid domain, the solution of RANS equations requires the discretization of the whole fluid domain. These aspects make RANSE codes the most computer intensive albeit realistic tools in the marine field.

A comprehensive review of the most recent advances in the use of CFD to predict seakeeping loads on ships was made by Temarel *et al.* (2016). According to the authors, potential flow solvers, with inclusion of a range of nonlinearities, still dominate due to their efficiency. Focus is now on the development of numerical methods capable of including nonlinear phenomena such as slamming, green water and sloshing. The use of RANSE solvers, in spite of the high computational resources required, is increasingly more popular and features improved accuracy. It is stressed by the authors that the need for validation against measurements remains essential in both cases.

2.2.4 Experimental Methods

Experimental measurements of the seakeeping responses of a vessel are an alternative to numerical methods and provide a way of validating their predictions. Experiments can be conducted in laboratories, usually at reduced scale, or in real conditions.

Most of the tests at model scale are conducted in towing tanks or wave basins, which provide ease of taking measurements and good control of the wave environment (Lloyd 1989). Regular and irregular wave patterns can be generated as required and re-produced during subsequent runs. The testing procedure and the data analysis, including the extrapolation of the results to real scale, can rely on extensive guidelines, developed in particular by the ITTC (e.g. ITTC (1999a, 1999b, 2002a, 2002b)). Seakeeping motion tests have been carried out extensively in the past and the choice of the measurement apparatus often depends on the facility's practice, the test objectives and on whether the model is towed by a carriage or equipped with its own propulsion system.

External pressures are usually measured with pressure transducers. Since these provide point measurements, the complete pressure field on the hull bottom is to be

reconstructed from arrays of transducers, as proposed by Rosén (2001, 2005) and Rosén and Garme (2004). An alternative to point measurements are slamming patches, which measure the hydrodynamic force exerted on a cut-out of a hull panel (e.g. Manganelli *et al.* (2003)). In this case, what is measured is the pressure over the entire patch rather than the pressure over the much smaller diaphragm area of a conventional transducer. Results are therefore to be regarded as averaged panel pressures.

Seakeeping experiments are also conducted to measure global loads on the hull girder. Ideally a 'hydro-structural' scaled model would be used to measure loads at any longitudinal position, however, due the practical complexities in satisfying the structural similarity at model scale, the use of a segmented model is most common (after ITTC (1999b, 2011)). The segmentation consists of cutting the hull shell into a number of segments so that the hull does not provide any continuous structural support. The hull girder strength is given by an internal backbone structure. Load measurements are taken at the segmentation cuts by means of strain gauges on the backbone beam or load cells connecting the segments. Two types of segmented model exist, depending on the stiffness of the connecting structure: rigid and elastic. A rigid segmented model has a much higher stiffness than the actual vessel and greater natural frequency than the wave encounter frequency. This ensures that the global loads measured on the beam that acts as a hull girder are free from vibratory responses such as whipping or springing. Wave-induced global loads can be measured and compared with theoretical results. Dynamic and impact load effects require the stiffness of the hull girder to be appropriately reproduced at scale. For these loads, an elastic segmented model that represents the rigidity of the prototype hull should be used, so that global loads, including the vibratory effects produced on the hull girder, can be extrapolated to real scale. A historical review of relevant tests with hydro-structural and flexible segmented models was edited by Marón and Kapsenberg (2014), while the most recent advances in the use of model tests to assess seakeeping loads on ships can be found in Temarel *et al.* (2016).

In spite of the numerous advantages of model testing, it should be recognised that scaling is problematic. The towing force only resembles the thrust of an actual propulsion system and the wave environment tends to lack the confused nature of the sea. To investigate the seakeeping of a vessel in real operational conditions, sea trials are

necessary. They are nevertheless expensive and time consuming, which is why they are not carried out on a regular basis. If conducted for design purposes, they also require a prototype vessel to be built first.

An example of full-scale tests conducted on an instrumented small high-speed naval craft (LWL=9.5m, V=+40kts) was presented by Rosén & Garme (1999). At a larger scale, other examples are the sea trials conducted with a wave-piercer catamaran (Jacobi *et al.* 2014) and those conducted with the research vessel Triton (Grassman and Hildstrom 2003, Renilson *et al.* 2004) as part of a programme to assess the trimaran hull form for implementation in future warship designs.

In addition to short-term dedicated sea trials, the recent technological advances have made feasible the monitoring of ship structures under normal operating conditions and for longer periods of time. Long-term and through-life monitoring systems find some practical application today. Amongst other features, reviewed by Salvino and Collette (2009), these systems enable designers to verify design assumptions in terms of design versus actual loads experienced, and to improve the calculation of design, lifetime and extreme loads.

2.2.5 Slamming

Loads from wave impacts (slamming) are important for small high-speed craft because they often govern the scantling design. These impact loads are usually named according to the area of the structure affected:

- Bottom slamming is due to significant heave and pitch motions and occurs when the hull bottom, emerged from the water, re-enters the water surface.
- Bow-flare slamming is due to significant heave and pitch motions that cause the bow to plunge into the water with high relative velocity.
- Stern slamming occurs on ships with a flat stern and is due to significant heave and pitch motions that cause the stern, emerged from the water, to re-enter the water surface with high relative velocity.
- Wed-deck slamming occurs on multihulls when the relative heave amplitude exceeds the height of the cross-structure connecting two adjacent side hulls.

- Sometimes considered under the term 'slamming', are also other impact loads due to: wave slaps, in particular from severe and breaking waves; and shipping of green water on deck, caused by the bow plunging into the water and displacing a large amount of water onto the deck.

The prediction of slamming-induced loads has been tackled for a long time, challenged by the complexity of the phenomenon. Slamming is strongly nonlinear and stochastic in nature. Slamming loads are sensitive to the relative motion and the impact angle between the structure and the water surface (e.g. significant pressures can rise for small hull deadrise angles, pronounced bow flares, flat stern shapes and flat deck cross-structures). Water impacts generate localised high pressure peaks that travel rapidly in space, affected by the three-dimensional shape of the body. The high loads imparted to the structure are of short duration and excite highly transient responses at both a local and a global level. A comprehensive list of the older theoretical, experimental and empirical approaches can be found in Daidola and Mishkevich (1995) and Kapsenberg (2011), while the most recent advances in computational techniques are reviewed by Temarel *et al* (2016).

The first theories for body impact with water were developed in the context of seaplane landing with the pioneering work of Von Kármán (1929) and Wagner (1932). The impact of the body with the water was idealised as the entry of a two-dimensional wedge through the calm water surface, solved by applying the momentum conservation principle. The body was assumed as rigid and the fluid incompressible. Several theories were later presented based on these fundamental ideas and most theoretical studies to date still treat the slamming problem as the impact of a two-dimensional body onto calm water.

For practical problems, where the shape of the body is more complex than that of a simple wedge, where the effect of gravity becomes important, and where the structure behaves elastically, analytical solutions are very difficult, which leaves CFD as a tool (Bertram 2012). Boundary element methods relying on the potential flow theory have been developed for two-dimensional cases (e.g. Zhao and Faltinsen (1993) and Zhao *et al.* (1997)). Strip theory and panel methods have been adopted to extend their

application to three-dimensional bodies. The rapid increase of computing power has promoted the use of volume of fluid methods based on solving the RANS equations. It seems that, so far, the focus has been mostly on the modelling of impact forces for predicting the whipping response. The prediction of local pressure peaks requires a small discretization of the impact zone and the modelling of the structure's hydroelasticity. Although single case studies exist, the computational requirements are likely to be the limitation for practical design work.

Experimental studies on slamming include seakeeping tests and drop tests. Seakeeping tests (Section 2.2.4) are conducted on hull models or on instrumented vessels. They may focus on local effects, with measurement of the local slamming pressures and of the local structural response, or on global effects, with measurement of the whipping stresses in the hull girder. Drop tests involve the free fall of a body, from different heights and inclination angles, through the water surface. These tests are mainly conducted to obtain a relation between the pressures and the impact velocity of the body. The literature on small and full scale drop tests is large. Most experiments have been conducted reducing the problem to two dimensions, by testing sections of flat panels and wedges with different deadrise angles (e.g. Chuang (1966)). The two-dimensional test results are useful to validate water-entry theories and to evaluate the effect of the hull form on the impact. If a structural model is employed, it is also possible to evaluate the structural response of the hull panel.

2.2.6 Experimental Pressure Measurements

Direct measurement of wave and slamming pressures seems a convenient option to generate loads for structural analysis. Several pressure-sensing technologies exist (piezoelectric, piezoresistive, capacitive, potentiometric, etc.) that provide transducers with different features. The common shortcoming is that measured pressures are values averaged over the diaphragm of the transducer, which should be relatively small to capture the magnitude of pressure peaks. The small sensing area requirement means that a transducer provides a 'point measurement' and that pressure fields can only be reconstructed from arrays of transducers.

Pressure transducers present other drawbacks. Kim et al. (2015) conducted a comparative study, reported by ITTC (2017), on sensor technologies typically used for sloshing experiments. They highlighted that, depending on the technology used, pressure sensors can exhibit the following limitations:

- Poor long-term stability with significant drift, which can be a practical limit for long-term measurements.
- Notable thermal shocks due to temperature differences, even relatively small, between the sensor and the medium (e.g. air, water).
- Sensitivity to changes of medium (e.g. from air to water), extendable to the case of a dry sensor that becomes in contact with water.
- Different measurements of peak pressure and peak rise time depending on the sensor used, but also between sensors of the same type, sensing diameter and linearity characteristics.
- In conclusion, pressure signals that differ depending on the sensor used.

Direct measurement of hull pressures presents also practical challenges. Transducers require holes through the hull shell and should be flush-mounted so as not to interfere with the fluid flow. If measurements are taken at model scale, extrapolation of pressure data to full scale is likely to be affected by scaling effects, which makes scaling laws paramount. As concluded by Daidola and Mishkevich (1995), extrapolation of slamming pressures to full scale should consider: scaling effects for different forms of hydrodynamic impact, in particular when air entrapment is involved; differences between two-dimensional and three-dimensional models; and differences between drop tests and tests at forward speed in waves.

2.2.7 Response Amplitude Operators

The study of the behaviour of a ship travelling in a seaway was considerably simplified by the development of linear theory (more rigorously the 'theory of linear response to a statistically stationary seaway'), to the point that most seakeeping predictions are still carried out within its framework. Introduced in the marine field by St. Denis and Pierson (1953), this technique finds its basis in ideas first developed in electronics and communications. The main assumptions of the theory are that:

- The sea can be described as a statistically stationary Gaussian random process.
- The amplitude of the ship responses is linearly proportional to the amplitude of the exciting wave, while the phase of the responses is invariant of the wave amplitude.

Its rigorous formulation, presented by the authors, has been reported in many textbooks (e.g. Lewis (1988b)). The concept, however, is well explained through an analogy with an electronic filter (reported by Lloyd (1989)). The input signal (waves) is composed by a number of different frequencies that are amplified or attenuated by the filter (ship) to produce the output signal (ship responses). This filter is linear, that is, the amplitude of the output signal, at any given frequency, is linearly proportional to the input signal.

The characteristics of the filter can be formalised into a quantity called Response Amplitude Operator (RAO), defined as the ratio of the amplitude of the response and the exciting regular wave amplitude. This definition was originally assigned to another term, the transfer function, while the RAO was defined as the square of the transfer function. In this thesis, however, the convention is followed whereby the RAO is taken to be the same as its transfer function and used in its unsquared form (see St. Denis and Pierson (1953), Lewis (1988b) and Lloyd (1989)). Since a stationary seaway can be represented as the superposition of an infinite number of regular sinusoidal waves of all frequencies (Hughes 1983, Lewis 1988b), the response of a ship in the seaway can be reconstructed from the responses in regular sinusoidal waves, hence from its RAOs. The complex problem of predicting and assessing the seakeeping motions and loads for a ship is thus broken down into two problems: the prediction of motions and loads in regular elementary waves, and the prediction of motions and loads in irregular waves, using a statistical description of the sea and the regular wave results.

2.3 Structural Response Analysis

2.3.1 Analytical Methods

Formulae used in structural engineering generally express relations between the material properties of a structural member, its form and dimensions, the loads applied to it and the resulting stresses and deformations. These formulae are valid within some limitations, as they are often the result of mathematical procedures that involve

approximations, and are based on assumptions regarding the properties of the material, the regularity of the shape and the boundary conditions. Handbook formulae are applicable to certain problems only and no calculated value of stress or deformation is to be taken as exact (Roark 1965).

Ship structural design has for long relied on classical engineering formulae. Due to the complexity of ship structures, the structural response is usually divided into categories, related to the (hierarchical) structural layout, the nature of the loading and the expected load responses (review after Lewis (1988a)). The global (primary) response is usually investigated by idealising the ship as a thin-wall box beam that acts in accordance to the classical beam theory. The (secondary) response of stiffeners and stiffened panels can be investigated through elastic beam theory, orthotropic plate theory or grillage theory, each incorporating some simplifying assumptions. For the (tertiary) response of individual unstiffened panels, it is usually assumed that the panel is supported at its edges, hence boundary conditions can be applied to represent the relative stiffness between the panel and the framing structure. Analytical methods have been widely implemented in classifications societies' rules and standards, often with corrections and tuning based on classification experience.

2.3.2 The Finite Element Method

"[...] *divide each of the difficulties under examination into as many parts as possible, and as might be necessary for its adequate solution"* (by René Descartes in his work "Discours de la méthode pour bien conduire sa raison et chercher la vérité dans les Sciences", 1637).

The finite element method (FEM), or finite element analysis (FEA), provides a numerical solution to a range of engineering problems (e.g. heat transfer, electromagnetism and fluid flow) and dominates in structural analysis. Its formulations are extensively covered in the open literature and can be found in many engineering textbooks.

The basic principles can be explained as follows (after Cook *et al.* (2002)). Let's assume that it is required to find the distribution of an unknown variable within a body. The body is divided ('discretized') into an assembly of elements ('finite elements') interconnected at joints ('nodes'). Within each finite element, a simple spatial variation

of the variable is assumed. The assembly of finite elements constitutes the 'finite element structure' of the body and the arrangement of the elements within the structure is called a 'mesh'. The mesh is numerically represented by a system of algebraic equations to be solved for unknowns at the nodes joining the finite elements. The nodal unknowns are the values taken by the variable at the nodes, which together with the field assumed for any given element, fully determine the variable's spatial distribution within that element. The distribution of the variable within the entire body is computed, element by element, through a piecewise solution.

The actual spatial distribution of a variable within the domain of a finite element is likely to be more complex than the simple distribution assumed to solve the problem. This implies that FEM leads to an approximate solution. Since the structure is discretized into elements, this solution can be generally improved by adopting element types that adequately represent the body and the field distribution of the variable, and by increasing the number of elements, hence decreasing their size.

It is obvious that, the more sophisticated is the element formulation and the finer is the mesh, the higher is the computational effort. Hence the choice of element type and mesh tends to follow the objective of the analysis and the level of detail required to adequately represent the body. Following the load classification previously presented, FEM for ship structures tends to fall into the following categories (after Phelps (1997)):

- Global or full ship models are developed with a coarse mesh and are based on simple line (rod, bar and beam) and area (shell) elements.
- Local models of a part of the ship's structure or a single structural member are developed with a fine mesh and may require the use of solid elements. Relevant global effects are included as boundary conditions, typically displacements, supplied by the global analysis.
- Detailed models to assess stress concentrations can require an even finer mesh. Depending on the scope of the analysis, however, global load effects do not necessarily need to be modelled. This is the case if the aim is simply to define stress concentration factors, in which case the analysis can be conducted with a unit load.

2.3.3 Experimental Methods

Experimental methods are a means of verifying design assumptions or even of monitoring the structural response in operating conditions. Measurements can be taken on test specimens, on the actual structure or models of it. The usual way of assessing a structure is based on strength and stiffness considerations, hence on the calculation of stresses and strains. Experimentally, the direct measurement of stresses is limited by practical complexities, hence an important branch of experimental stress analysis relies on the principle of measuring strains (Hoffmann 1989).

Strain occurs on the surface of an object, which makes it is accessible for measurements, and it is on the surface that it often takes up the maximum values, of importance for design calculations which are often concerned with the maximum stresses and strains within the object. The stress in the material can be found from the resulting deformation thanks to Hooke's Law, which is considerably simplified if the material stiffness can be assumed as constant.

A review of the different types of strain transducers, with a focus on the most popular foil resistive strain gauges, and their use within the Wheatstone Bridge circuit, is provided by Hoffmann (1989). The state-of-the-art in ship structural monitoring systems, in terms of both technologies used and range of applications, has been reviewed by Slaughter *et al.* (1997), Salvino and Collette (2009) and Phelps and Morris (2013), and guidelines for their development have been edited by classification societies (e.g. American Bureau of Shipping (2015)).

2.4 Summary

A wide-ranging review was given of methods for seakeeping load prediction and for structural response analysis, leading to the following conclusions:

- The structural design of high-speed craft has for long relied on semi-empirical methods, assuming that a transient non-uniform pressure distribution can be modelled as static and uniform. A first limitation of this approach is that a uniform static pressure simply cannot resemble the actual pressure field, for example induced

by slamming, in terms of both bending and shear stresses generated. Moreover, advanced structural assessments based on semi-empirical pressures are questionable, since these pressures are formulated from assumptions on the load-carrying structure. The main limitation however is that, because of their formulation, semi-empirical methods are unsuitable for explicit calculations of the actual loads sustained during operation.

- CFD for seakeeping load predictions features continuous improvement. The most popular potential flow solvers are in principle inappropriate for high-speed craft whose seakeeping is highly nonlinear, although inclusion of nonlinearities broadens their scope. More advanced RANSE solvers require another level of computational resources but can feature improved accuracy. In both cases, there is still not enough confidence to base the design of a craft solely on CFD predictions and validation against measurement is still essential.
- Seakeeping experiments are an attractive alternative to CFD predictions and a means of validating their results. Tests at small scale have been carried out extensively and can rely on comprehensive guidelines. Load measurement is however limited by the complexities of satisfying both the hydrodynamic and structural similarity at model scale. Moreover, extrapolation of the results to real scale should take into account scaling effects and is always challenging. To overcome the limitations of scaled model tests, sea trials are necessary. These require conspicuous resources and, if conducted for a new design, a prototype vessel. Sea trials therefore remain a powerful tool to investigate the seakeeping of a real vessel in a real wave environment but cannot be always regarded as an accessible option for design.
- Direct assessments of the structural response are essentially FEM-based and range from global strength to detailed stress analyses. Experimental assessments are by large based on strain measurements, since the direct measurement of stresses is limited by practical complexities.

None of the existing methods is capable of solving the load prediction problem on its own and generate loads suitable for direct structural analysis. Different methods can however be combined, thereby overcoming the limitations of each. This is the approach followed in this study.

Chapter 3

Overview of the Approach

3.1 Introduction

Because of the complex hydrodynamics and load effects that dominate the loading scenario at high speed and planing regime, the structural design of high-speed craft has traditionally relied on simplified approaches. For practical design purposes, semi-empirical methods, such as those implemented as basic standards by many classification societies and the RNLI's own load prediction method, are often used and have proved to be successful. These methods are, however, not suitable for direct calculations of the structure's response to the actual loads sustained in operation (Lim *et al.* 2018).

Numerical tools are increasingly more popular. The less sophisticated, such as potential flow solvers, seem to be the state of the art, but with reservations on their ability to capture the planing hydrodynamics. Advanced RANSE solvers are increasingly more popular and have successfully been used for single case studies. Yet, in addition to their computational requirements, there is often not enough confidence to base the design solely on their results. Experimental measurements are an alternative to numerical simulations and a way of validating their predictions. Tests at model scale, in towing

tanks or wave basins, are now standard practice. Although they provide ease of measurements and control over the waves that are generated, scaling is always problematic and the wave environment lacks the confused nature of a real seaway. Seakeeping trials are an attractive solution to these shortcomings, although they require significant resources and a prototype vessel (Lim *et al.* 2018). They also require transformation of the measurements into quantities useful to the analysis of the structural behaviour and construction of distributions from discrete measurement points, such as a pressure field from pressure measurements taken at the locations of the pressure sensors.

Without the availability of a single reliable means to predict all the possible loading situations during operation in waves, a systematic approach that combines different methods was developed and validated on the Severn Class lifeboat operated by the RNLI.

3.2 The RNLI and the Severn Class Lifeboat

The RNLI is a charity that exists to save lives at sea. Since it was founded in 1824, it has saved more than 142.000 lives (Royal National Lifeboat Institution 2018). The RNLI now provides a 24-hour maritime search and rescue service, flood rescue service and seasonal lifeguard service in the United Kingdom and the Republic of Ireland, in addition to other prevention and international activities.

Continuous search and rescue cover is guaranteed up to a distance of 50 miles offshore within three hours of launching. As of 2018, the active RNLI's fleet counted more than 350 lifeboats, ranging from 3.8m to 17m in length, launched from 238 lifeboat stations. These lifeboats, which are at all effects dedicated search and rescue vessels, are divided into two categories. The inshore lifeboats are specifically designed to operate close to the shore and in surf, on rivers, in shallow water, close to cliffs and in caves. The fleet comprises a range of fully inflatable boats, rigid inflatable boats (RIBs), rigid hull boats and hovercraft, ranging in length from 3.8 to 10.5m. The all-weather lifeboats have a length of 12 to 17m and are capable of operating safely in all weather conditions. They can be launched from a carriage, or a slipway and lie afloat, depending on the class and geographic location, and all have self-righting capability after capsize.

The Severn (Figure 3.1) is the largest all-weather lifeboat class of the RNLI's fleet. With an overall length of 17 metres and a displacement of 42 tons, it is capable of a maximum speed of 25 knots and has an operational range of 250 nautical miles. Its principal particulars are outlined in Table 3.1. In this thesis, the seakeeping of the Severn is evaluated for a range of operating speeds. Table 3.2 reports speed values in knots and the correspondent Froude number values.

Figure 3.1. The Severn Class lifeboat.

Length overall	LOA	17.00	m
Length waterline	LWL	15.50	m
Beam overall	BOA	5.62	m
Draught	T	1.37	m
Displacement (light load)	Δ	36.5	t
Displacement (full load)	Δ	42.0	t
Speed max	V	25	kts
Fuel		5600	lt
Range		250	NM
Construction		FRP	
Crew		7	
Survivor capacity (self-righting)		28	
Survivor capacity (not self-righting)		124	

Table 3.1. Severn Class main particulars.

knots	Fn
5	0.2
10	0.4
15	0.6
20	0.8
25	1.0

Table 3.2. Severn Class speed conversion from knots to Froude numbers.

The original design of the Severn, which was subject to subsequent modifications during the construction and the evaluation stages, can be found in Hudson *et al.* (1993). In the final design, the hull is a single chine with a deep 'vee' forward and a reduced deadrise aft. The propulsion system has shaft lines and deep propeller tunnels delimited by a centreline skeg. Sacrificial side keels are fitted to protect the propellers and rudders should the lifeboat take the ground. These also serve to keep the vessel upright in the event of a complete grounding.

The structure is comprised of composites with unidirectional, biaxial and multi-axial E-glass and hybrid E-glass/aramid reinforcements impregnated with an epoxy resin matrix. PVC foams of different densities are used for the sandwich panel core material, and for the longitudinal stiffener and transverse frame supports. The hull bottom is of stiffened single skin construction, while the hull topsides, deck, internal subdivision bulkheads and the superstructure are of sandwich construction. Details of sample laminate layups are reported in Tables 3.3-3.4, whilst the mechanical properties of reinforcement plies and foams are reported in Tables 3.5-3.7.

Below decks, the hull is divided into six watertight compartments: steering gear room, engine room, fuel tank space, survivor space, fore cabin and fore peak. These are delimited by five continuous transverse bulkheads and two intercostal longitudinal bulkheads positioned off-centreline and symmetrically. The longitudinal bulkheads provide most of the compartments with double sides (or wing tanks). Six top hat longitudinals run from the transom to the bow. In the engine room, four of these are enhanced as girders to support engines and gearboxes, while, in the survivor space, an additional centreline girder supports the lower deck sole. Web frames run between the transverse bulkheads to support the longitudinals and the lower deck sole, and to stiffen the wing tanks. In the survivor space and in the fore cabin, the sole is bonded to the bulkheads, providing these compartments with a watertight double bottom. The deck is mainly supported by the bulkheads and by transverse beams connected to the web frames. A continuous centreline deck girder, supported by pillars, runs longitudinally in the engine room. The transom is strengthened by two stiffeners that continue from the inboard engine girders, while the stem is thickened by a foam infill covered by an extra laminate.

Area	Structural Member	Laminate	Layup
Hull	Bottom	Single Skin	1 x RE210 2 x YE1597 4 x QEA1200 2 x YE1597
Hull	Transom	Sandwich	1 x RE210 2 x QEA1200 H130 @ 40mm thk 2 x QE1600
Hull	Side	Sandwich	1 x RE210 3 x QEA1200 H130 @ 100mm thk 2 x QE1200
Hull	Deck	Sandwich	1 x RE210 1 x QE600 1 x QE1200 H100 @ 30mm thk 1 x QE1200 1 x QE600
Hull	Long. Bulkhead	Sandwich	1 x QE1200 H80 @ 30mm thk 1 x QE1200
Hull	Transv. Bulkhead/ Web Frame	Sandwich	1 x XE450 1 x XE900 1 x QE1200 H80 @ 20, 30 or 50mm thk 1 x QE1200 1 x XE900 1 x XE450
Hull	Floor	Top Hat	H80 Foam 1 x XE900 6 x UE800 (flange only) 1 x XE900 6 x UE800 (flange only) 1 x XE900 6 x UE800 (flange only) 1 x XE900 6 x UE800 (flange only) 2 x XE900 1 x UE800 (flange only) 1 x XE900
Hull	Long. Stiffener	Top Hat	H45 Core 2 x XE900 (hand lam.) 1 x XE900 4 x UE800 (flange only) 1 x XE900 4 x UE800 (flange only) 1 x XE900 4 x UE500(flange only) 2 x XE900
Hull	Deck Beam	Top Hat	H80 Core 1 x XE900 5 x UE800 (flange only) 1 x XE900 5 x UE800 (flange only) 1 x XE900 5 x UE800 (flange only) 1 x XE900 5 x UE800 (flange only) 1 x XE900

Table 3.3. Sample hull laminates of the Severn Class.

Area	Structural Member	Laminate	Layup
Wheelhouse	Forward & Side	Sandwich	1 x RE210 1 x QE1200 H80 @ 30mm thk 1 x QE1200
Wheelhouse	Top	Sandwich	1 x RE210 2 x QE1200 H100 @ 30mm thk 2 x QE1200
Wheelhouse	Aft	Sandwich	1 x RE210 2 x QE1200 H80 @ 30mm thk 2 x QE1200
Wheelhouse	Transv. Bulkhead	Sandwich	1 x RE210 1 x QE1200 H80 or H100 @ 30mm thk 1 x QE1200 1 x RE210
Wheelhouse	Transv. Beam	Top Hat	H80 Core 1 x XE900 4 x UE800 (flange only) 1 x XE900 4 x UE800 (flange only) 1 x XE900 2 x UE800 (flange only) 1 x XE900

Table 3.4. Sample wheelhouse laminates of the Severn Class.

Reinforcement		UE500		UE800		RE210	
Material		E-Glass		E-Glass		E-Glass	
Fabric		Unidir. Woven		Unidir. Woven		Biaxial Woven	
Fibre Orientation		[0°]		[0°]		[0°/90°]	
Dry Ply Weight	[g/m^2]	500		800		210	
Resin		Epoxy	Epoxy	Epoxy	Epoxy	Epoxy	Epoxy
Lam Type		Wet Lam	PrePreg	Wet Lam	PrePreg	Wet Lam	PrePreg
Fibre Content (Volume)		0.44	0.56	0.44	0.56	0.45	0.48
Long. Tensile Modulus	[N/mm^2]	33180	41420	33180	41420	19360	20740
Long. Tensile Strength	[N/mm^2]	597	808	597	808	290	311
Long. Compressive Modulus	[N/mm^2]	28650	36470	28650	36470	18970	20330
Long. Compressive Strength	[N/mm^2]	344	620	344	620	209	224
Transv. Tensile Modulus	[N/mm^2]	5690	7600	5690	7600	19360	20740
Transv. Tensile Strength	[N/mm^2]	26	34	26	34	290	311
Transv. Compressive Modulus	[N/mm^2]	7850	10000	7850	10000	18970	20330
Transv. Compressive Strength	[N/mm^2]	118	150	118	150	209	224
Interlam. Shear Modulus	[N/mm^2]	2910	3910	2910	3910	2980	3270
Interlam. Shear Strength	[N/mm^2]	44	59	44	59	36	39
In-Plane Shear Modulus	[N/mm^2]	4320	5500	4320	5500	4261	4676
In-Plane Shear Strength	[N/mm^2]	52	83	52	83	45	44
Density	[kg/m^3]	1762	1972	1762	1972	1778	1859
Cured Ply Thickness	[mm]	0.44	0.34	0.70	0.55	0.18	0.17
Cured Ply Weight	[g/m^2]	771	674	1233	1078	317	311

Table 3.5. Sample laminae's mechanical properties (1 of 2). Supplied by the RNLI.

Reinforcement		XE450		XE900		QE600	
Material		E-Glass		E-Glass		E-Glass	
Fabric		Double Bias Stitched		Double Bias Stitched		Quadriaxial Stitched	
Fibre Orientation		[±45°]		[±45°]		[0°/90°/±45°]	
Dry Ply Weight	[g/m^2]	450		900		600	
Resin		Epoxy	Epoxy	Epoxy	Epoxy	Epoxy	Epoxy
Lam Type		Wet Lam	PrePreg	Wet Lam	PrePreg	Wet Lam	PrePreg
Fibre Content (Volume)		0.46	0.52	0.46	0.52	0.41	0.51
Long. Tensile Modulus	[N/mm^2]	20150	22640	20150	22640	15220	18930
Long. Tensile Strength	[N/mm^2]	302	340	302	340	228	284
Long. Compressive Modulus	[N/mm^2]	19750	22190	19750	22190	18040	19510
Long. Compressive Strength	[N/mm^2]	217	244	217	244	207	283
Transv. Tensile Modulus	[N/mm^2]	20150	22640	20150	22640	15220	18930
Transv. Tensile Strength	[N/mm^2]	302	340	302	340	228	284
Transv. Compressive Modulus	[N/mm^2]	19750	22190	19750	22190	18040	19510
Transv. Compressive Strength	[N/mm^2]	217	244	217	244	207	283
Interlam. Shear Modulus	[N/mm^2]	3050	3600	3050	3600	5270	6720
Interlam. Shear Strength	[N/mm^2]	37	43	37	43	63	81
In-Plane Shear Modulus	[N/mm^2]	4362	5148	4362	5148	7683	8324
In-Plane Shear Strength	[N/mm^2]	46	49	46	49	93	112
Density	[kg/m^3]	1786	1895	1786	1895	1731	1919
Cured Ply Thickness	[mm]	0.39	0.35	0.76	0.67	0.59	0.47
Cured Ply Weight	[g/m^2]	702	659	1233	1078	317	311

Reinforcement		QE1200		QE1600		QEA1200	
Material		E-Glass		E-Glass		E-Glass/Aramid	
Fabric		Quadriaxial Stitched		Quadriaxial Stitched		Quadriaxial Stitched	
Fibre Orientation		[0°/90°/±45°]		[0°/90°/±45°]		[0°/90°/±45°]	
Dry Ply Weight	[g/m^2]	1200		1600		1200	
Resin		Epoxy	Epoxy	Epoxy	Epoxy	Epoxy	Epoxy
Lam Type		Wet Lam	PrePreg	Wet Lam	PrePreg	Wet Lam	PrePreg
Fibre Content (Volume)		0.48	0.52	0.48	0.52	0.44	0.52
Long. Tensile Modulus	[N/mm^2]	18410	19910	18410	19910	17830	21270
Long. Tensile Strength	[N/mm^2]	276	299	276	299	267	319
Long. Compressive Modulus	[N/mm^2]	18040	19510	18040	19510	17930	21270
Long. Compressive Strength	[N/mm^2]	198	254	198	254	170	234
Transv. Tensile Modulus	[N/mm^2]	18410	19910	18410	19910	17830	21270
Transv. Tensile Strength	[N/mm^2]	276	299	276	299	267	319
Transv. Compressive Modulus	[N/mm^2]	18040	19510	18040	19510	17930	21270
Transv. Compressive Strength	[N/mm^2]	198	254	198	254	170	234
Interlam. Shear Modulus	[N/mm^2]	3190	3600	3190	3600	5700	7030
Interlam. Shear Strength	[N/mm^2]	38	43	38	43	68	84
In-Plane Shear Modulus	[N/mm^2]	7683	8324	7683	8324	7700	8400
In-Plane Shear Strength	[N/mm^2]	81	79	81	79	102	122
Density	[kg/m^3]	1809	1883	1809	1883	1632	1744
Cured Ply Thickness	[mm]	0.99	0.92	1.33	1.22	1.26	1.07
Cured Ply Weight	[g/m^2]	1797	1727	2398	2305	2056	1866

Table 3.6. Sample laminae's mechanical properties (2 of 2). Supplied by the RNLI.

Foam		H45	H80	H100	H130
Material		PVC	PVC	PVC	PVC
Nominal Density	[kg/m^3]	48	80	100	130
Compressive Strength	[N/mm^2]	0.6	1.4	2.0	3.0
Compressive Modulus	[N/mm^2]	50	90	135	170
Tensile Strength	[N/mm^2]	1.4	2.5	3.5	4.8
Tensile Modulus	[N/mm^2]	55	95	130	175
Shear Strength	[N/mm^2]	0.56	1.15	1.6	2.2
Shear Modulus	[N/mm^2]	15	27	35	50

Table 3.7. Sample foams' mechanical properties (from Diab Group (2018)).

The superstructure is bonded to the deck and creates one watertight space, on the basis that the hatches and wheelhouse door are closed. It is mainly stiffened by two partial transverse bulkheads and four transverse frames. The bulkheads and two deck beams provide the support for the flybridge.

3.3 Calculation of Seakeeping Loads and Response

3.3.1 Foundations of the Work

This work aims at providing the analyst with a functional tool for the direct calculation of the seakeeping loads and of the structural response. It is therefore developed with a practical perspective, whereby 'simplified' solutions are adopted to enable the modelling of the ship-wave system. While details will be given in the following chapters, it is anticipated that these solutions are not different from what is already accepted as standard practice:

- The principle whereby loads are classified according to the frequency at which they occur is at the basis of the different types of ship structural analysis (broadly: static, quasi-static and dynamic (Hughes 1983, Lewis 1988a)) and of the experimental measurement of ship loads and responses (e.g. Boller *et al.* (2009)).
- The breakdown of the structure according to the loads carried and the associated responses is at the basis of the ship structural design and of the calculations on global and local strength proposed by classification societies (e.g. American Bureau of Shipping (2014), Det Norske Veritas (2012a) and Lloyd's Register (2014)).

- The validation of numerical results through comparison with experimental measurements is the core of the engineering practice.
- Statistical trends to predict short and long term extreme loads have been extensively used to formulate design load values (e.g. Clarke (1986) and Schellin *et al.* (2015)).
- The use of global and local finite element models for direct structural analyses is now part of the advanced design procedures of many classification societies (e.g. American Bureau of Shipping (2011a) and Det Norske Veritas (2012b)).
- The modelling of slamming pressures as equivalent static uniform pressures has been at the basis of most semi-empirical design methods (e.g. Heller and Jasper (1960) and Allen and Jones (1972)).
- Simplified load distributions, often with corrections to account for the additional dynamic load effects, have found wide application (e.g. Clarke (1986) and Phelps (1997)).

3.3.2 General Outline

This study focuses on the following seakeeping loads, classified according to the breakdown from Chapter 2:

- **Hydrostatic loads:** static buoyancy pressures of the vessel, and pressures and forces from self-weight and contents.
- **Wave-induced loads:** wave-induced pressures from the combination of the passing waves and the resulting oscillatory vessel motions, and inertial reactions of the vessel and its contents resulting from the accelerations of the vessel travelling in waves.
- **Slamming-induced loads:** slamming pressures from wave impacts and transient hull girder vibrations (whipping) induced by these.

The following principles are followed:

- Loads and load responses are classified according to the timescale at which they occur and according to the level of the structure at which they act (local, global or both).

- The entire loading is broken down into load components, which are calculated separately and superimposed in the generation of a load case for the structural analysis.
- Wave-induced loads are not significantly affected by elastic deformations (which is generally the case for high-speed monohulls, as suggested by the American Bureau of Shipping (2011a)). Wave pressures can therefore be computed through a motion analysis and applied to the structure to obtain the elastic response.
- The generation of extreme load values is based on statistical methods that do not consider abnormal or freak waves.
- The loading definition is limited to the case of a vessel at forward speed in infinitely deep water.
- The effect of motion control devices, such as trim tabs, is not modelled. It is expected that their influence to the response of the craft can be superimposed onto the naked hull case.
- The prediction of extreme loads does not account for voluntary speed reductions and changes of course.

An overview of the approach is graphically presented in Figure 3.2. This consists of numerical seakeeping simulations based on linear potential theory (CFD Simulations), finite element analyses for the computation of the structural response (FE Analysis), and experimental tests at both model scale (Small-Scale Tests) and full scale (Full-Scale Tests).

The workflow can be partitioned into a hydrodynamic and a structural problem. The first leads to the determination of the load components, with the hydrostatic and the wave terms predicted numerically and the slamming term determined from full-scale test data. The load components are combined in the generation of a load case, which constitutes the input to the structural problem. This yields to the response of the structure. The accuracy of the structural analysis depends, in first place, on the correctness of the loading formulation, which partially relies on the accuracy of the numerical results. A validation task is therefore embedded into the workflow to verify, through comparison against experimental data, the validity of the CFD model.

The hydrodynamic and the structural problems are evidently connected, as one constitutes the input to the other. This implies that, to perform the structural analysis, loads need to be defined in a suitable form, that is, in terms of pressures or forces that can be applied to the structural model. Different methods are adopted. The schematic overview of the workflow will be expanded in the next chapters and a detailed outline of the direct procedure for the calculation of the seakeeping loads and response will be presented as part of the conclusions.

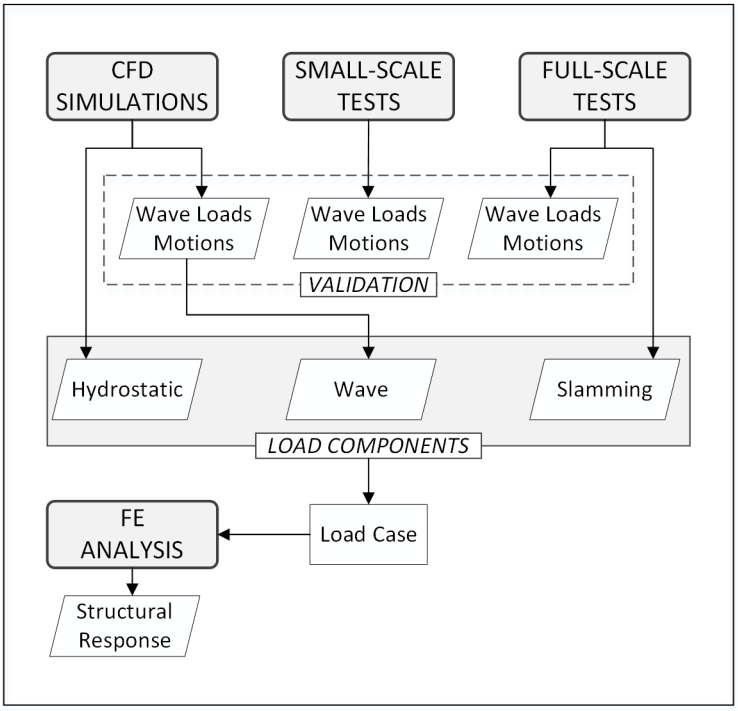

Figure 3.2. Overview of the approach.

3.3.3 Validation

It is generally accepted that static buoyancy pressures and the pressures and forces from self-weight and contents, can be estimated numerically with a high degree of confidence (Phelps 1997). Moreover, on a small high-speed craft these loads tend to be largely exceeded by the wave and slamming loads, hence they represent only a minor component of the total loading. The hydrostatic load term is therefore computed numerically.

Estimation of the wave loads relies on the capability of the CFD model to predict the hull pressures and the inertial reactions of the vessel resulting from the waves and the

vessel motions. These loads depend on the accuracy of the seakeeping simulations and, in turn, on the validity of the underpinning theory. The linear strip theory adopted is common for seakeeping simulations at displacement speeds, but could be questionable for semi-planing and planing speeds, both relevant because of the possible different operation modes of high-speed craft (from displacement to planing). The seakeeping simulations are therefore verified, or validated, through comparison against experimental data.

The 'validation' (Figure 3.2) takes place at a result level and comprises the RAOs of rigid body motions and sectional global wave loads. The results from the seakeeping simulations are superimposed onto those determined from experimental measurements for comparison. The experimental results, in particular those from the sea trials, could, in principle, be taken as reference for evaluating the seakeeping simulations. In practice, even experiments are affected by uncertainties and errors that make the validation task more complex. The following criteria, based on the implications for the structure of the vessel, are adopted to assess the validity of the wave loads predicted numerically:

- The CFD model is evaluated by assessing some of the simulation outputs. It is assumed that if motions and sectional wave loads are accurately predicted, the associated wave pressures can be used with confidence.
- If the numerical RAOs well encompass the experimental results, the numerical model can be considered conservative and therefore still suitable.
- If the trend of the RAO plots and the location of the peak along the abscissa (that is the wavelength that produces the maximum response) are accurate, an equivalent extreme (or design) wave can be calculated.
- Following from the above, if the magnitude of the RAOs is underestimated, a correction, in terms of a scaling factor, can be applied to the wave pressure to reach the sectional wave loads measured experimentally.

The CFD model developed for the hydrostatic and wave loads is not useful for the prediction of slamming loads because of the linear strip theory at the basis of the computations. These loads are therefore estimated from direct measurements taken at full scale.

For practical work, the relative importance of each of the load components should also be considered. As an example, a 30% underestimation of a minor load component can still make little difference to the whole loading, while the same 30% error relative to a major load component may result in a significant underestimation of the implications to the structure.

Chapter 4

Numerical Simulations

4.1 Framework

Computational methods are a convenient option for generating loads compatible with finite element structural analysis, as many codes output external hull pressures that can be directly applied to a structural model. Amongst the computational methods available for seakeeping problems, those working under the assumption of linearity still carry consistent advantages, which make them suitable to investigate the large number of operating conditions of a high-speed craft. Moreover, the presentation of motion and load results in terms or RAOs simplifies their assessment and the prediction of extreme loads can be based on well proven statistical methods.

One of the limitations of linear codes is the impossibility to capture nonlinearities, such as slamming impacts and relative loads. In this study, the use of computational hydrodynamics is therefore limited to the prediction of hydrostatic and wave loads. Hydrostatic pressures are computed from the balance of gravity and buoyancy forces. Wave-induced pressures are found from a seakeeping analysis based on linear potential

theory, which also outputs the correspondent motions and sectional global loads in terms of RAOs.

The computation of the structural response is based on the finite element method, widely used for direct structural analyses. The strength assessment is conducted at a global level with a full-ship model, where the structure is represented in its entirety. The level of detail is chosen accordingly and makes the finite element model suitable to assess the global strength and to identify structural members, or areas, that require enhanced modelling.

Both the generation of the load in a suitable form for the computation of the structural response and the structural response analysis itself rely on a numerical description of the vessel. The modelling and the load generation tasks are made easier by using the same model for the seakeeping and the finite element analysis, as part of a software package that combines the hydrodynamic and the structural problem. Many commercial programs couple standalone hydrodynamic and finite element solvers. Others (e.g. AVEVA Marine, NAPA) have the capability to export both mesh and loads to several general-purpose FEM software packages (e.g. Nastran, Ansys, Abaqus). The most comprehensive suites (e.g. Sesam, MAESTRO) bind together tools for pre-processing, hydrodynamic analysis, structural analysis and post-processing. Amongst these, the marine design program MAESTRO (2017) was chosen for the following features: integration of hydrostatic, hydrodynamic and structural analysis through a hydrostatic balance tool, a potential flow solver and a linear finite element solver; determination of short and long term extreme wave load values; modelling of composite materials; and computation of the global structural response.

4.2 The Marine Design Package MAESTRO

4.2.1 Finite Element Modelling

Because it is intended as a comprehensive naval architecture design tool, the MAESTRO philosophy differs from that of a generic finite element program. A MAESTRO global model is naturally organised into a hierarchy of parts. The structure is broken down into a number of substructures, modules and strakes, down to an element level. The basic

building block often corresponds to a structural element, such as a plate (stiffened or unstiffened), a girder, or a floor. Stiffeners do not necessarily need to be modelled as actual finite elements because their contribution to the structural stiffness can be accounted for through an increased bending stiffness of the finite elements representing the stiffened panel. As a consequence, finite elements can be relatively large and the mesh 'coarse'. This allows large ship models to be constructed with a limited number of nodes and elements, which makes efficient the computation of the structural response.

Single or groups of finite elements can be collected into strength assessment entities called 'patches'. A patch serves to represent a supported panel, a beam span or other structural elements, as per the traditional top-down structural hierarchy of a ship. Through the definition of patches, the true boundary conditions and spans of structural elements are used to calculate and assess their limiting failure modes.

The mesh generation task is different from that of most finite element software, which feature embedded mesh generation tools once the geometry has been defined. In MAESTRO the generation of the discretized model coincides with the construction of the geometry. This means that a coarse mesh finite element model can differ significantly from its respective geometrical model. The characteristic requirements of the finite element method, for example in terms of element size, skewness, warping and aspect ratio, are balanced against seeking a realistic structural behaviour through an adequate representation of the shape.

Because of the relative coarse mesh, and because conventional ships are thin-plated structures, MAESTRO is based on line (1D) and area (2D) elements only. The most common finite element is a 4-node flat shell with each node having 6 degrees of freedom. It is an orthotropic quadrilateral element, which can include the additional bending rigidity of the stiffeners, if these are not modelled as actual finite elements. The second type of area element is a 3-node flat shell with 6 degrees of freedom per node. This is a degeneration of the quadrilateral form and is a typical constant strain element. Because of the approximate solution for stresses and strains within the element domain, triangles are only used on a limited basis and mainly as filler elements in the mesh

generation. Both shells accept the layered definition for the modelling of composite materials, and the output of stresses and strains at each layer of the laminate layup.

The other fundamental element is a hybrid beam with 2 nodes and 6 degrees of freedom per node. The term 'hybrid' stands for the different methods used to calculate the flexural and axial stiffness when the element is used to model frames, girders or beams that are attached to the plating. In this case, the flexural properties are calculated taking into account the contribution of the plating through an effective breadth that acts as a beam flange. The axial properties are instead calculated for the beam only, because the in-plane stiffness of the plating is accounted for by the plate element. The other common line element is the rod, a pin-jointed bar that carries axial forces and torsion only. Currently neither of these two line elements accepts the layered definition. The material properties of composite beams and rods should therefore be determined separately and input as homogeneous orthotropic properties.

Details of other elements such as springs and restraints, not used for this study, can be found in the MAESTRO user manual (2017).

4.2.2 Loading Definition

A structural analysis in MAESTRO requires the definition of a load case, which is the combination, or superposition, of all the loads that act on the structure at the same time. This implies that loads that do not act simultaneously should be part of separate load cases, unless their interaction is negligible.

Numerous loading patterns are used to generate the load case, including: masses; mass distributions; plate pressures; point forces and moments; longitudinal or transverse hull girder bending moment distributions; and additional accelerations. Since MAESTRO is essentially a static analysis tool (with modal analysis capabilities), none of these load patterns can be a function of time. This implies that if the load case has to include loads that are dynamic in nature, some approximate equivalent static load should be determined.

4.2.3 Restraints and Static Equilibrium Balance

Appropriate restraints should be applied to solve the global finite element equations. A MAESTRO model can be balanced through the application of rigid restraints that prevent nodal displacements and/or rotations. However, unrealistic deformations can occur when the structure is either excessively or poorly constrained. Fictitious stress concentrations in way of the restrained nodes are also to be expected. To avoid these issues, MAESTRO includes another restraint option based on calculating a static equilibrium balance.

Static equilibrium is reached by applying two types of balance (Ma *et al.* 2012, Zhao *et al.* 2013, MAESTRO Version 11.5.0 2017): hydrostatic and inertia relief. The first provides equilibrium in heave, pitch and roll by iteratively adjusting draught, trim and heel of the vessel. The latter adjusts additional accelerations to reach equilibrium in surge, sway and yaw. The inertia relief tool can be used as the restraint method for running any structural analysis. This feature has become common in many finite element software packages and supersedes the application of rigid restraints.

The static equilibrium balance is also used before running any hydrodynamic analysis. Equilibrium on the still waterline is sought to define the attitude of the vessel and the wetted elements to be used by the hydrodynamic solver. Static equilibrium balance can also be used to compute hydrostatic pressures that can form part of a load case. For this purpose, the vessel can be rebalanced on a sinusoidal wave rather than on the still waterline.

4.2.4 The Hydrodynamic Solver MAESTRO-Wave

The MAESTRO-Wave plugin integrated into the software suite is a computational tool to predict hydrodynamic rigid body motions and wave-induced loads for a vessel. Currently the tool is based on linear potential flow theory and features three different codes, which can be employed for both frequency and time-domain simulations:

- 2D (or 'classical') strip theory that ignores the forward speed term in the formulation of the free surface boundary condition. The velocity potential therefore satisfies a

'zero-speed free surface condition'. The assumption usually holds at low-to-moderate Froude numbers, typically Fn≤0.4.

- 2.5D (or 'high-speed') strip theory that considers the forward speed term in the formulation of the free surface boundary condition. The velocity potential therefore satisfies a 'forward-speed free surface condition'. This code is recommended when running cases at high Froude numbers, typically Fn>0.4.
- 3D panel method with different discretization options: one based on the structural elements, where a source strength is computed for each finite element; others based on groups of elements, where the same source strength is assigned to all the elements of the group.

All the aforementioned codes were used in this study, with simulations run in the frequency domain. The simulation output consists of ship motions and wave-induced loads. The first are produced in terms of displacements, velocities and accelerations; the second in terms of sectional hull girder loads and hydrodynamic panel pressures. Since the equations of motion are formulated using the structural mesh, panel pressures are mapped directly onto the structural model. The codes implemented into MAESTRO-Wave are described in detail by Salvesen *et al.*(1970), Ma *et al.* (2012, 2014), Zhao *et al.* (2013) and Zhao and Ma (2016).

4.2.5 Extreme Load Analysis

The output from MAESTRO-Wave feeds into an extreme load analysis module, which provides the statistical tools to predict the maximum wave loads experienced over a given period. Both sort-term and long-term statistics can be employed. The first requires the input of a sea spectrum, the second requires also a wave scatter diagram and an operational profile.

4.2.6 Structural Response Analysis

The structural response is computed through a static linear finite element analysis. The output consists of stresses, strains and displacements. For composite shell elements, stresses and strains can be recovered for each layer of the laminate. In addition, post-processing tools are available to investigate possible failure modes of the structure. Since

these are only implemented for steel and aluminium structures but not for composites, a review of these failure mode evaluation methods is not given.

The mesh of any portion of the global model can be refined maintaining the material properties and the applied loads. The fine mesh analysis can be run in two ways: as part of the global finite element analysis, by replacing the coarse mesh portion of the model with the fine mesh, or after the global analysis, by applying the computed displacements as boundary conditions to the fine mesh model (for completeness, it is acknowledged that MAESTRO can also perform natural frequency analyses and progressive collapse analyses with a simplified nonlinear finite element method).

4.3 The MAESTRO Model of the Severn Class

4.3.1 Finite Element Modelling

MAESTRO was used to construct the global finite element model of the Severn Class (Figure 4.1 & Table 4.1). Geometry and structural layout were determined from technical construction drawings supplied by the RNLI. The model is inclusive of those structural elements that are expected to contribute to the global strength: hull plating, deck, superstructure, internal subdivisions, primary and secondary reinforcements, central skeg, and bilge keels.

A combination of shell, beam and bar elements was used for modelling the Severn. The laminates' mechanical properties were embedded as layered orthotropic for shells, uniform orthotropic for beams, and isotropic for rods. The mechanical properties of the plies within each laminate were recovered from data supplied by the material manufacturer and the RNLI. Sample material properties and laminate layups are reported in Section 3.2.

The types of finite elements and the geometry construction tools available in the program are well suited for conventional steel and aluminium ship structures. For a composite structure, the modelling paradigm of MAESTRO required some adaptation:

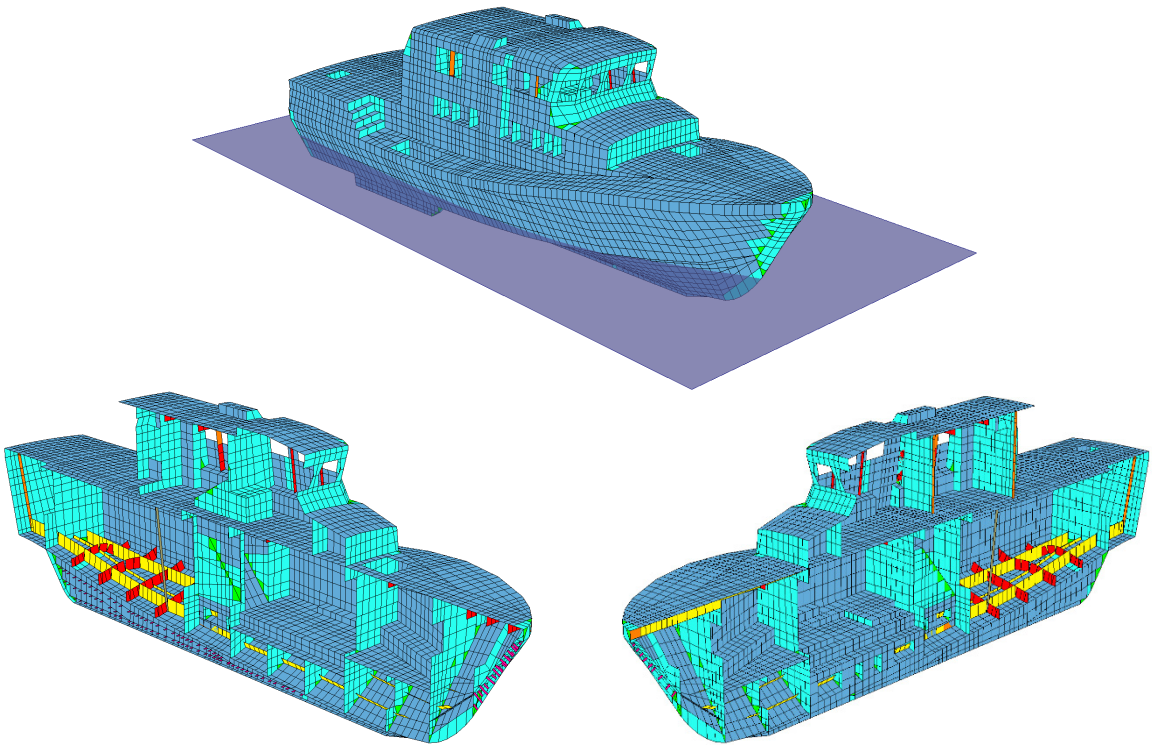

Figure 4.1. MAESTRO model of the Severn class.

MAESTRO MODEL MAIN PARTICULARS	
Number of nodes	12458
Number of elements	15489
Total length	17.00 m
Total Width	5.62 m
Total Height	5.93 m

Table 4.1. MAESTRO model main particulars.

- The mesh was finer than what would be required to assess hull girder stresses in a global strength analysis. A fine mesh was needed to model the variations in shape and laminate layup associated with the use of fibre-reinforced composites and to locate areas of high stress due to local pressure loads. The minimum element size was determined by the thickness of the sandwich laminates, modelled with shell elements. Shells, suitable for analysing thin to moderately-thick structures, need planar dimensions much larger than the through-thickness dimension, which imposes a limit to the minimum element size. The representative size of quadrilateral elements was 0.15-0.25m.

- All the structural reinforcements were modelled as actual finite elements. The philosophy whereby stiffeners can be accounted for through an increased flexural stiffness of the attached plating was not adopted.
- Composite beams of 'top-hat' cross-section were modelled with an equivalent 'T' cross-section, which consists of a T-section with a web thickness that is the sum of the thicknesses of the top-hat webs. The approximation, necessary due to software limitations, is substantial but conservative. The T-section can be deemed to have equivalent flexural stiffness on the vertical plane, but is likely to possess lower torsional stiffness, and it also fictitiously increases the unsupported width of the attached plate, as shown in Figure 4.2.

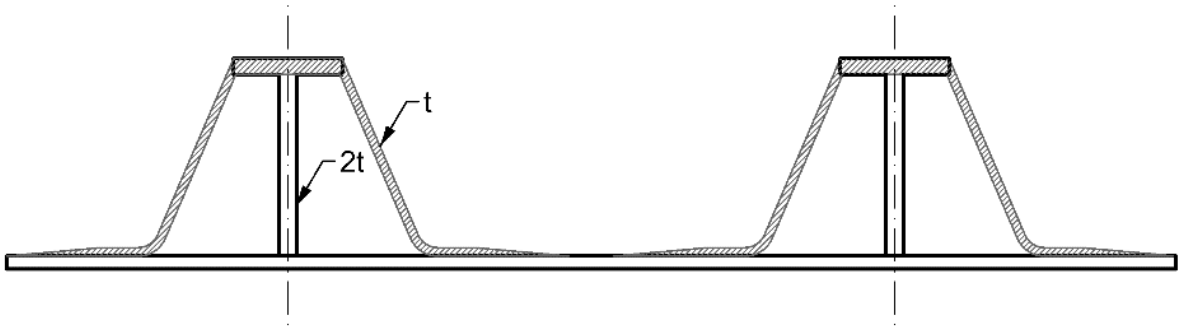

Figure 4.2. 'Top-hat' cross-section and equivalent 'T' cross-section of composite beams.

4.3.2 Loading Condition and Hydrostatic Balance

The structural mass was automatically computed based on the finite elements and their associated material properties. Other weights were represented, according to their nature, as: volumes; plate and nodal masses; scaled-up structural mass; large solid masses whose centre of gravity lies at a distance from the supporting nodes (e.g. engines and gearboxes); and longitudinally distributed mass.

For the seakeeping simulations presented in this chapter, load displacement and CG position were determined through a statistical analysis of the inclining test data of the Severn fleet. The target and achieved values are reported in Table 4.2. Static equilibrium was reached from the balance of weight and buoyancy forces (Section 4.2.3). The resulting weight and buoyancy distributions are shown in Figures 4.3 & 4.4.

For the small-scale experiments, the same loading condition was taken as target for the setup and ballasting of the hull models. Simulation results produced with this loading condition are therefore re-presented in Chapter 5, together with small-scale test data. Differently, comparison of the simulations with full-scale experiments required tuning of the MAESTRO model's loading condition according to the loading condition of the lifeboat used for the sea trials. Details of this second loading condition are presented in Chapter 6, where simulation results are plotted together with full-scale data.

SEVERN CLASS LIFEBOAT			TARGET	ACHIEVED
Loading condition			Full load	Full load
Displacement	Δ	[kg]	43170	43164
Centre of gravity (x)	LCG	[m]	6.45	6.44
Centre of gravity (z)	TCG	[m]	0.00	0.00
Centre of gravity (y)	VCG	[m]	2.32	2.20
Roll radius of gyration	k_4	[m]	N.A.	1.89
Pitch radius of gyration	k_5	[m]	N.A.	3.97
Yaw radius of gyration	k_6	[m]	N.A.	3.99

Table 4.2. MAESTRO model loading condition.

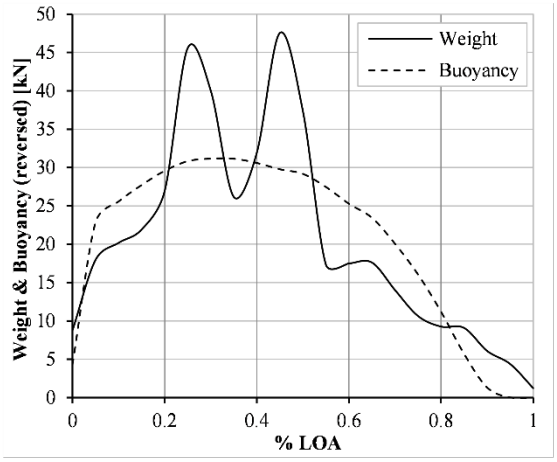

Figure 4.3. Longitudinal weight and buoyancy distribution. Full load condition.

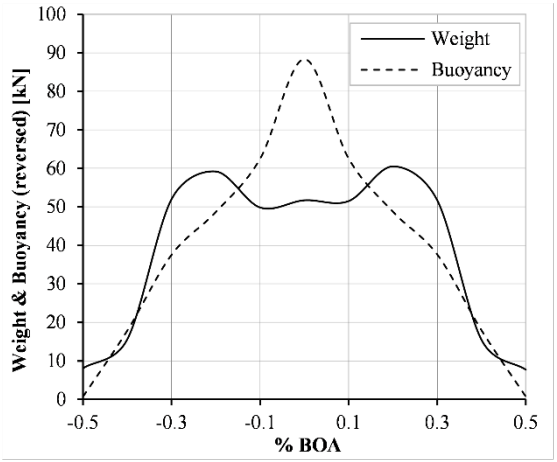

Figure 4.4. Transverse weight and buoyancy distribution. Full load condition.

4.4 Hydrodynamic Analysis

MAESTRO-Wave was used to predict the wave loads of the vessel. To assess the differences between the three codes implemented into the software, initial simulations

were compared against small-scale test data from Chapter 5. An example is given in Figures 4.5-4.8, which show heave and vertical bending moment at amidships for two speeds: 10 and 20kts (Fn=0.4 and 0.8). There is a transition zone at Fn≈0.4 where the 2D strip theory progressively loses accuracy in favour of the 2.5D strip theory, as it would be expected from their supposed range of applicability. The 3D panel method predicts well the position of the RAO peaks along the wavelength axis. However, in spite of the more realistic representation of the geometry in the three dimensions, motion and load magnitudes are unrealistically over-predicted, or at least heavily undamped. Whilst some error would be expected at higher speeds because of the linear theory and potential flow assumptions, the error at lower speeds was unexplainable. The panel method was therefore disregarded for subsequent simulations.

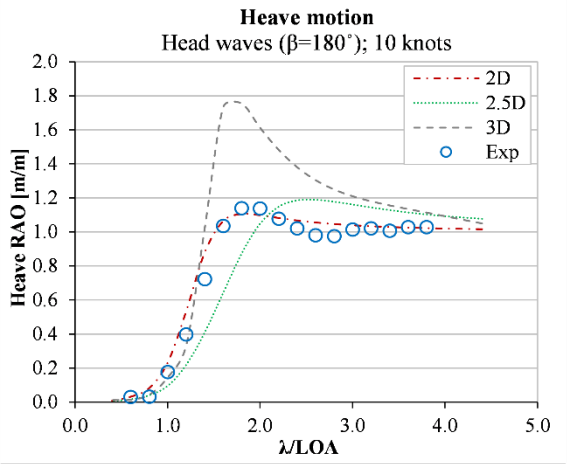

Figure 4.5. Heave in head waves at 10kts.

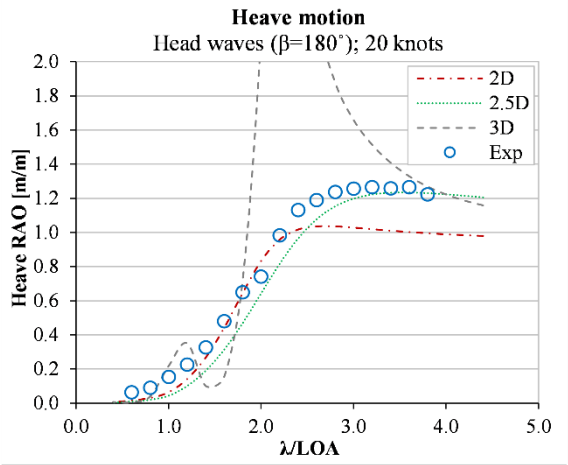

Figure 4.6. Heave in head waves at 20kts.

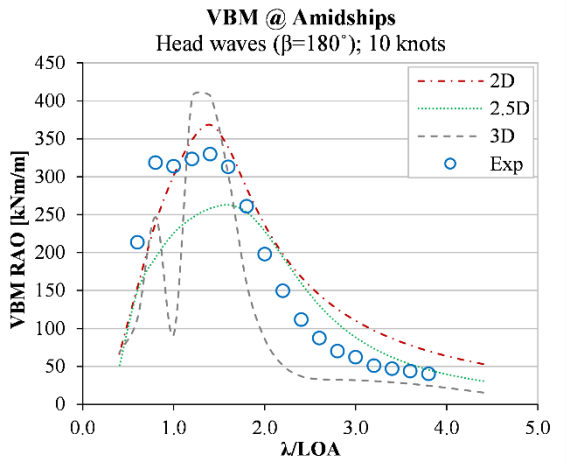

Figure 4.7. VBM at 0.50LWL in head waves at 10kts.

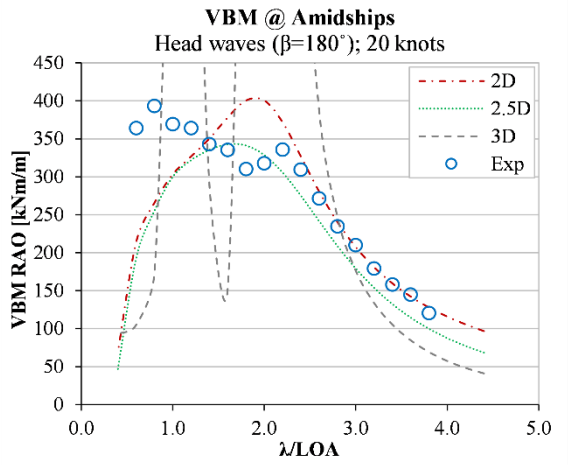

Figure 4.8. VBM at 0.50LWL in head waves at 20kts.

From this point forward numerical data will be presented for the two strip theory codes, used as follows:

- 2D strip theory at Froude numbers Fn≤0.4
- 2.5D strip theory at Froude numbers Fn>0.4

All the simulations were run in the frequency domain at wavelength-to-hull length ratios λ/LOA=0.4, 0.6,..., 4.4. The hull was divided into 24 strips between the transom and the fore perpendicular. A correction factor was applied to the roll damping coefficient to include the viscous damping effects not accounted for by the potential flow theory. The correction was applied by estimating a value for the critical damping ratio, defined as:

$$k = \frac{B_{44,\Phi} + B_{44,v}}{B_{44,crit}} \tag{4.1}$$

where $B_{44,\Phi}$ is the potential flow roll damping; $B_{44,v}$ is the viscous roll damping; $B_{44,crit}$ is the critical roll damping, that is the damping for which the system returns to equilibrium without oscillating and in the shortest possible time; and k is the critical damping ratio, expected to take values up to 0.2 for conventional vessels. For the Severn it was taken k=0.1, which was the value found by tuning the roll RAOs in beam waves at zero speed according to those determined from small-scale tests. Assuming that $B_{44,\Phi}$ is small compared to $B_{44,v}$, the total damping coefficient was computed as:

$$B_{44} = B_{44,\Phi} + kB_{44,crit} \tag{4.2}$$

where B_{44} is the total damping; and $kB_{44,crit}$ is the correction introduced to account for the viscous roll damping (MAESTRO Version 11.5.0 2017).

Simulation results consist of rigid body motions (displacement, velocities and accelerations) and wave-induced loads (sectional hull girder loads and panel pressures). Since the analyses were run in the frequency domain, all the results produced are for waves of unit amplitude. Examples of simulation outputs are shown in Figures 4.9-4.10.

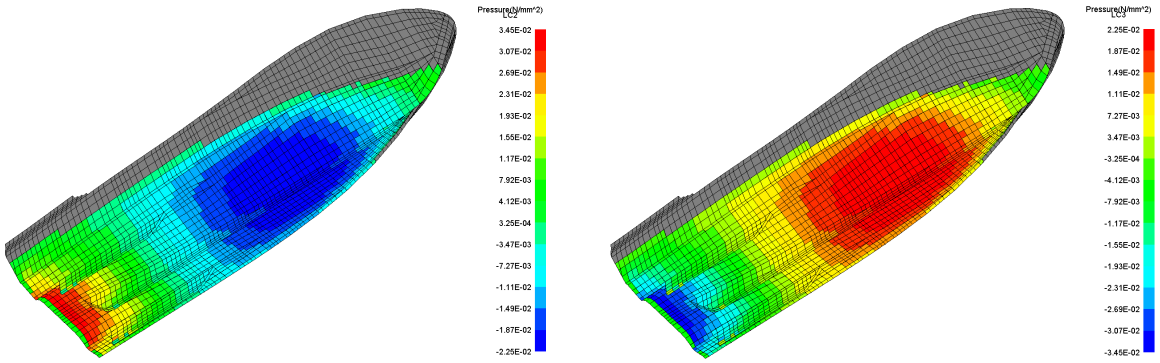

Figure 4.9. Panel pressure output from MAESTRO-Wave. Sagging (left) and hogging (right).

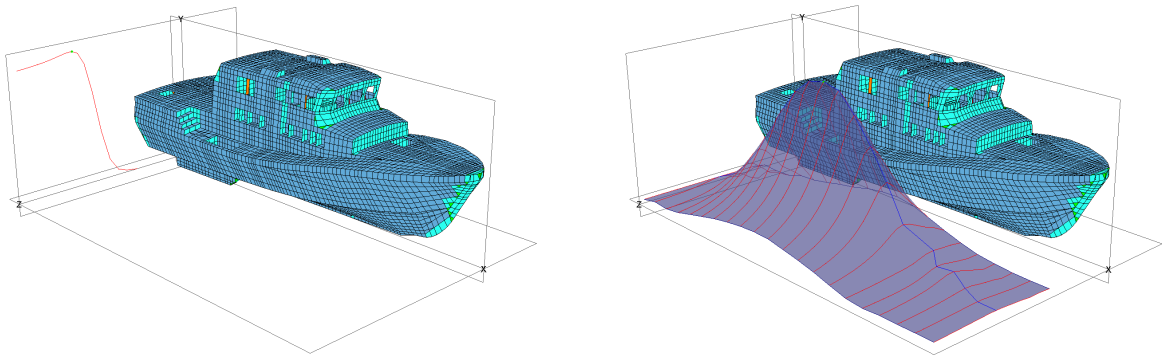

Figure 4.10. Motion and load output from MAESTRO-Wave. Heave RAOs (left) and VBM RAOs (right).

4.5 Seakeeping Results

Only a subset of the seakeeping data produced is presented here. The subset gives an overview of the motions and loads assessed, most of which will be re-presented in the next chapters and compared against experimental data from small and full scale tests.

Figures 4.11-4.40 show Response Amplitude Operators (RAOs), calculated as the ratio of the amplitude of the response and the exciting wave amplitude:

$$Heave\ RAO = \frac{\eta_{30}}{\zeta_0} \tag{4.3}$$

$$Roll\ RAO = \frac{\eta_{40}}{\zeta_0} \tag{4.4}$$

$$Pitch\ RAO = \frac{\eta_{50}}{\zeta_0} \tag{4.5}$$

$$VBM\ RAO = \frac{VBM_0}{\zeta_0} \tag{4.6}$$

$$HBM\ RAO = \frac{HBM_0}{\zeta_0} \tag{4.7}$$

$$VSF\ RAO = \frac{VSF_0}{\zeta_0} \tag{4.8}$$

Where: η_{30}, η_{40}, η_{50} are the amplitudes of heave, roll and pitch motion respectively; VBM_0, HBM_0, VSF_0 are the amplitudes of vertical bending moment, horizontal bending moment and vertical shear force respectively; and ζ_0 is the wave amplitude.

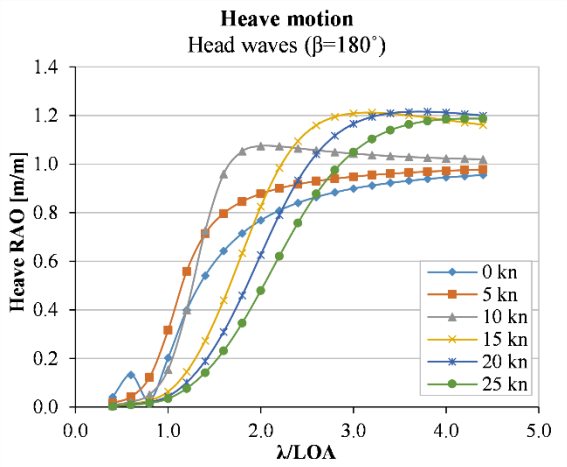

Figure 4.11. Heave in head waves. Varying speed.

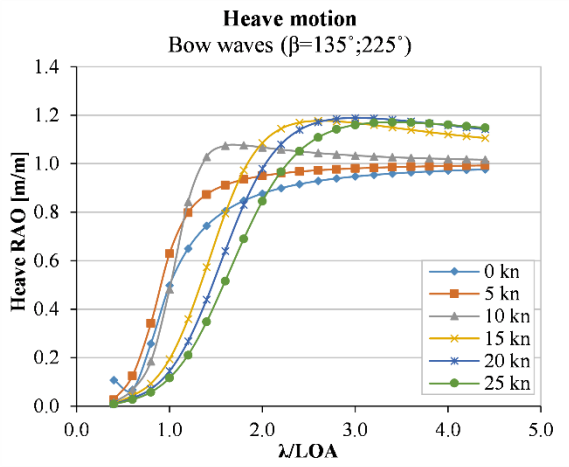

Figure 4.14. Heave in bow quartering waves. Varying speed.

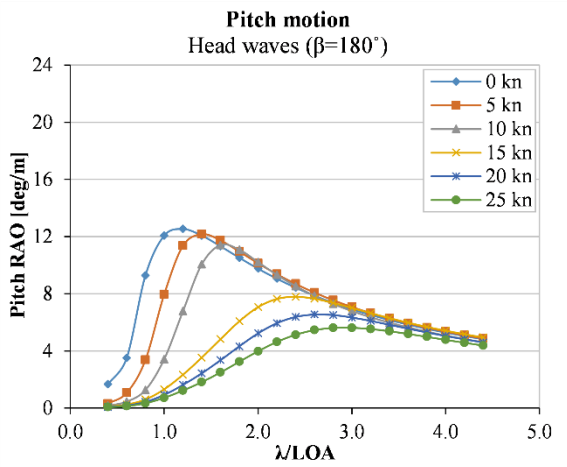

Figure 4.12. Pitch in head waves. Varying speed.

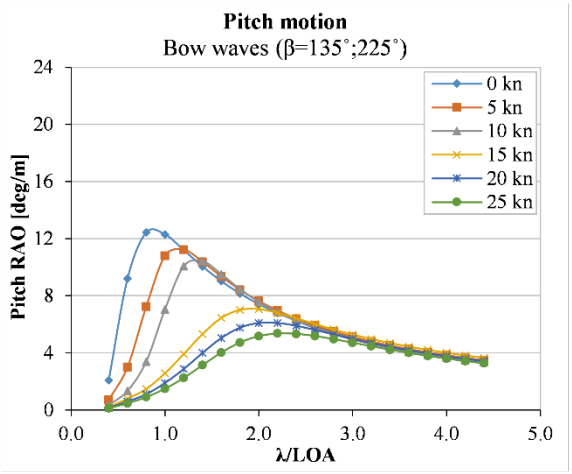

Figure 4.15. Pitch in bow quartering waves. Varying speed.

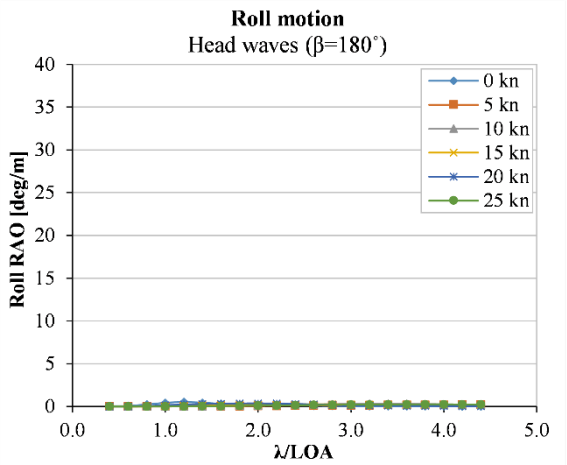

Figure 4.13. Roll in head waves. Varying speed.

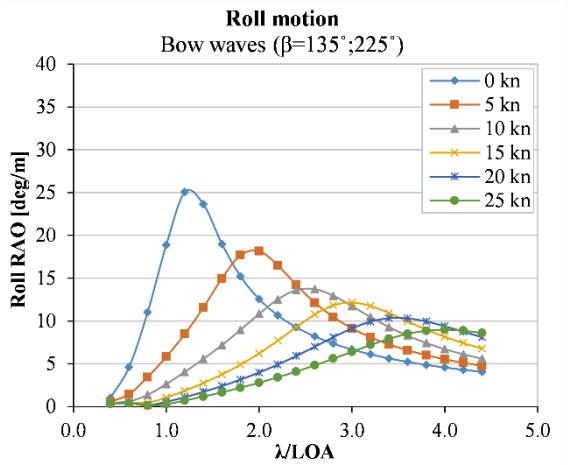

Figure 4.16. Roll in bow quartering waves. Varying speed.

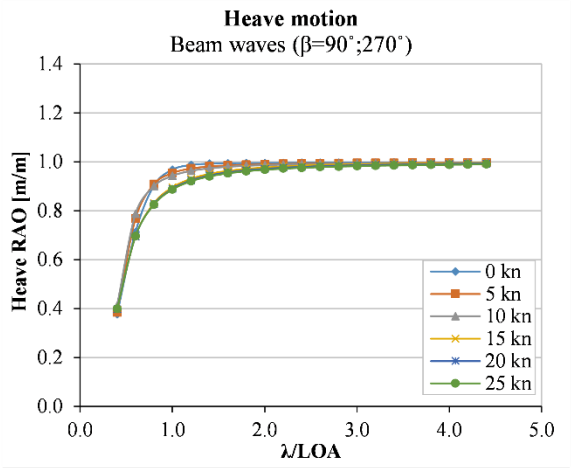

Figure 4.17. Heave in beam waves. Varying speed.

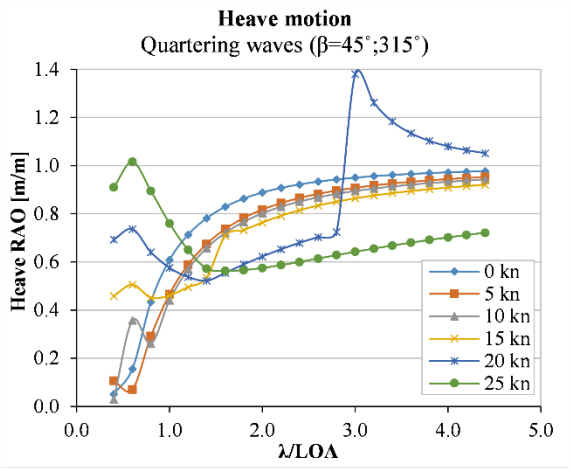

Figure 4.20. Heave in stern quartering waves. Varying speed.

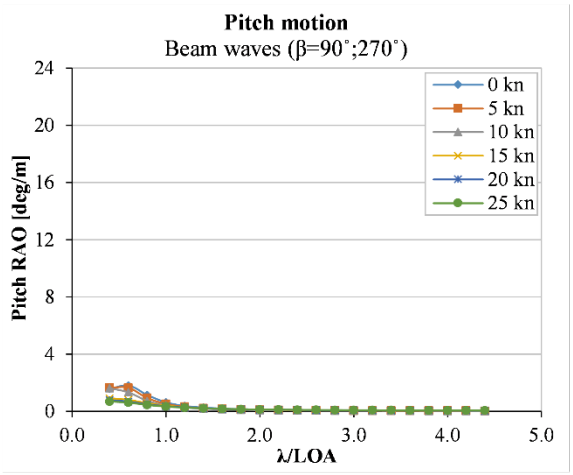

Figure 4.18. Pitch in beam waves. Varying speed.

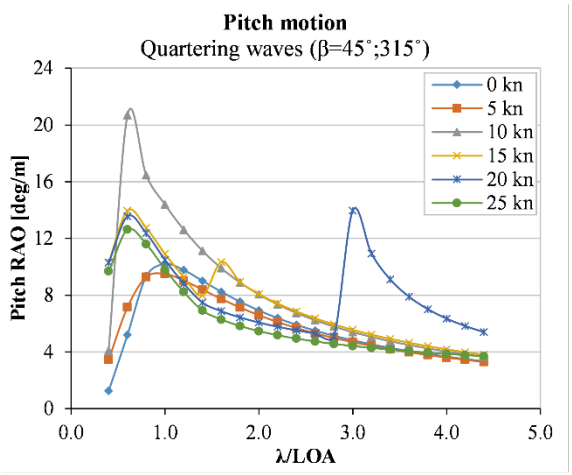

Figure 4.21. Pitch in stern quartering waves. Varying speed.

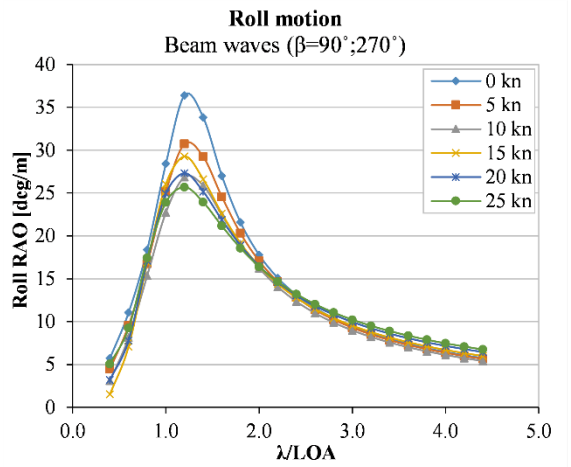

Figure 4.19. Roll in beam waves. Varying speed.

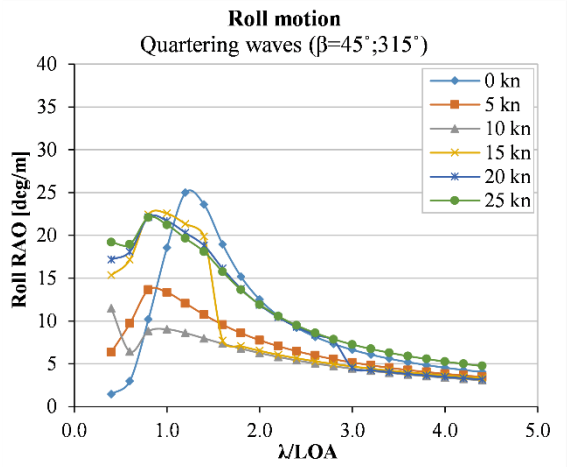

Figure 4.22. Roll in stern quartering waves. Varying speed.

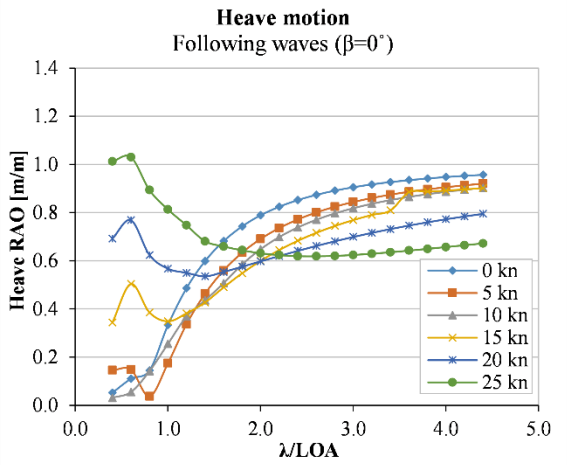

Figure 4.23. Heave in following waves. Varying speed.

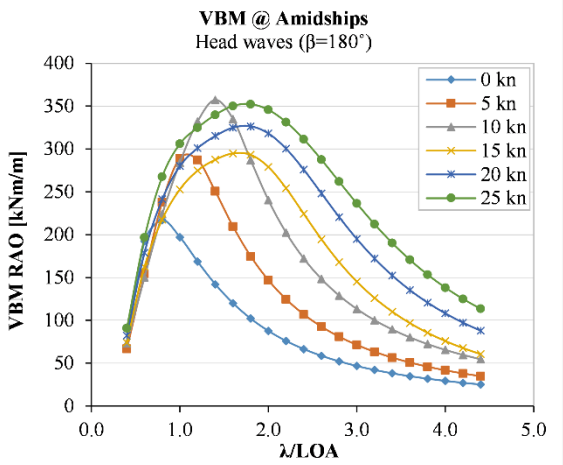

Figure 4.26. VBM at 0.50LOA in head waves. Varying speed.

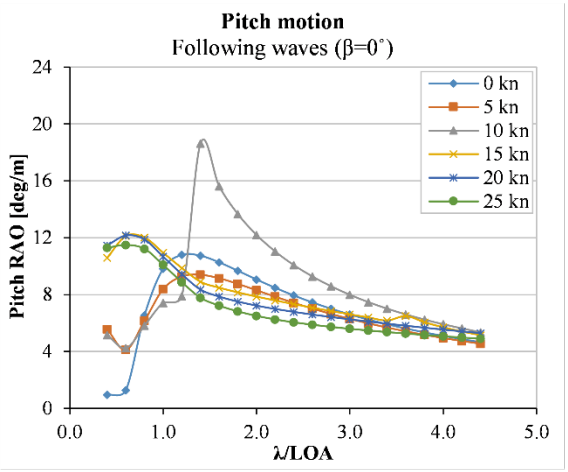

Figure 4.24. Pitch in following waves. Varying speed.

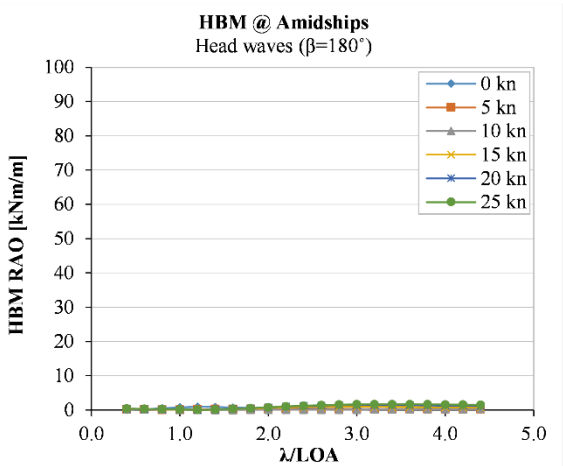

Figure 4.27. HBM at 0.50LOA in head waves. Varying speed.

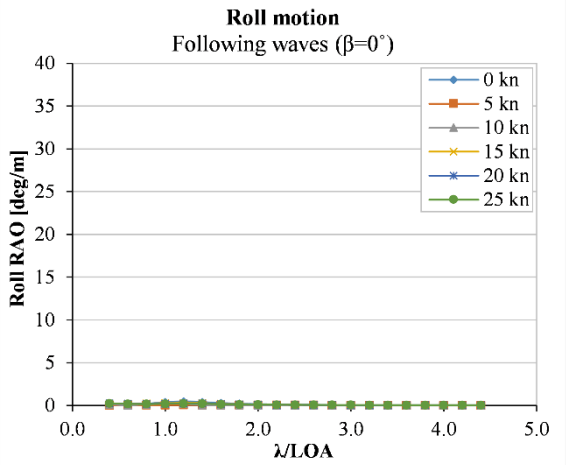

Figure 4.25. Roll in following waves. Varying speed.

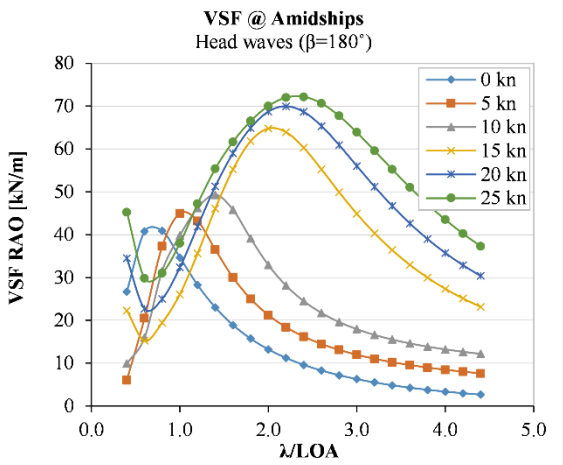

Figure 4.28. VSF at 0.50LOA in head waves. Varying speed.

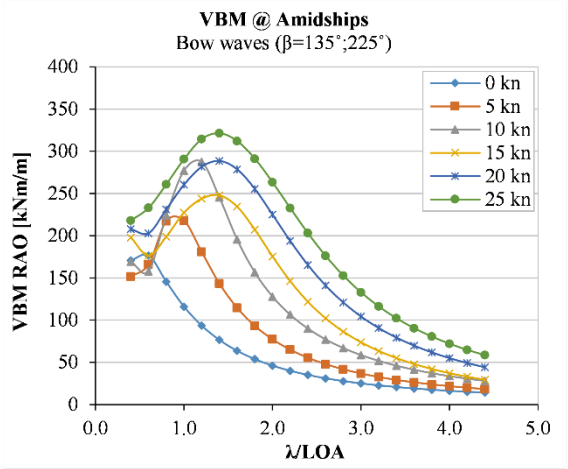

Figure 4.29. VBM at 0.50LOA in bow quartering waves. Varying speed.

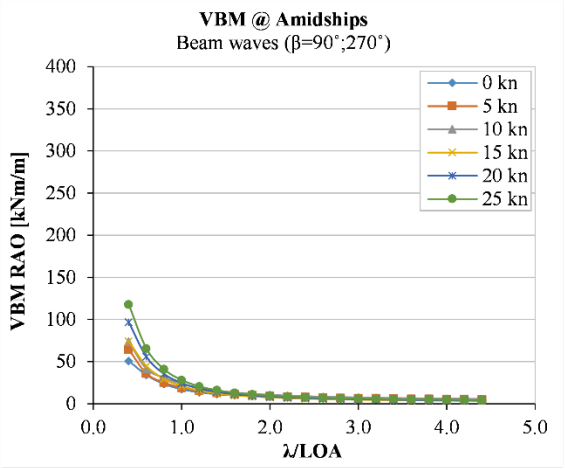

Figure 4.32. VBM at 0.50LOA in beam waves. Varying speed.

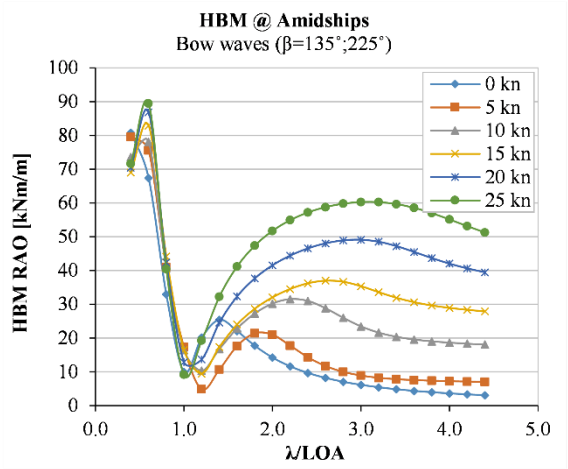

Figure 4.30. HBM at 0.50LOA in bow quartering waves. Varying speed.

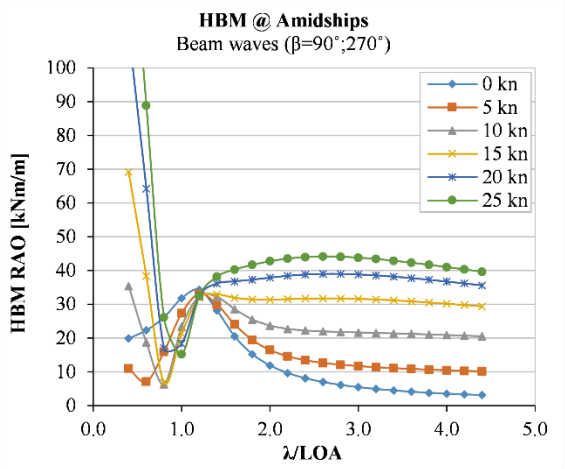

Figure 4.33. HBM at 0.50LOA in beam waves. Varying speed.

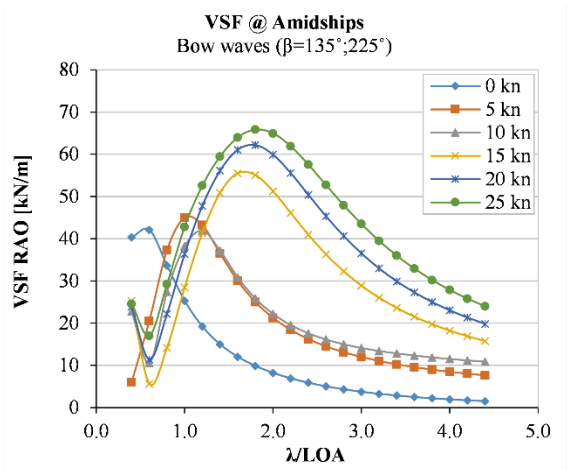

Figure 4.31. VSF at 0.50LOA in bow quartering waves. Varying speed.

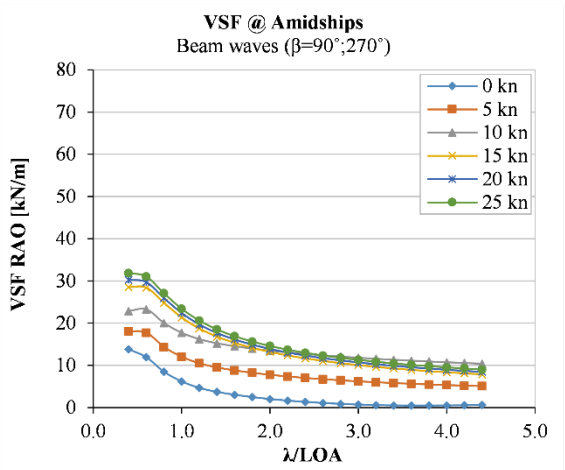

Figure 4.34. VSF at 0.50LOA in beam waves. Varying speed.

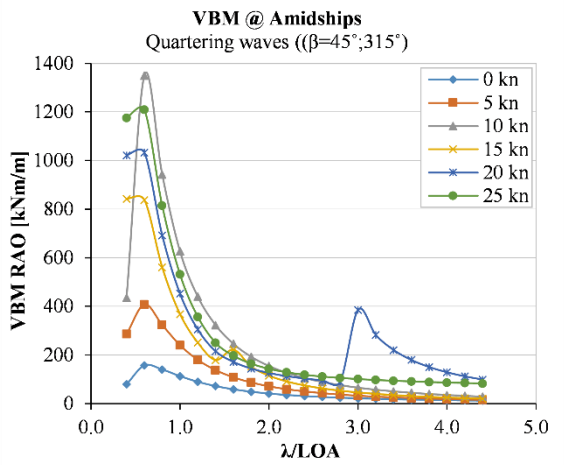

Figure 4.35. VBM at 0.50LOA in stern quartering waves. Varying speed.

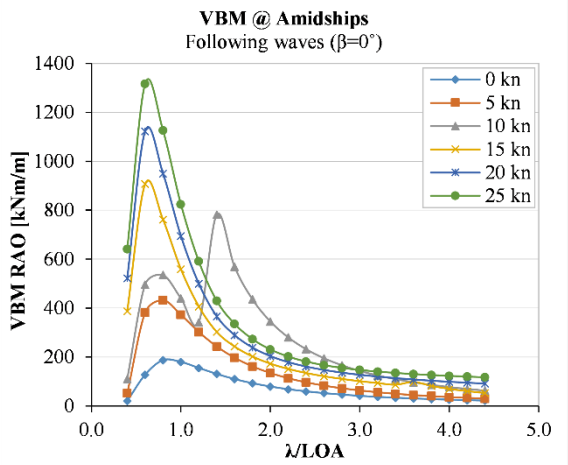

Figure 4.38. VBM at 0.50LOA in following waves. Varying speed.

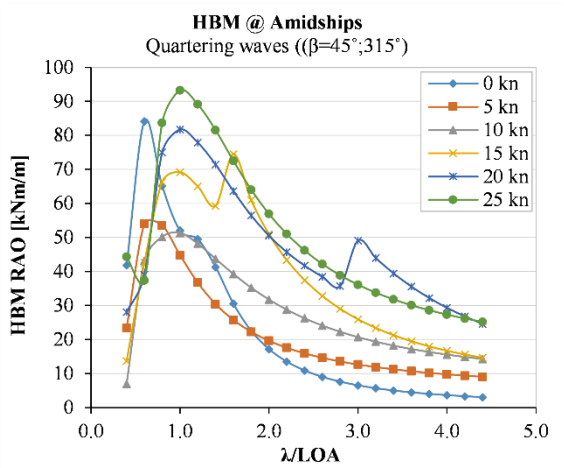

Figure 4.36. HBM at 0.50LOA in stern quartering waves. Varying speed.

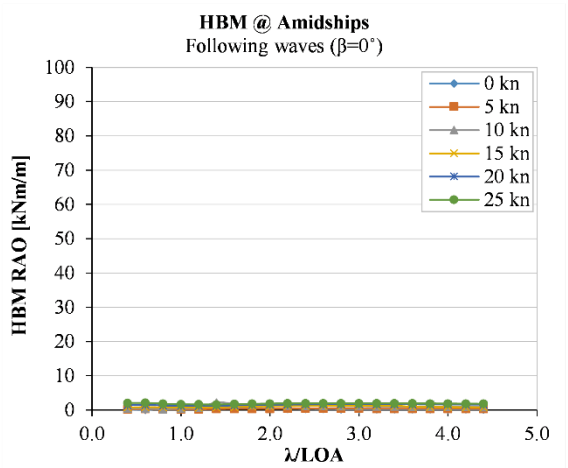

Figure 4.39. HBM at 0.50LOA in following waves. Varying speed.

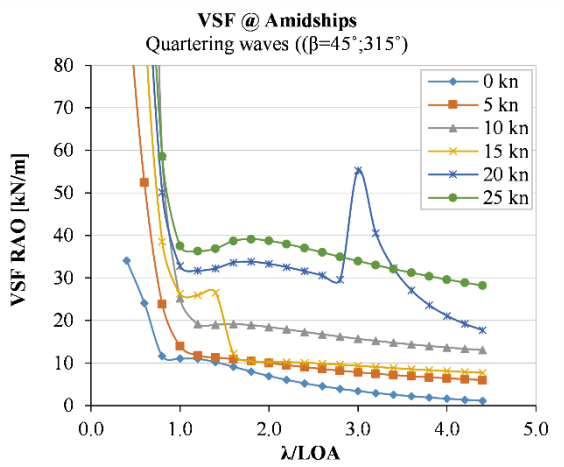

Figure 4.37. VSF at 0.50LOA in stern quartering waves. Varying speed.

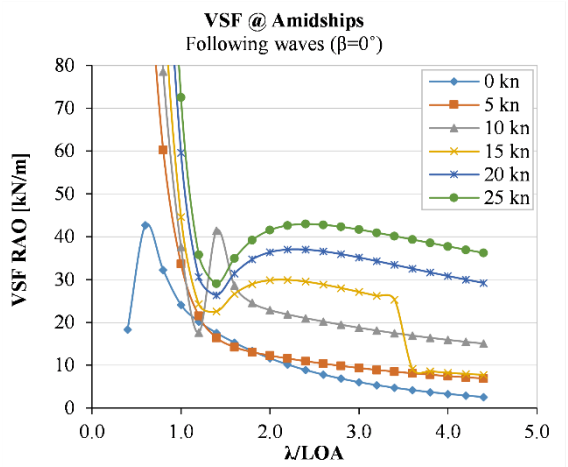

Figure 4.40. VSF at 0.50LOA in following waves. Varying speed.

4.6 Discussion

The accuracy of the simulations is assessed, at this stage, only qualitatively. A detailed discussion is presented in the next chapters, where the simulation results are directly compared against experimental data.

Strip theory introduces several simplifications to solve the ship-wave interaction problem (Chapter 2), with the following main consequences for the simulations:

- The assumption of wall sidedness implies that the same values of vertical bending moment and vertical shear force are predicted for bending in both sagging and hogging.
- The assumption of zero fluid viscosity implies that motion damping can only be attributed to wave radiation, which is generally adequate for most motions with the exception of roll. A correction factor was therefore applied to account for the viscous damping in the prediction of roll motions.
- The assumption of a two-dimensional flow within each hull strip implies that the flow velocity in the longitudinal direction should be negligible, which becomes a limitation at low frequencies of encounter.

Following from the high frequency assumption of strip theory methods, the simulations seem more valid in head and bow quartering waves than in following and stern quartering waves, where the encounter frequency reduces significantly as the vessel speed increases. In stern quartering waves, discontinuities in the motion and load RAO plots appear at 20kts for $\lambda/LOA \approx 3$ as well as at 15kts for $\lambda/LOA \approx 1.6$ (Figures 4.20-4.22 & 4.35-4.37). In following waves, similar discontinuities appear at 10kts for $\lambda/LOA \approx 1.4$ and at 15kts for $\lambda/LOA \approx 3.6$ (Figures 4.23, 4.24, 4.38 & 4.40). Moreover, in both stern quartering and following waves, the maximum RAO values of vertical bending moment and vertical shear force appear unrealistic. On headings abaft the beam, the simulation results are therefore questionable, at least for speeds above 5kts.

4.7 Summary

The work described in this chapter is summarised in Figure 4.41. A structural model of the Severn Class lifeboat was developed with the software MAESTRO. The seakeeping solver MAESTRO-Wave was used to determine: hydrostatic pressures through a hydrostatic balance calculation; and wave-induced pressures through seakeeping simulations based on two linear strip theory methods. The seakeeping simulations output motions, global sectional loads and associated panel pressures. The first two terms, presented in terms of RAOs, will be validated against experimental results in the next chapters.

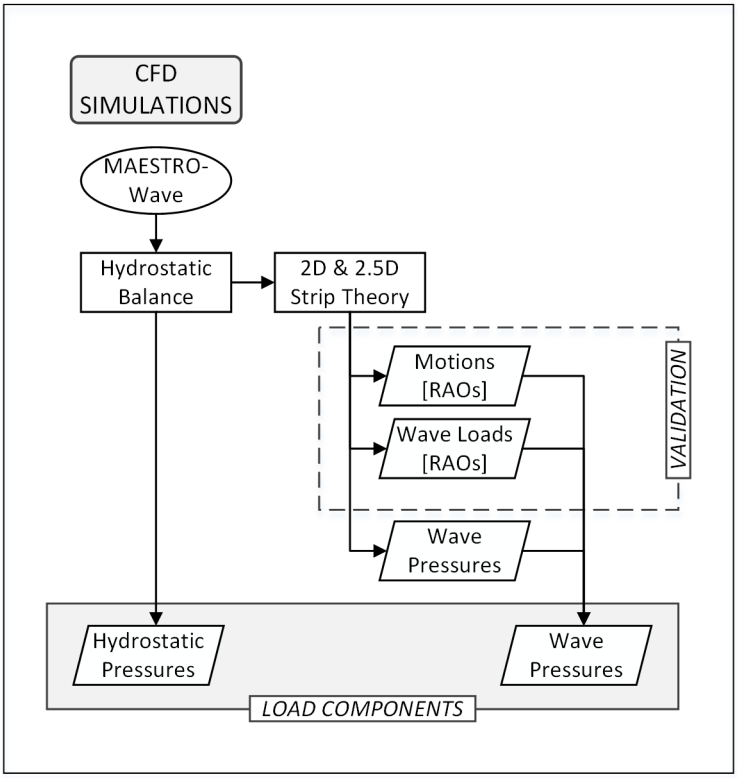

Figure 4.41. Direct calculation approach – CFD simulations.

Chapter 5

Small-Scale Tests

5.1 Framework

Tests at scale, in towing tanks and wave basins, have been carried out extensively by numerous researchers and can rely on extensive guidelines for their execution, which make them an effective solution for design and for validating numerical calculations. For tests in waves, the measurement of seakeeping motions, amongst other quantities, is conventional. With a focus on the structure of the vessel, towing tank tests become more valuable if seakeeping loads can also be measured directly.

Hydrostatic and hydrodynamic hull pressures can only be determined, experimentally, through pressure measurements. The use of pressure sensors was not considered practical (Section 2.2.6): a pressure field would still need to be constructed from discrete measurement points; pressure sensors suffer several drawbacks, including temperature shocks and sensitivity to change of medium; and extrapolation of the pressure data to full scale is likely to be affected by scaling effects. The realisation of a hydro-structural model, which would enable direct measurements of the structural behaviour, was also considered impractical because of the impossibility to achieve both the structural and

the hydrodynamic similarity at scale. Since the external pressures on the hull have an effect on the structure at a global level, seakeeping loads were measured with a segmented model. The loads measured were sectional global loads.

Following the load breakdown from Chapter 2, global effects occur as a result of hydrostatic, wave and slamming loads. The measurement of the hull girder response to hydrostatic pressures is not straightforward for merely practical reasons. A segmented model typically makes use of sensors that need to be zeroed at some set condition. If this condition cannot be the hull at rest in still water, which represents the measurement condition, some other reference state has to be found. Since hydrostatic loads are easily predicted numerically and represent a relatively small load component, they were not measured experimentally. The whipping response of the hull girder can be measured, at scale, with an elastic segmented model. Although achievable, this involves scaling the stiffness of the hull girder so that the rigidity of the scaled model represents that of the prototype, which introduces further complexities in the hull model design. Whipping of the hull girder was therefore not measured with the small-scale tests, which were limited to the measurement of rigid body motions and wave-induced sectional global loads, the latter assuming a rigid hull.

Without leading to the determination of any of the load components that make up the input for the structural response analysis, the value of the small-scale tests resides in the direct validation of the numerical model. The seakeeping experiments were conducted in regular waves, which simplifies the data analysis and the computation of the RAOs of the vessel responses. These can be directly compared with the results of the ship motion analysis (Chapter 4).

5.2 The Small-Scale Tests of the Severn Class

Two scaled models of the Severn Class were designed and built for seakeeping tests: a solid model and a rigid segmented model (Figure 5.1). The first was a conventional hull for measuring rigid body motions at scale. The second, geometrically similar to the first, was made of four hull segments, held together by an internal structure fitted with

sensors. The segmented model enabled measurement of global wave loads at the interface between the hull segments.

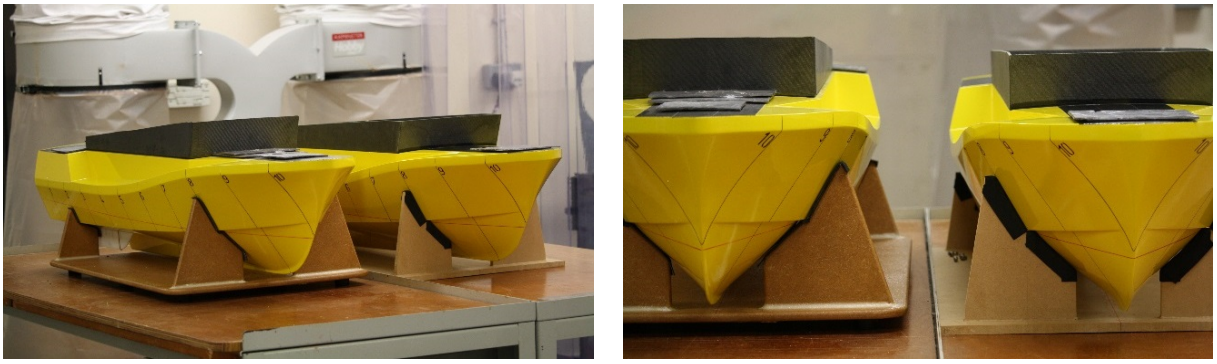

Figure 5.1. Severn class scaled hull models (these models may be viewed at Newcastle University (see Appendix 1)).

The segmented model was built as a solid hull and preliminary tests were carried out to ensure that both models had the same baseline seakeeping characteristics prior to one being segmented. The same tests were carried out, after the segmentation, measuring global wave loads. The consequences of an increased hull surface roughness and of a hull girder stiffness provided by an independent structure rather than the hull itself, were evaluated by comparing the two sets of tests. The effect of the hull discontinuity on the seakeeping of the vessel was thus evaluated.

The scope of the task was limited to the following conditions:

- Forward speed by towing (not self-propelled model)
- One displacement condition
- Hull in the naked condition with centreline skeg and bilge keels (no trim tabs, rudders, shafts, A-brackets, propellers and bow thruster openings)
- Seakeeping evaluated using classical deep-water formulae, hence assuming that the water is deep compared to the wave length.

5.3 Description of the Tests

5.3.1 The Facility

The tests were performed at Newcastle University's towing tank, with main particulars listed in Table 5.1. The tank is a conventional long narrow basin with a monorail along its length and a towing carriage powered by a winch. Waves are generated by a wave

maker at one end of the tank and absorbed by a beach at the opposite end. A series of wave probes located along the tank measure the water surface elevation.

TOWING TANK SPECIFICATIONS	
Length	37 m
Width	3.7 m
Maximum Water Depth	1.25 m
Maximum Carriage Speed	3.5 m/s
WAVEMAKER CAPABILITIES	
Wave Period	0.5-2.0 s
Wave Height (period dependent)	0.02-0.12 m

Table 5.1. Towing tank main particulars.

5.3.2 Scaling and Construction

The Severn Class hull models were realised from the hull lines provided by the RNLI at a scale 1:13.5. The model size was identified, based on the scope of the experiments and on the size of the facility, to ensure that the tests were going to be conducted clear from tank wall interference, blockage and shallow water effects. This is shown in Appendix 2, which reports the specifications for the design and construction of the models. Table 5.2 reports the main particulars of the Severn at both real and model scale.

High structural stiffness was required by the segmented model to transfer the seakeeping loads from the hull segments to the connecting structure without losses due to local deformations. Light weight was also required to leave room for ballast and achieve the target inertial properties. The models were therefore built with advanced fibre-reinforced composites.

The same moulds were used for both models to ensure high geometrical similarity. The moulds consisted of two female parts, one for the hull shell and one for the deck, both CNC-machined out of high-density foam blocks. The models were manufactured in carbon fibre, epoxy resin and foam core, with vacuum bag moulding technique. Hull shell and deck were made of a sandwich laminate, occasionally tapered to monolithic as per standard practice. The central skeg was hand-laminated separately and attached to

the hull at a later stage. The bilge keels were 3D-printed in plastic and bolted onto the hull shell. The models were also fitted with a spray deflector to avoid water entering.

The internal structural layout differed between the solid and the segmented model, since the latter had to accommodate additional structural members to hold the hull segments together (Figures 5.2-5.3). The solid model's hull shell was stiffened by three bulkheads at 25, 50 and 75% LWL. The segmented model had, at the same locations, three sets of bulkheads. Each set comprised two ring frames, spaced by 3mm, which stiffened each of the segments and served as guides for cutting of the hull shell. Moreover, an intercostal top hat stiffener and a channel beam of monolithic construction ran along the model length at the centreline. A series of floors, strengthened the top-hat stiffener, ensuring that the loads carried by the segments were transferred entirely to the connecting structure. The channel beam accommodated a 'strength bar' rigidly held by clamping plates, which allow removal or replacement of the bar (Figure 5.4). Details of the strength bar and its instrumentation are given in following sections.

SEVERN CLASS PARTICULAR			REAL SCALE	MODEL SCALE
Scale Factor			1	13.50
Length Overall	LOA	[m]	17.00	1.259
Length Waterline	LWL	[m]	15.57	1.153
Beam Overall	BOA	[m]	5.62	0.416
Beam Waterline	BWL	[m]	5.00	0.370
Draught (at amidships)	T	[m]	1.46	0.108
LCG (aft of amidships)	LCG	[m]	1.30	0.096
LCG (from transom)	LCG	[m]	6.45	0.478
Displacement	Δ	[kg]	43170	17.12
Speed max	V	[kts]	25	6.80
Speed max	V	[m/s]	12.86	3.50
Wet Surface Area	WSA	[m^2]	94.73	0.520

Table 5.2. Severn Class main particulars at real and model scale.

Figure 5.2. Internal structure of the solid model.

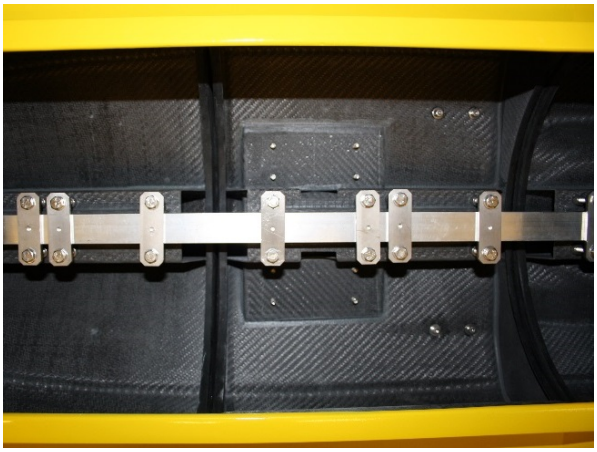

Figure 5.3. Internal structure of the segmented model.

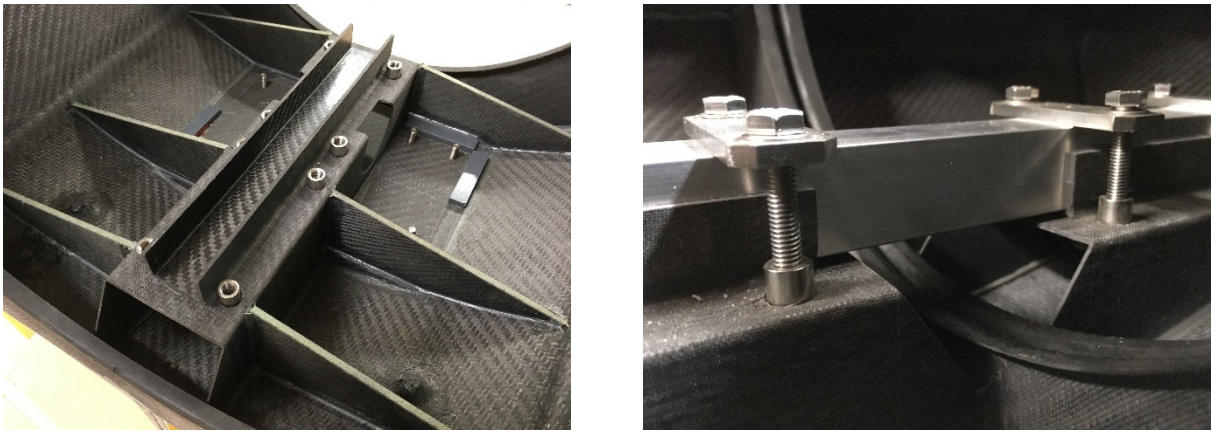

Figure 5.4. Structural details of the segmented model. Top hat stiffener and channel beam of one segment (left). Strength bar connecting two adjacent segments (right).

5.3.3 Towing Point

The towing arrangement had the following requirements: to tow both models at the same point; to accommodate for the high pitch angles experienced during tests in waves; and to minimise the artificial trim moments introduced by the towing force. The last requirement is generally fulfilled by towing at the centre of gravity or at the intersection between the propeller shaft line and the vertical passing through the CG. However, the internal structure of the segmented model required the development of a bespoke solution. A towing rig (Figure 5.5) was manufactured to connect the dynamometer to the hull shell. The rig consisted of a truss and two feet with bearings on either side of the centreline. The model pitching point, hence the point of application of the towing force, was thus at the intersection of the propeller shaft line with the vertical passing through the CG.

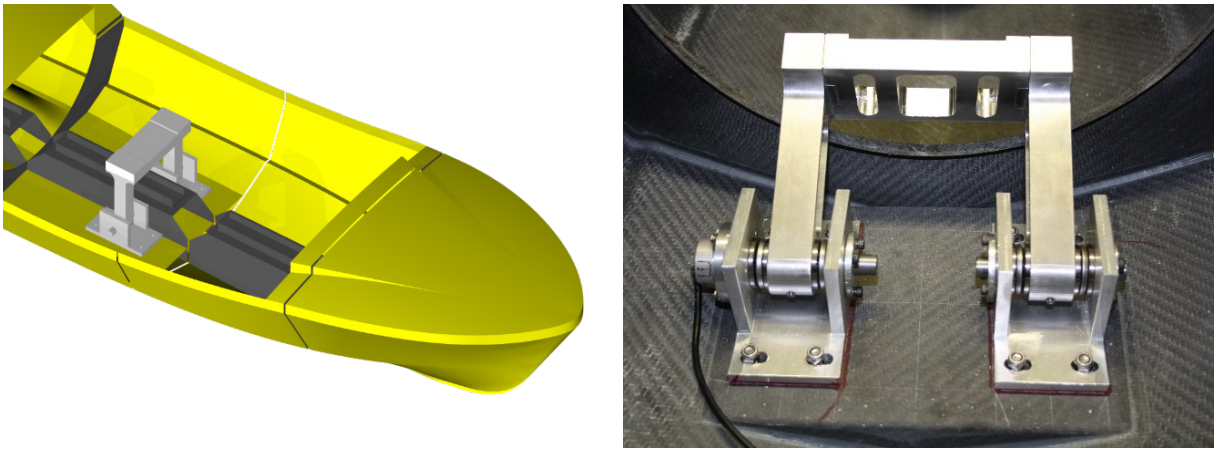

Figure 5.5. Towing rig on the segmented model (left) and solid model (right).

5.3.4 Turbulence Stimulation

When testing ship models, scaling is done according Froude's similitude, which ensures that gravity forces, hence surface waves and wave-related forces, are correctly scaled. Due to the physical impossibility to fulfil both Froude's and Reynolds' similitudes at scales that are not the real one, Reynold's number, hence similarity of viscous forces, is not appropriately represented and tends to assume values lower than at real scale. The fluid flow over a model hull will be at least partially laminar, whilst it would be almost entirely turbulent over the real hull. This effect is even more pronounced on appendages that lie outside the hull boundary layer and have smaller characteristic linear dimensions. To achieve fluid flow similarity during ship model tests and enable reliable extrapolation of the results to full scale, it is standard practice to establish turbulent flow through turbulence stimulation devices. Several methods have been devised and are commonly used by testing facilities. A first review can be found in ITTC (2002a).

From an analysis of previous towing tank tests conducted by the RNLI, it was found that turbulence stimulators mounted on the bow would have not been effective at high speed, where the hydrodynamic lift causes the bow to emerge from the water. Instead, a probe mounted on the carriage and piercing the water in front of the model was used. Around the bilge keels, which typically lie outside the hull boundary layer, turbulent flow was generated by trip wires bonded near the keels' leading edge.

5.3.5 Setup and Ballasting

The loading condition tested was the full load departure as taken in Chapter 4. Both models were ballasted to achieve the same displacement, centre of gravity and mass moments of inertia. For the segmented model, the correct weight distribution and inertial properties were sought at both a global level and for each segment.

The ballast consisted of lead plates bonded to the hull, in some cases supported by polystyrene blocks to increase the vertical centre of gravity. All the major masses, such as engines, gearboxes, tanks and capstans, were placed at their designated position and only the remaining ballast was adjusted.

The ballasting followed the procedure detailed by Lloyd (1989) and Bhattacharyya (1978). The LCG was determined by placing one end of the model on a scale and the other end on a wedge and weighing the model. The VCG was determined through an inclining experiment and the TCG was visually adjusted with trim gauges. The radii of gyration for roll, pitch and yaw were determined using a bifilar swing and the CG position was checked again after the adjustment of the radii of gyration.

The segmented model was ballasted, prior to its segmentation, for preliminary tests. After the segmentation and the installation of strain gauges on the backbone structure, ballasting was carried out again, hanging the bundle of cables connecting the strain gauges above the model and with some slack. It was found that heeling and swinging of the model were affected by the cables. It was therefore possible to re-determine only displacement, LCG and TCG with an acceptable accuracy. The consequences on the test results are discussed later in the chapter. The target and actual values achieved are detailed in Tables 5.3 & 5.4.

			TARGET (Small-Scale)	SOLID MODEL	SEGMENTED MODEL (before segm'n)	SEGMENTED MODEL (after segm'n)
Displacement	Δ	[kg]	17.12	17.15	17.20	17.00
Centre of gravity (x)	LCG	[mm]	477	478	478	481
Centre of gravity (z)	TCG	[mm]	0	visually adjusted	visually adjusted	visually adjusted
Centre of gravity (y)	VCG	[mm]	163	170	162	N.A.
Roll radius of gyration	k_4	[mm]	140	128	166	N.A.
Pitch radius of gyration	k_5	[mm]	294	287	290	N.A.
Yaw radius of gyration	k_6	[mm]	296	313	343	N.A.

Table 5.3. Hull model loading condition. Small-scale values.

			TARGET (Full-Scale)	SOLID MODEL	SEGMENTED MODEL (before segm'n)	SEGMENTED MODEL (after segm'n)
Displacement	Δ	[kg]	43164	43250	43376	42872
Centre of gravity (x)	LCG	[m]	6.44	6.45	6.45	6.49
Centre of gravity (z)	TCG	[m]	0.00	visually adjusted	visually adjusted	visually adjusted
Centre of gravity (y)	VCG	[m]	2.20	2.30	2.19	N.A.
Roll radius of gyration	k_4	[m]	1.89	1.73	2.24	N.A.
Pitch radius of gyration	k_5	[m]	3.97	3.87	3.92	N.A.
Yaw radius of gyration	k_6	[m]	3.99	4.23	4.63	N.A.

Table 5.4. Hull model loading condition. Full-scale values.

5.3.6 Segmented Model – Strength Bar

On the segmented model, the stiffness of the hull girder is provided by a strength bar, which holds the hull segments together and carries the hull girder loads. The strength bar determines the stiffness of the hull girder at the cuts. For a rigid segmented model, this should be much higher than the stiffness of the prototype and should have a higher natural frequency than the maximum wave encounter frequency. Nevertheless, deformations of the strength bar should be large enough to be sensed by strain gauges.

Three independent aluminium 6082 T6 beams of square hollow section were used, one for each segmentation cut. Preliminary seakeeping simulations were run with MAESTRO-Wave to estimate the load magnitudes that would have been sustained during tests. For any given beam size, correspondent strains could thus be calculated.

The acceptable maximum strain was limited to 500με (tensile or compressive), a compromise between the low strains that would result from a stiff hull girder and the typical measuring range of a conventional strain gauge. The size of the beams making up the strength bar was chosen accordingly. The final design consisted of beams of 1" x 1" x 16SWG at 25 and 50% LWL, and ¾" x ¾" x 16SWG at 75% LWL. Figures 5.6-5.7 show the design of the strength bar.

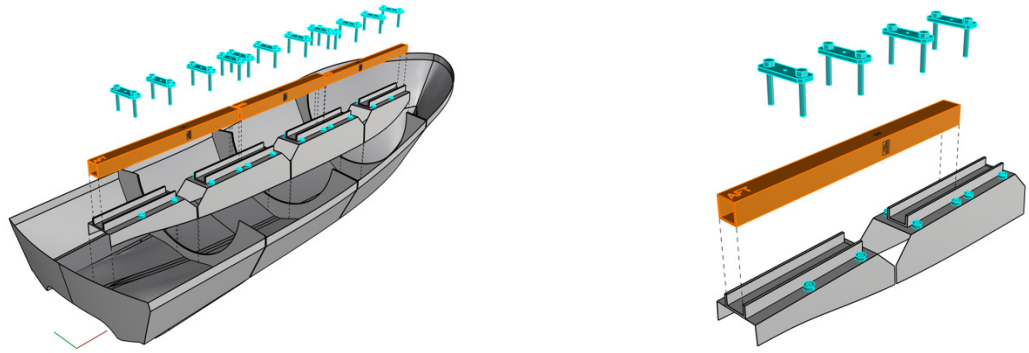

Figure 5.6. Strength bar layout.

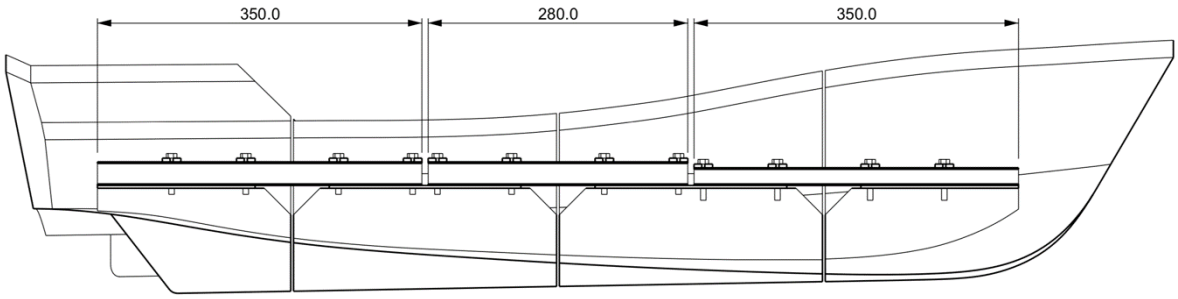

Figure 5.7. Strength bar. Longitudinal section taken at the hull centreline.

5.3.7 Segmented Model – Global Load Measurement

Load measurements with a segmented model can only be taken at the segmentation cuts, whose position should be decided based on the objectives of the test. The number of segments is generally a compromise. A high number of measurement points along the hull can be required to reconstruct the longitudinal distribution of the load. Each segment should, however, have the same weight and inertial characteristics as the corresponding segment on the full-scale prototype, which restricts how small each segment can be. The number of signals to be recorded can also be limited by the capabilities and cost of the acquisition system.

The Severn Class model was segmented where bending moment and shear force tend, in general, to be maximum: at amidships (50% LWL) for bending moment and the quarters of the length (25 & 75% LWL) for vertical shear force. Recognising that three measurement points along the hull would not allow to reconstruct longitudinal load distributions, the task was limited to generating results for the validation of numerical simulations. At each segmentation cut, the strength bar was fitted with foil resistive strain gauges to measure:

- Vertical bending moment (VBM)
- Horizontal bending moment (HBM)
- Vertical shear force (VSF)

The strain gauge layout is shown in Figure 5.8. Vertical bending moment was measured with the linear strain gauges SG1 & SG5; horizontal bending moment was measured with the linear strain gauges SG3 & SG7; and vertical shear force was measured with the shear strain gauges SG2, SG4, SG6 & SG8, oriented at 45° from the longitudinal axis of the beam. Since the webs required three strain measuring grids oriented at 45° from each other, rectangular triaxial rosettes were used in lieu of a combination of linear and shear gauges. The reasons for this were mainly practical since the operating principle remains unaltered. The position and orientation of the strain gauges with respect to the symmetry planes of the beam enables isolation of each of the three load components. A rigorous demonstration can be found in Hoffmann (1989).

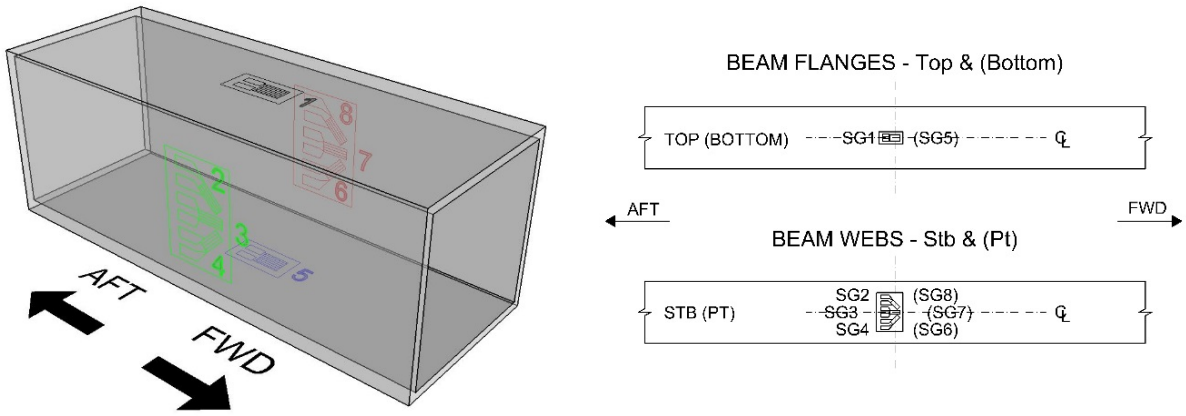

Figure 5.8. Strain gauge layout.

The strain gauge layout would suit the use of a half Wheatstone bridge for vertical and horizontal bending moments, and a full Wheatstone bridge for vertical shear force. However, to have better control over the data recorded, and to facilitate the detection of malfunctions, all the strain gauges were wired into quarter bridge circuits and their signals were acquired separately. This resulted in 8 channels per segmentation cut and a total of 24 channels. The averaging of the strain signals to isolate the loading component of interest (VBM, HBM or VFS) was done at the data processing stage. The mathematics involved is similar to that computed within a Wheatstone bridge in half or full configuration:

$$\varepsilon_{VBM} = \frac{\varepsilon_{SG5} - \varepsilon_{SG1}}{2} \tag{5.1}$$

$$\varepsilon_{HBM} = \frac{\varepsilon_{SG5} - \varepsilon_{SG1}}{2} \tag{5.2}$$

$$\varepsilon_{VSF} = \frac{\varepsilon_{SG4} - \varepsilon_{SG2} + \varepsilon_{SG6} - \varepsilon_{SG8}}{4} \tag{5.3}$$

where ε_{VBM}, ε_{HBM} and ε_{VSF} are the strains due to VBM, HBM and VFS and ε_{SG1}, ε_{SG2},..., ε_{SG8} are the strains measured by the strain gauges SG1, SG2,..., SG8.

Experimental load analysis requires the conversion of the measured quantity - microstrains (με) - into a load magnitude. This relation was constructed through direct calibration, by applying a known load and reading the response of the measuring system.

A test rig was used to set the instrumented beams under bending and strain readings were taken at fixed loads covering the whole expected loading range of the beams. Four-point bending (Figure 5.9 (left)), generating constant bending moment and zero shear between the loading rollers, was used for the calibration of the strain gauges measuring bending moment. Three-point bending (Figure 5.9 (right)), which causes constant shear and linearly varying bending moment on either side of the loading roller, was used for calibrating the strain gauges measuring vertical shear force.

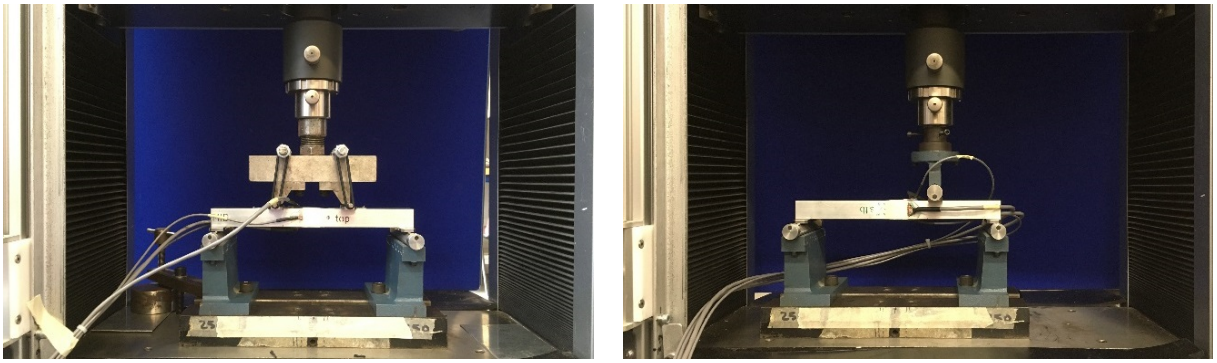

Figure 5.9. Backbone beam calibration. 4-point bending setup (left) and 3-point bending setup (right).

The load magnitude correspondent to the applied vertical force can easily be calculated using the equilibrium equations. A correlation between the applied load and the measured strain was constructed and compared against theoretical values calculated with the following equations.

For bending moment:

$$\sigma = \frac{My}{I} \tag{5.4}$$

$$\varepsilon = \frac{\sigma}{E} \tag{5.5}$$

where σ is the bending stress; M is the applied bending moment; y is the distance of the measuring point from the neutral axis; I is the section modulus of the cross-section; E is the modulus of elasticity; and ε is the bending strain.

For shear force:

$$\tau = \frac{TQ}{It} \tag{5.6}$$

$$\gamma = \frac{\tau}{G} \tag{5.7}$$

where τ is the shear stress; T is the applied shear force; Q and I are the first and second moments of area of the cross-section about the neutral axis; t is the thickness of the cross-section in the direction perpendicular to the shear; G is the shear modulus; and γ is the shear strain. Since γ is a deformation angle, which cannot be measured directly by a strain gauge, it is determined by measuring the strain at 45° from the shear plane. The following relation applies at the level of the neutral axis, where bending moment is zero:

$$\varepsilon_{45^\circ} = \frac{1}{2}\gamma \tag{5.8}$$

The complete set of calibration graphs is reported in Appendix 3. Figures 5.10-5.11 show typical graphs for vertical and horizontal bending moments measured with the couples of strain gauges SG1 & SG5 and SG3 & SG7 respectively. The theoretical relation between measured strain and correspondent load is superimposed on the experimental values and on the best linear fit used as calibration factor. The error between the linear fit and any data point is generally within 1%. The discrepancy between the theoretical and the experimental lines, highlights how direct calibration takes into account inaccuracies in the installation of the strain gauges and imperfections of the structure, both neglected by theoretical calculations.

Calibration of vertical shear force measured with the strain gauges SG2, SG4, SG6 & SG8 involved a further step. It was found that the strain readings were biased by vertical bending strain sensed by the gauges, hence a correction was applied to compensate the readings for the 'parasitic' bending strain. The correction factor was found through the calibration tests and applied as a percentage of the bending strain at the beam flanges sensed by the gauges SG1 & SG5. Figures 5.12 & 5.13 show an example calibration plot without and with correction respectively. The error between the linear fit and any data point is generally within 1%.

5.3.8 Segmented Model – Segmentation and Sealing

After preliminary tests, the segmented model was cut into four segments. The segments were put back together with a larger spacing and held by the backbone beams. Sealing of the gaps was achieved with thin latex strips bonded on the hull shell with fluid silicon. The segments were then squeezed back to the original spacing. This procedure leaves the latex strips indented toward the inside, preventing them from constraining relative motions between the segments. The segmentation and sealing are shown in Figure 5.14.

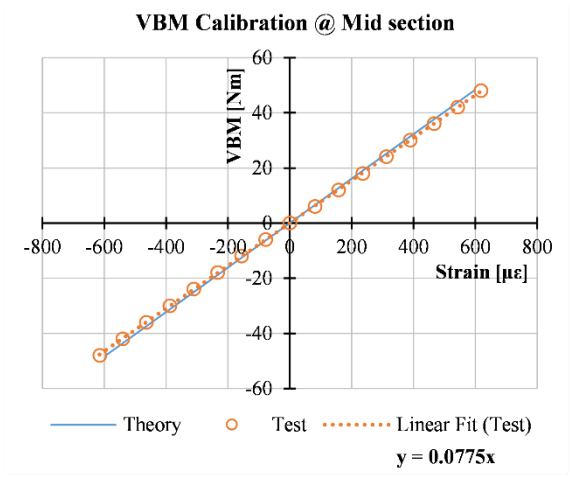

Figure 5.10. Calibration of the strain gauges measuring VBM at 0.50LWL.

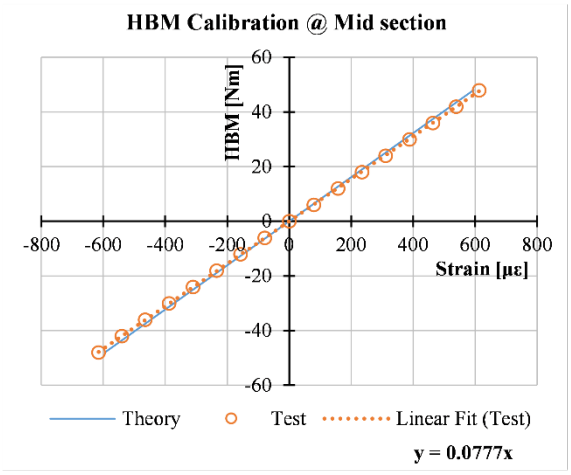

Figure 5.11. Calibration of the strain gauges measuring HBM at 0.50LWL.

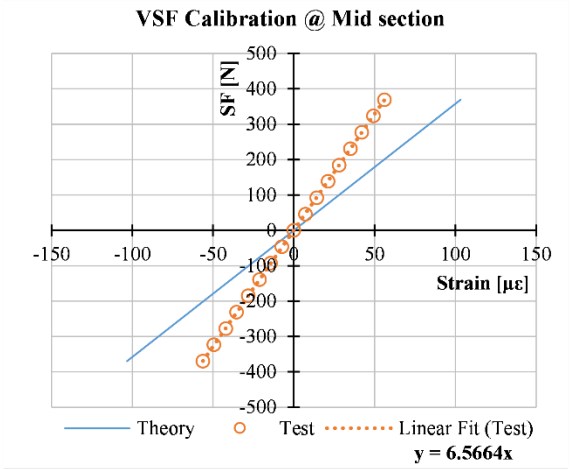

Figure 5.12. Calibration of the strain gauges measuring VSF at 0.50LWL. The readings are affected by bending strain sensed by the shear gauges.

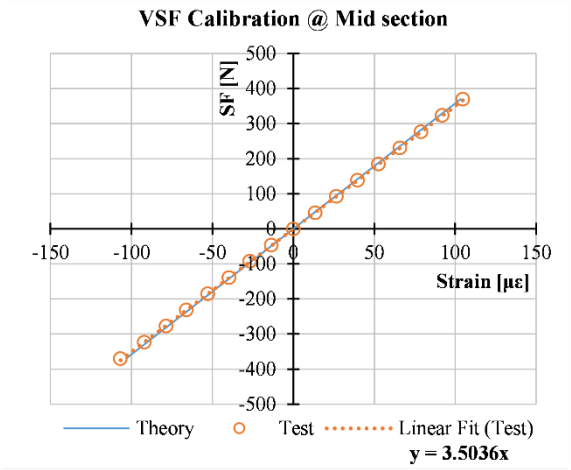

Figure 5.13. Calibration of the strain gauges measuring VSF 0.50LWL. A correction factor is applied to account for the parasitic bending strain.

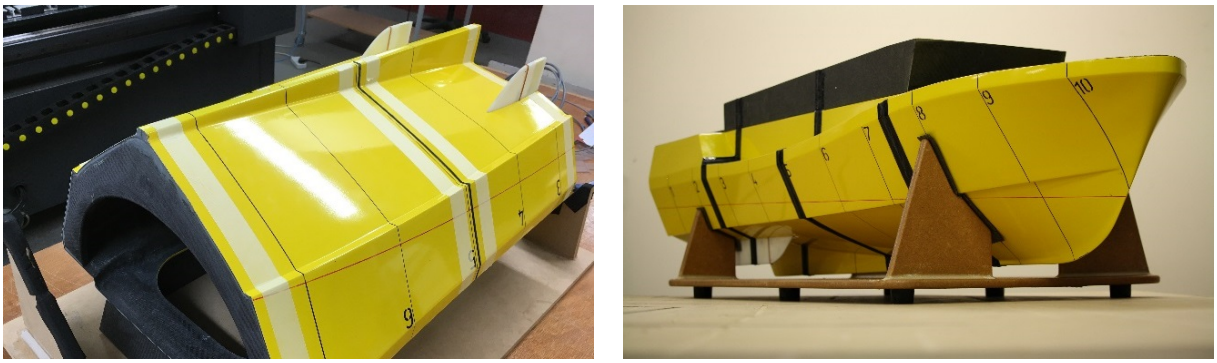

Figure 5.14. Hull model segmentation and sealing.

5.3.9 Test Apparatus and Procedure

The experiment matrix involved two groups of tests:

- ***Forward-speed tests***
  - Resistance in calm water at speeds V_M=0.7, 1.4,..., 3.5m/s (V_S=5, 10,..., 25kts).
  - Seakeeping in regular head waves at wavelength-to-hull length ratios λ/LOA in the range 0.4-3.4; at speeds V_M=0.7, 1.4,..., 2.8m/s (V_S=5, 10,..., 20kts).

- ***Zero-speed tests***
  - Seakeeping in regular waves at wavelength-to-hull length ratios λ/LOA in the range 0.4-2.6; at headings β=0˚, 45˚,..., 315˚.

The first group was conducted with the model attached to a standard towing carriage (Figure 5.15). Drag and side forces were measured with a dynamometer free to heave and pitch, positioned at the bottom end of the heave post. Two potentiometers measured heave (or sinkage) and pitch (or trim). For seakeeping tests, the towing carriage and the data recording equipment were synchronised with the wave maker to minimise interference of waves reflected by the tank walls.

Tests at zero speed were carried out with the model positioned at the centre of the tank. A set of mooring lines, fitted with spring dampers, constrained the model in yaw, surge and sway (Figure 5.16). Rigid body motions in the six degrees of freedom were recorded with a motion capture system (Qualisys Motion Capture Systems 2018), consisting of two infrared cameras on the side of the basin and four retroreflective markers on the vessel.

The water depth was set to 1045mm and waves were generated with a nominal wave height of 74mm for tests at $V_M \leq$2.1m/s and 44mm for tests at V_M=2.8m/s. These correspond to full-scale values of 1m at $V_S \leq$15kts and 0.6m at V_S=20kts and should only be taken as a reference. The actual wave height generated by the wave maker was a function of the wave period and differed from its nominal value. For the analysis of the vessel responses, and calculation of their RAOs, the actual wave height was used. This was determined for each test by measuring the wave elevation with a wave probe located at the tank midspan.

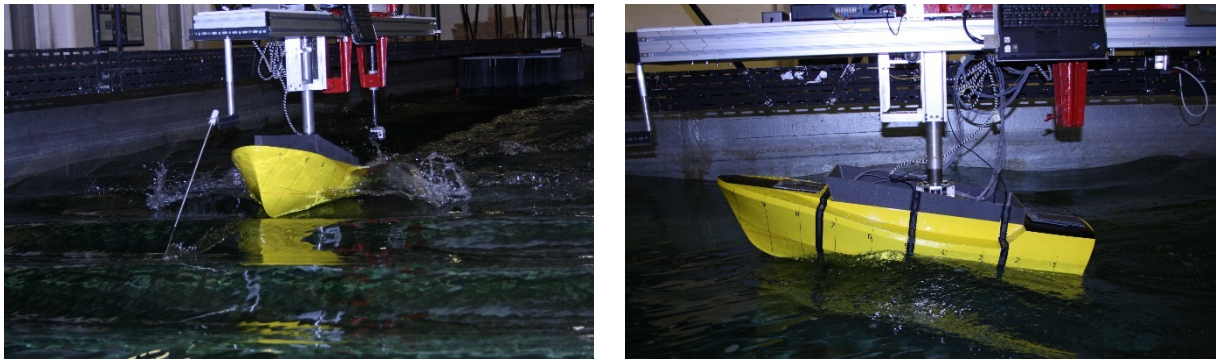

Figure 5.15. Test at forward speed with the hull model attached a free-to-heave-and-pitch dynamometer. Solid model (left) and segmented model (right).

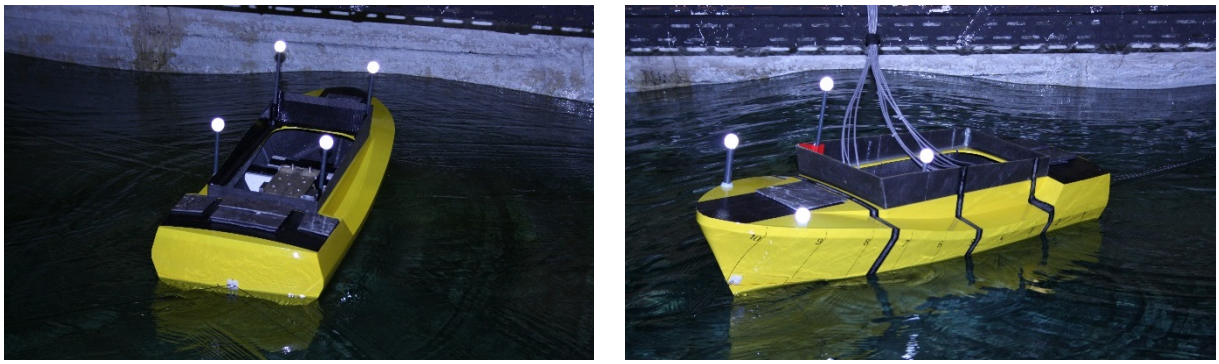

Figure 5.16. Test at zero speed with the hull model constrained by a set of mooring lines. Solid model (left) and segmented model (right).

5.3.10 Data Acquisition and Analysis

During any test the following quantities were recorded continuously through one or more data acquisition systems:

- Drag & side force (forward speed tests only)
- Motions (heave and pitch at forward speed; 6 degrees of freedom at zero speed)
- Hull girder loads (segmented model only)
- Wave elevation (seakeeping tests only)
- Carriage speed (forward speed tests only)

The data acquisition relied on 'oversampling'. Motions, drag, side forces, wave elevation and carriage speed were sampled at 100Hz whilst hull girder loads at 1000Hz. The data analysis confirmed that the sampling rates exceeded the minimum requirements. The raw signals were trimmed to remove any transients and a Savitzky-Golay smoothing filter with a short frame length was applied to suppress electrical noise.

Results from resistance tests were derived by averaging the instantaneous measured values over the measuring interval. For tests at V_M=3.5m/s (V_S=25kts), which produced only 4 seconds worth of data, two consecutive runs were combined to double the sample.

From seakeeping tests, results were produced in terms of mean amplitude of the sinusoidal signal computed through a peak-to-peak analysis, described by the ITTC (2002c). The method consists of searching the peak and trough values of each oscillation cycle and computing the amplitude of the cycle from the following equation:

$$y_0 = \frac{|y_p - y_t|}{2} \tag{5.9}$$

where y represents the quantity on the ordinate of a time-history plot; and the subscripts 0, p and t represent the amplitude, peak and trough of a cycle respectively. In this analysis, y could take any of the following forms: heave (η_3), roll (η_4), pitch (η_5), vertical bending moment (VBM) or wave elevation (ζ). The mean signal amplitude was obtained by averaging the amplitudes of all the cycles within the measuring interval. Although the mathematics is straightforward, equation 5.9 has important implications for the vessel responses. The same value is indeed computed for positive and negative motions, and for loads in sagging and hogging condition. Also, as long as the signal preserves its periodicity, an amplitude value can always be found, even when the signal loses its sinusoidal character.

The signal frequency was estimated through a short-term Fourier transform to verify that it corresponded to the expected value of either wave frequency or wave encounter frequency, depending on the quantity analysed and on the test setup. Figure 5.17 shows an example of data analysis for heave motions recorded during a seakeeping test.

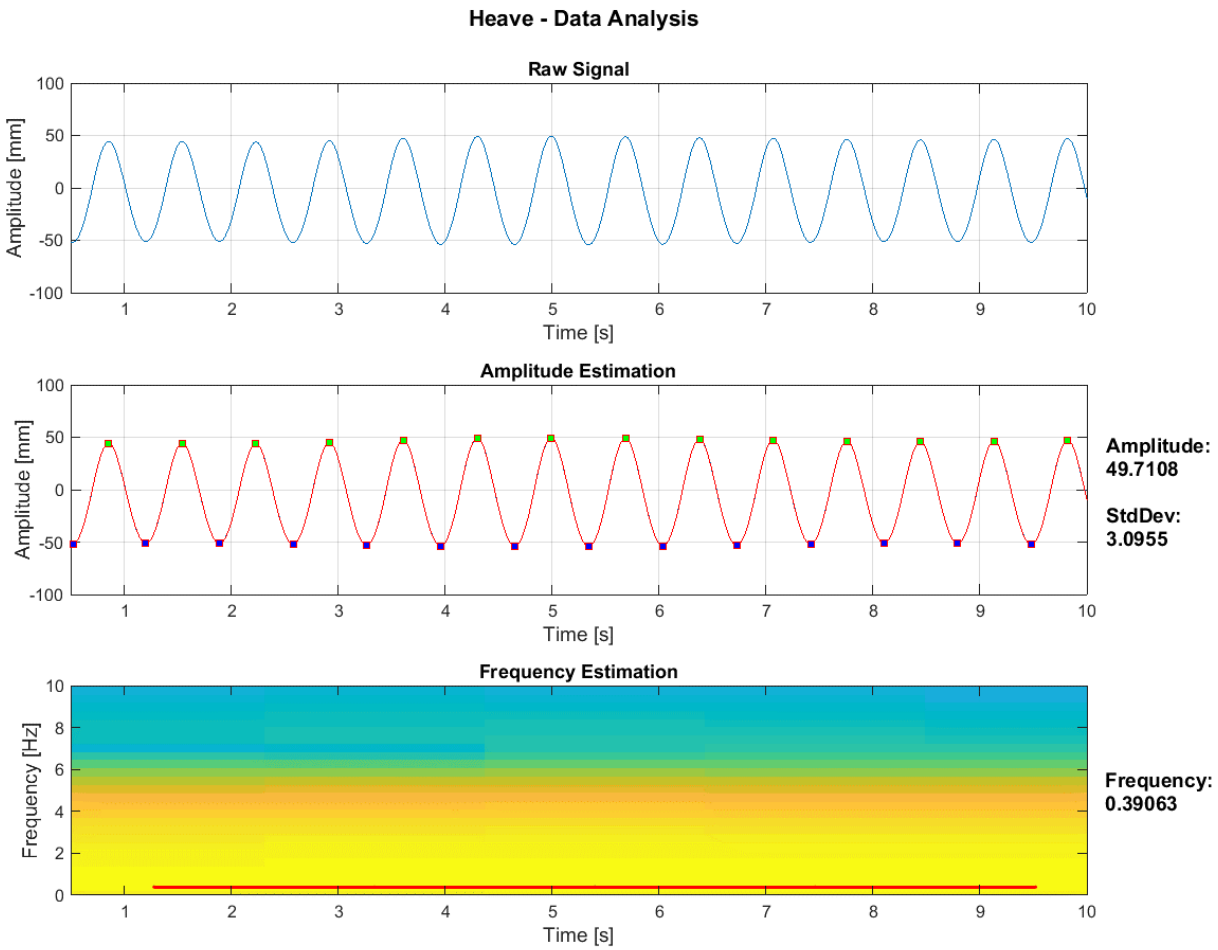

Figure 5.17. Data analysis for heave motions. Raw signal (top). Filtered Signal and estimation of its mean amplitude through a peak-to-peak analysis (middle). Spectrogram and estimated signal frequency (bottom).

5.4 Results

5.4.1 Data Series

In general, results are presented for three data series:

- Solid model (***Solid***)
- Segmented model preliminary tested as solid (***Segm (P)***)
- Segmented model after its segmentation (***Segm***)

The test matrix of a seakeeping experiment tends to be large because of the number of variables that are needed to obtain a complete picture of the behaviour of the vessel. To keep the task within practical limits, not all headings and wave frequencies were tested with the three setups. This is reflected in the results presented in the following sections, where it will be noted that the data series and the number of data points within each

series vary. Seakeeping results are also compared against the numerical predictions from Chapter 4. The numerical data was obtained with the following codes:

- 2D strip theory (***2D***) for speeds $V_M \leq 1.4$ ($V_S \leq 10$ kts)
- 2.5D strip theory (***2.5D***) for speeds $V_M > 1.4$ ($V_S > 10$ kts)

5.4.2 Resistance

Figures 5.18-5.20 show total drag, sinkage and running trim from tests in calm water. These tests were conducted with the main objectives of assessing the correlation between the solid and the segmented model and the effect of the segmentation on the latter. Results from calm water tests are presented at model scale, as measured, and as a function of the carriage speed. Although a secondary x-axis reporting the correspondent full-scale vessel speeds is shown, extrapolation of the measured quantities to full scale should be carried out in accordance with accepted procedures (e.g. ITTC).

5.4.3 Seakeeping

Seakeeping results are presented in terms of Response Amplitude Operators (RAOs), computed as the ratio of the amplitude of the response and the exciting wave amplitude:

$$Heave_{RAO} = \frac{\eta_{30}}{\zeta_0} \tag{5.10}$$

$$Roll_{RAO} = \frac{\eta_{40}}{\zeta_0} \tag{5.11}$$

$$Pitch_{RAO} = \frac{\eta_{50}}{\zeta_0} \tag{5.12}$$

$$VBM_{RAO} = \frac{VBM_0}{\zeta_0} \tag{5.13}$$

where η_{30}, η_{40}, η_{50} are the amplitudes of heave, roll and pitch motion respectively, VBM_0 is the vertical bending moment amplitude and ζ_0 is the wave amplitude. All terms were computed from Equation 5.9.

Stationary seakeeping tests were conducted to verify the correct ballasting of the models and to obtain a first comparison against the numerical simulations. Motion and load results are presented for different headings and, since beam and quartering waves were tested for both port and starboard, the RAO mean value is used. Figures 5.21-5.35 show

heave, pitch and roll motions, whilst Figures 5.36-5.50 show the vertical bending moment at three stations correspondent to the three load measurement sections on the segmented model. The RAOs are plotted against the non-dimensional ratio λ/LOA.

For vertical bending moment an additional representation is possible, which emphasises how the load varies longitudinally rather than with the wave length. The RAO is plotted against the distance of the station under consideration from the aft end, whilst the wavelength, expressed as λ/LOA, appears as a parameter. These plots are shown in Figures 5.51-5.55.

The seakeeping of the vessel at different speeds is assessed with the model towed by the carriage. Figures 5.56-5.63 show heave and pitch motions. Figures 5.64-5.75 show vertical bending moment at the three measurement sections on the segmented model.

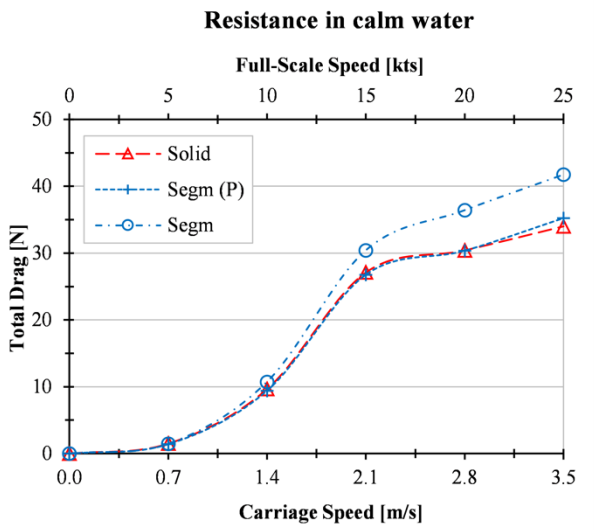

Figure 5.18. Resistance in calm water.

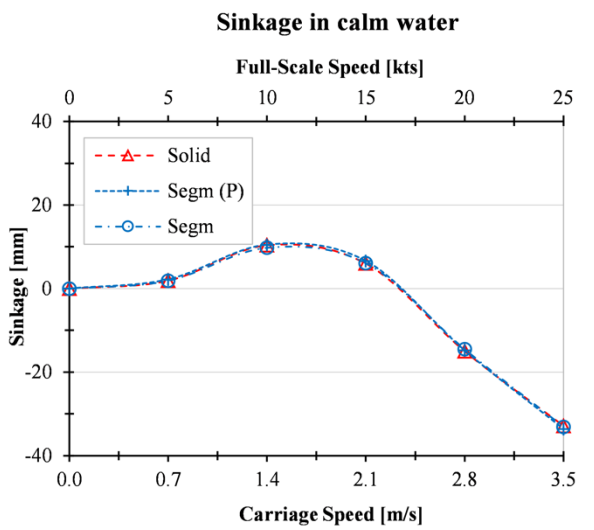

Figure 5.19. Sinkage in calm water.

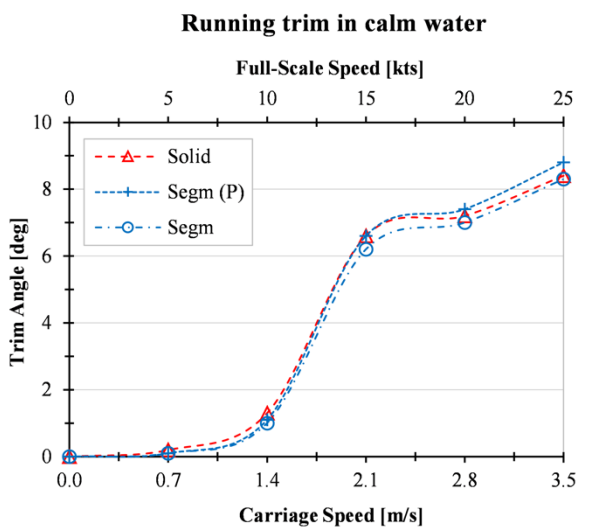

Figure 5.20. Running trim in calm water.

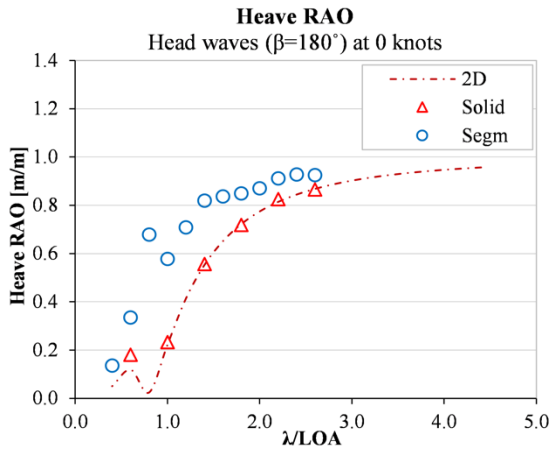

Figure 5.21. Heave in head waves at 0kts.

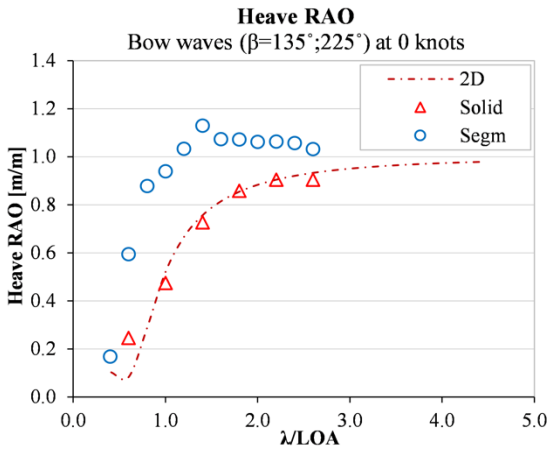

Figure 5.24. Heave in bow quartering waves at 0kts.

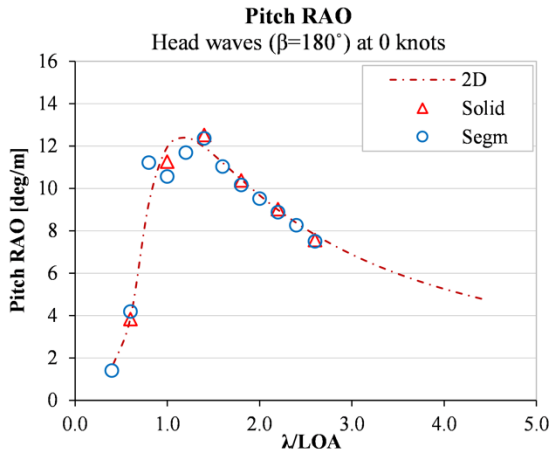

Figure 5.22. Pitch in head waves at 0kts.

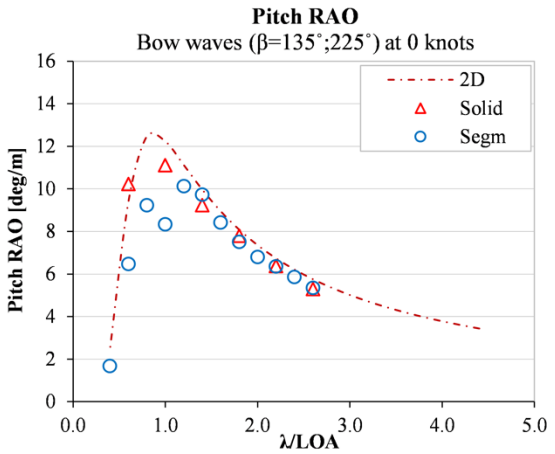

Figure 5.25. Pitch in bow quartering waves at 0kts.

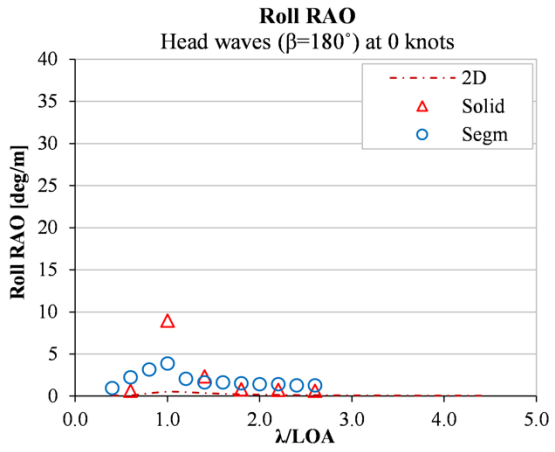

Figure 5.23. Roll in head waves at 0kts.

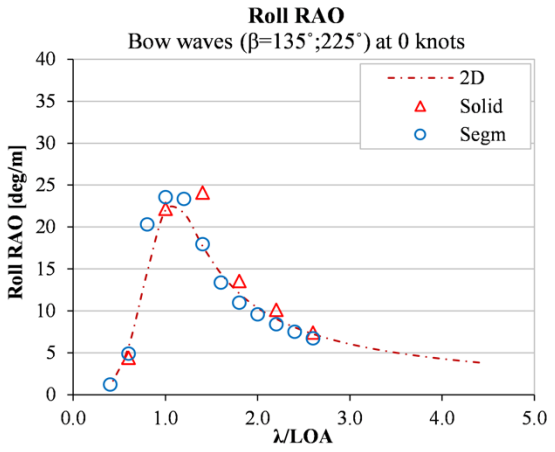

Figure 5.26. Roll in bow quartering waves at 0kts.

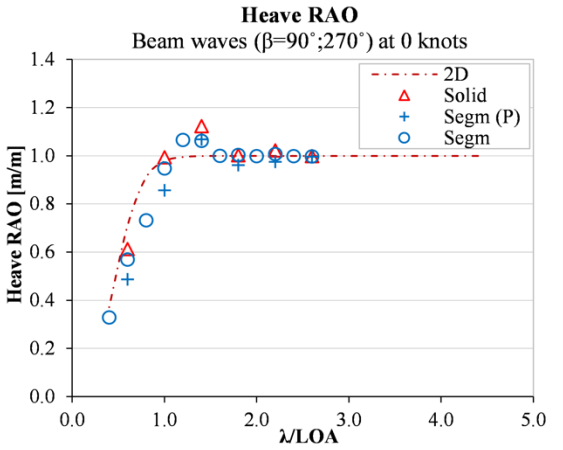

Figure 5.27. Heave in beam waves at 0kts.

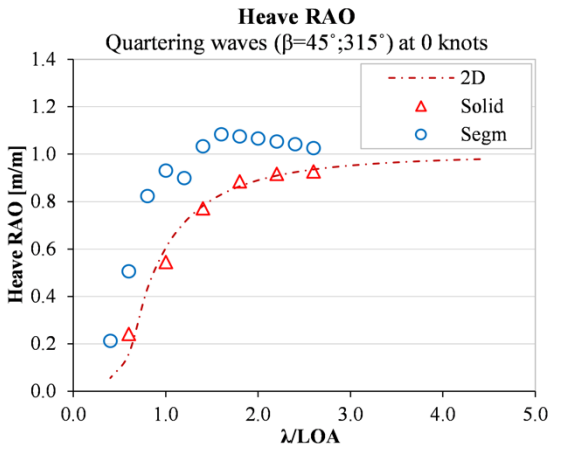

Figure 5.30. Heave in stern quartering waves at 0kts.

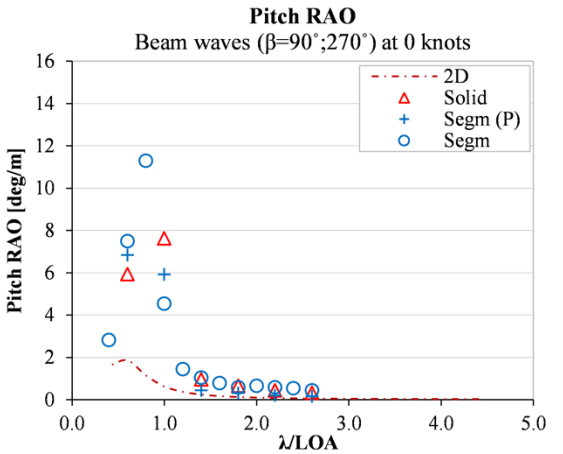

Figure 5.28. Pitch in beam waves at 0kts.

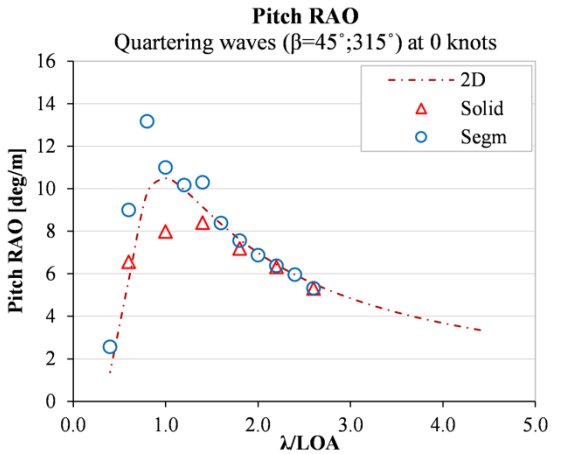

Figure 5.31. Pitch in stern quartering waves at 0kts.

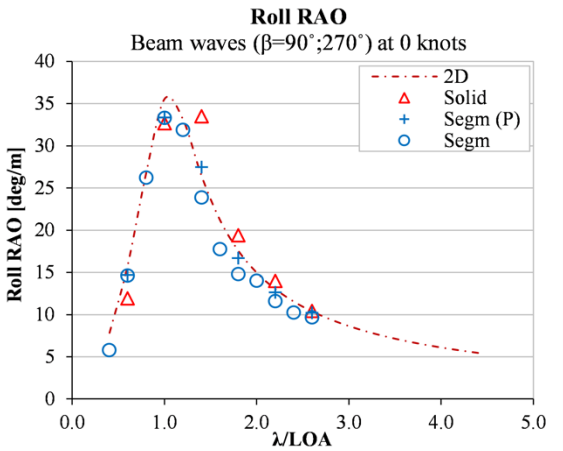

Figure 5.29. Roll in beam waves at 0kts.

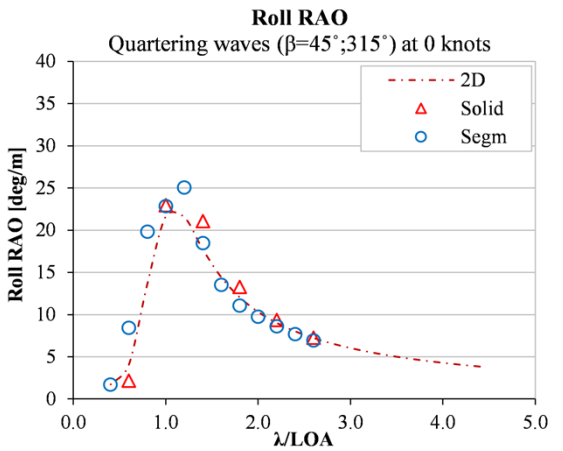

Figure 5.32. Roll in stern quartering waves at 0kts.

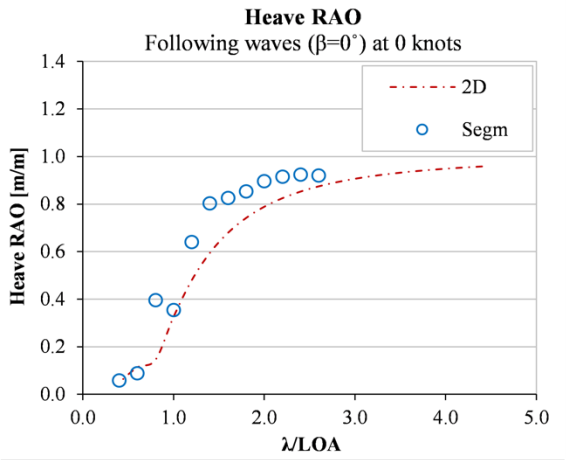

Figure 5.33. Heave in following waves at 0kts.

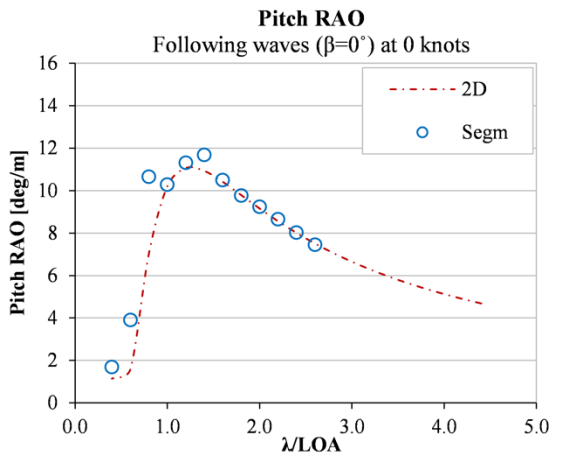

Figure 5.34. Pitch in following waves at 0kts.

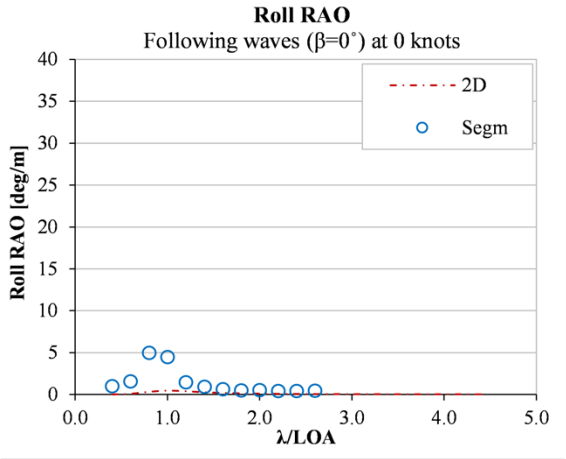

Figure 5.35. Roll in following waves at 0kts.

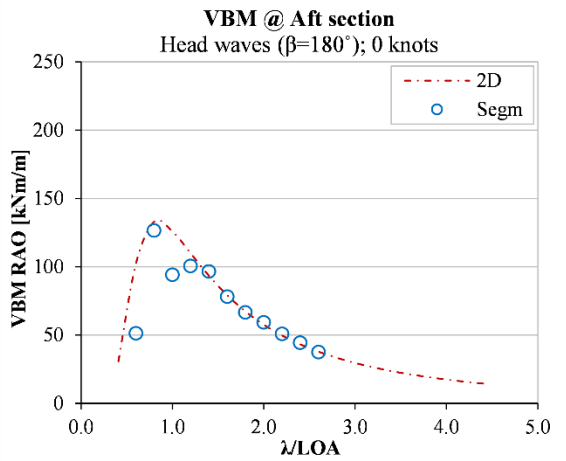

Figure 5.36. VBM at 0.25LWL in head waves at 0kts.

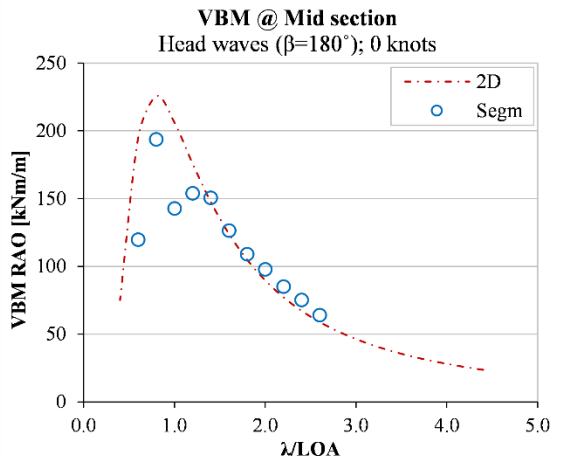

Figure 5.37. VBM at 0.50LWL in head waves at 0kts.

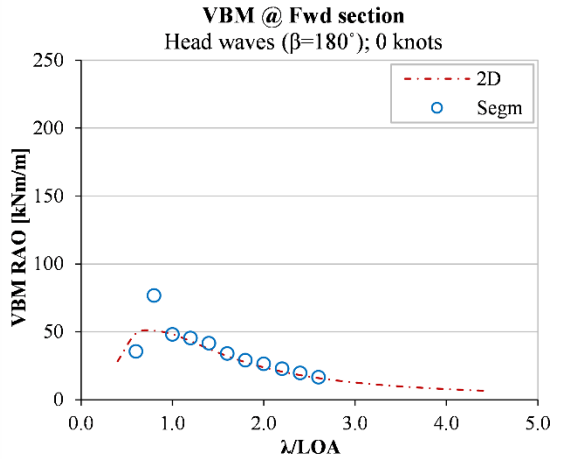

Figure 5.38. VBM at 0.75LWL in head waves at 0kts.

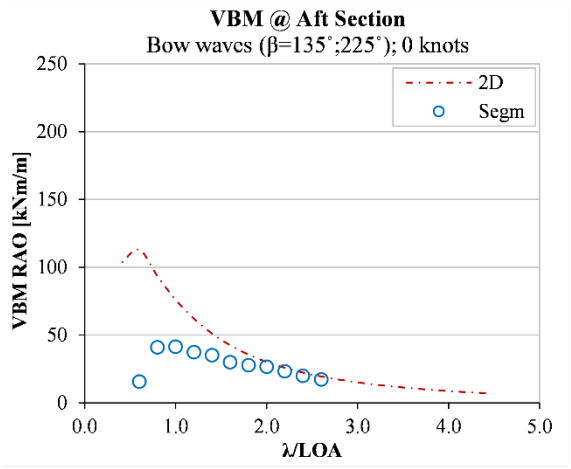

Figure 5.39. VBM at 0.25LWL in bow quartering waves at 0kts.

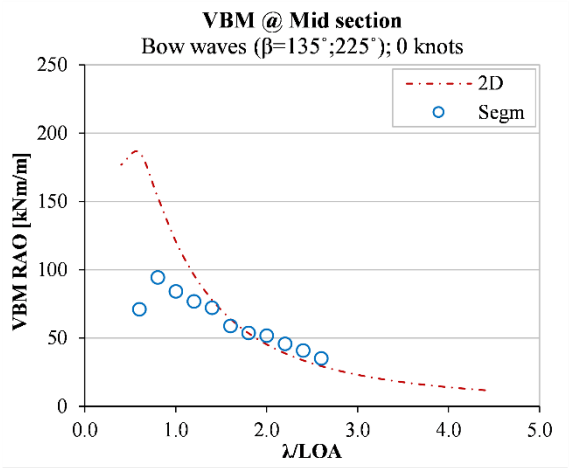

Figure 5.40. VBM at 0.50LWL in bow quartering waves at 0kts.

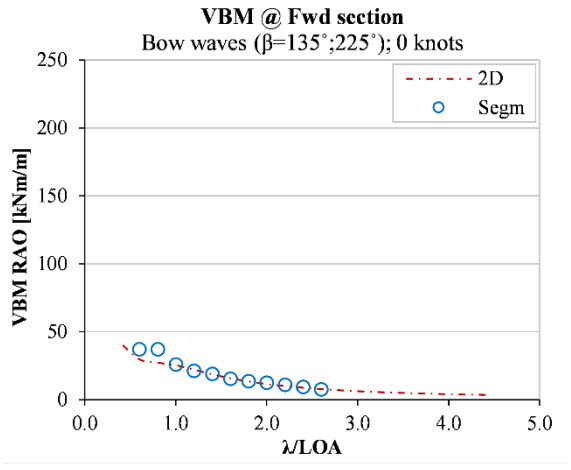

Figure 5.41. VBM at 0.75LWL in bow quartering waves at 0kts.

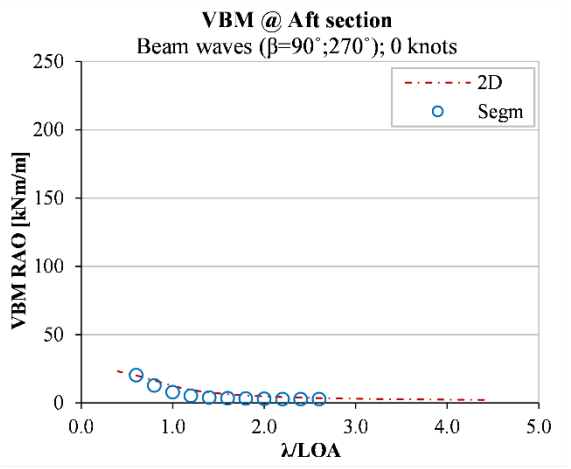

Figure 5.42. VBM at 0.25LWL in beam waves at 0kts.

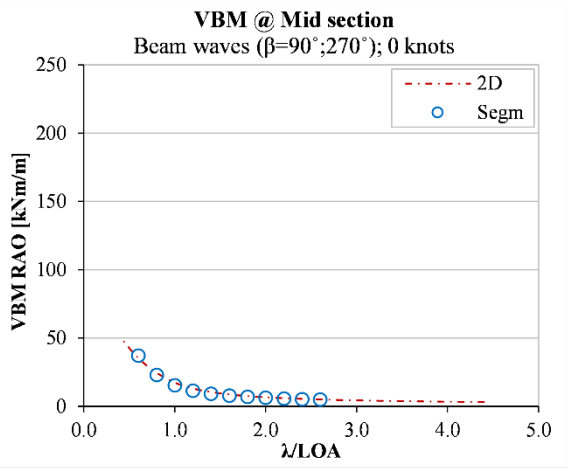

Figure 5.43. VBM at 0.50LWL in beam waves at 0kts.

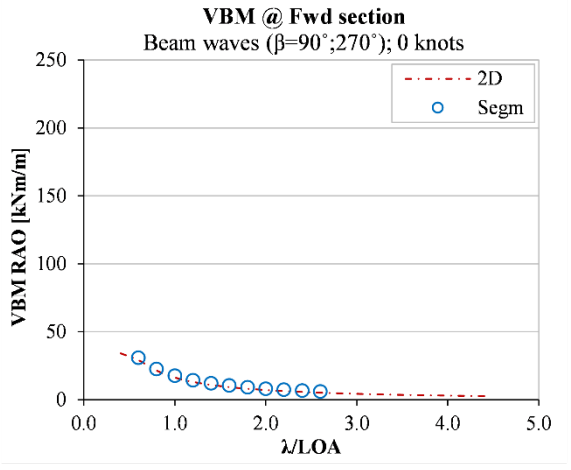

Figure 5.44. VBM at 0.75LWL in beam waves at 0kts.

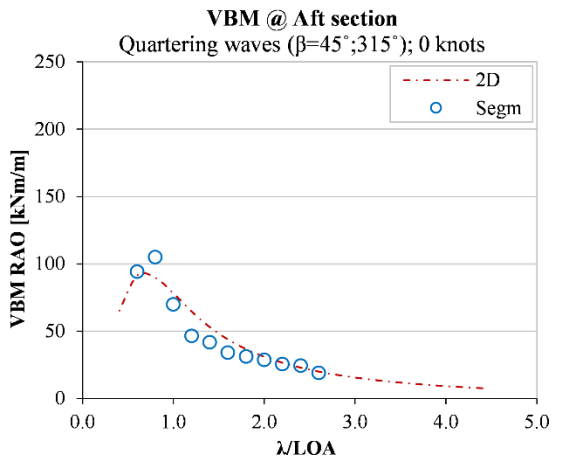

Figure 5.45. VBM at 0.25LWL in stern quartering waves at 0kts.

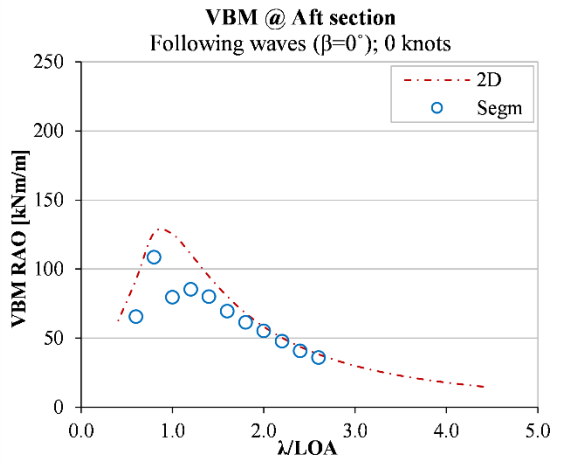

Figure 5.48. VBM at 0.25LWL in following waves at 0kts.

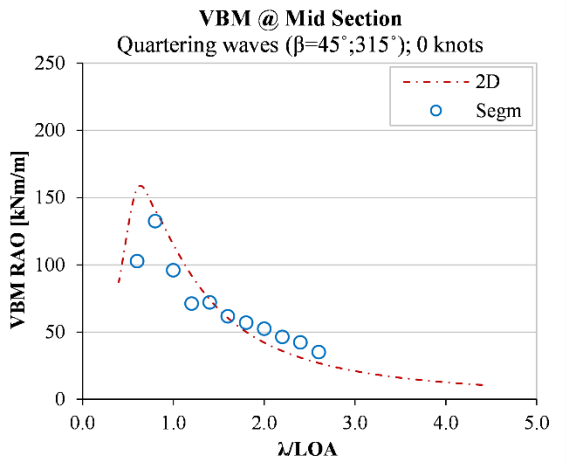

Figure 5.46. VBM at 0.50LWL in stern quartering waves at 0kts.

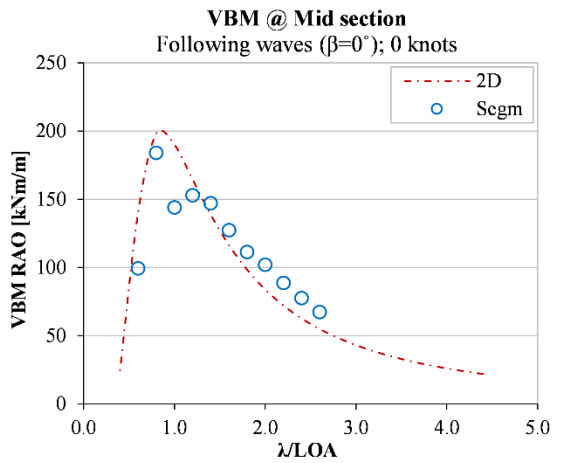

Figure 5.49. VBM at 0.50LWL in following waves at 0kts.

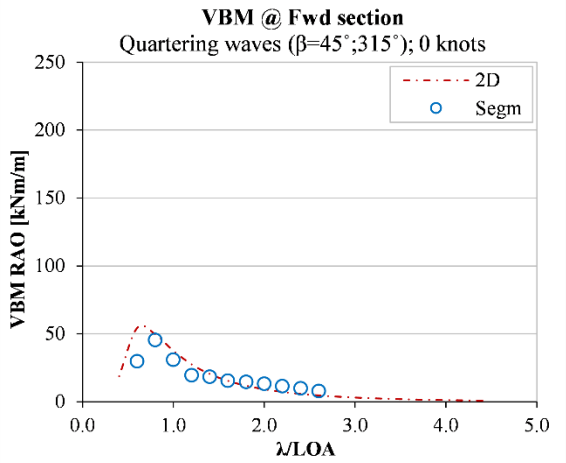

Figure 5.47. VBM at 0.75LWL in stern quartering waves at 0kts.

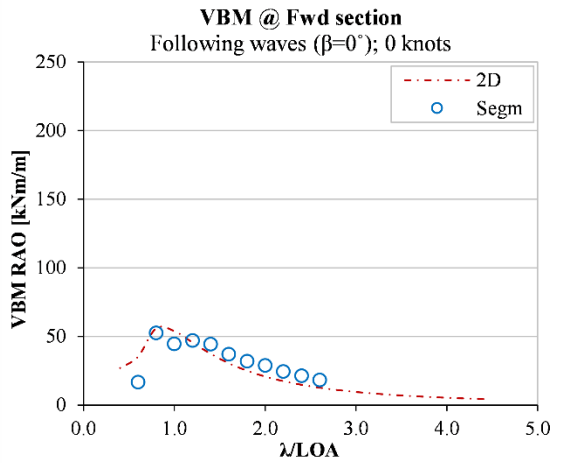

Figure 5.50. VBM at 0.75LWL in following waves at 0kts.

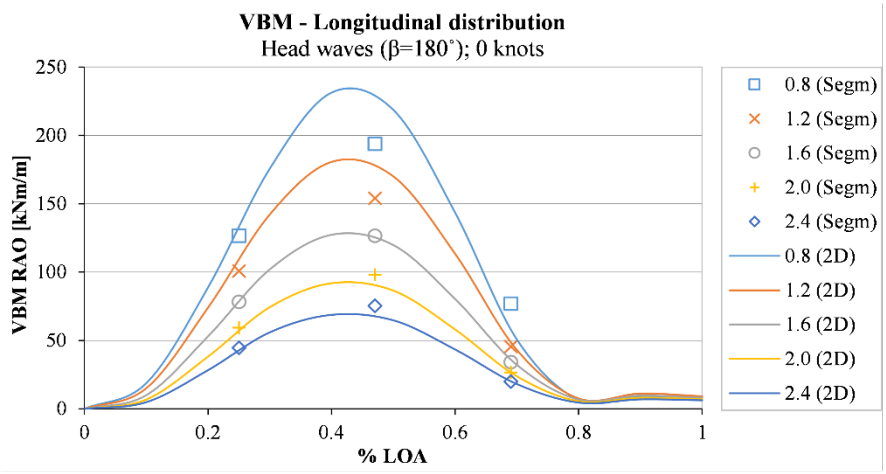

Figure 5.51. VBM longitudinal distribution in head waves at 0kts.

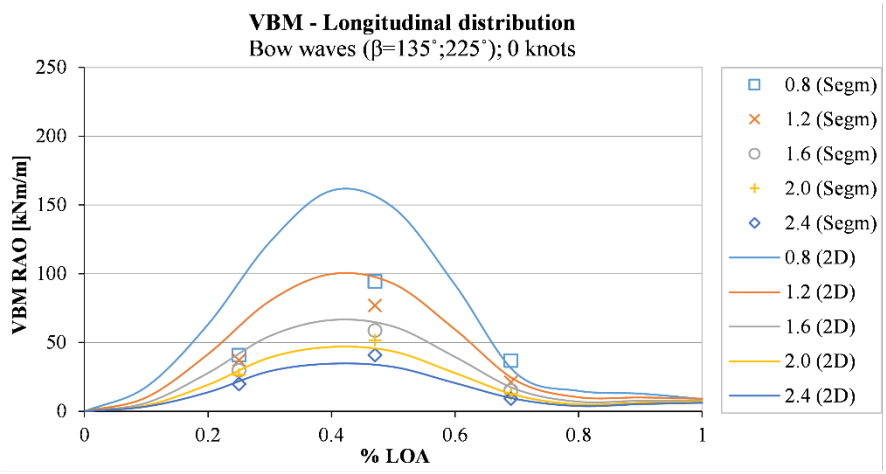

Figure 5.52. VBM longitudinal distribution in bow quartering waves at 0kts.

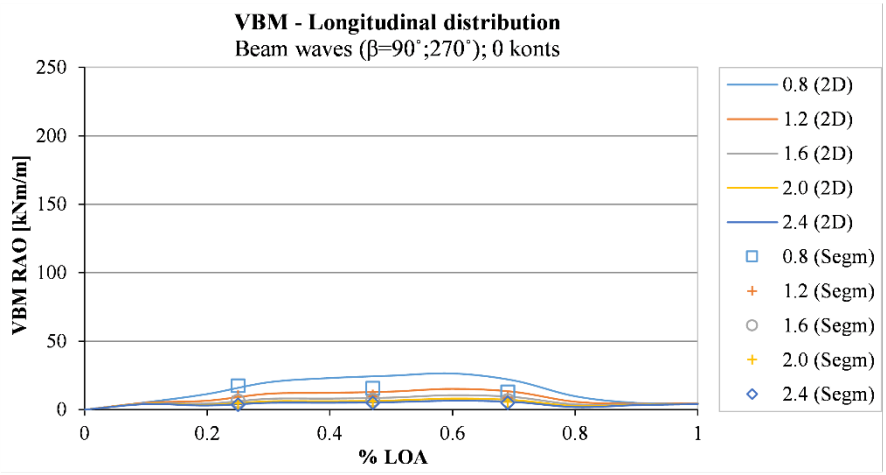

Figure 5.53. VBM longitudinal distribution in beam waves at 0kts.

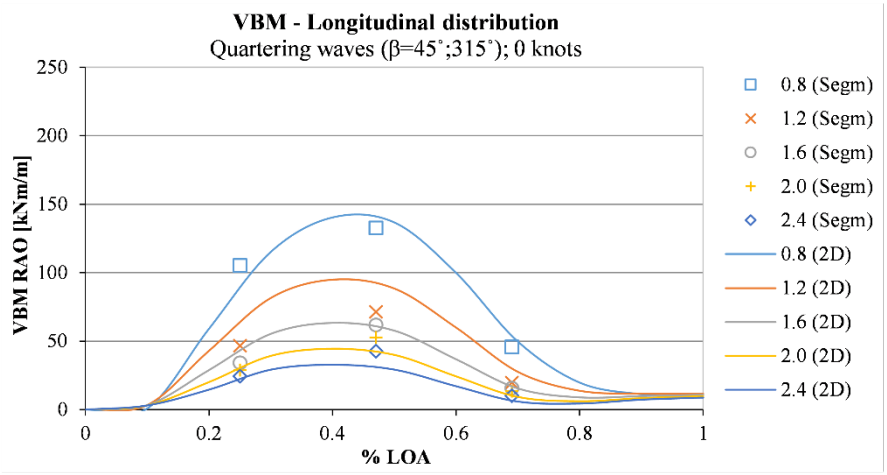

Figure 5.54. VBM longitudinal distribution in stern quartering waves at 0kts.

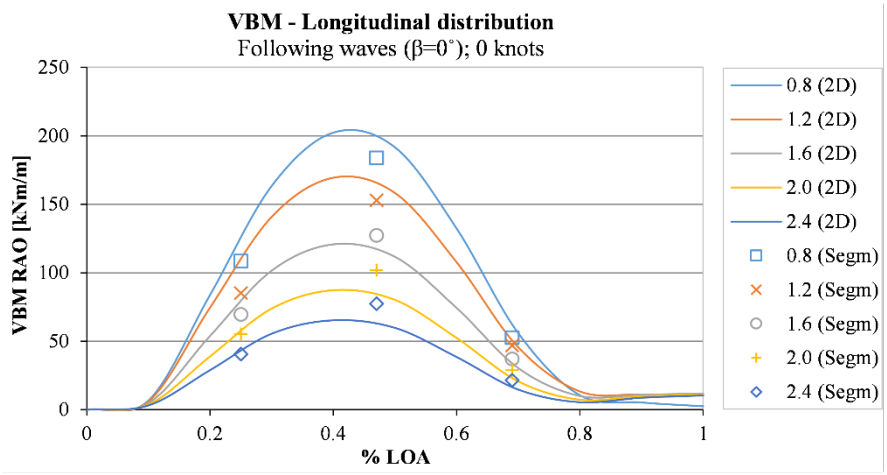

Figure 5.55. VBM longitudinal distribution in following waves at 0 kts.

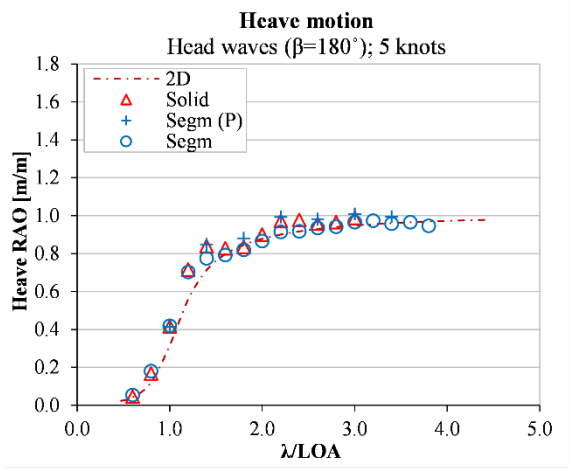

Figure 5.56. Heave in head waves at 5kts.

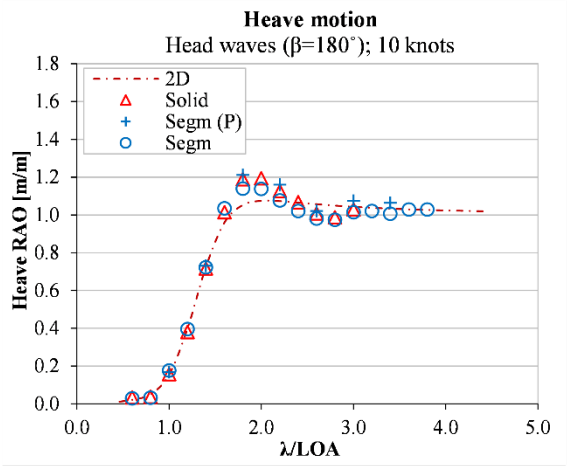

Figure 5.58. Heave in head waves at 10kts.

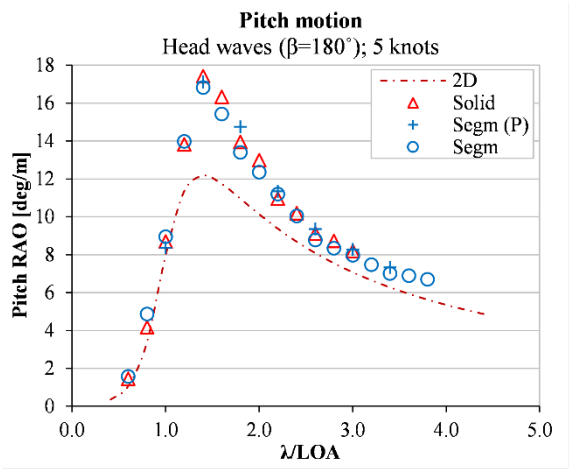

Figure 5.57. Pitch in head waves at 5kts.

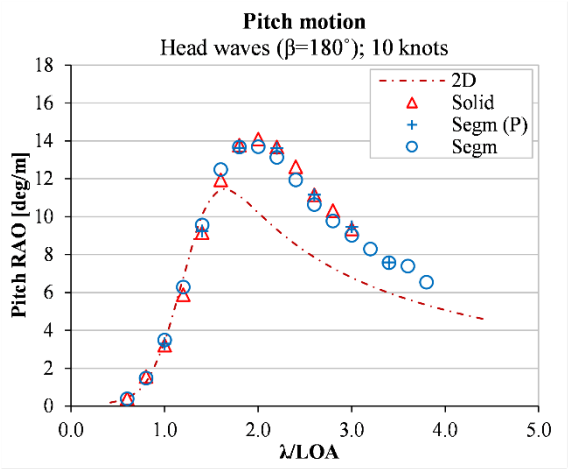

Figure 5.59. Pitch in head waves at 10kts.

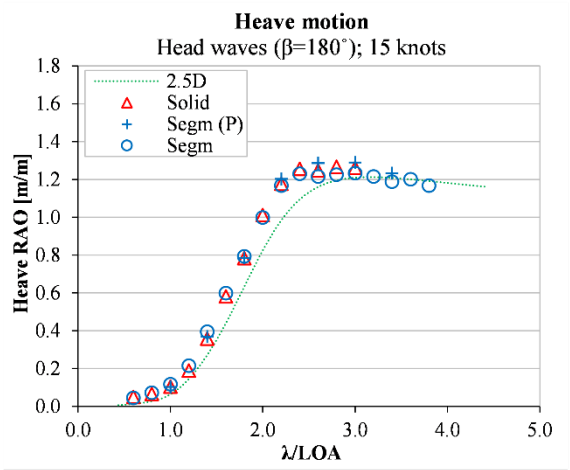

Figure 5.60. Heave in head waves at 15kts.

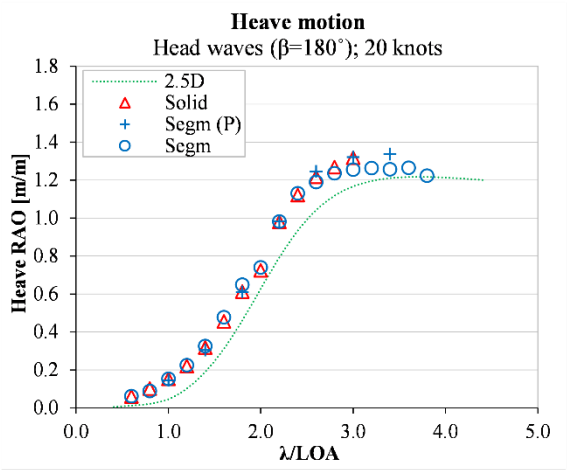

Figure 5.62. Heave in head waves at 20kts.

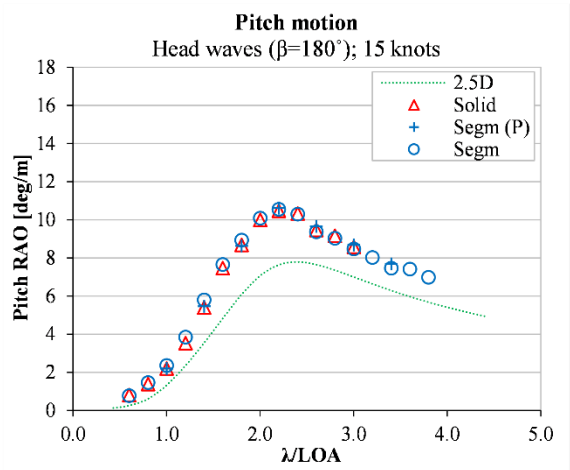

Figure 5.61. Pitch in head waves at 15kts.

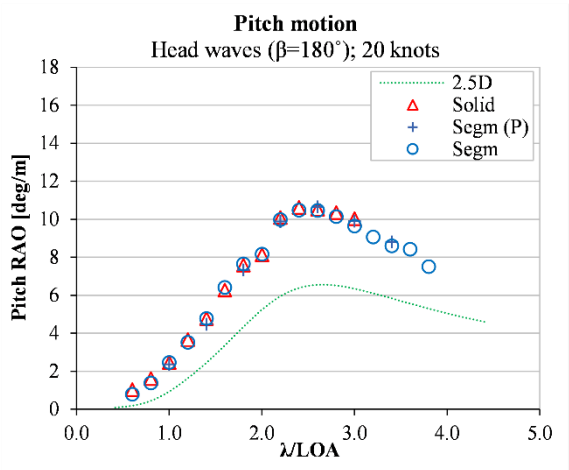

Figure 5.63. Pitch in head waves at 20kts.

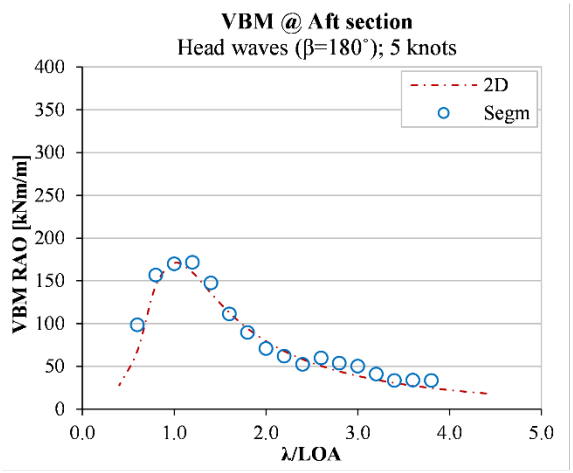

Figure 5.64. VBM at 0.25LWL in head waves at 5kts.

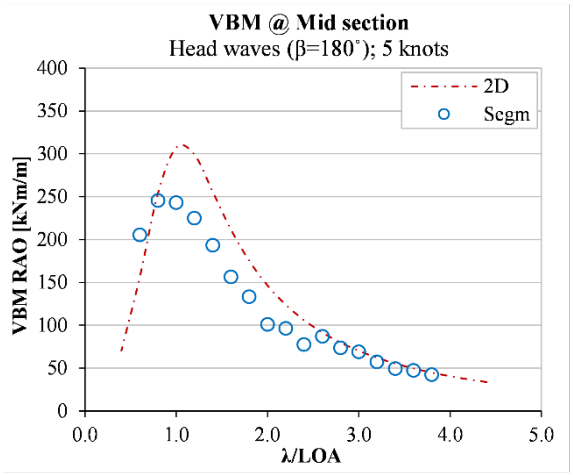

Figure 5.65. VBM at 0.50LWL in head waves at 5kts.

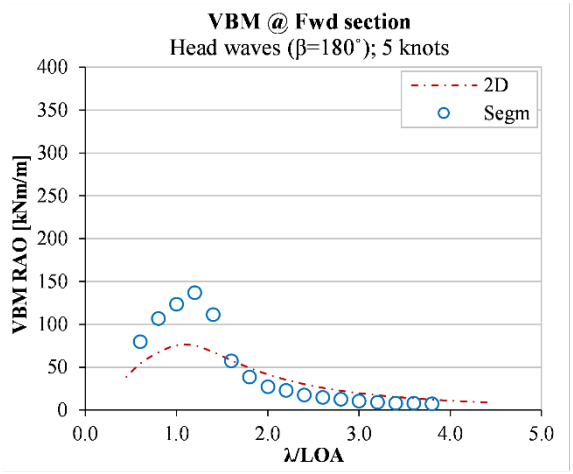

Figure 5.66. VBM at 0.75LWL in head waves at 5kts.

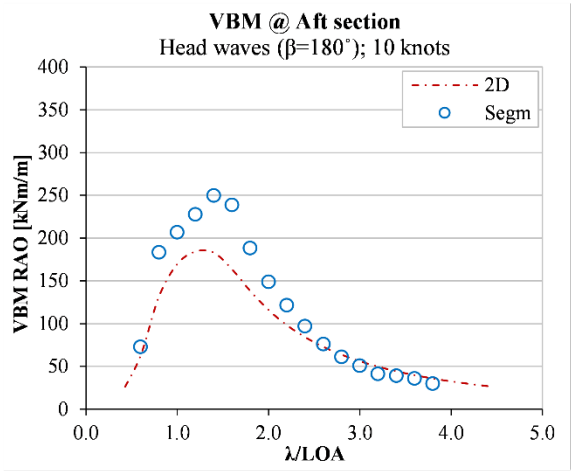

Figure 5.67. VBM at 0.25LWL in head waves at 10kts.

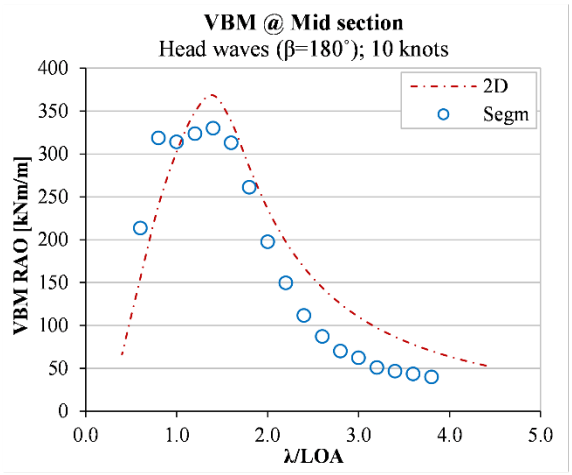

Figure 5.68. VBM at 0.50LWL in head waves at 10kts.

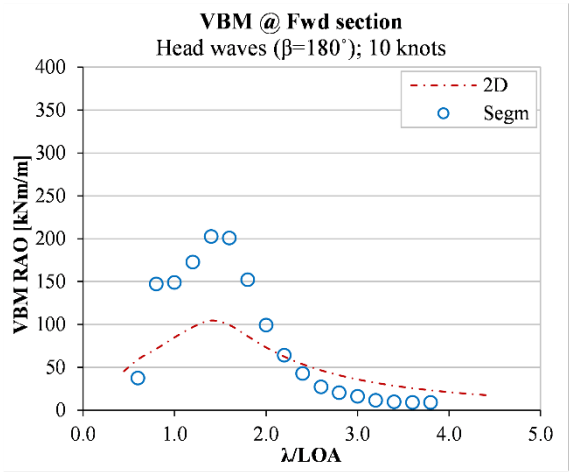

Figure 5.69. VBM at 0.75LWL in head waves at 10kts.

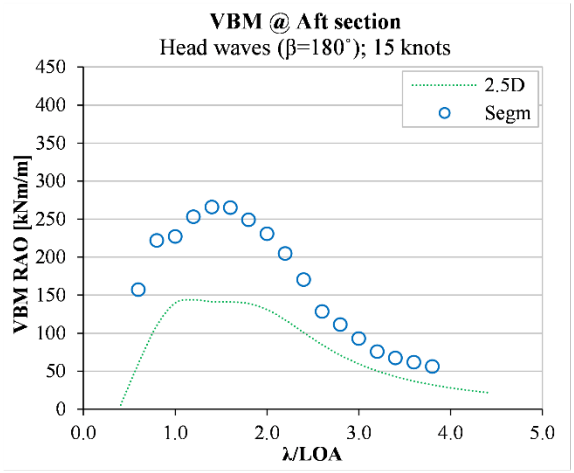

Figure 5.70. VBM at 0.25LWL in head waves at 15kts.

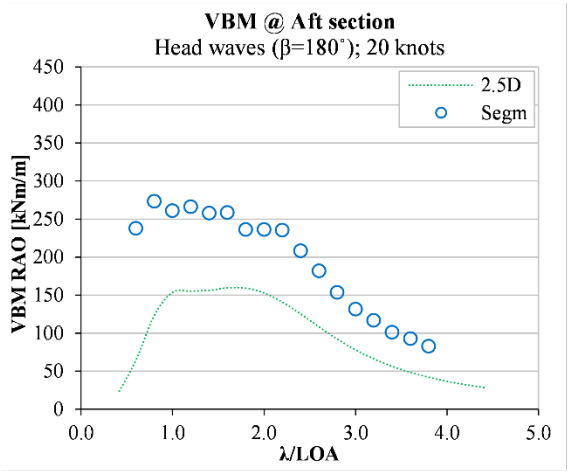

Figure 5.73. VBM at 0.25LWL in head waves at 20kts.

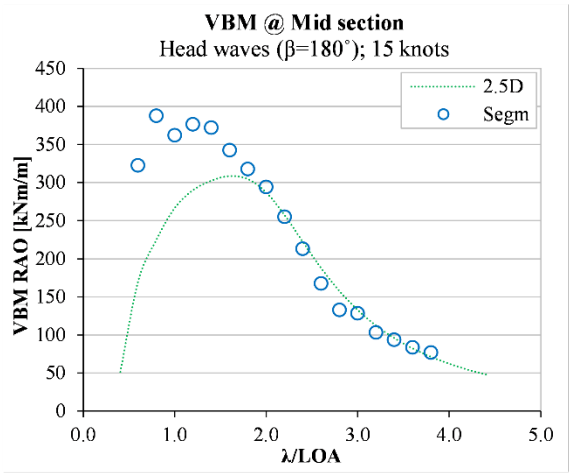

Figure 5.71. VBM at 0.50LWL in head waves at 15kts.

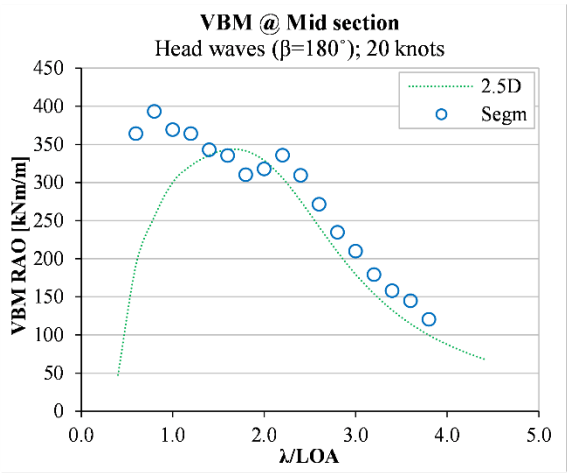

Figure 5.74. VBM at 0.50LWL in head waves at 20kts.

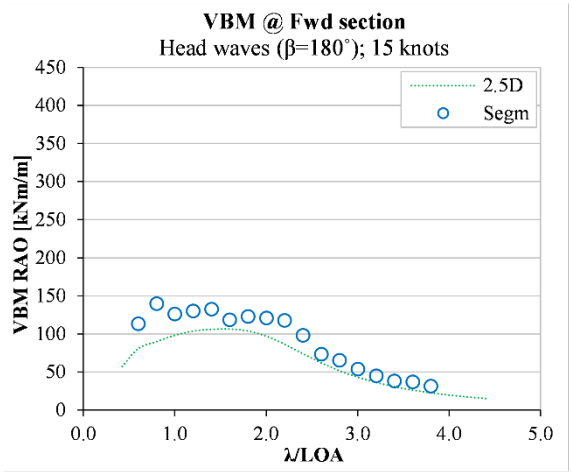

Figure 5.72. VBM at 0.75LWL in head waves at 15kts.

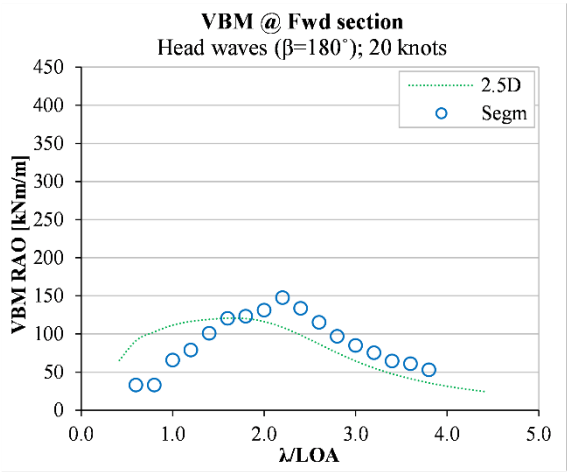

Figure 5.75. VBM at 0.75LWL in head waves at 20kts.

5.5 Discussion

5.5.1 Accuracy of the Measurement System

System sensitivity and presence of noise affected the measurement of small quantities:

- Motions and loads recorded at high wave encounter frequencies (approximately $\lambda/LOA \leq 0.6$ at zero speed and $\lambda/LOA \leq 1.0$ at forward speed in head waves).
- Roll in head/following waves as well as pitch in beam waves.
- Vertical bending moment in beam waves.
- Sinkage and trim at low speed ($V_M \leq 0.7$m/s).
- Sinkage where the hydrodynamic lift balances the downward forces causing no elevation (approximately V_M=2.0-2.5m/s as shown in Figure 5.19).

The poor accuracy of these test results becomes of little relevance because relative to operating conditions that are not of great interest. It is still recognised that a rigorous uncertainty analysis would be required to appropriately evaluate the quality of the data collected and that such an analysis could be performed on the entire dataset.

Seakeeping calculations adopted the classical formulae for deep water. These assume that the depth of the water is infinite or, with a more practical restriction, that the water depth is greater than one half of the wave length. This was not the case for tests in wavelengths $\lambda/LOA \geq 1.0$. Improvements in the data analysis could be achieved by introducing corrections for shallow-water waves.

Tests at zero speed are, in principle, never clear from interactions with the tank walls and reflected waves. Calibration of the mooring lines in order to minimise their influence on the vessel's motions whilst keeping it stationary is challenging. Moreover, it was found that the cable harness attached to the segmented model, and necessary for load measurements, visibly affected the vessel's motions at zero speed. This was not the case during tests at forward speed, where the cable harness appeared to be effectively supported by the carriage.

5.5.2 Similarity between the Hull Models

The *Solid* and *Segm (P)* series show the hydrodynamic characteristics of the two models prior to one being segmented, therefore informing on the consistency of results achieved from two similar hull models.

Figures 5.18-5.20 show drag, sinkage and trim in calm water for the two test series. The difference of the *Segm (P)* series with respect to the *Solid* series is within 3.5% for drag; 2.1% for sinkage (except for one data point at 2.1m/s. See Section 5.5.1); and 4.8% for trim. Motion responses can be firstly evaluated from Figures 5.27-5.29 showing heave, pitch and roll in beam waves at 0kts. There is certainly a larger scatter in the data and for short waves ($\lambda/LOA \leq 1.4$) rather than long ones. This is not surprising since the influence of the mooring lines on the motions of the two models was found stronger for waves generating high frequency responses. The RAO trends are the very same. Motion responses are closer in Figures 5.56-5.63, showing heave and pitch RAOs in head waves at forward speed. The average difference of the *Segm (P)* series with respect to the *Solid* series is 2.4% for heave and 2.2% for pitch.

The two series of tests on the same hull model, first as solid (*Segm (P)*) and later as segmented (*Segm*), show the effect of the segmentation on the vessel's running attitude in calm water and on its motions in waves.

Figure 5.18 clearly shows an increase of total drag, due to the segmentation of the hull, which peaks at 3.5m/s with a +18.6% of the *Segm* series on the *Segm (P)* series. This increase in resistance is explained by the augmented surface roughness of the segmented hull shell, due to the gaps between the hull segments and the sealing material. There is a much smaller effect on sinkage and trim, as shown in Figures 5.19 & 5.20 respectively. Sinkage in particular is the least influenced, with a difference at 3.5m/s of only -1.5%. At the same speed trim shows a drop of -5.7%. The influence on the seakeeping of the vessel can be firstly seen from Figures 5.27-5.29 showing heave, pitch and roll in beam seas. The distance between the two series varies with the wave length and a larger scatter is present (see Section 5.5.1), but the two series, *Segm (P)* and *Segm*, show the same trend. A better assessment can be based on the tests at forward speed, which were less affected by interference with reflected waves and the testing apparatus. Figures 5.56-5.63 show

that both heave and pitch RAOs have the same trend throughout the range of speeds and wavelengths tested. The average error of the *Segm* series on the *Segm (P)* series is 5.4% for heave and 4.1% for pitch. Whilst there is no correlation with speed, the *Segm* series, consistently shows smaller heave and pitch values in long waves, that is approximately for $\lambda/LOA>2$.

To understand if the differences in running attitude and motions should be entirely attributed to the hull discontinuity, or also to differences in the trimming and ballasting, further work would be required. It remains, however, that the largest effect is the additional drag induced by the segmentation, and that differences in the loading condition, as reported in Table 5.3, are likely to have played a minor role. It also stands out that the segmentation did not significantly alter the seakeeping of the vessel.

Conclusions on the correlation between the solid and the segmented model (*Solid* and *Segm* series respectively) can be drawn from the observations just made between the *Solid* and the *Segm (P)* series and between the *Segm (P)* and the *Segm* series. Broadly the two models show similar running attitude in calm water and similar motions in waves, but with a larger scatter from tests at zero speed, which is mainly attributed to interaction with reflected waves and the mooring lines. There are two further aspects worth noting.

The first is that the segmentation of the hull shell, and the consequent re-ballasting, did not always cause the behaviour of the segmented model to move further away from that of the solid model. This can be seen in Figures 5.19-5.20 for sinkage and trim and it is clear in Figures 5.56-5.63 for heave and pitch, where some data points of the *Segm* series are closer to the *Solid* series than those of the *Segm (P)* series. Again, this is likely to be the effect of a different loading condition, but the possibility that the segmentation affected the fluid flow, which in turn changed the forces in play, should not be excluded a priori.

The second aspect is not due to the segmentation itself but is a consequence of it. The cable harness used to measure hull girder loads on the segmented model seems to have significantly amplified heave motions at 0 speed, as visible from Figures 5.21, 5.24, 5.30

& 5.33. The effect on the rotations is less evident if not negligible (Figures 5.22, 5.23, 5.25, 5.26, 5.31 & 5.32) and the agreement with the numerical simulations, treated later in the chapter, would suggest that neither vertical bending moment was significantly affected (Figures 5.36-5.55).

5.5.3 Comparison with Numerical Simulations

The accuracy of the seakeeping simulations is evaluated according to the criteria described in Chapter 3, by comparing the three experimental data series (*Solid*, *Segm (P)* and *Segm*) against the numerical simulations (*2D* and *2.5D*).

A baseline comparison can be made from Figures 5.21-5.35 showing motions at zero speed and at different headings. The 2D strip theory (*2D*) well predicts the trends of the RAOs and is considered satisfactory in terms of magnitude of the responses. Exceptions are roll in head/following waves (Figures 5.23 & 5.35) and pitch in beam waves (Figure 5.28). In addition to the considerations made in Section 5.5.1, it is possible that differences between ideal simulations and practical tests become evident here. Figures 5.56-5.63 show that the RAO trends of heave and pitch are also well predicted by the *2D* series up to 10kts and by the *2.5D* series at higher speeds, with only minor exceptions. At 10kts the experiments show a light hump in the heave RAO plot (Figure 5.58), which is not captured by the simulations, and show the peak in the pitch RAO plot (Figure 5.59) for slightly longer wavelengths. At speeds above 10kts similar heave response magnitudes are predicted, but consistently for slightly longer waves (Figures 5.60 & 5.62). There appear to be a shift of the 2.5D series along the wavelength axis and towards the right.

In terms of response magnitude, the simulations seem to realistically capture heave motions, whilst there are notable differences for pitch. The experiments show higher pitch responses at all the speeds tested (Figures 5.57, 5.59, 5.61 & 5.63). It is possible that the linear strip methods did not correctly capture the pitching of the vessel. This could be the case at higher speeds but would not explain large differences at low displacement speeds. Instead, a bias in the experimental data could have been introduced by the towing force, which only resembles the thrust of an actual propulsion system. When

towing the model along the tank, a constantly horizontal towing force acts in place of the actual thrust, whose direction in the vertical plane would follow the attitude of the vessel. The difference between numerical and experimental estimates of pitch motions is therefore attributed to an artefact in the towing tank experiments, introduced by the towing force.

Another comparison can be made in terms of vertical bending moment, for which relevant experimental data consists of the *Segm* series only. Figures 5.36-5.50 show how the loads measured at the three instrumented stations along the hull match the 2D strip theory (*2D* series) at zero speed and at different headings. The agreement in long waves (λ/LOA>1.4) is taken as excellent, especially considering the limited size of the segmented model and the small forces in play. In shorter waves it is not surprising that differences become visible, but the 2D series still well encompasses the experimental data points. This is better shown in Figures 5.51-5.54, where the same data is rearranged to highlight how the load varies along the hull rather than with the wavelength. The 2D strip theory remains adequate also at higher speeds, as shown in Figures 5.64-5.69. The vertical bending moment RAOs at 5-10kts in head waves resemble those estimated from measurements. Differences can be observed, mainly at 0.25 and 0.75LWL, but it should be considered that at these points the longitudinal load envelope has its steepest slope, dropping from the maximum near amidships to zero at the fore and aft ends. What appears as a large gap between the two sets of data becomes less evident when considering the load distribution along the length of the vessel. At higher speeds the *Segm* series should be compared against the *2.5D* series, as presented in Figures 5.70-5.75 for head waves at 15 and 20kts. The agreement between the two series appears dependent on the wavelength. In longer waves (λ/LOA>2.0) numerical and experimental RAOs have the same trend. In shorter waves the 2.5D strip theory underestimates the loads experienced. The largest differences in the magnitude of the response seem to be towards the stern, as shown in Figures 5.70 & 5.73.

Motion and load results proved that that the classical strip theory (2D), as implemented in MAESTRO, is an appropriate tool to investigate the seakeeping of the Severn at displacement speeds (Fn≤0.4). At semi-planing and planing speeds (Fn>0.4), the high-speed strip theory (2.5D) was used and yielded reasonable motion predictions, at least

for heave. Loads were, however, underestimated, which becomes an important limitation if the objective is the load generation for structural analysis. The small-scale tests seem, therefore, to frame the applicability of the simulations within the displacement regime.

5.6 Practical Considerations

Because of the practical complexities of measuring wave loads at small scale, great emphasis was given to the technical solutions adopted for the construction and setup of the hull models. The seakeeping tests with structural load measurements were broadly successful and the results confirmed that it is possible to obtain good accuracy in the measurements even with a relatively small hull model and, therefore, small forces in play. The following considerations are given for future reference:

- The cable harness connecting the strain gauges on the segmented model to the data acquisition unit made the ballasting and testing tasks considerably more challenging, and visibly interacted with the vessel motions during stationary seakeeping tests. It is likely that larger models would be less affected, but it is advised that the harness be as light and flexible as possible. Other options could be the installation of the data acquisition unit on board or the use of wireless telemetry. The latter was not viable because of interference with the towing tank environment but other facilities may have less limitations.
- Watertightness of the hull shell successfully relied on latex strips sealing the gaps between the hull segments. A potential drawback is the latex's limited longevity in contact with water, which does not make it a long-lasting solution. It also affects the smoothness to the outer hull shell, causing considerable hydrodynamic drag that would not be present on the real vessel. Another common practice is the use of tape. Although tape is less elastic and it is difficult to ensure a good bond around complex hull forms, it is likely to result in a smaller additional drag.

5.7 Summary

The work described in this chapter is summarised in Figure 5.76. Towing tank tests were conducted with a solid and a rigid segmented hull model of the Severn Class. Motions and sectional global wave loads were measured during stationary and forward speed tests in regular waves. The tests were used to validate CFD simulations through a direct comparison of the results, presented in terms of RAOs.

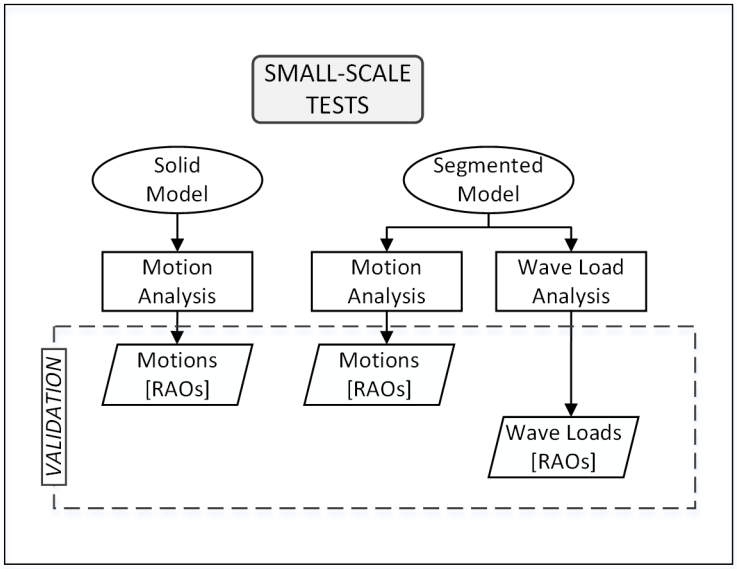

Figure 5.76. Direct calculation approach. Small-scale tests.

Chapter 6

Full-Scale Tests

6.1 Framework

Tests at full scale have traditionally been the way of validating theoretical models and laboratory tests. The technology now available, which makes full-scale experiments practically and economically viable, opens up the possibility to broaden their application. "*Using the real world as a laboratory*" (Lim *et al.* 2018), has the advantage of accounting for the complexity of the real-world phenomena, which usually impose theoretical and physical models to adopt some simplification. Full-scale tests become not only a validation tool but an aid to the design and operation of vessels.

The tests, which contribute to validating the numerical simulations and generating loads for the structural analysis, are based on the principle of measuring motions and strains. With a focus on the structure rather than on the loading, strain measurements have scientific and practical advantages compared to pressure measurements. The structural response of the vessel is measured directly and loads that have generated it are found by reverse calculation. This inherently supersedes the need to model pressures accurately enough to reproduce a realistic structural response. Data sampling rates adequate for

capturing transient responses of the structure are typically lower than those required for modelling transient pressure loads. Strain sensors do not present the shortcomings of pressure sensors (Section 2.2.6) and can be relatively easy to install.

6.2 Testing Procedure

6.2.1 Description of the Trials

The tests were conducted in the North Sea, approximately 15 nautical miles offshore from Tynemouth (UK), and consisted of several one-day dedicated seakeeping trials. The trial days were selected based on the expected sea state and each trial was conducted at a given speed and at a number of headings.

Throughout each trial the speed over ground was kept constant by adjusting the engines RPM as required. The trim tabs were set to 'rest' position, fully lifted, and never adjusted, consistently with the scope of the work (Chapter 3). Data was collected continuously from on-board sensors and wave buoys, whilst a record sheet was used to manually record additional information.

All the trials were conducted with full fuel tanks at departure from the lifeboat station. Displacement and centre of gravity position of the lifeboat were already known from previous inclining tests. For further estimates of the loading condition the total crew weight was assessed based on the crew members aboard on the day, the fuel consumed was recorded at the end of each trial and draft mark readings were taken in conjunction with measurements of the water density before and after each trial.

6.2.2 Test Matrix

The size of the test matrix was a compromise between the cost and effort of the task, and the need to collect data in conditions wide-ranging enough to provide a good picture of the loads experienced during operation. The scope of the experiment was limited to one lifeboat and one sea area. The combination of sea states and speeds to test, reported in Table 6.1, was found as follows:

- The sea state was judged in terms of wave height only, recognising that the sea spectral shape would have been unique for each trial and that including the wave period as a variable into the test matrix was not practically feasible. The state of the sea (significant wave height Hs or Douglas Sea Scale) was divided into 4 tiers: calm (Hs≤1.25m, Douglas 1-3); moderate (1.25<Hs≤2.5m, Douglas 4); rough (2.5<Hs≤4m, Douglas 5) and extreme (Hs>4m, Douglas 6-9,). In the North Sea, which is partially sheltered, the probability of an extreme sea to occur is very low. The last tier was therefore not considered, since the possibility of carrying out a trial in those sea conditions would have been a rare occasion.
- The trial speeds were chosen as 5, 15 and 25 knots to cover the whole speed range of the Severn. It was anticipated that travelling at 15 or 25 knots would have not always been possible in rough sea conditions. The test matrix was therefore modified and trials in rough seas were conducted at 5, 10 and at the maximum allowable constant speed that the crew deemed to be safe on the day chosen for that specific trial.

One trial was repeated because the sea conditions were not those expected and because of technical issues with the data acquisition system that made necessary the collection of extra data for redundancy. The actual test matrix is reported in Table 6.2.

5 knots Calm	5 knots Moderate	5 knots Rough
15 knots Calm	15 knots Moderate	10 knots Rough
25 knots Calm	25 knots Moderate	Max allowable Rough

Table 6.1. Target sea trial matrix.

5 knots Hs=0.6m, Tp=3.8s, Tz=3.3s	5 knots Hs =1.6m, Tp=6.9s, Tz=4.8s	5 knots Hs=3.0m, Tp=8.7s, Tz=6.5s
15 knots Hs =0.4m, Tp=5.1s, Tz=3.9s	15 knots Hs =1.7m, Tp=4.9s, Tz=4.6s	10 knots Hs=4.5m, Tp=10.0s, Tz=7.8s
25 knots Hs =1.3m, Tp=11.7s, Tz=5.9s	25 knots Hs =1.5m, Tp=10.3s, Tz=5.9s	20 knots Hs=3.1m, Tp=10.3s, Tz=7.1s

Table 6.2. Achieved sea trial matrix.

6.2.3 Trial Area and Trajectory

The tests took place offshore from Tynemouth (UK). A minimum distance from the shore had to be maintained to avoid systematic errors in the results due to shallow waters and coastal effects. Based on theoretical knowledge and experience of the local crew, a minimum distance of 5-6 nautical miles from the shoreline, corresponding to a water depth of 50 metres, was considered appropriate to avoid coastal effects. A practical restriction to conduct seakeeping calculations under the deep-water assumption is that waves should be of length inferior to twice the water depth. The chosen water depth would therefore make the deep-water formulae applicable to waves up to 100m long, hence over five times the length of the Severn. Based on the size of the vessel, the expected sea states and associated wavelengths, a 50m water depth was also considered suitable to adopt the formulae for deep water in the seakeeping calculations. Furthermore, the 50-metre bathymetry line is easily identifiable on navigation charts, which is practical for positioning and orienting the trial trajectory according to the principal wave direction on the day of the trial.

Dedicated seakeeping tests often involve runs at different headings to understand the vessel behaviour in a range of operating conditions. An appropriate sequence can minimise the gap between the runs and the average distance from a wave measuring device, such as a wave buoy. The first aspect becomes important to minimise the downtime and the risk of the sea conditions changing during the trial. The second is even more relevant if the ship responses are to be related to the exciting waves. A long distance from the wave measuring device means that wave measurements could be unrepresentative of the wave conditions seen by the vessel. An appropriate sequence of legs can also minimise the effect of factors that, by changing during the trial, such as displacement and tidal currents, influence the results.

Johnson (2004) reviewed common trial trajectories. The simplest involve five legs covering head sea, following sea and bow quartering, beam and stern quartering sea on one side only, either port or starboard. Such a trajectory is reported for example by Lloyd (1989). Johnson instead recommends eight legs at 45° intervals as a minimum to fully account for the effect of the seaway on the ship responses. An octagonal trajectory represents the easiest option, with the drawback that it can have a large diameter.

The trajectory adopted for the trials was a 'star' devised to test headings from head to following sea, both port and starboard, at 45° intervals. This results in the 8-legs star pattern shown in Figure 6.1, which has the advantage of minimising the average distance from the wave buoy as compared to a simple octagon. As commented by Johnson, the disadvantage would be the increased time spent in turns, but this becomes irrelevant for a small craft.

The time spent on any one heading determines the number of motion and load cycles recorded, which should be high enough to create a statistically significant sample. The presence of tidal currents that affect the wave spectrum also plays a role. As suggested by Johnson (2004), short trials tend to be bound to a larger systematic error than long trials, which are more likely to include slack water and current in both directions. On the other hand, the data analysis is simpler if it can be considered that the sea has remained uniform and statistically stationary during the whole trial. This is the case for a limited amount of time, typically 1 to 4 hours (Lewis 1988a).

A compromise was found by setting the time spent at each heading so that a minimum of 100 wave encounters would have occurred, as suggested by Lloyd (1989). The leg time was found from an analysis of the wave scatter diagrams for the North Sea (Bales *et al.* 1981, Lee and Bales 1984, Lee 1995). The significant wave height was divided into 4 tiers, as described in the previous section. For calm to rough seas, the minimum, most probable and maximum modal periods were extracted. The associated wave length and celerity were found using the classical formulae for deep water. These, combined with the vessel heading and speed, returned an estimate of the time needed to encounter 100 waves, on top of which a 15% contingency was added. In following and stern quartering seas the calculated wave encounter period can be very long, meaning that in those conditions the vessel would tend to ride the same wave with consequently long encounter cycles. This is mostly due to the simplified calculations that only consider the modal period of the sea spectrum, which is in fact a combination of waves of different lengths and periods. In those cases the leg duration was limited to what was practically achievable.

Since the wave period tends to increase with the wave height, the longest time is usually required in rough seas. It was also found that the most probable wave period of a rough sea approximately includes the maximum wave period of a moderate or calm sea. Hence the rough sea was adopted as a reference for all the sea states, the advantage being that, for a given speed, the same star pattern could be used in different sea states in spite of the actual sea conditions during the trial, whilst being conservative in calm and moderate seas.

A consequence of this approach is that the legs of the star trajectory have different lengths depending on the heading. This becomes clear if it is considered that the encounter frequency is a function of the heading and ergo that to encounter the same number of waves less time is required in head sea than in following sea. The conceptual star pattern represented in Figure 6.1 becomes asymmetric (Figure 6.2). A 9th leg that would be needed to return towards the wave buoy is also added.

The wave encounter period is also a function of the vessel speed. At speeds as low as 5 knots the effect is almost negligible and a symmetric star with equal time spent at each heading could in theory be adopted. At higher speeds less time is required in head sea and a much longer time is required in following sea. At 25 knots the difference becomes considerable, with head sea runs that require approximately 10 minutes against following sea runs that could require over 1 hour. Within this time more than 25 nautical miles would be travelled and the distance from the wave buoy would be too large to relate the vessel responses to the wave spectrum measured at the buoy location. For speeds of 15 knots and above, the star pattern was modified by splitting up stern quartering and following sea legs into two or more legs. The modified star decreases in diameter and so does the distance from the wave buoy. Its shape for a trial at 25 knots is shown in Figure 6.3. Recognising that the abovementioned calculations had the objective of ensuring the collection of enough data at each heading, manual adjustments were made at the final stage for practical reasons. The details of each star trajectory as undertaken are reported in Tables 6.3-6.7 and in Appendix 4.

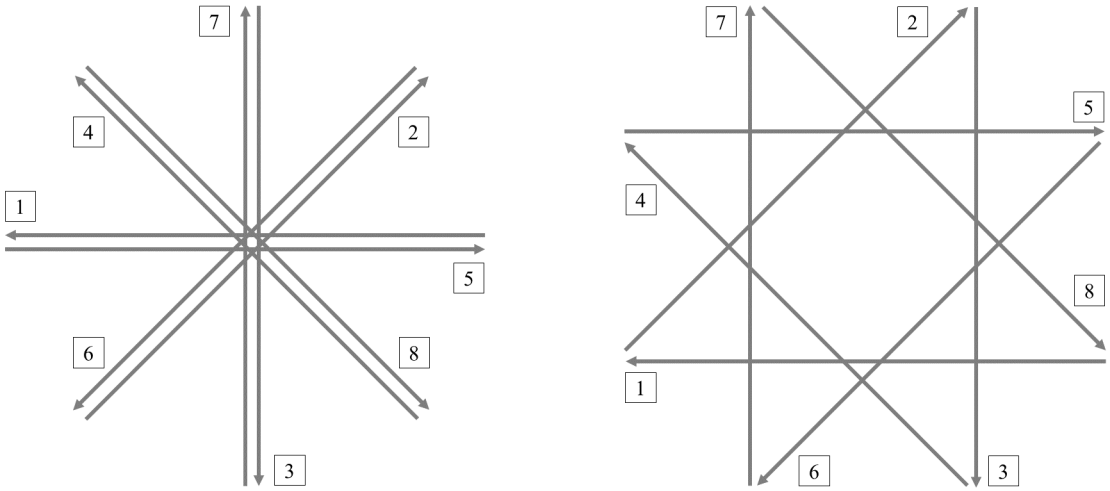

Figure 6.1. Trial trajectory. Symmetric 'star' pattern with 8 legs at 45° intervals.

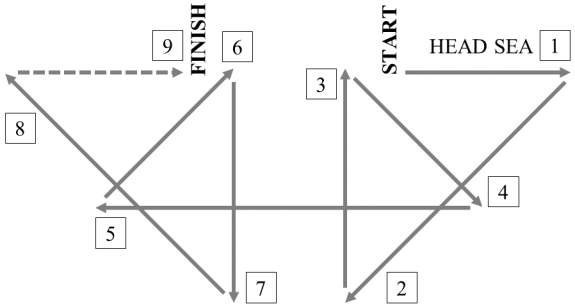

Figure 6.2. Trial trajectory. Asymmetric 'star' pattern with 8(+1) legs at 45° intervals.

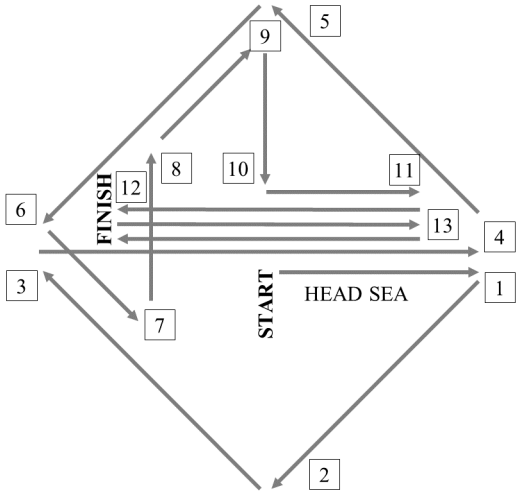

Figure 6.3. Trial trajectory. Asymmetric 'star' pattern modified for high-speed trials.

Speed [kts]	Leg [No]	Heading	[deg]	Duration [mins]	Distance [NM]
5	1	Head	180	16	1.3
	2	Stern Quartering Pt	225	22	1.8
	3	Beam Stb	90	18	1.5
	4	Bow Quartering Pt	225	16	1.3
	5	Following	0	22	1.8
	6	Bow Quartering Stb	135	16	1.3
	7	Beam Pt	270	18	1.5
	8	Stern Quartering Stb	45	22	1.8
	9	Head	180	16	1.3
Total				**166**	**14**

Table 6.3. Sea trial trajectory at 5kts. Leg breakdown.

Speed [kts]	Leg [No]	Heading	[deg]	Duration [mins]	Distance [NM]
10	1	Head	180	15	2.5
	2	Stern Quartering Pt	225	25	4.2
	3	Beam Stb	90	18	3.0
	4	Bow Quartering Pt	225	15	2.5
	5	Following	0	30	5.0
	6	Bow Quartering Stb	135	15	2.5
	7	Beam Pt	270	18	3.0
	8	Stern Quartering Stb	45	25	4.2
	9	Head	180	15	2.5
Total				**176**	**29**

Table 6.4. Sea trial trajectory at 10kts. Leg breakdown.

Speed [kts]	Leg [No]	Heading	[deg]	Duration [mins]	Distance [NM]
15	1	Head	180	14	3.5
	2	Stern Quartering Pt	315	30	7.5
	3	Beam Stb	90	18	4.5
	4	Bow Quartering Pt	225	14	3.5
	5	Following	0	20	5.0
	6	Bow Quartering Stb	135	14	3.5
	7	Beam Pt	270	18	4.5
	8	Stern Quartering Stb	45	30	7.5
	9	Head	180	20	5.0
	10	Following	0	20	5.0
	11	Head	180	14	3.5
Total				**212**	**53**

Table 6.5. Sea trial trajectory at 15kts. Leg breakdown.

Speed [kts]	Leg [No]	Heading	[deg]	Duration [mins]	Distance [NM]
20	1	Head	180	13	4.3
	2	Stern Quartering Pt	315	17	5.7
	3	Stern Quartering Stb	45	17	5.7
	4	Head	180	24	8.0
	5	Stern Quartering Stb	45	17	5.7
	6	Stern Quartering Pt	315	17	5.7
	7	Bow Quartering Pt	225	13	4.3
	8	Beam Stb	90	18	6.0
	9	Bow Quartering Stb	135	13	4.3
	10	Beam Pt	270	18	6.0
	11	Following	0	25	8.3
	12	Head	180	25	8.3
	13	Following	0	25	8.3
Total				**242**	**81**

Table 6.6. Sea trial trajectory at 20kts. Leg breakdown.

Speed [kts]	Leg [No]	Heading	[deg]	Duration [mins]	Distance [NM]
	1	Head	180	12	5.0
	2	Stern Quartering Pt	315	23	9.4
	3	Stern Quartering Stb	45	23	9.4
	4	Head	180	36	15.0
	5	Stern Quartering Stb	45	23	9.4
	6	Stern Quartering Pt	315	23	9.4
25	7	Bow Quartering Pt	225	12	5.0
	8	Beam Stb	90	18	7.5
	9	Bow Quartering Stb	135	12	5.0
	10	Beam Pt	270	18	7.5
	11	Head	180	12	5.0
	12	Following	0	23	9.6
	13	Head	180	16	6.7
	14	Following	0	23	9.6
Total				**272**	**113**

Table 6.7. Sea trial trajectory at 25kts. Leg breakdown.

6.3 Data Acquisition

6.3.1 Sea State Measurement

A measurement of the sea state is necessary to correlate motions and structural response to the wave environment. A comprehensive review of techniques for ocean wave measurements can be found in Johnson's work (2004). Visual estimates of the wave height and period were the only option before the advent of technological devices for wave measurement. Relations between observed and measured values were later proposed, as summarised by Lloyd (1989). In addition to the obvious limits to the reliability of visual estimates, even observations made by experienced sailors lack a complete description of the spectral shape. This is important if one of the objectives is to recover the RAOs of a ship response or to assess some aspects, such as slamming, that are largely dependent on the wave period in addition to the wave height. Wave estimation through ship motion analysis has also been attempted (Tannuri *et al.* 2003, Nielsen 2006, Drouet *et al.* 2013), although a more rigorous method is nowadays considered a requisite for seakeeping trials.

An important aspect that drives the analysis of data from sea trials is whether the measurement is taken at the vessel position or in the trial area. In the first case, an event

in the vessel response can be related to the wave that has generated it. Wave measurements at the vessel can be obtained through on-board systems, such as bow-mounted radars and wave radars. Considerations on the wave data that these technologies provide are not discussed, since neither of these options was practical: bow-mounted radars could not be mounted on an operational lifeboat because of the risk of damaging the equipment during rescues; and wave radars still come at a prohibitive cost and are not proven to be reliable in rough and confused seas. Wave measuring devices not mounted on board exclude the possibility to directly relate a ship response to a wave, since the device will be at some distance from the vessel or will provide averaged values for an area of sea surface. Within this category of devices there are wave buoys, satellite altimetry radars and mathematical hindcast models. As concluded by Johnson (2004), wave buoys were rated as the best compromise, combining accuracy, ease of handling, reliability and cost.

A wave buoy, deployed central to the trial area and left free to float for the whole duration of each trial, was used as the principal source of wave data. The buoy was a Directional Waverider DWR-G4 (de Vries *et al.* 2003, Jeans *et al.* 2003, Datawell B.V. 2014), which consists of a sphere with a diameter of 0.4m and a weight of 17kg. It was easy to store on deck, and to deploy and recover in any sea condition without davits. Due to its small size, a danbuoy was loosely tied to it to increase its visibility.

Forward (North), transverse (West) and vertical (heave) displacements are generated through a GPS-based motion sensor installed on the wave buoy. The GPS technology supersedes the need for calibration of accelerometer and compass based sensors, and it is not affected by spinning or manual handling. One potential disadvantage is that wave wash on the buoy's GPS antenna or extreme tilting could mask the signal and interrupt the measurement. In fact, this only happened sporadically and for a few seconds during the whole deployment time. Displacements are sampled at 1.28Hz, which allows to capture wave periods as short as 1.6s (≈4m wavelength). Despite the relatively small size of the vessel, this was enough to calculate, through a spectral analysis, the RAOs of the ship responses for the whole range of wavelengths of interest.

Additional wave data was obtained from two wave buoys moored approximately 10 nautical miles North ('Newbiggin' buoy) and 23 nautical miles East-South-East ('Tyne/Tees' buoy) from Tynemouth, respectively operated by the Channel Coastal Observatory (CCO) and the Centre for Environment, Fisheries and Aquaculture Science (Cefas) in the UK. Visual observations were taken at the start and end of each trial. These mainly relied on the crew's experience and on wind-to-sea state correlation pictures (National Oceanic and Atmospheric Administration 1987, Met Office 2010).

6.3.2 On-Board Instrumentation

To explain the quantities measured during the tests and the choices made for the data acquisition, it is worth re-stating the main objectives of the task:

1. Validate the numerical simulations in terms of motions and wave loads.
2. Include into the loading envelope the highly dynamic load effects neither captured numerically nor at small scale.
3. Collect data on accelerations experienced by the crew to support the RNLI in separate work.

Based on a preliminary feasibility study, the trials involved the measurement of the following quantities:

- Rigid body motions (objectives 1 & 3)
- Hull girder bending moments (objective 1)
- Hull bottom pressure (objective 1)
- Hull bottom and bow flare slamming (objective 2)
- Green water impacts on deck (objective 2)
- Accelerations in the wheelhouse (objective 3)

System specifications

In addition to the typical requirements for on-board data collection, the system had to allow the lifeboat to be on call during the trial period, which was protracted for several months. The design of the data acquisition system largely benefited from the RNLI's experience of past trials and from the expertise of the research team behind this work.

Data was collected through three separate systems, detailed in Table 6.8. The cabling was shielded to prevent electrical interference with other on-board equipment and the cable routing was realised to maintain the watertight integrity and the self-righting ability of the lifeboat (Figures 6.4-6.5). Part of the apparatus was devised to be disembarked after each trial to minimise the disruption to SAR operations (Figures 6.6-6.7). The remainder was devised to be stripped off, without damaging the structure, at completion of the task.

Sensor layout

The sensor layout can be found in the technical drawings reported in Appendix 5. Motion data was collected with an accelerometer and a rate gyro positioned at the centreline, close to the centre of gravity of the vessel. These recorded accelerations and angular velocities, from which displacements could be found through integration over time. Additional acceleration data useful to the RNLI was collected from a standalone data recorder in the wheelhouse.

Hull girder bending strains were measured at five stations along the hull. Depending on the structural layout, each station was instrumented with either three or four strain gauges, positioned on the hull bottom and on the deck. On the hull bottom, the strain gauges were bonded to either primary longitudinal supports or to the centreline keel (Figure 6.8). On the deck, the hull-to-deck joint was used instead of a primary structural member, as it was deemed to be stiff enough to deform under global loads only (Figure 6.9). The strain gauge layout was always symmetric with respect to the centreline to enable isolation of the vertical and horizontal bending strains from a complex loading scenario.

The local deformation of a structural panel due to water pressure was measured on ten panels: six on the hull bottom, two at the bow and two on the fore deck. Except for the deck, the panels instrumented were symmetric port and starboard. Each panel was instrumented with four strain gauges oriented along the longitudinal centreline of the panel: two near the supported edges and two at the panel midspan (Figures 6.10 & 6.11).

Sys	Type	Description	No	Supplier	Model
	Strain gauge	Monoaxial, foil type	58	VPG MM	CEA-00-250UW-350
	Accelerometer	Triaxial	1	MEAS	7132A
A	Rate gyro	Triaxial	1	MEAS	31206B
	Thermocouple		2	RS	Type K
	Data logger unit	Main data logger	1	VPG	System 7000
	Accelerometer	Triaxial			
B	GPS sensor		1	Dyena	120301-04
	Data logger unit	Standalone data logger			
C	HF receiving antenna HF link receiver	Wave data receiver	1	Datawell	RX-C

Table 6.8. On-board instrumentation.

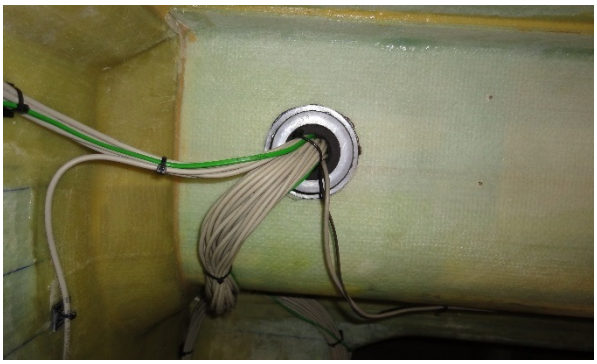

Figure 6.4. Cable routing to maintain watertightness of the compartments.

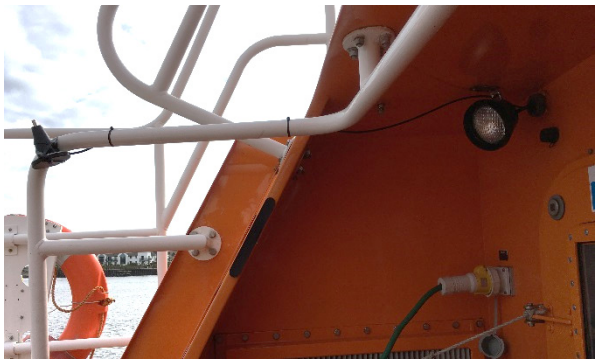

Figure 6.5. HF antenna cable routing to maintain watertightness of the wheelhouse.

Figure 6.6. Data acquisition unit secured to a survivor seat.

Figure 6.7. HF link receiver and laptops secured to the stretcher.

This layout was devised to retrieve both the strain due to highly dynamic loads, such as slamming or green water on deck, and the strain due to quasi-static wave loads.

A sufficient strain gauge size was required to obtain readings representative of the strain in the laminate rather than of microstructural strain fluctuations occurring at the interface between fibres and compound or between warp/weft fibres. General guidance (e.g. Lang and Chou (1998), Vishay Precision Group (2014)) is that the size of the measuring grid, mostly its length, should to be large with respect to the inhomogeneities of the underlying material. Based on the reinforcement plies used for the Severn, strain gauges with a measuring grid of 6.35x4.57mm were selected.

Strain signals were compensated for unwanted temperature effects. These consist of the thermal expansion, or contraction, of the structure due to temperature variations during the trial, which produce a thermally-induced strain output from the strain gauges. The compensation made use of two thermocouples, one in the engine room and one in the survivor space bilge. Each strain gauge was assigned to one of the two thermocouples, depending on its location. The compensation was applied at a data processing level using the temperature readings and the thermal output coefficients of the strain gauges.

Sampling frequency

In Chapter 2 a classification of seakeeping structural loads was made according to the frequency at which the loads occur. The sampling frequency was chosen based on the same principle, hence signals were sampled at different frequencies depending on their nature: accelerations and strains due to local pressure loads were sampled at 2048Hz; angular velocities and strains due to hull girder loads at 256Hz. The resultant measurement types and sampling frequencies are detailed in Table 6.9.

With regard to slamming, a 2kHz sampling rate may seem, at first, insufficient. In the literature, values as high as 5-10kHz are not unheard of, but what is usually in question is the slamming pressure, typically measured with pressure sensors. The difference is substantial: whilst a pressure front due to slamming travels rapidly, requiring very high sampling frequencies, the response of a structure to the same pressure front does not necessarily happen at the same rate. In fact, a structure such as a supported hull bottom

panel, would tend to react at its natural frequencies. The results obtained gave confidence that the data was adequately sampled and that it was possible to detect and measure the magnitude of rapid strain peaks due, for example, to slamming.

Measurement	Sensor	Sampling Frequency [Hz]	No. of axes	Quantity	Channels
Hull girder bending moments	Strain gauge	256	1	18	18
Hull bottom slamming	Strain gauge	2048	1	24	24
Bow flare slamming	Strain gauge	2048	1	8	8
Green water impacts	Strain gauge	2048	1	8	8
Temperature compensation	Thermocouple	256	1	2	2
Whole boat accelerations	Accelerometer	2048	3	1	3
Whole boat angular velocities	Rate gyro	256	3	1	3
Total				**62**	**66**

Table 6.9. Measurements and sampling frequencies.

Figure 6.8. Strain gauge bonded to a primary longitudinal structural member.

Figure 6.9. Strain gauge bonded on the deck in way of the hull-to-deck joint.

Figure 6.10. Strain gauges bonded to a hull bottom panel.

Figure 6.11. Strain gauges bonded to two bow panels on the port and starboard side.

6.3.3 Manually Recorded Data

Further information to aid the data analysis was recorded manually on a trial record sheet, reported for reference in Appendix 6. This information is summarised as follows:

- Sea and wind state assessments at the start and end of the trial
- Local high water times on the day of the trial
- Water specific gravity and draft marks readings before and after the trial
- Structural integrity visual inspection before and after the trial (rough seas only)
- Fuel consumed for the whole trial
- GPS coordinates at the turning points
- Times at the turns
- Compass heading
- Speed over ground and through water
- Trim angle
- Engines RPM
- Buoy GPS position

6.4 Data Analysis Basics

Whilst full-scale trials are invaluable for assessing the response of the actual vessel in a real seaway, the data analysis is challenging and can significantly affect the outcome. Broadly three aspects are at the basis of the data analysis conducted.

The first is related to the frequency at which the vessel responses occur. Quantities changing slowly over time would be observed as drift, a low frequency component or even a slowly moving trend; wave-induced responses are cyclic and related to the wave encounter frequency; and slamming-induced responses tend to be vibratory and to occur at higher frequencies, typically the natural frequency of the structure or the structural member reacting to the load. These effects are all superimposed in a raw signal. The analysis relies on frequency-based filters to isolate the response of interest from the raw signal.

The second aspect concerns the conversion of the quantity measured into a quantity useful to the study. Central to the data analysis is the calculation of sectional and pressure loads from strain measurements, but a similar task would be required to convert accelerations and angular velocities to body displacements. Whilst there is no single theory that suits all cases, different methods can be adopted depending on the nature of the conversion required.

The third aspect is related to the wave information. A directional wave buoy provides a comprehensive description of the wave environment during the whole trial, but this is relative to the buoy's location and not the vessel's. Since it is impossible to relate an event in the vessel response to the exciting wave, and because of the irregular and random character of the sea, data is to be treated with appropriate statistical theories.

The following sections expand these three aspects through the assessment of wave and slamming induced loads. Data filtering, strain-to-load conversion and statistical analysis are undertaken in the most convenient sequence, which varies depending on the dataset analysed.

6.5 Analysis of Wave Data

6.5.1 Visual Estimates

Visual observations of the sea state were made at the start and end of each trial and included estimates of the wave height H_{obs}, wave period T_{obs} (calculated from the estimated wave length defined in 'hull lengths') and wave direction Dir_{obs}. Averaged values for each trial are presented in Table 6.10 against wave buoy measurements. Visual estimates of the wave height (H_{obs}) correspond reasonably well to measurements of the significant wave height Hs, with an average error below 10%. Visual estimates of the wave period (T_{obs}) are closer to the measured zero-crossing wave period Tz than the spectrum peak period Tp. The average error of T_{obs} with respect to Tz is less than 15%. Visual estimates of the wave direction (Dir_{obs}) can differ significantly from the measured primary (spectrum peak) wave direction Dirp, in particular for multimodal or confused seas. This does not imply that visual estimates should be regarded as unreliable, but rather that the wave spread cannot always be ignored. For reliable comparisons the

entire wave direction spectrum (as shown later in Section 6.9.3) should be considered, which is only possible when using a directional wave buoy as opposed to a non-directional one.

Trial	Visual Assessment	Deployed Wave Buoy
5 knots Calm	H_{obs}=0.7m T_{obs}=3.6s Dir_{obs}=180°	Hs=0.6m Tp=3.8s, Tz=3.3s Dirp=122°
15 knots Calm	H_{obs}=0.4m T_{obs}=3.6s Dir_{obs}=065°	Hs=0.4m Tp=5.1s, Tz=3.9s Dirp=068°
25 knots Calm	H_{obs}=1.0m T_{obs}=3.6s Dir_{obs}=045°/135°	Hs=1.3m Tp=11.7s, Tz=5.9s Dirp=015°
5 knots Moderate	H_{obs}=1.8m T_{obs}=5.0s Dir_{obs}=160°	Hs=1.6m Tp=6.9s, Tz=4.8s Dirp=122°
15 knots Moderate	H_{obs}=1.9m T_{obs}=3.6s Dir_{obs}=250°	Hs=1.7m Tp=4.9s, Tz=4.6s Dirp=254°
25 knots Moderate	H_{obs}=1.5m T_{obs}=5.0s Dir_{obs}=020°	Hs=1.5m Tp=10.3s, Tz=5.9s Dirp=025°
5 knots Rough	H_{obs}=2.9m T_{obs}=6.2s Dir_{obs}=100°	Hs=3.0m Tp=8.7s, Tz=6.5s Dirp=087°
10 knots Rough	H_{obs}=4.3m T_{obs}=6.2s Dir_{obs}=085°	Hs=4.5m Tp=10.0s, Tz=7.8s Dirp=072°
20 knots Rough	H_{obs}=2.7m T_{obs}=6.2s Dir_{obs}=135°	Hs=3.1m Tp=10.3s, Tz=7.1s Dirp=060°

Table 6.10. Sea state visual observations and wave buoy measurements.

6.5.2 Wave Buoy Data

Information on the sea state (Section 6.3.1) was gathered from the following sources: visual observations, moored wave buoys ('Newbiggin' and 'Tyne/Tees'), and a deployable wave buoy. A preliminary assessment confirmed the reliability of the data collected by the wave buoy deployed in the trial area, which was used for the data analysis.

6.5.3 Displacement Time Histories

Datawell's Directional Waverider buoys (Datawell B.V. 2014), such as the DWR-G4, currently generate raw North, West and vertical displacements that are processed by the buoy to produce wave spectra and descriptive statistics. Both the raw and the processed data are stored in the buoy's data logger and output through a radio link.

Whilst the 'live' data received via radio from the wave buoy provided useful feedback on the sea conditions and principal wave direction during the trials, the data analysis relied on the data stored in the buoy's data logger. This was not affected by temporary losses of radio signal due to the large distance that there was, at times, between the vessel and the wave buoy.

6.5.4 Wave Spectrum

In oceanography the use of Fourier analysis to transform the time history of an irregular wave system into its wave spectrum is wide-spread. If measurements of the sea state are taken with a wave buoy, the wave spectrum can be found from the time history of the buoy's displacements.

The term 'wave spectrum' is in fact a shorter name for what, as stated by Hughes (1983), is the 'mean square spectral density function'. It can be demonstrated that, for any kind of wave, the energy enclosed by a bandwidth of the wave spectrum is proportional to the total energy of the components which lie within that band. This has promoted the use of the Energy Spectral Density (ESD) function and of the terms 'wave energy spectrum' or 'wave energy density spectrum', as noted for example by Lloyd (1989). For ocean waves, which are in the majority a stochastic process whose total energy over all time is generally infinite, it is more rigorous to refer to power rather than energy. This has promoted the use of the Power Spectral Density (PSD) function instead of the energy equivalent, with the result of an ambiguity regarding the spectral density of ocean waves, although the units used are generally the same: m^2s or m^2/Hz (Topper 2013). In this thesis the term wave spectrum describes a PSD function with units m^2/Hz.

The method adopted by Datawell to process the raw data from its Waverider buoys produces wave spectra covering 30mins of measurements. Displacements are sampled

at a frequency fs=1.28 Hz. A Fourier transform can be applied to the displacement time histories to compute the relative single-sided energy spectra in the frequency range 0 to fs/2=0.64 Hz, with a resolution fs/N=0.005. During 1800 seconds, 9 consecutive spectra of 200 seconds each are averaged to produce the half-hour wave spectrum and its relative parameters.

Two spectra are produced by the wave buoy: a wave height spectrum and a wave direction spectrum. The first is based on the vertical displacements and is the most common spectrum that can be obtained from non-directional wave measurements. It provides information on the wave height and period. The second includes into the analysis the North and West displacements, providing information on the wave direction, wave spread and wave ellipticity.

For the data analysis presented in this chapter, the two spectra are used to different extents. Information on the wave direction and wave spread was used for a general assessment of the experiments and to identify those trials conducted in seas with significant wave spread or different wave systems. The wave direction spectrum output by the wave buoy was used without any further processing. The more rigorous data analysis and the calculation of the RAOs of the vessel responses relied on the wave height spectrum. This was re-computed from the raw wave data following the method developed by Datawell (2014), but without discarding any wave frequency defining the spectrum.

6.5.5 Wave Encounter Spectrum

The wave spectra defined in the previous section are relative to the buoy's frame of reference, which can be approximated to that of a fixed point at sea. The data analysis in this chapter is based on the separation of the load components according to the frequency at which they occur and on the principle that wave-induced load cycles occur at the frequencies at which waves are encountered by the vessel. The RAOs of the vessel responses also require combining the response spectrum to the exciting wave spectrum. These tasks all require transforming the wave spectrum to an encounter spectrum based on the frame of reference of the moving vessel.

The transformation is based on the assumption that waves are 'long crested', hence that the wave crests remain straight and parallel. The first step involves defining the spectral ordinates based on the wave encounter frequency by shifting the wave spectrum along the frequency axis. Each frequency of encounter can be found from the respective wave frequency through the following equation:

$$\omega_e = \omega\left(1 - \frac{2\pi\omega V cos\beta}{g}\right) \tag{6.1}$$

where $\omega_e$is the wave encounter frequency in Hz; ω is the correspondent wave frequency in Hz; V is the vessel speed in m/s; and β is the vessel heading with respect to the wave direction. Equation 6.1 differs from that presented by other authors (e.g. Lloyd (1989) and Bhattacharyya (1978)) by a factor 2π, since frequencies are defined in Hz instead of rad/s.

It can be demonstrated that the area enclosed by a wave height spectrum is proportional to the total energy, per square metre of sea surface, of the complete wave system. Since the transformation does not change the energy of the system, but only its frame of reference, the area under the spectrum must be the same, irrespective of whether it is defined per wave frequency of wave encounter frequency.

The second step involves adjusting the ordinates of the wave encounter spectrum so that the area within any infinitesimal wave frequency range is reproduced as an equal area in the correspondent infinitesimal encounter frequency range. Each spectral ordinate of the wave encounter spectrum can be found from the respective spectral ordinate through the following equation:

$$S_\zeta(\omega_e) = S_\zeta(\omega)\frac{g}{g - 4\pi\omega V cos\beta} \tag{6.2}$$

where $S_\zeta(\omega_e)$ is the spectral ordinate, in m^2/Hz, relative to the wave encounter frequency ω_e; and $S_\zeta(\omega)$ is the correspondent spectral ordinate relative to the wave frequency ω. Also Equation 6.2 differs from that presented by other authors by a factor 2π because frequencies are defined in Hz instead of rad/s.

An example of the transformation is shown in Figure 6.12. As per Equations 6.1 & 6.2, the calculation of the wave encounter spectrum requires the vessel's speed V and

heading β to be known. Mean values of V and β were estimated for each leg of the trial trajectories based on expert judgement and with the aid of on-board instrumentation. The accuracy of the transformation is therefore dependent on the estimates made for V and β and can be largely affected by misalignment of the trial trajectory with respect to the wave direction.

Wave spectra computed from a Directional Waverider buoy are defined within a range of wave frequencies 0-0.64 Hz (Section 6.5.4). Any wave encounter spectrum computed from the buoy's displacements will be therefore defined within a correspondent range of encounter frequencies. For the data filtering, the following sections will often refer to the mean and maximum wave encounter frequency. These should be taken as follows:

- **mean**($\boldsymbol{\omega_e}$): mean wave encounter frequency, computed from the ratio of the first to the zeroth spectral moment of the wave spectrum.
- **max**($\boldsymbol{\omega_e}$): Maximum encounter frequency at which the wave encounter spectrum, calculated based on the wave buoy's vertical displacements, is defined.

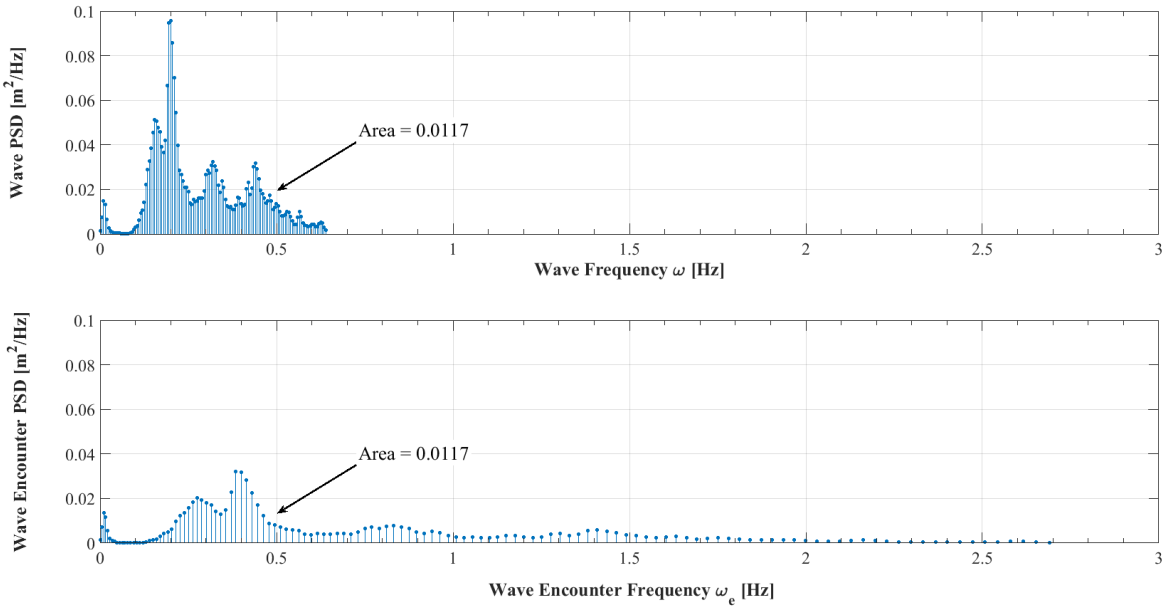

Figure 6.12. Wave height PSD transformation from wave frequency to wave encounter frequency. The total energy under the spectrum, hence the area, is preserved by the transformation.

6.6 Analysis of Global loads

6.6.1 Data De-Trending

The raw strain signals were affected by drift that could not be always attributed to any slowly changing factor, such as the displacement. It was convenient to remove the drift prior to combining strain readings from different strain gauges. A high-pass filter with the following characteristics was applied to all raw strain signals:

$$F_{stop} = 0.01\ Hz \tag{6.3}$$

$$F_{pass} = 0.05\ Hz \tag{6.4}$$

where F_{pass} and F_{stop} are the passband and stopband frequency respectively. An example of how each of the raw strain signals was de-trended is shown in Figure 6.13.

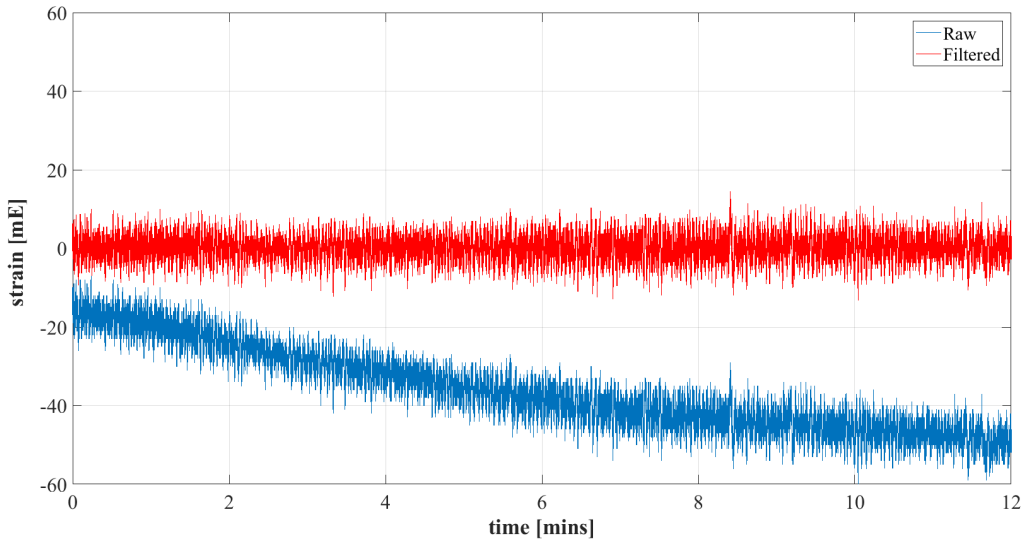

Figure 6.13. Raw strain signal de-trended.

6.6.2 Strain to Bending Moment Conversion

The conversion from strain to hull girder load relies on the classical beam theory and its underlying assumptions. The hull girder is idealised as a beam with material properties and dimensions of the actual vessel. The procedure to recover the vertical bending moment from strain measurements is outlined here. Horizontal bending moment could be estimated in a similar fashion.

The symmetrical position of the strain gauges with respect to the centreline of the vessel implies that two strain gauges on the deck, port and starboard, will measure the same vertical bending strain and opposite horizontal bending strain. Depending on the sign used to combine, or average, the signals of the two strain gauges, either vertical or horizontal bending can be isolated whilst the other neutralised. This approach is at the basis of strain measurement and resembles the theory behind the use of strain gauges in a half or a diagonal Wheatstone Bridge circuit (Hoffmann 1989). Any superimposed global axial load will be compensated in the successive steps. Superimposed global torsional loads will only be partially compensated. However, because of the stiffness and the size of the craft, and because of the orientation of the strain gauges, the magnitude of the parasitic torsional loads was considered negligible.

From the averaging explained above two vertical bending strain signals can be found, one close to the hull bottom and one close to the deck. The arithmetic to recover the magnitude of the vertical bending moment is based on the relations between strain, stress and load on a bending beam, namely:

$$\sigma = \varepsilon E \tag{6.5}$$

$$M = \frac{\sigma I}{y} \tag{6.6}$$

where ε is the strain; E is the modulus of elasticity; σ is the stress; I is the section modulus of the cross-section; y is the distance of the measuring point from the neutral axis; and M is the bending moment.

The vertical bending strain ε was measured at the deck and at the hull bottom. The modulus of elasticity E was estimated based on the material properties of all the reinforcement plies of the cross section and, for each cross-section, one value for E was determined. The stress σ could then be calculated by assuming a linear relationship between stress and strain. In order to determine the bending moment M that imparts a stress σ to the structure (Equation 6.6), values for I and y are also required.

The section modulus I was computed using the finite element model of the Severn (Chapter 4). The distance y between the measuring point and the neutral axis could

have also been retrieved from the finite element model. This was not necessary because the vertical distance between the strain gauges on the hull bottom and those on the deck was known from the technical drawings of the vessel. Equations 6.5 & 6.6 can be applied to both the hull bottom and the deck strain signals, and they must return the same vertical bending moment. The two equations can then be combined into one that does not depend on y, but only on the distance between the strain gauges on the hull bottom and those on the deck. For a positive bending moment in sagging condition Equations 6.5 & 6.6 yield to:

$$VBM = \frac{IE}{y_{BD}}(\varepsilon_{Bottom} - \varepsilon_{Deck}) \tag{6.7}$$

where ε_{Bottom} is the strain measured at the hull bottom; ε_{Deck} is the strain measured at the deck; y_{BD} is the vertical distance between the strain gauges at the hull bottom and those at the deck; and VBM is the resulting vertical bending moment. From Equation 6.7 it also becomes clear that any global axial strain would be compensated, as it would occur with the same sign at both the hull bottom and the deck. Global torsional strain is only partially compensated, since it does occur with the same sign, deck and hull bottom, but not necessarily with the same magnitude.

A time history of vertical bending moment can be found for each of the five instrumented stations. Each time history is made by a bending moment induced by waves and a superimposed bending moment due to the transient vibrations of the hull girder induced by slamming impacts. Noise is also present. Springing is not considered because, due to the high stiffness of the hull girder and its high natural frequency, does not occur on the Severn.

6.6.3 Wave-Induced Bending Moment

To isolate the wave-induced component, a low-pass filter was applied to the bending moment signal found in the previous section. Wave-induced bending moment is assumed to be a function of the wave encounter frequency, according to the principles of linear theory (Chapter 2). The wave encounter frequency is, in turn, a function of the heading and speed of the vessel, and can vary significantly for a high-speed vessel. The characteristics of the filter were therefore set as a function of the wave encounter

frequency. This allows to automate the data analysis whilst taking into account the large range of encounter frequencies that results from different combinations of headings and speeds. The passband and stopband frequencies of the filter were set to:

$$F_{pass} = mean(\omega_e) + \frac{max(\omega_e) - mean(\omega_e)}{1.5} \tag{6.8}$$

$$F_{stop} = max(\omega_e) \tag{6.9}$$

where F_{pass} and F_{stop} are the passband and stopband frequency respectively; $mean(\omega_e)$ is the mean wave encounter frequency; and $max(\omega_e)$ is the maximum wave encounter frequency. $mean(\omega_e)$ and $max(\omega_e)$ are found from the wave energy spectrum(Section 6.5.5). An example of how the wave-induced bending moment is isolated from a vertical bending moment signal is shown in Figure 6.14.

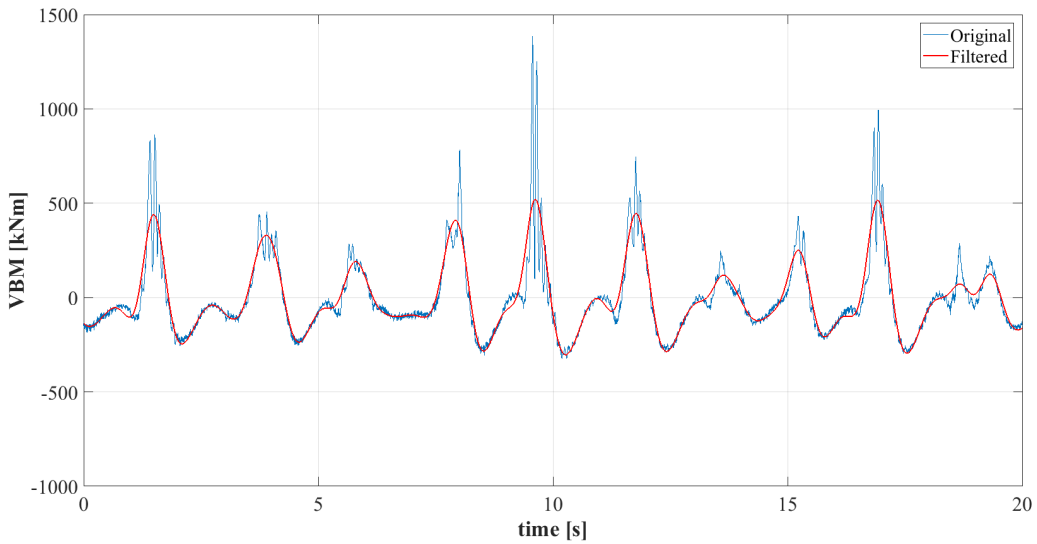

Figure 6.14. Wave-induced vertical bending moment signal filtered.

6.6.4 Slamming-Induced Bending Moment

The global response of ship structures to a slamming impact tends to occur as a transient vibration of the hull girder in the vertical plane. This vibration, which translates into vertical bending moment, can be expected to occur at the wet natural frequency of the hull girder. From an analysis of the vertical bending moment signals, represented in the frequency domain, the wet natural frequency of the hull girder was estimated at 10 Hz.

Some variability was found, attributed to the variation of added mass that results from a decreased wetted surface as the vessel travels at higher speeds.

In theory, the slamming-induced bending moment could be isolated from the bending moment signal by applying a high-pass filter to attenuate all frequencies below 10 Hz. This would have the drawback of attenuating also those frequencies that are higher than the maximum wave encounter frequency, and therefore not attributed to waves, but lower than the hull girder natural frequency. Although these frequencies should be, in principle, of small amplitude, neglecting an entire frequency range could result in the underestimation of the combined wave-slamming bending moment. The stopband and passband frequencies of the filter where therefore set according to those used in Section 6.6.3 for isolating the wave bending moment, but in reversed order, as shown in Equations 6.10 & 6.11.

Higher frequency components, attributed to local structural deformations sensed by the strain gauges, were also present. These appear in the bending moment signal as vibrations with a fundamental frequency and higher harmonics. Also in this case the fundamental frequency showed some variability, attributed again to the variation of added mass that results from a decreased wetted surface as the vessel travels at higher speeds. From an analysis of the strain signals plotted in the frequency domain, the minimum fundamental frequency of local structural vibrations was estimated at 15 Hz. Instead of a high-pass filter, a band-pass filter with the following characteristics was adopted to isolate the slamming-induced bending moment:

$$F_{stop1} = mean(\omega_e) + \frac{max(\omega_e) - mean(\omega_e)}{1.5} \tag{6.10}$$

$$F_{pass1} = max(\omega_e) \tag{6.11}$$

$$F_{pass2} = 13\ Hz \tag{6.12}$$

$$F_{stop2} = 15\ Hz \tag{6.13}$$

where F_{stop1} and F_{pass1} are the lower stopband and passband frequencies respectively; F_{pass2} and F_{stop2} are the higher passband and stopband frequencies respectively; $mean(\omega_e)$ is the mean wave encounter frequency; and $max(\omega_e)$ is the maximum wave

encounter frequency. An example of how the slamming-induced bending moment is isolated from a vertical bending moment signal is shown in Figure 6.15.

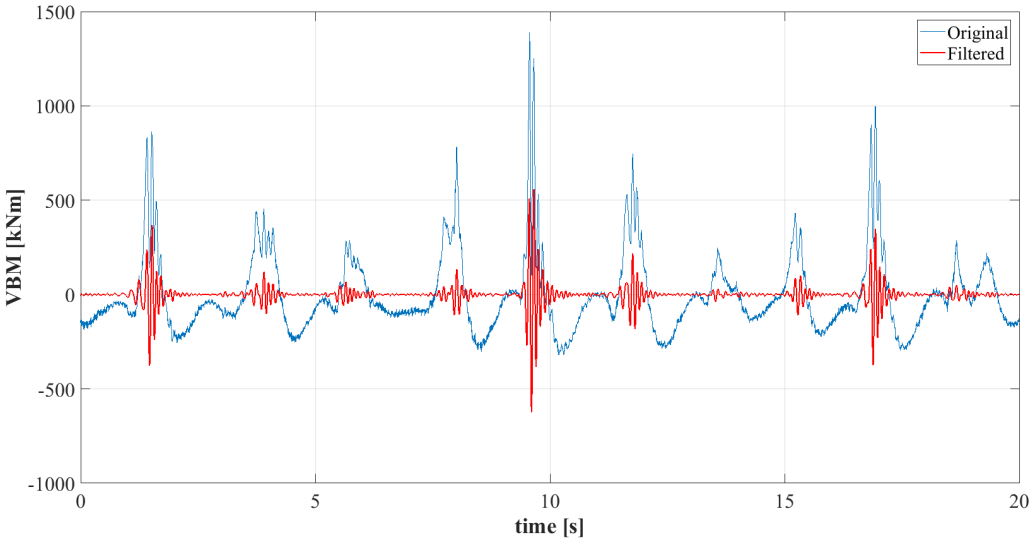

Figure 6.15. Slamming-induced vertical bending moment signal filtered.

6.6.5 Descriptive Statistics

The processed global loads were analysed through descriptive statistics. Maximum, minimum, mean, standard deviation, highest 1/3rd and highest 1/10th values of vertical bending moment were computed for all the headings of each of the trials conducted. Whilst the definition of these parameters is well known, the procedure to determine the dataset is crucial.

For wave-induced bending moment, the statistical values were calculated from datasets of load cycles, in particular of maximum and minimum values taken during each wave encounter. These values would be relatively easy to identify for tests in regular waves, for which motion and load responses tend to be periodic and sinusoidal. For tests in irregular waves, the construction of the dataset largely depends on what is deemed to be a wave encounter. For slamming-induced bending moment similar considerations apply, with the difference that what is analysed are the maximum and minimum values recorded during a transient vibration of the hull girder as the result of a slam.

The mean wave encounter frequency was used to determine the number of wave encounters, hence load cycles, that occurred during any one leg. Local maxima (peaks)

of the signal were found from the vertical bending moment time history of the leg considered. A minimum peak prominence and a minimum peak-to-peak separation were set to ignore local peaks resulting from small signal fluctuations. Their threshold values were set so as to obtain a number of peaks equal to, or larger than, the number of expected load cycles. The same analysis was repeated for local minima (troughs), thus generating two datasets from each time history: one for peaks and one for troughs. These were then sorted in descending order and trimmed according to the number of load cycles that was deemed to have occurred during the leg considered. For vertical bending moment, peaks and troughs can be regarded to as sagging and hogging bending peaks respectively. An example of peak and trough detection is shown in Figure 6.16. Since only major load cycles are detected, this method is only suitable for predicting extreme loads. For fatigue life calculations, small load cycles should also be considered.

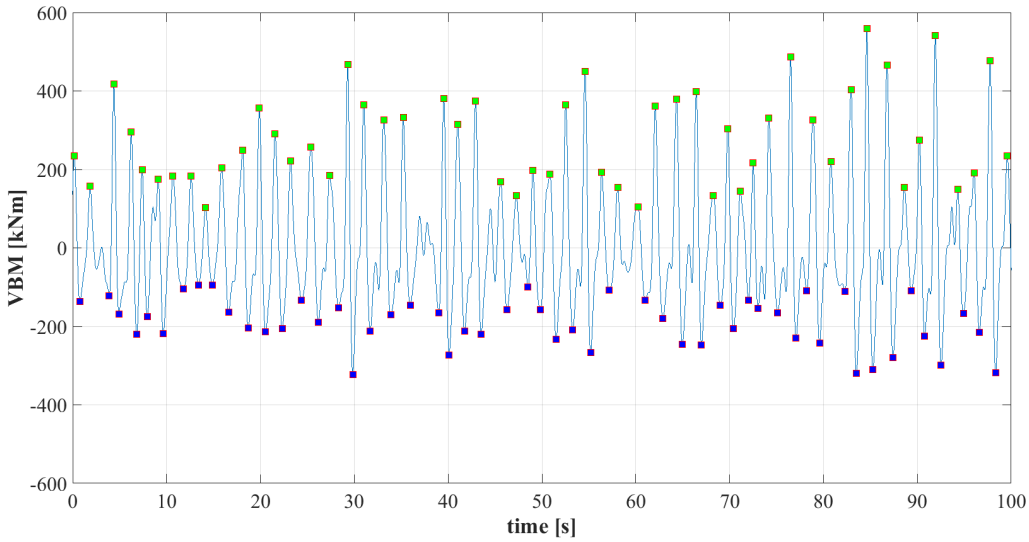

Figure 6.16. Detection of sagging and hogging bending moment peaks.

6.6.6 Spectral Analysis

Based on the assumption that some vessel responses are linearly proportional to the wave height, at any given speed, heading and wave frequency, data was also analysed according to the principles of linear theory. In this section only, difference will be made between the term 'transfer function' and 'response amplitude operator' (RAO), which is actually the square of the transfer function.

The transfer functions of the vessel responses were estimated from measurements of the responses and of the sea state, in particular from the response spectrum and the wave height spectrum. The procedure, called 'spectral analysis', is widely used in seakeeping calculations and its basics have been rigorously presented by many authors (Bhattacharyya 1978, Hughes 1983, Lewis 1988b, Lloyd 1989, Faltinsen 1990).

The transfer functions were produced for wave-induced vertical bending moment, although the analysis could be extended to the horizontal bending moment measured with the same strain gauge system and to the rigid body motions measured with a combination of accelerometer and rate gyro.

The vertical bending moment spectrum and the wave spectrum were first calculated. Whilst the first is defined according to the vessel's frame of reference, the second requires transformation to an encounter spectrum (Section 6.5.5). The vertical bending moment RAO, for any given encounter frequency, was calculated as the ratio of the relative spectral ordinate of the vertical bending moment spectrum and that of the wave encounter spectrum:

$$\left(\frac{VBM_0}{\zeta_0}\right)^2 = \frac{S_{VBM}(\omega_e)}{S_\zeta(\omega_e)} \tag{6.14}$$

where VBM_0 is the vertical bending moment amplitude; ζ_0 is the wave amplitude; $S_{VBM}(\omega_e)$ is the vertical bending moment power spectral density; and $S_\zeta(\omega_e)$ is the wave height power spectral density defined according to the vessel's reference frame (encounter spectrum).

The vertical bending moment transfer function was found by taking the square root of the RAO. Equation 6.14 can be reformulated as follows:

$$\frac{VBM_0}{\zeta_0} = \sqrt{\frac{S_{VBM}(\omega_e)}{S_\zeta(\omega_e)}} \tag{6.15}$$

By applying Equation 6.15 to all the encounter frequencies defining the spectra, it is possible to create graphs that show the amplitude of vertical bending moment, normalised with the wave amplitude, as a function of the wave encounter frequency. To

change the representation of the transfer functions from encounter frequency to λ/LOA, the transfer function ordinates are 'shifted' along the frequency axis. The encounter frequencies can be converted back to wave frequencies and the classical formulae for deep water used to relate these to wave lengths.

The procedure to estimate the transfer functions from measurements of the seakeeping responses of the vessel (e.g. VBM) and the concurrent sea state is reported schematically in Figure 6.17. Since these transfer functions are based on the wave height spectrum and not on the wave direction spectrum, it is evident that the wave spreading is neglected and that the transfer functions obtained are based on the assumption of long crested seas.

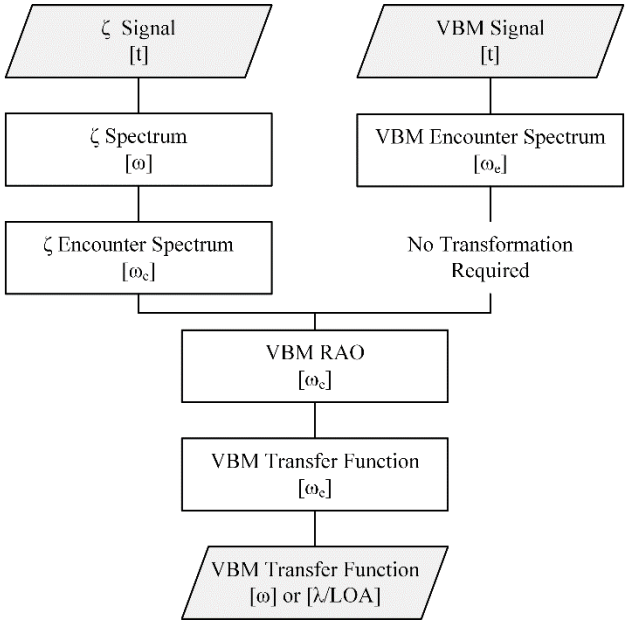

Figure 6.17. Calculation of the VBM transfer function.

6.7 Analysis of Local Loads

6.7.1 Data De-Trending

Similarly to the strain signals measuring global loads, also those measuring local loads on the hull bottom, bow and fore deck panels were affected by offset and slowly moving trends. These were removed, before combining strain readings from different strain gauges. A high-pass filter with the same characteristics as those used to filter the strains due to global deformations (Section 6.6.1) was applied to all raw strain signals:

$$F_{stop} = 0.01\ Hz \tag{6.16}$$

$$F_{pass} = 0.05\ Hz \tag{6.17}$$

where F_{stop} and F_{pass} are the stopband and the passband frequency respectively.

6.7.2 Wave-Induced Strain

As for global wave loads, a low-pass filter can be applied to isolate the strain caused by wave pressures from that induced by slamming effects at a global and local level. For consistency, the characteristics of the filter could be kept the same as those used for the wave-induced bending moment (Section 6.6.3):

$$F_{pass} = mean(\omega_e) + \frac{max(\omega_e) - mean(\omega_e)}{1.5} \tag{6.18}$$

$$F_{stop} = \max(\omega_e) \tag{6.19}$$

where F_{pass} and F_{stop} are the passband and stopband frequency respectively; $mean(\omega_e)$ is the mean wave encounter frequency; and $max(\omega_e)$ is the maximum wave encounter frequency (Section 6.5.5).

The filtered signal would still embed mainly two components: axial strain due to bending of the hull girder and bending strain of the panel under local wave pressures (torsion of the hull girder is again neglected). These two strain components can hardly be distinguished from one another because they tend to occur at the same frequency: the wave encounter. All four strain gauges become necessary to isolate the local pressure load from the axial load. This can be attempted based on the principle that the four strain gauges will sense approximately the same axial strain due to hull girder bending but different bending strain due to the local pressure on the panel. Beam and plate theories, or more sophisticated methods based on finite element analysis, could be applied to estimate the two strain components and isolate one from the other.

6.7.3 Slamming-Induced Strain

The analysis of the local slamming loads relied on the two strain gauges located at the midspan of the instrumented panels of the hull bottom and of the bow. The two strain

gauges were positioned close enough that their signals could be averaged to obtain one strain signal. A high-pass filter was applied to isolate the strain component due to slamming.

The features of the filter were chosen so as to attenuate all those frequencies that characterise the strain induced by loads other than the slamming pressures on the panel under consideration. This includes not only the low frequency global and local wave loads, but also the axial load due to the vibration of the hull girder that results from a slamming impact. The stopband and passband frequencies of the filter were chosen the same as those used for isolating the slamming-induced bending moment (Section 6.6.4), but in reversed order:

$$F_{stop} = 13\ Hz \tag{6.20}$$

$$F_{pass} = 15\ Hz \tag{6.21}$$

where F_{stop} and F_{pass} are the stopband and the passband frequency respectively. An example of how the slamming-induced strain is isolated from a raw strain signal is shown in Figure 6.18.

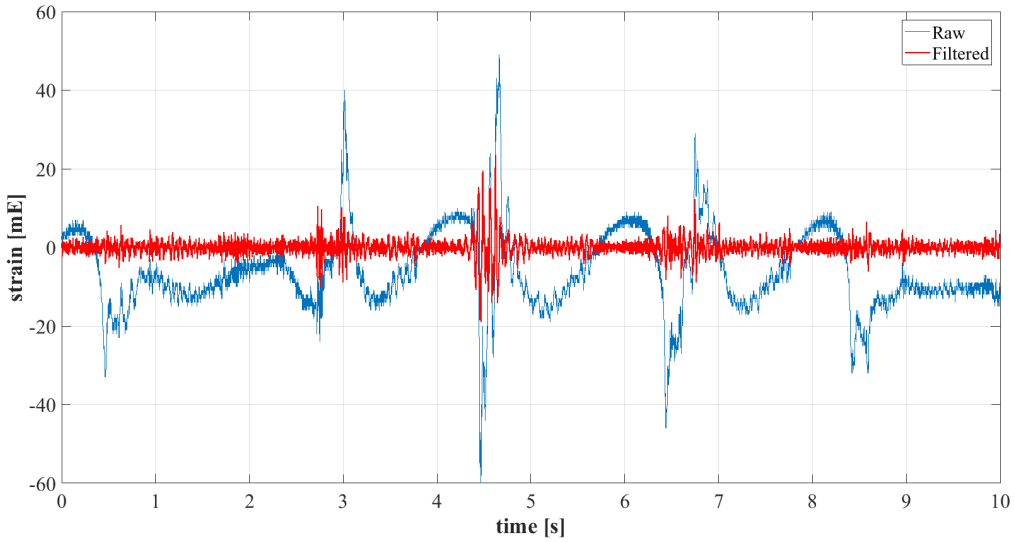

Figure 6.18. Slamming-induced strain signal filtered.

6.7.4 Strain-to-Pressure Conversion

Wave pressures on the hull structure fluctuate as the vessel travels through the waves. In addition to these, the structure may be subject to slamming impacts, which are typically characterised by a pressure front that travels rapidly across the bow or the hull bottom, and by transient loads due to large amounts of sea water flowing on the deck. Attempting to recover a dynamic pressure field from strain readings taken at only some points across the hull structure was considered neither practical nor easily achievable. If a dynamic pressure field was found, it would still need to be applied to a finite element model for the computation of the structural response. Applying the pressure load as a function of time to retain its dynamic nature would certainly increase the complexity of the finite element analysis, whilst converting it to a static load would nullify the effort of reconstructing the pressure load in the time domain.

The analysis of local loads on the hull structure relied on the determination, for each of the instrumented panels, of an equivalent static uniform pressure. This is the pressure that, if applied to the whole panel, produces the same strains at the points instrumented as those produced by the actual pressure field. A static pressure envelope, which represents the effect of dynamic loads on the entire hull structure, can then be constructed by combining the equivalent static pressures found for each of the panels. A strain-pressure conversion was found from local finite element models of the instrumented panels through linear static structural analysis. This study was limited to the effect of slamming on the hull bottom and on the bow but could readily be extended to the case of green water loads on the fore deck.

The extent of structure modelled was determined based on the supporting members of the structural panel instrumented. For hull bottom panels, supporting members were identified as the adjacent transverse frames, the centreline joint and the chine. For bow panels, supporting members were identified as the adjacent ring frame, the stem and the hull-to-deck joint. The same material properties as those used for the global finite element model (Chapter 4) were used. Geometrical models were discretised with 4-node quadrilateral shell elements and the laminate properties were assigned ply by ply, using the shell layered definition. An example of geometrical and meshed model for one of the hull bottom panels is shown in Figures 6.19 & 6.20. Boundary conditions in the form of

rigid restraints were applied in lieu of the supporting structural members and a uniformly distributed pressure of 1 MPa was applied to the outer side of the plating, as shown in Figure 6.21. The structural analysis was performed with Abaqus FEA software as linear and static. Surface strains along the strain gauges' active direction were output for evaluation. An example for one of the hull bottom panels is shown in Figure 6.22. The strain value computed at the location of the strain gauges was used to relate the pressure load to the measured strain.

Strain to pressure conversion factors were thus produced for each of the instrumented panels. For one panel, the strain value computed was found unrealistic and therefore adjusted based on expert judgement. The final conversion factors adopted are reported in Table 6.11. Further details of this analysis are presented in Appendix 7, whilst the construction of static pressure envelopes is covered in Chapter 7, as part of the definition of the load cases for the computation of the structural analysis.

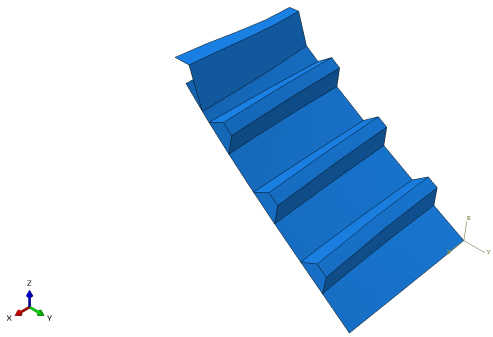

Figure 6.19. Hull bottom panel. Geometrical model.

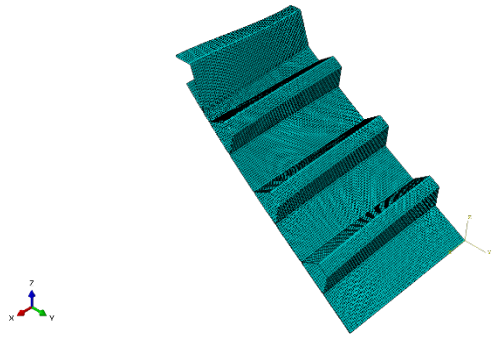

Figure 6.20. Hull bottom panel. Meshed model.

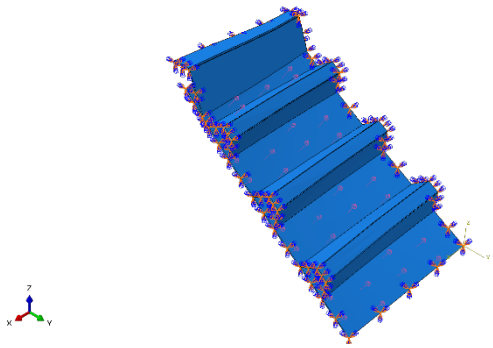

Figure 6.21. Hull bottom panel. Boundary conditions and loads.

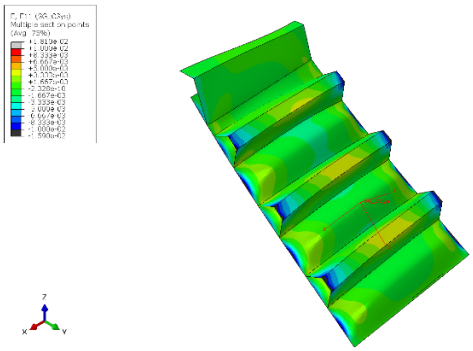

Figure 6.22. Hull bottom panel. Surface strain in the strain gauges' active direction (x8 magnification).

Model	Panel position	Distance from aft end [m]	Pressure [MPa]	Strain [με]
Model 1	Hull bottom	7.14	1	866
Model 2	Hull bottom	8.84	1	866
Model 3	Hull bottom	11.39	1	866
Model 4	Bow	16.15	1	2440

Table 6.11. Strain to pressure conversion.

6.8 Results

The analysis of the sea trial data was completed for three load components: global wave loads, global slamming loads and local slamming loads. In this chapter results are presented for the first component because the wave-induced vertical bending moment was also predicted numerically and measured at scale (Chapters 4 & 5). Results on slamming loads will be presented in Chapter 7.

The results for vertical bending moment are presented graphically with figures that consist of five data sets, each for every frame instrumented along the hull (from aft to fore: FR03, FR05, FR08, FR10 & FR12). Each figure is in turn relative to one of the nine trials selected for the study, identified by the nominal trial speed and the mean significant wave height measured during the trial. Two sets of results are presented: polar plots and RAO plots.

Figures 6.23-6.31 show polar plots of wave-induced vertical bending moment. Each figure consists of highest 1/3rd and maximum values of sagging and hogging bending moment measured at eight headings (0˚,45˚,...,315˚). The heading system follows the standard seakeeping convention (see Nomenclature and Sign Conventions).

Figures 6.32-6.40 show RAO plots of wave-induced vertical bending moment. Each figure consists of two sets of RAO plots: as a function of λ/LOA and as a function of the distance of the station under consideration from the aft end. For this second type, a number of λ/LOA values is selected as a parameter. For all the RAO pots, the heading is limited to head sea and data is presented for two legs, the first and the last head sea legs of the trial trajectory (Leg01 & Leg09, Leg11 or Leg13 depending on the trajectory).

In Figures 6.32-6.40, the sea trial results are also compared against the numerical predictions from Chapter 4. The numerical results were obtained with the following codes:

- 2D strip theory (***2D***) for speeds V≤10kts
- 2.5D strip theory (***2.5D***) for speeds V>10kts

For these simulations, the MAESTRO model's loading condition was tuned to that of the lifeboat used for the trials, which was determined from historical inclining test data. The target and achieved values are reported in Table 6.12.

TYNEMOUTH LIFEBOAT			TARGET	ACHIEVED
Loading condition			Full load	Full load
Displacement	Δ	[kg]	42370	42363
Centre of gravity (x)	LCG	[m]	6.42	6.41
Centre of gravity (z)	TCG	[m]	0.00	0.00
Centre of gravity (y)	VCG	[m]	2.28	2.29
Roll radius of gyration	k_4	[m]	N.A.	2.11
Pitch radius of gyration	k_5	[m]	N.A.	4.01
Yaw radius of gyration	k_6	[m]	N.A.	4.02

Table 6.12. MAESTRO model loading condition tuned to sea trial vessel.

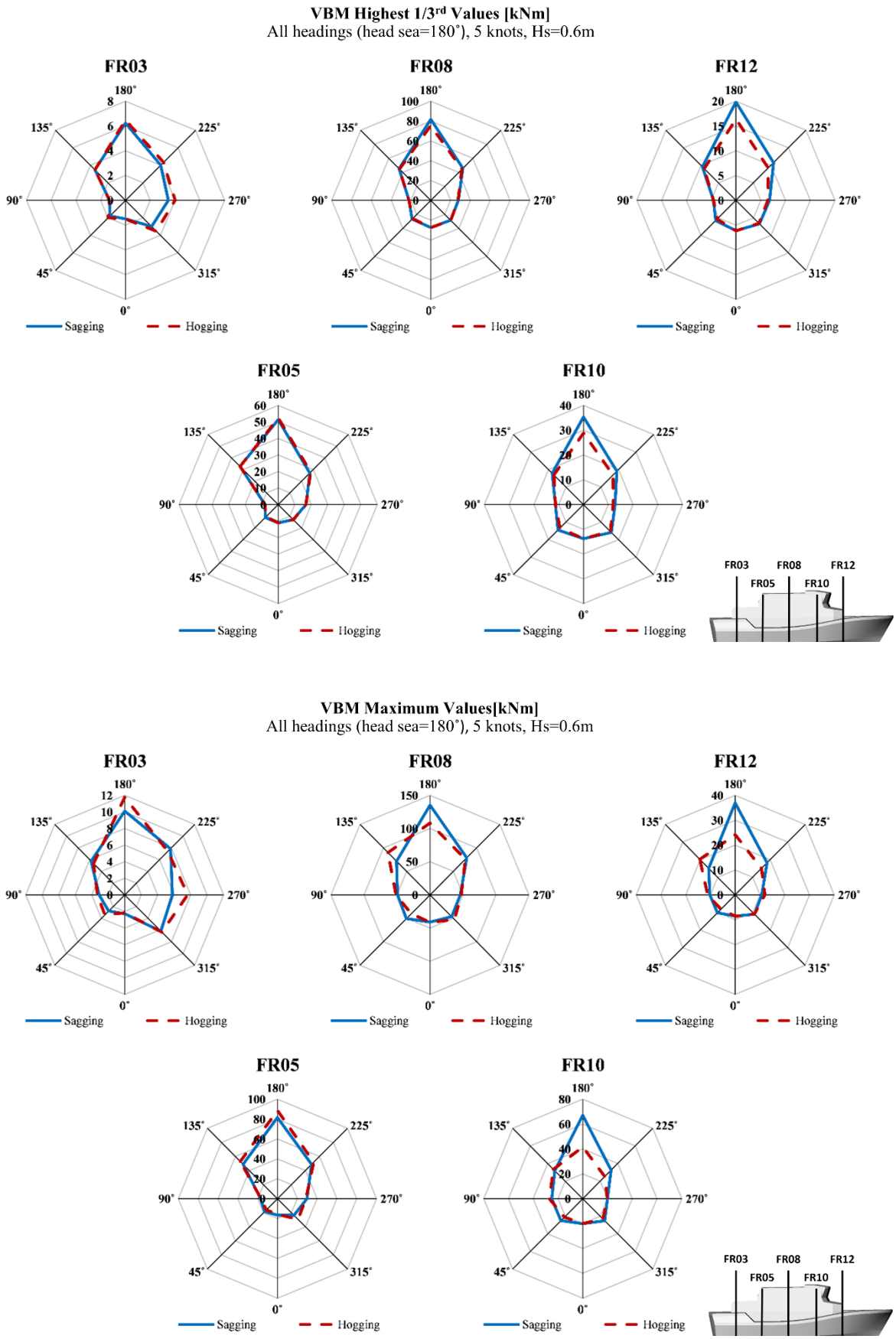

Figure 6.23. Wave-induced VBM. Highest 1/3rd and maximum values. All headings, 5kts, Hs=0.6m.

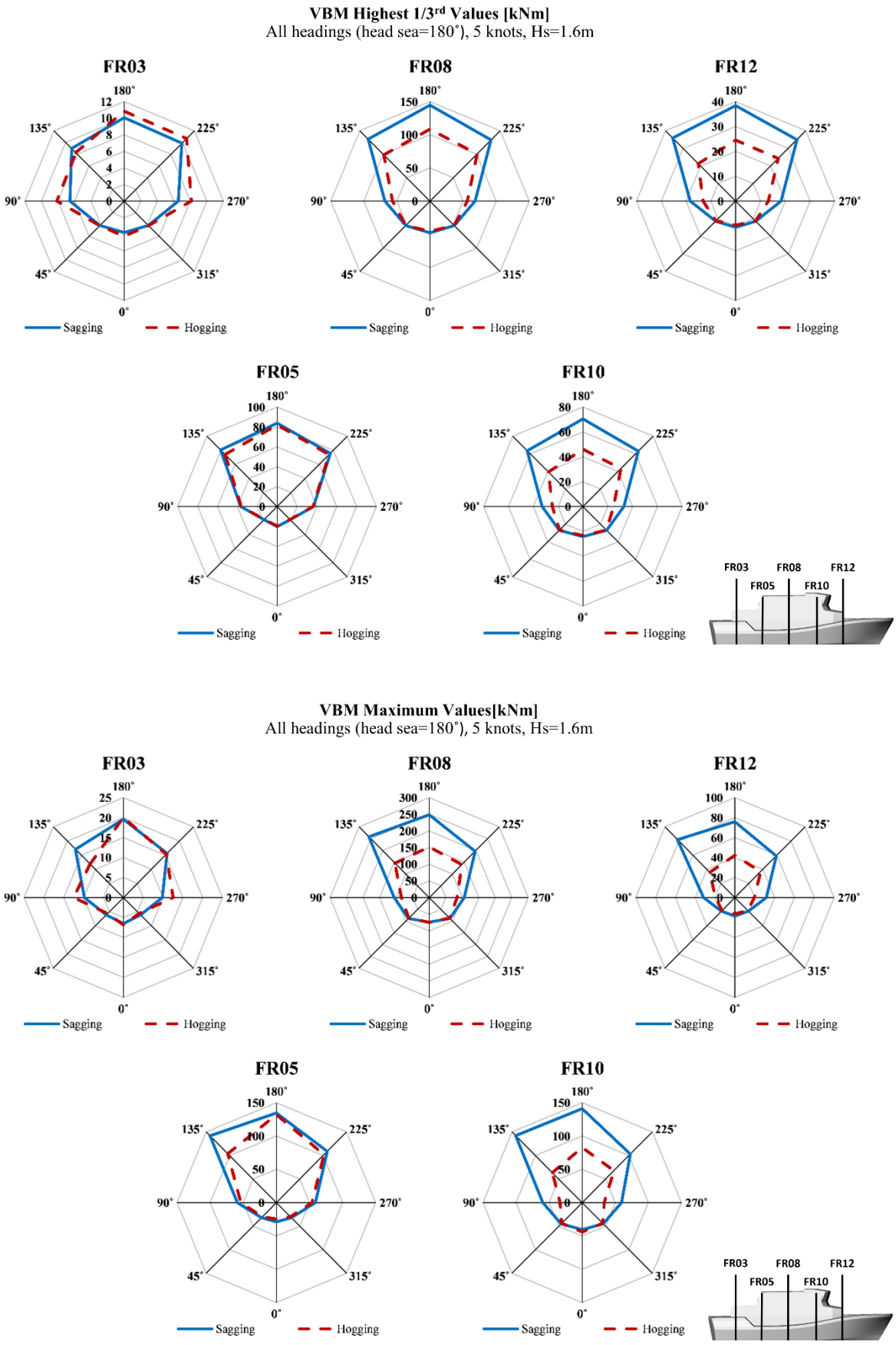

Figure 6.24. Wave-induced VBM. Highest 1/3rd and maximum values. All headings, 5kts, Hs=1.6m.

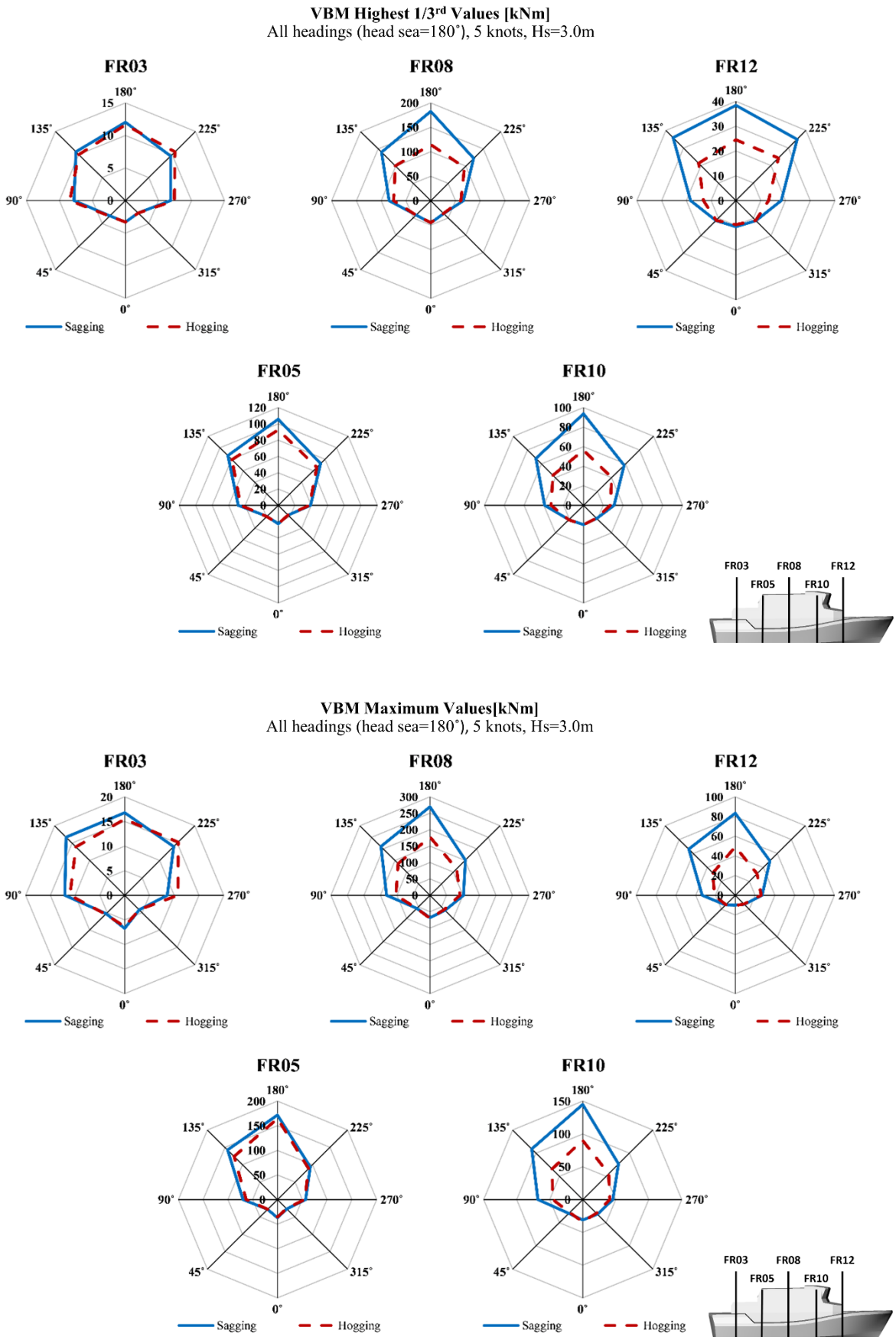

Figure 6.25. Wave-induced VBM. Highest 1/3rd and maximum values. All headings, 5kts, Hs=3.0m.

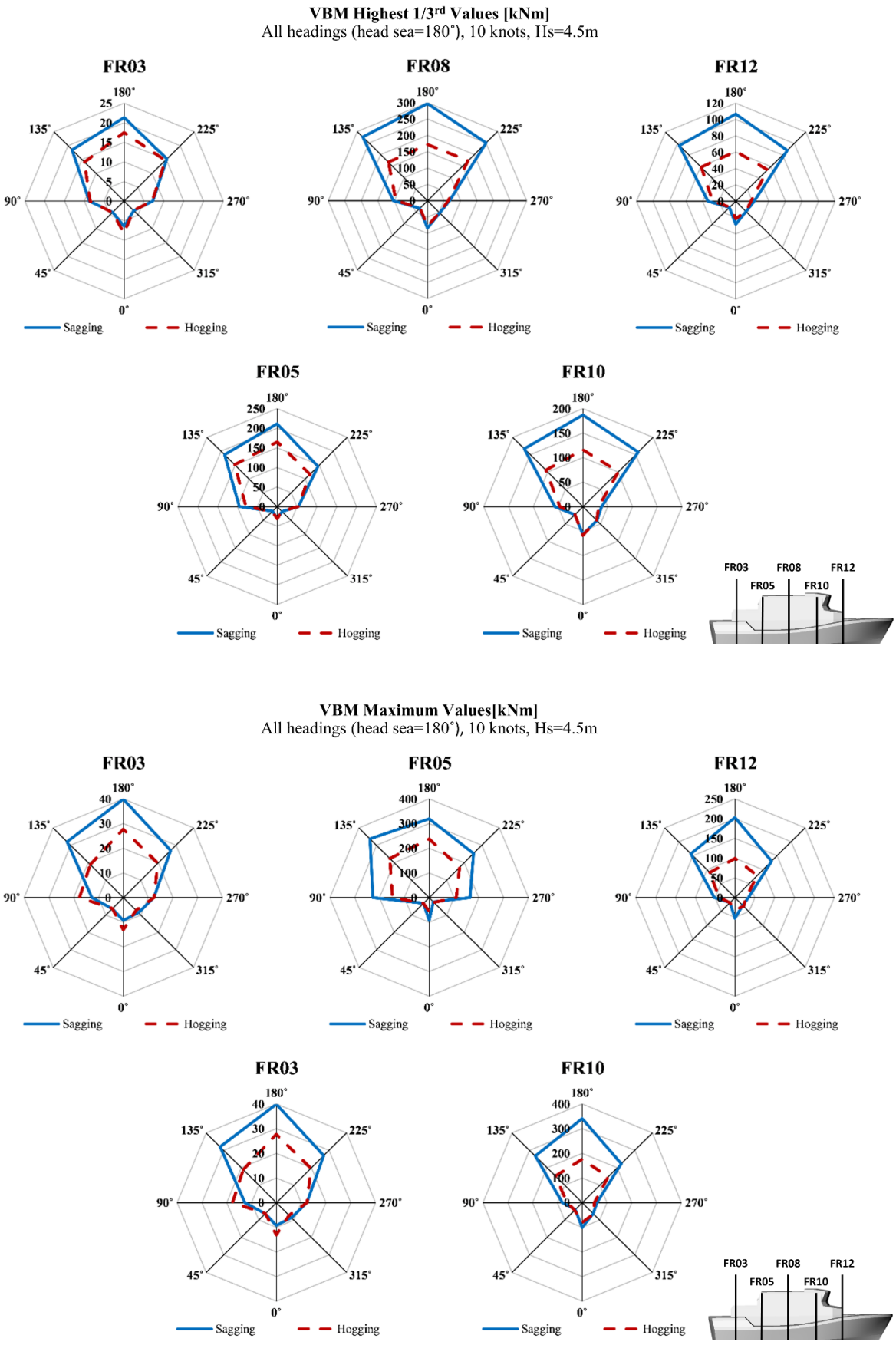

Figure 6.26. Wave-induced VBM. Highest 1/3rd and maximum values. All headings, 10kts, Hs=4.5m.

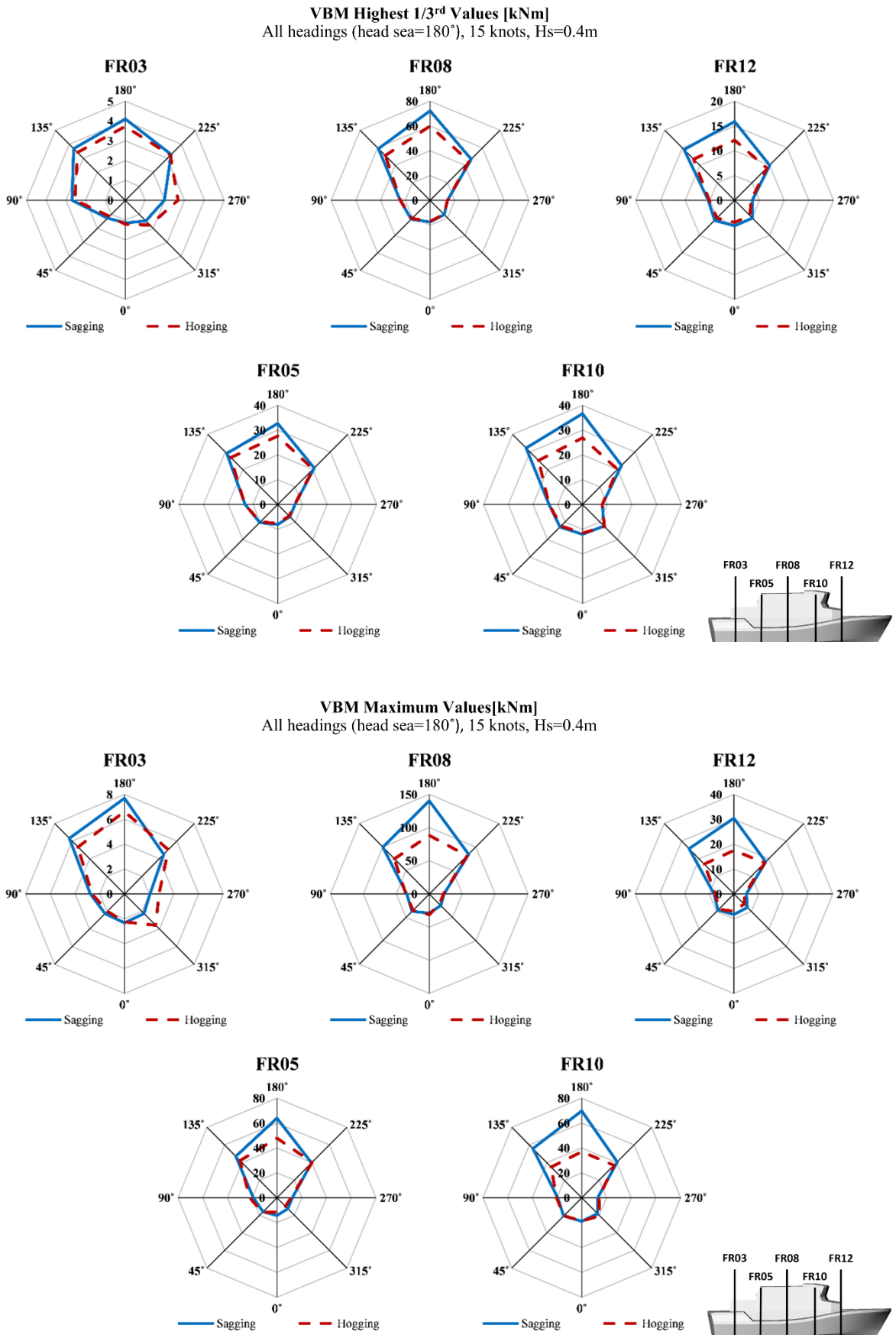

Figure 6.27. Wave-induced VBM. Highest 1/3rd and maximum values. All headings, 15kts, Hs=0.4m.

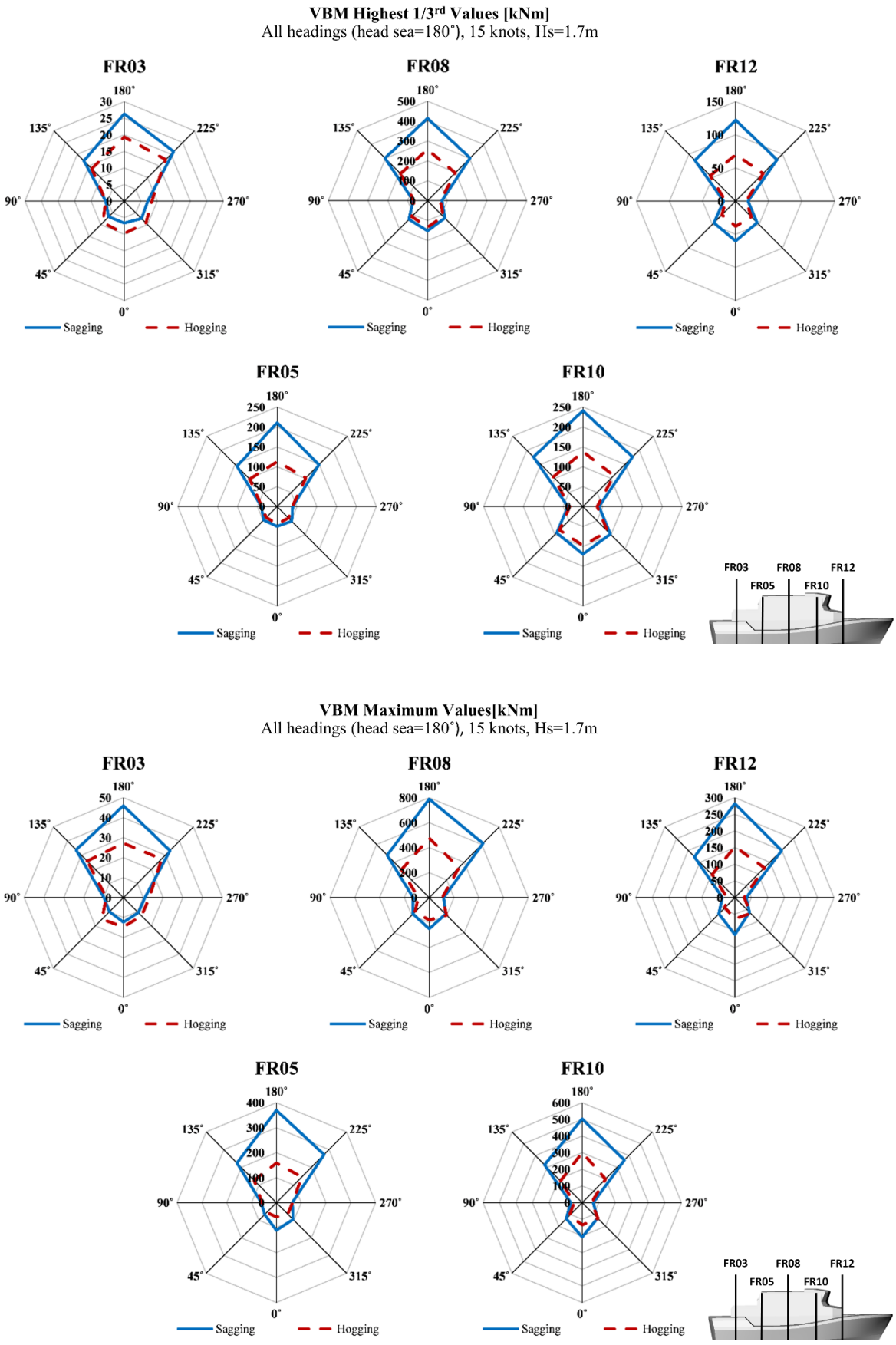

Figure 6.28. Wave-induced VBM. Highest 1/3rd and maximum values. All headings, 15kts, Hs=1.7m.

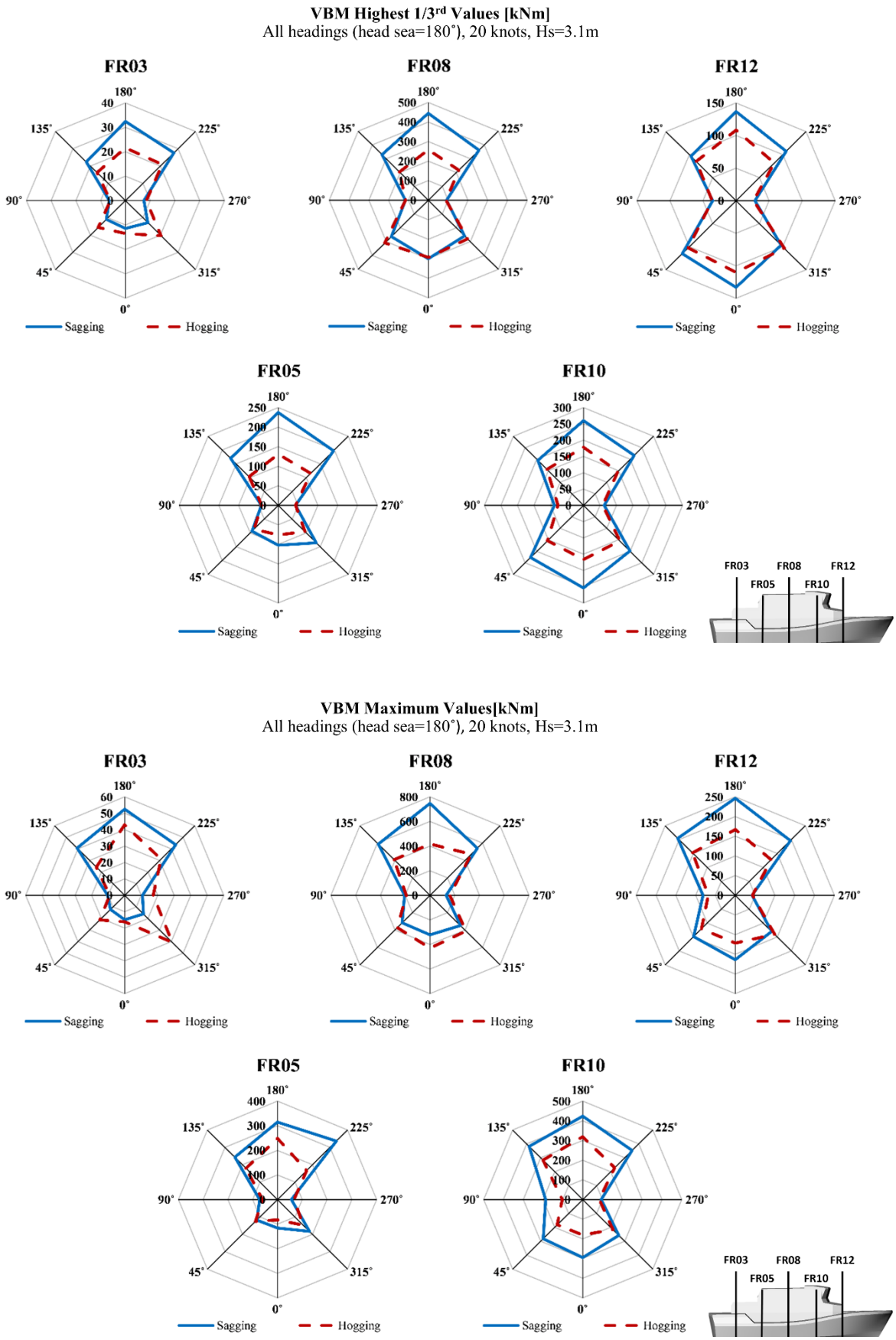

Figure 6.29. Wave-induced VBM. Highest 1/3rd and maximum values. All headings, 20kts, Hs=3.1m.

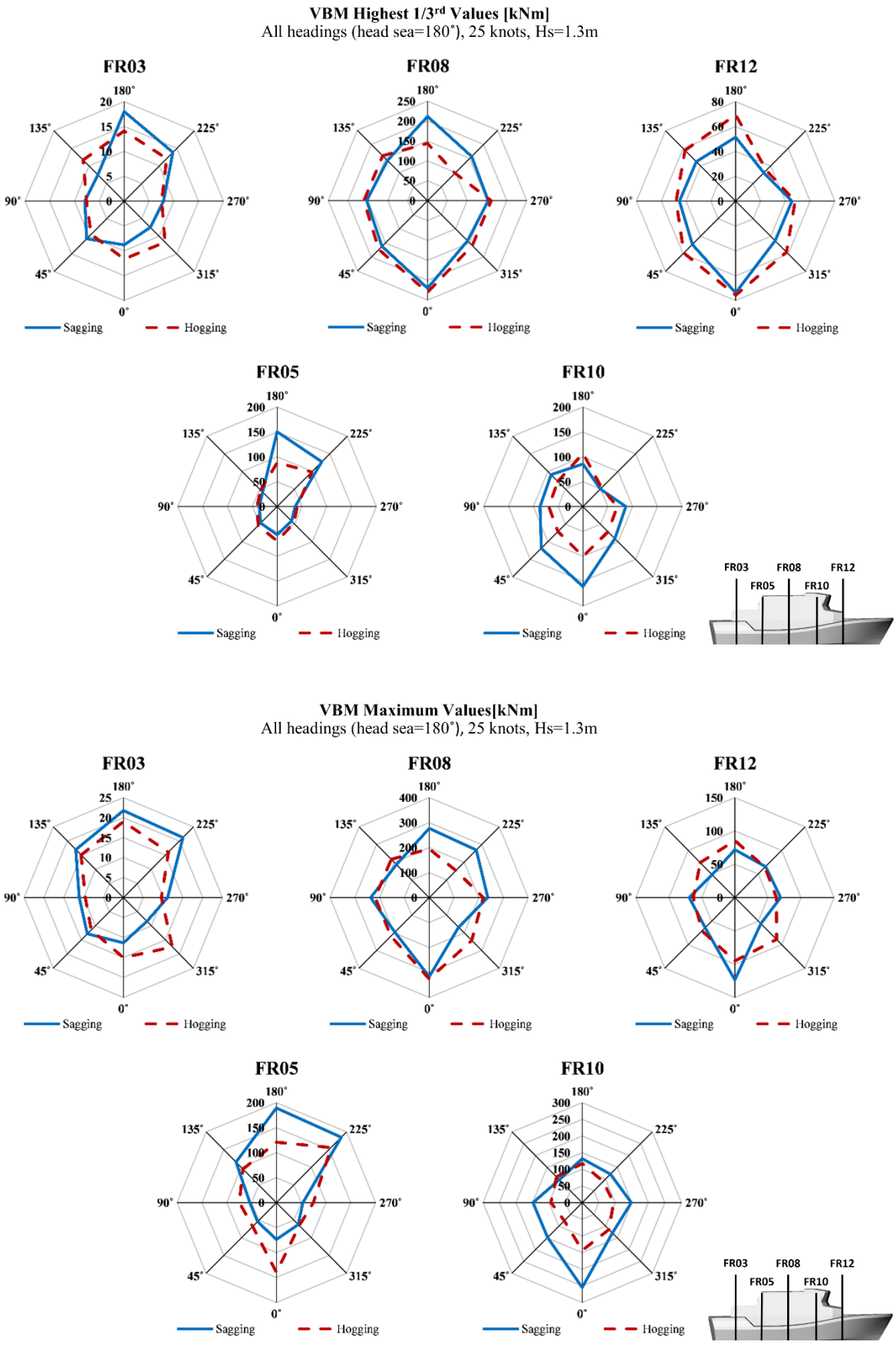

Figure 6.30. Wave-induced VBM. Highest 1/3rd and maximum values. All headings, 25kts, Hs=1.3m.

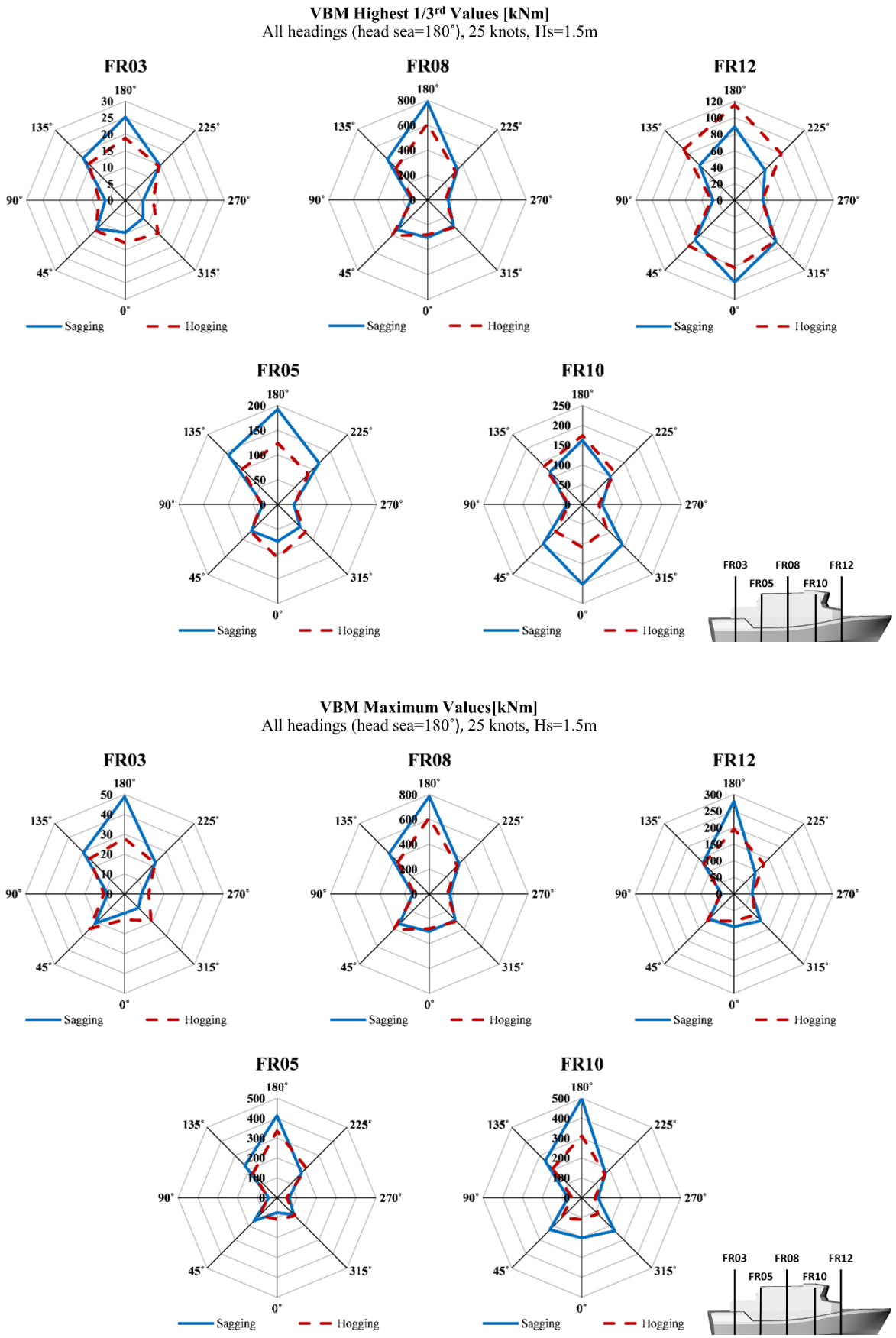

Figure 6.31. Wave-induced VBM. Highest 1/3rd and maximum values. All headings, 25kts, Hs=1.5m.

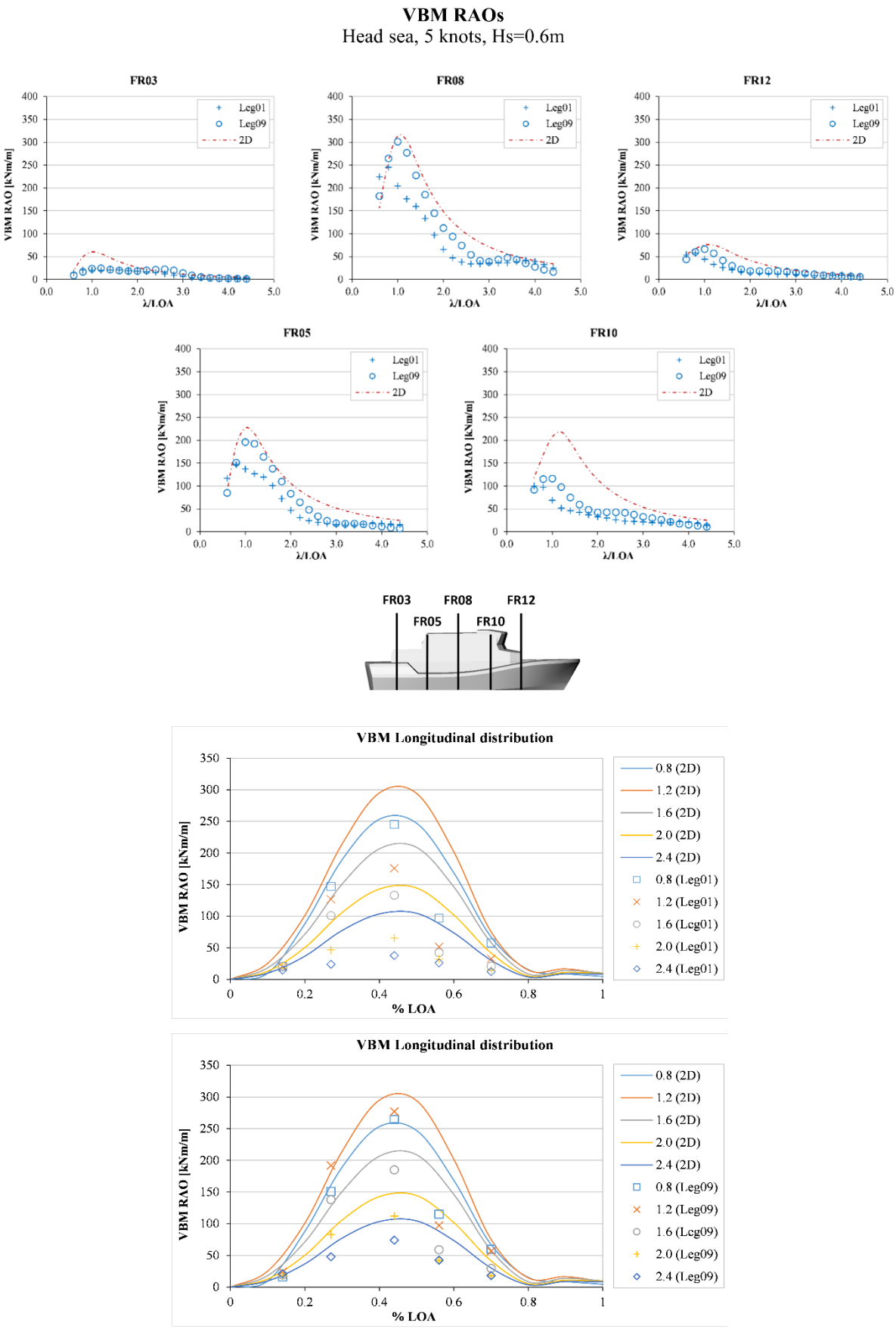

Figure 6.32. Wave-induced VBM RAOs. Head sea, 5kts, Hs=0.6m.

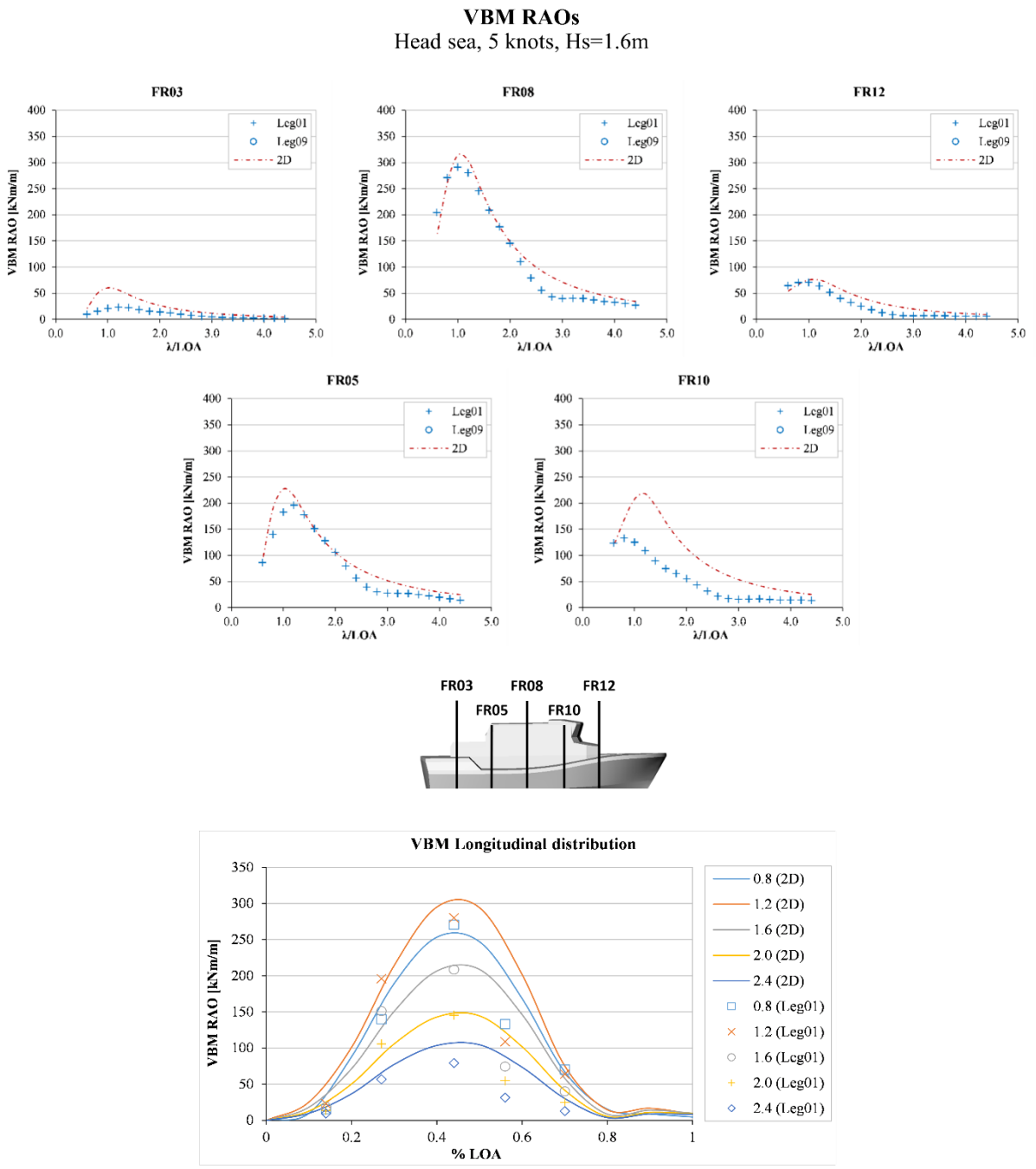

Figure 6.33. Wave-induced VBM RAOs. Head sea, 5kts, Hs=1.6m.

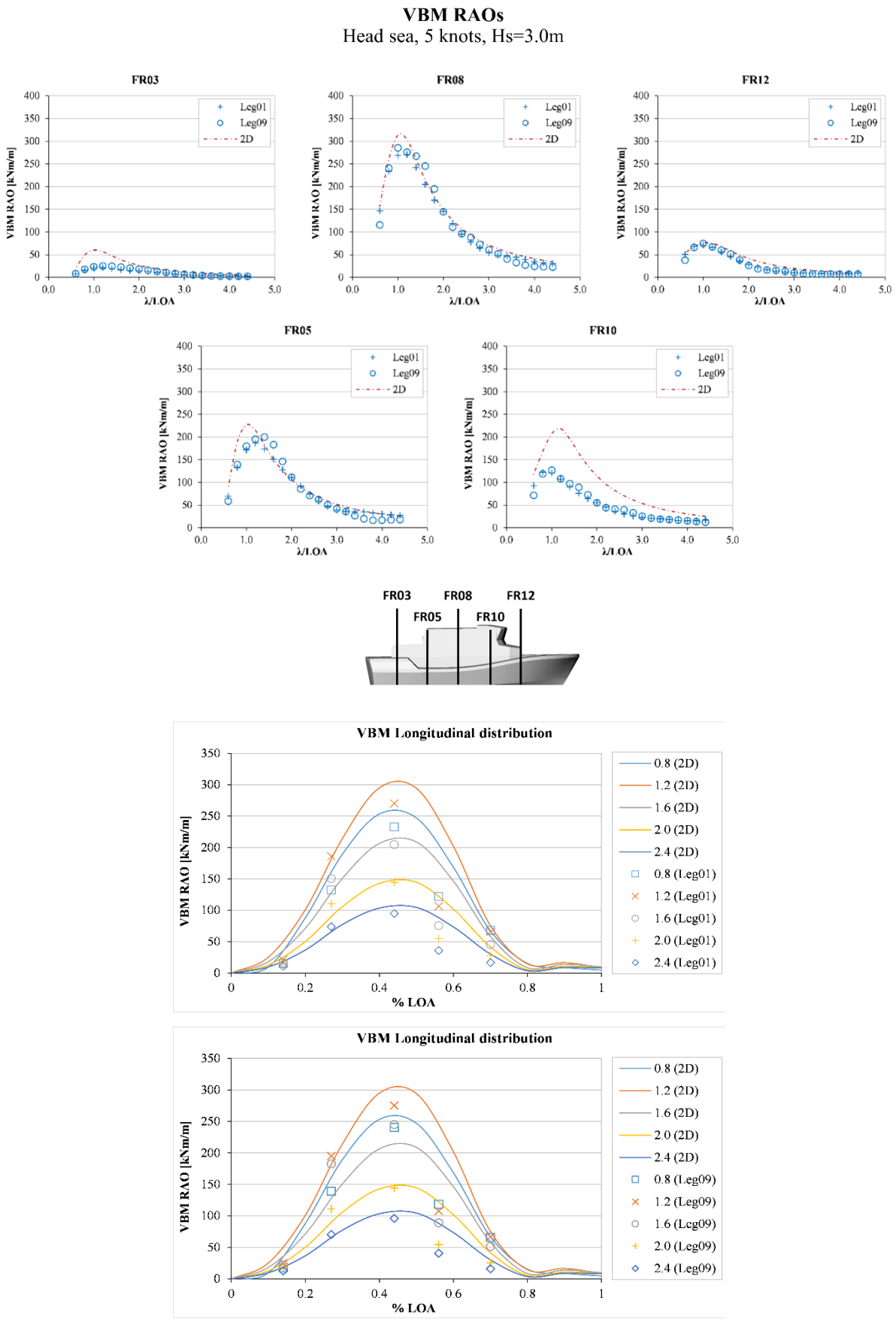

Figure 6.34. Wave-induced VBM RAOs. Head sea, 5kts, Hs=3.0m.

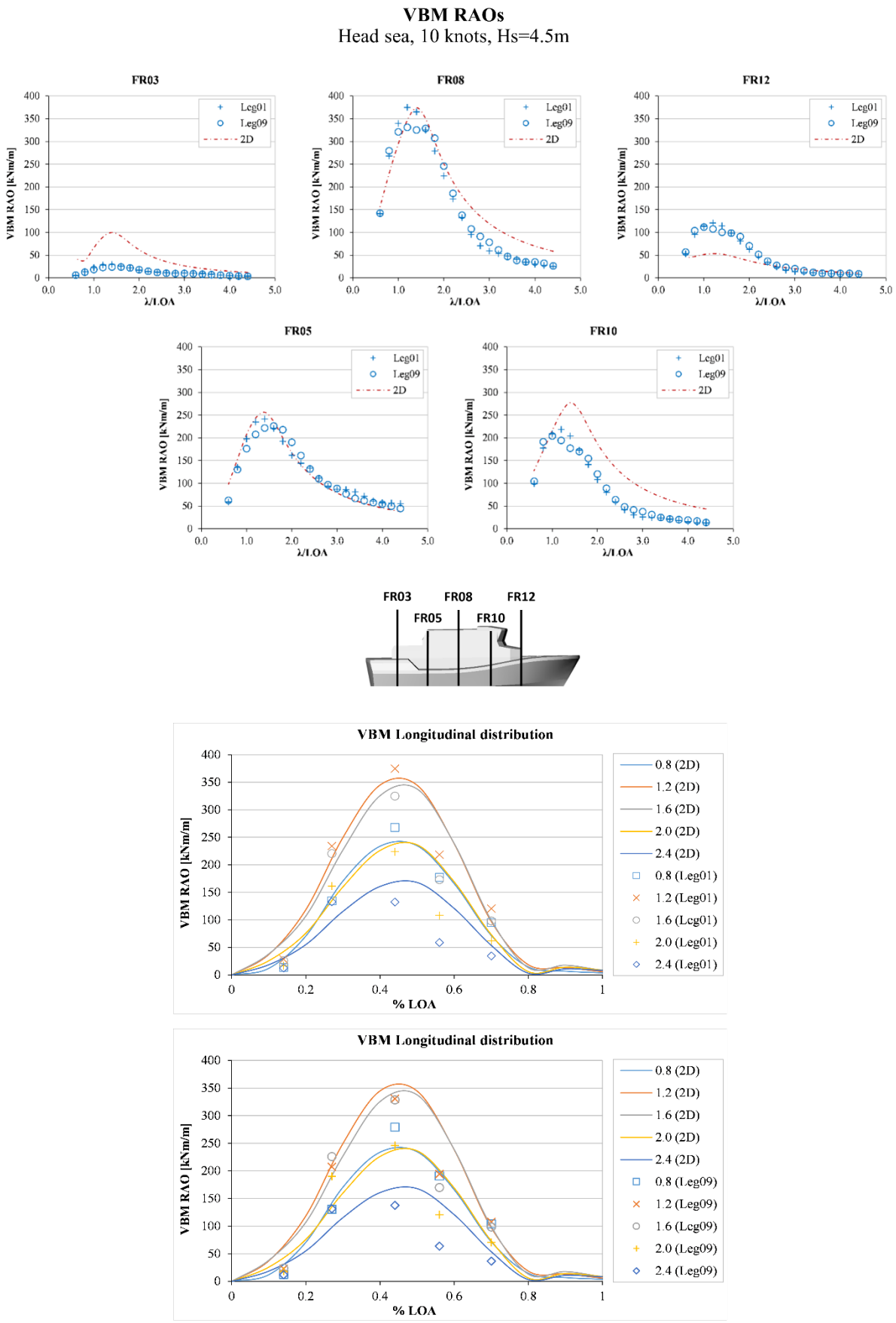

Figure 6.35. Wave-induced VBM RAOs. Head sea, 10kts, Hs=4.5m.

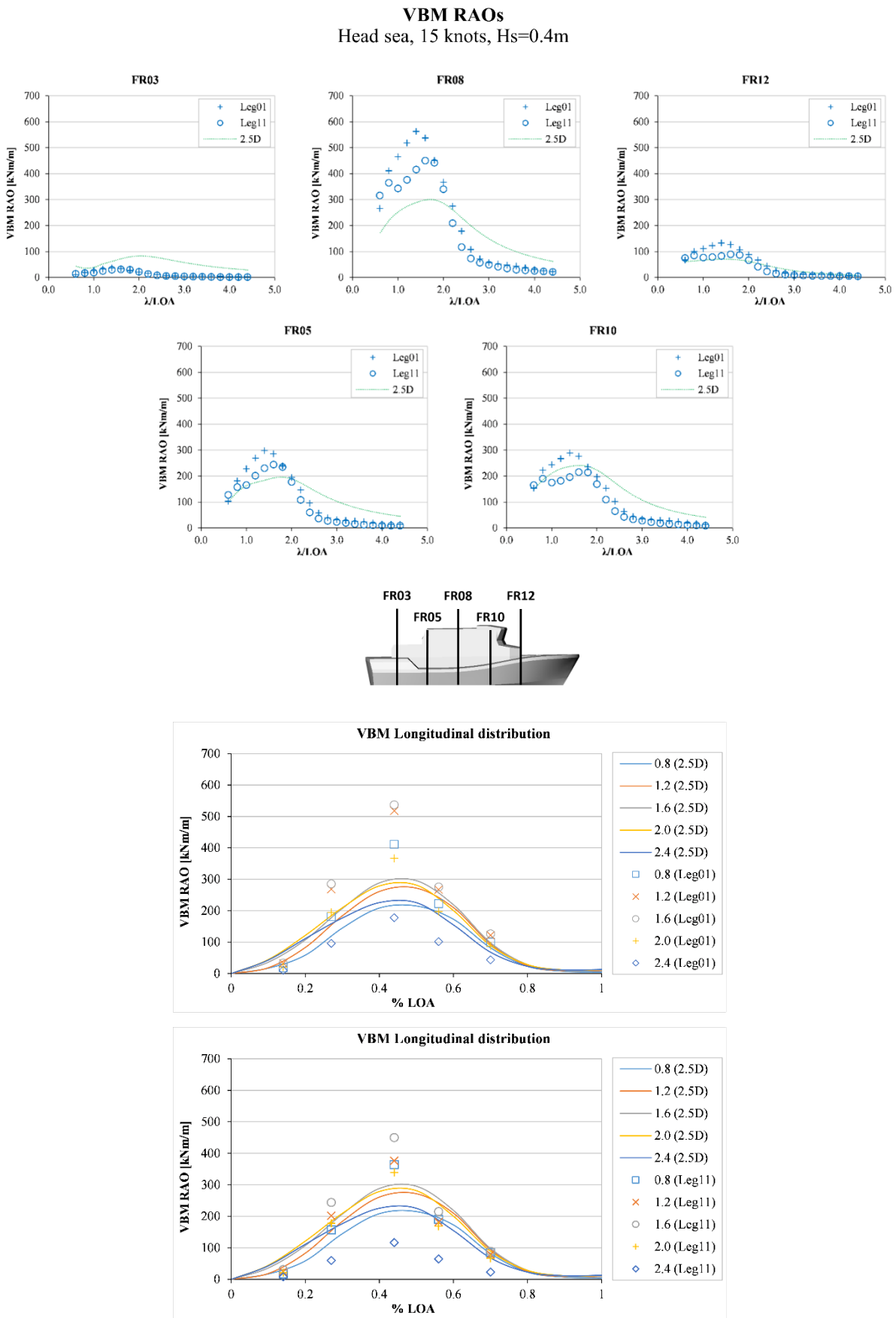

Figure 6.36. Wave-induced VBM RAOs. Head sea, 15kts, Hs=0.4m.

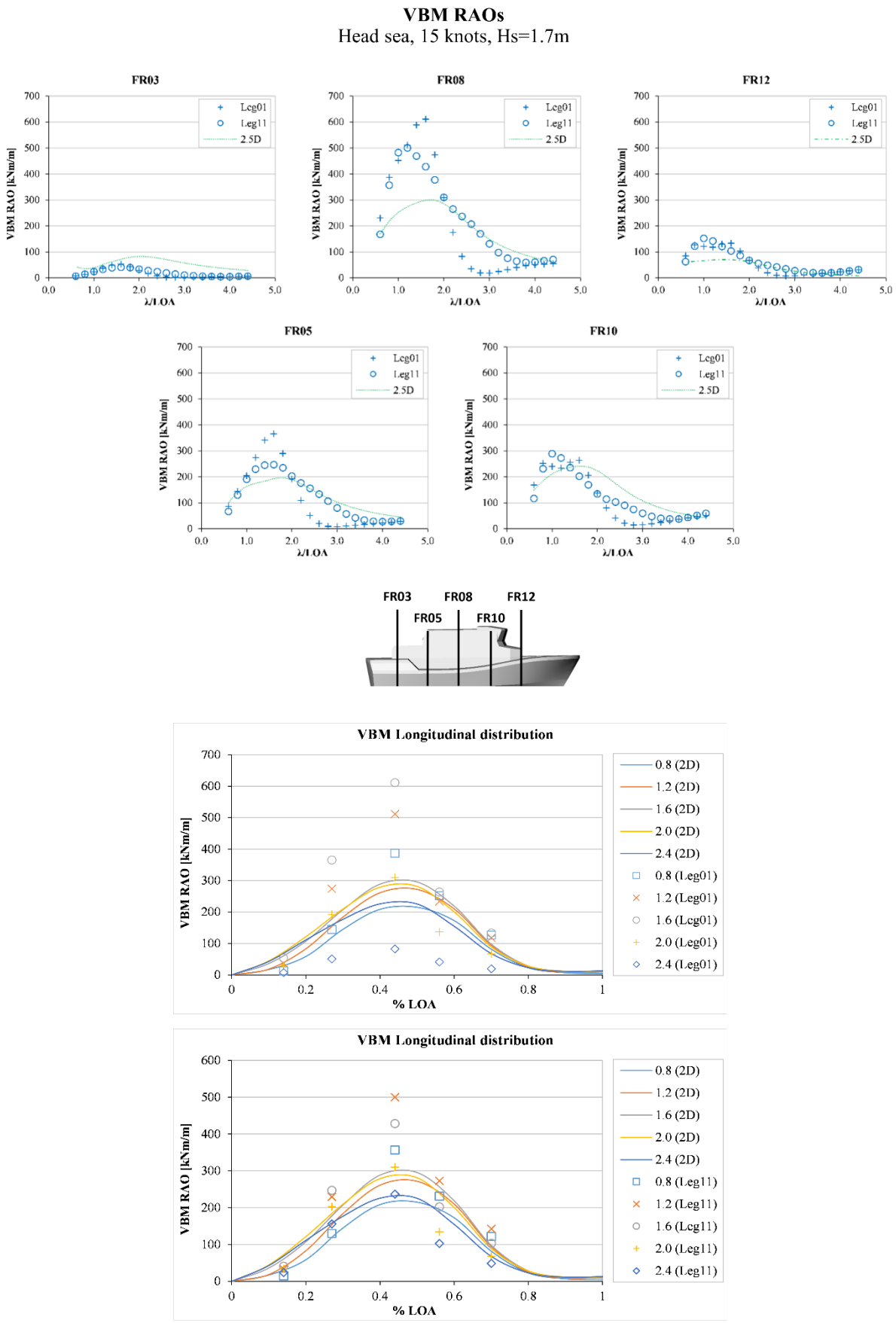

Figure 6.37. Wave-induced VBM RAOs. Head sea, 15kts, Hs=1.7m.

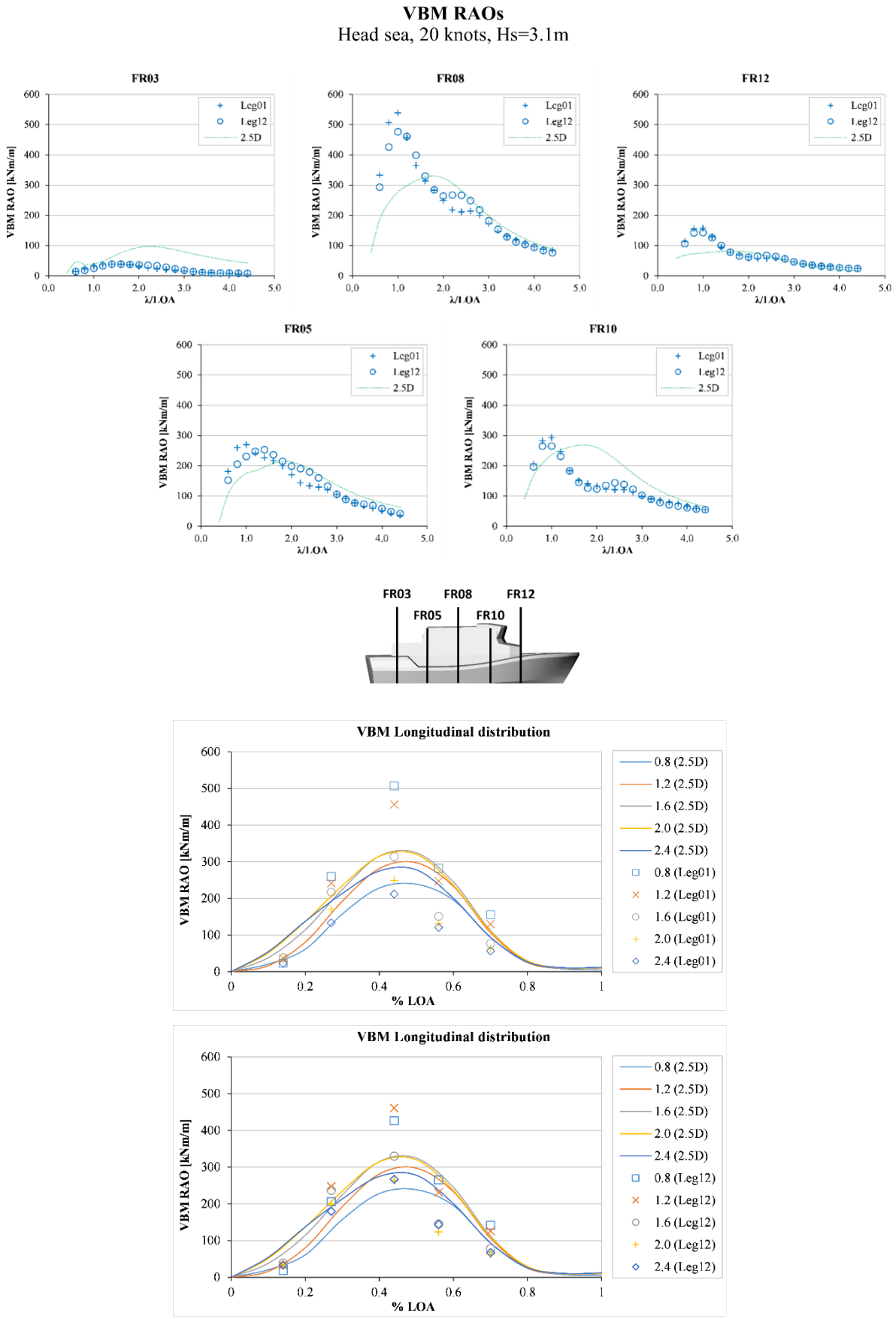

Figure 6.38. Wave-induced VBM RAOs. Head sea, 20kts, Hs=3.1m.

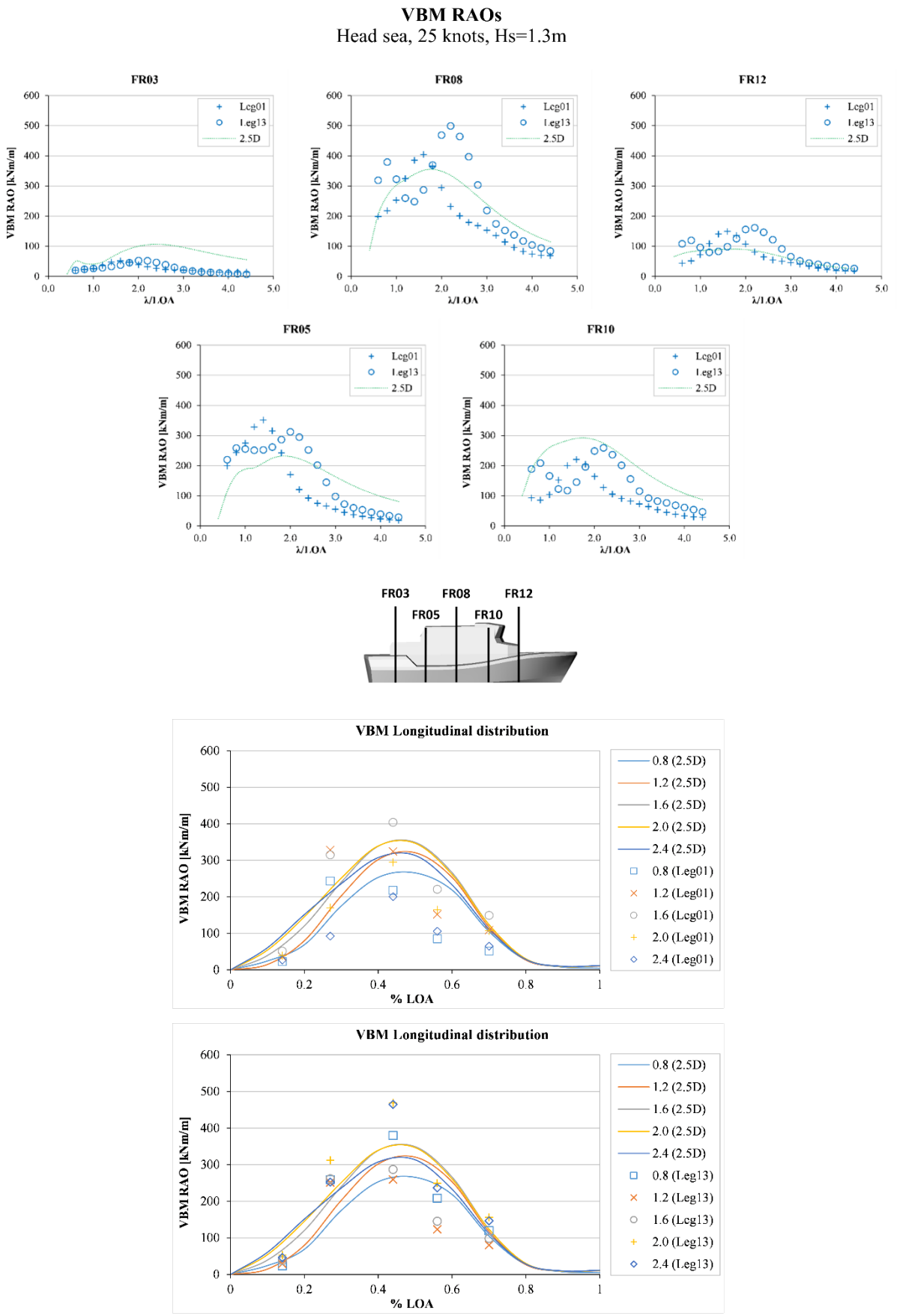

Figure 6.39. Wave-induced VBM RAOs. Head sea, 25kts, Hs=1.3m.

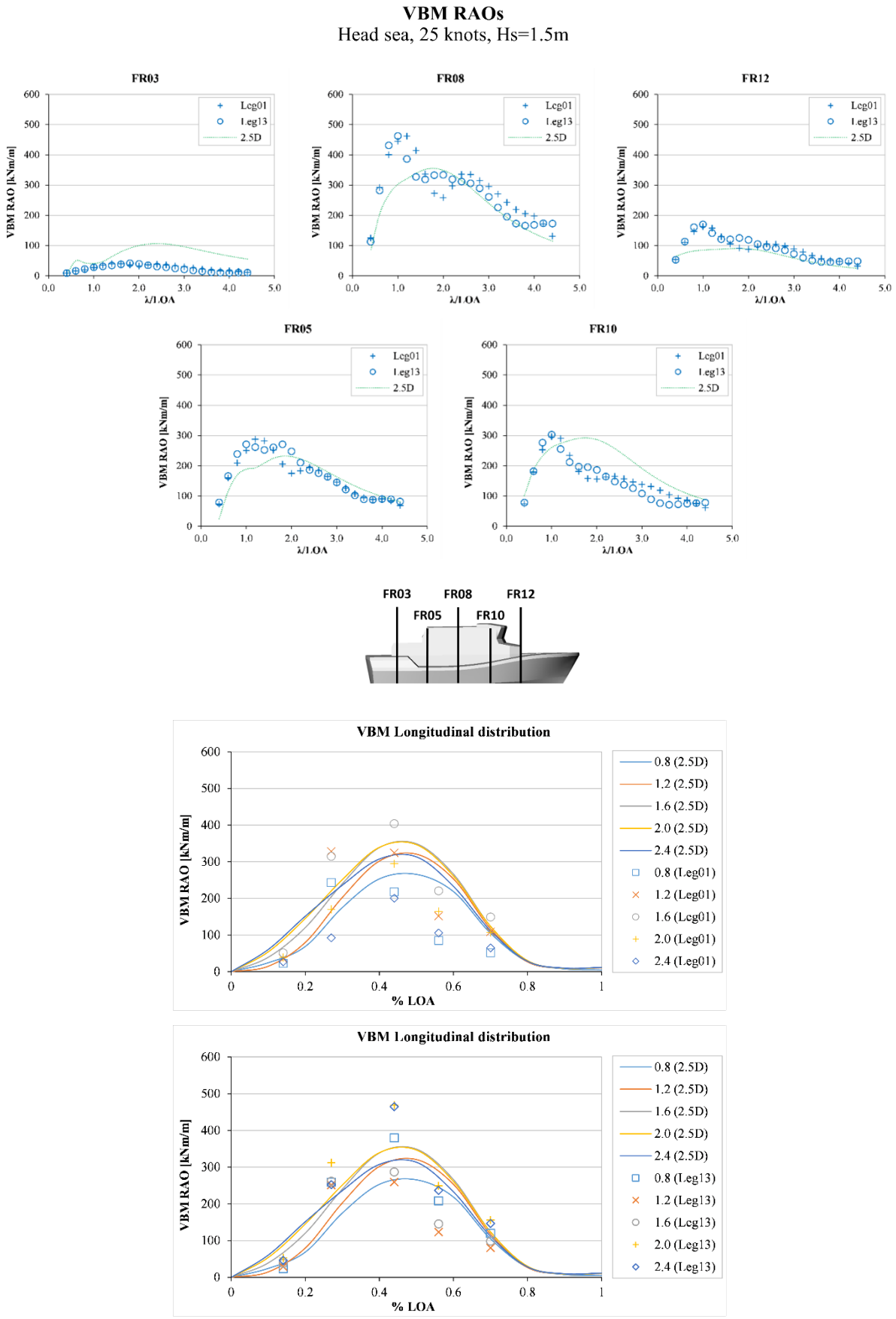

Figure 6.40. Wave-induced VBM RAOs. Head sea, 25kts, Hs=1.5m.

6.9 Discussion

6.9.1 Accuracy of the Measurements

Results of seakeeping trials are generally dependent on factors that introduce some variability in the data sets. Some of the main sources of uncertainty are briefly discussed:

- The effect of wind and current on the vessel responses was not considered explicitly in the data analysis and can be expected to have introduced some uncertainty.
- The wave directionality was considered through an assessment of the wave direction spectra. The wave spread, and the resulting effect on the vessel responses, was not explicitly considered and part of the data analysis was carried out under the assumption of long crested waves. Results found to be affected by misalignment of the trial trajectory with respect to the wave direction and by presence of multiple wave systems will be pointed out in the following sections.
- The principal wave direction and the relative vessel heading were estimated during the trials with best judgement. The vessel speed was estimated from the on-board GPS tracker. A mean value was assigned to each leg of the star trajectory and used for the data analysis. Some uncertainty in the results should therefore be attributed to differences between the nominal and the actual heading, and between the mean and the instantaneous speed kept during each leg of the trial trajectory.
- The effect of the displacement changing during the trial was attenuated by filtering out drift and slowly moving trends in the vessel responses. The difference in displacement between trials was also minimised. Although some variability was present, it is believed that other factors played a major role and that the variability in the loading condition between the trials could be at first neglected.
- The stiffness of the hull girder limited the measurement of small strain values. This was mainly the case of the hull girder strains towards the stern (FR03). The polar plots of vertical bending moment (Figures 6.23-6.31) show some scatter in the significant and maximum values measured at different headings. The RAO plots (Figures 6.32-6.40) also show that the vertical bending moment measured is appreciably smaller than what was predicted numerically.

6.9.2 Wave Period

The wavelength, and the associated wave period, have a large influence on the vessel responses. A systematic assessment based on sea trials, if ever possible, would certainly require a much larger test matrix. It is still worth considering the sea conditions found during the trials to define a range of use for the data collected. Part of the results presented in the thesis are indeed 'valid' for similar seas and are expected to be different for sea conditions that deviate substantially from the reference ones.

The quantity considered is the wave modal or peak period Tp, which is the period associated with the peak of the wave energy spectrum. The sea conditions found during the trials are reported on top of wave scatter diagrams of the North Sea, showing the joint frequency of occurrence of wave height and period for an average year. Figure 6.41, from Lee (1995), is relative to a grid point in the centre of the North Sea. Figure 6.42, from the Southampton Oceanography Centre (2001), is relative to a grid point closer to the trial area. This plot shows also lines of constant steepness calculated as the ratio Hs/λ. For both diagrams a range of peak periods with maximum frequency of occurrence and wide enough to encompass most of the conditions found during the sea trials is shown. Except for the two trials at V=25kts, all the others fit reasonably within the proposed envelope. The trials at V=5kts were also conducted in waves of similar steepness.

6.9.3 Wave Direction and Spread

Differences between the actual and the nominal wave direction can be somehow appreciated from the polar plots of vertical bending moment. It is reasonable to assume that, in absence of systematic errors introduced by wind, current or significant wave spread, a polar plot of a vessel response would show a port-starboard symmetry, provided that there are no large errors in the estimation of the nominal heading. For a 8-heading plot, any of these effects is likely to manifest itself as a rotation of the polar plot with a consequent port-starboard asymmetry. The polar plots of wave-induced VBM presented in Figures 6.23-6.31 show, by large, a reasonable port-starboard symmetry, more evident in the significant (highest $1/3^{rd}$) than the maximum values, as it can be expected.

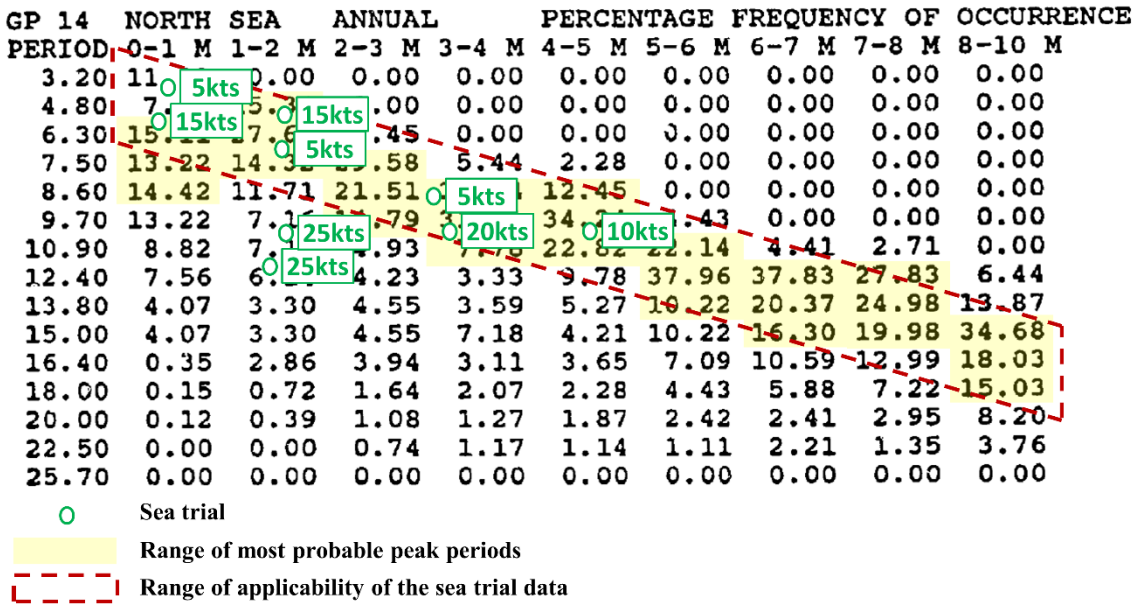

Figure 6.41. Wave scatter diagram for the North Sea showing the sea conditions (Hs & Tp) found during the sea trials (adapted from Lee (1995)).

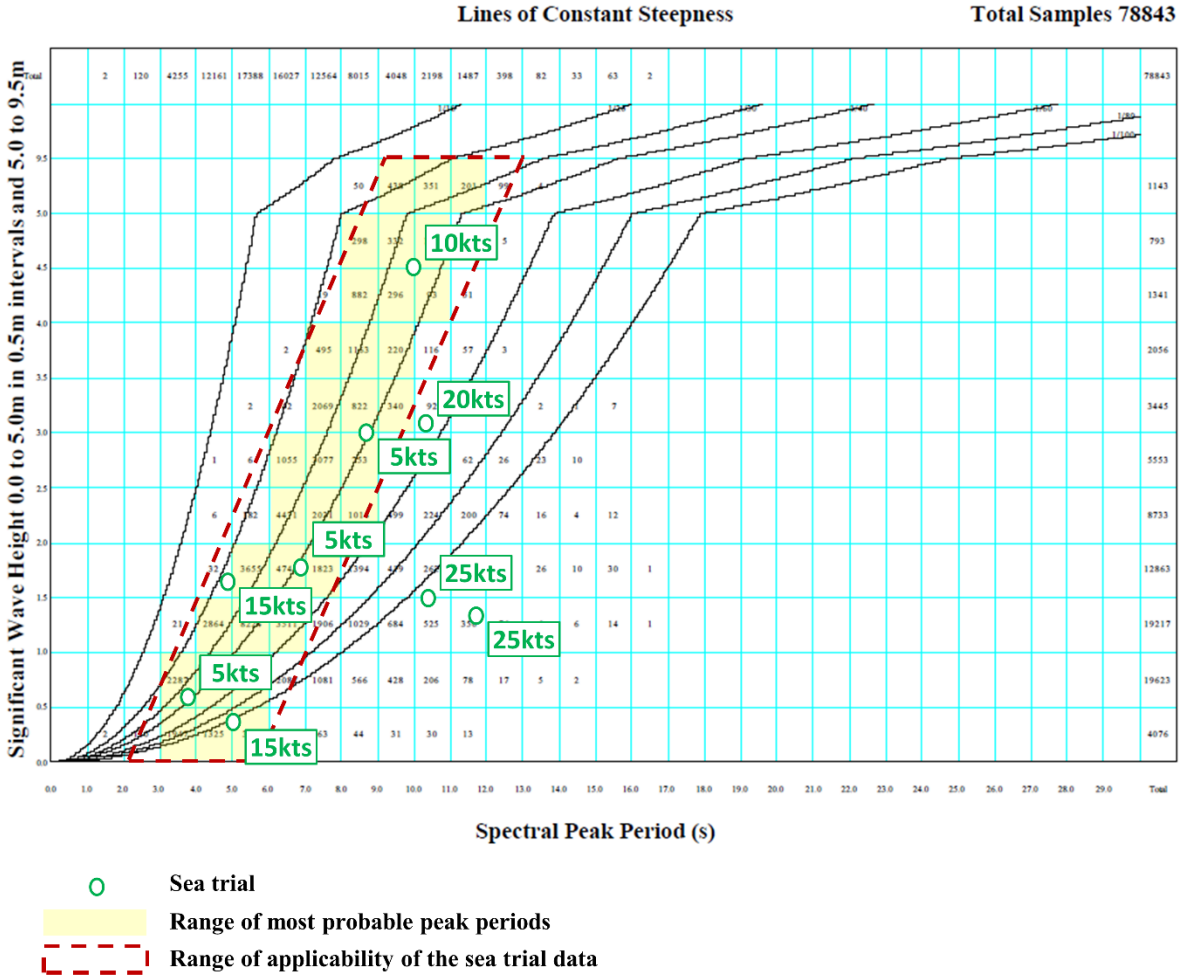

Figure 6.42. Wave scatter diagram for the North Sea showing the sea conditions (Hs & Tp) found during the sea trials (adapted from Southampton Oceanography Centre (2001)).

This suggests that the trial trajectories were reasonably well oriented according to the principal wave direction and that the results are not affected by significant errors due to wind, current or wave spread. There are some exceptions.

Figure 6.26 shows the results relative to a trial at V=10kts in Hs=4.5m. The significant and maximum values are larger in waves from the port bow than from the starboard bow, and in waves from the starboard quarter than from the port quarter. This is likely due to a misalignment of the trial trajectory, as suggested by the difference, shown in Figure 6.43, between the principal wave direction calculated from wave measurements and the compass heading adopted for head sea. Similar observations can be made for the trial at V=20kts in Hs=3.1m (Figure 6.29). The difference between the principal wave direction and the head sea compass heading kept is shown in Figure 6.44.

Slightly different is the cause attributed to the skewness of the polar plots shown in Figure 6.27 for the trial at V=15kts in Hs=0.4m. Figure 6.45 highlights the presence of two wave systems, a lower frequency swell and higher frequency wind waves, with directions 90° apart. Similar and more apparent is the effect of different wave systems on the results presented in Figure 6.30 for the trial at V=25kts in Hs=1.3m. The presence of swell and wind waves is evident in Figure 6.46.

Improvement of the results could be possible by adopting more sophisticated analysis methods that account for the effect of the wave directionality. Partitioning of the wave and vessel response spectra has the potential to correct the bias introduced by the presence of multiple wave systems. This has not been attempted, hence the results relative to the trials at V=15kts in Hs=0.4m and at V=25kts in Hs=1.3m should be considered with care. The latter, in particular, could be considered 'unreliable', with also RAOs that diverge significantly from the expected trends, as discussed in the following sections.

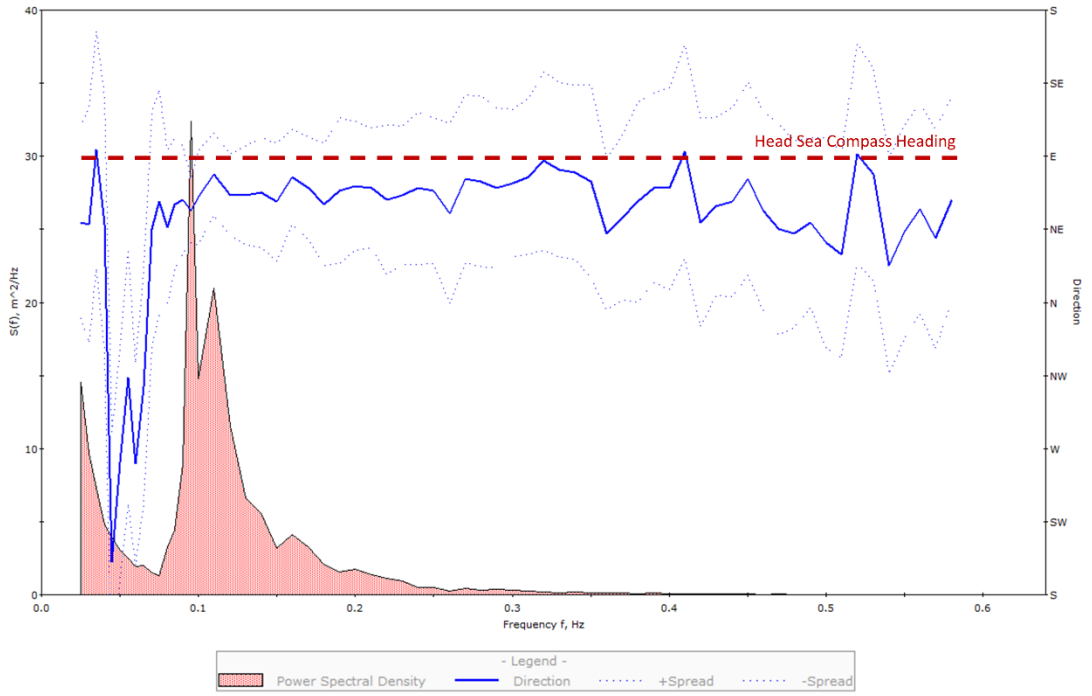

Figure 6.43. Estimated and actual wave direction. Trial at 10kts in Hs=4.5m.

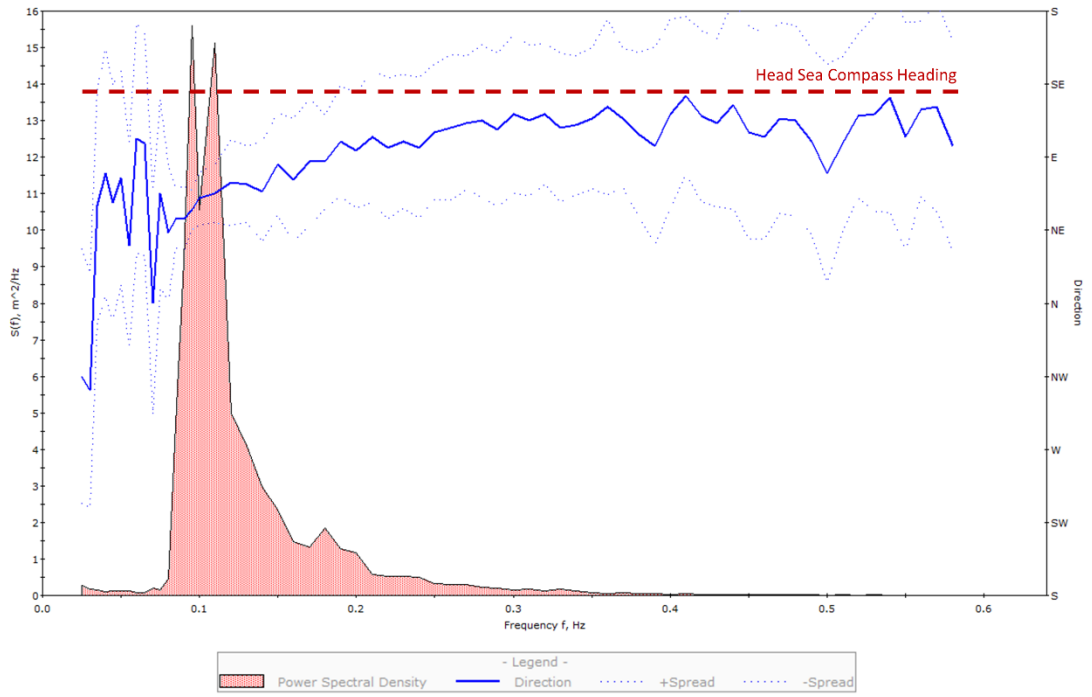

Figure 6.44. Estimated and actual wave direction. Trial at 20kts in Hs=3.1m.

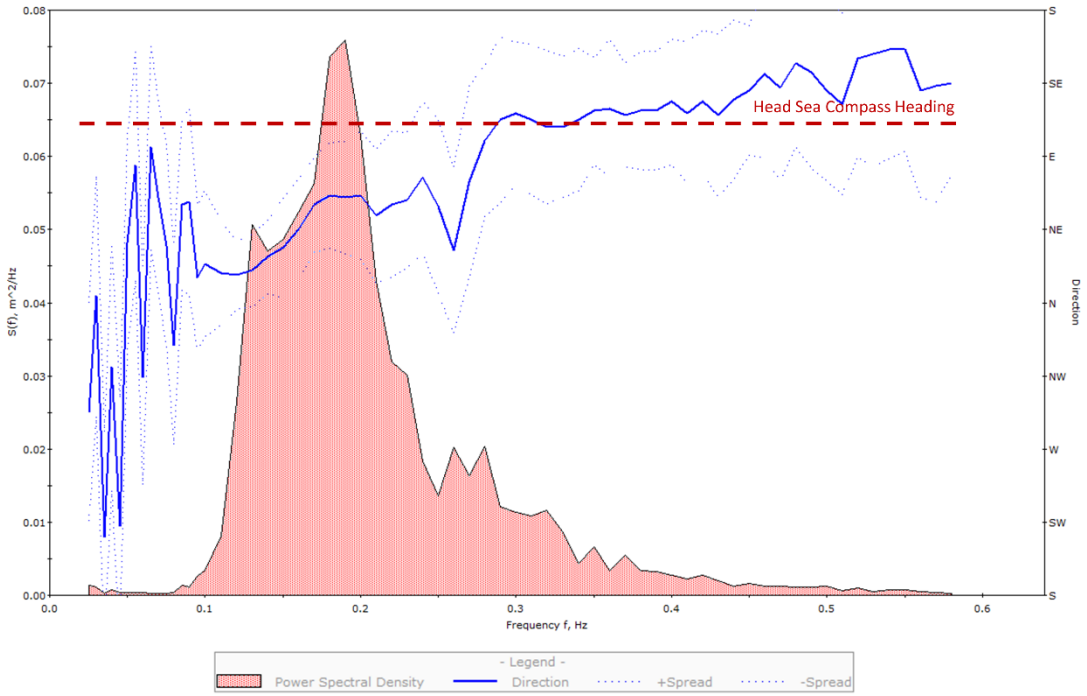

Figure 6.45. Estimated and actual wave direction. Trial at 15kts in Hs=0.4m.

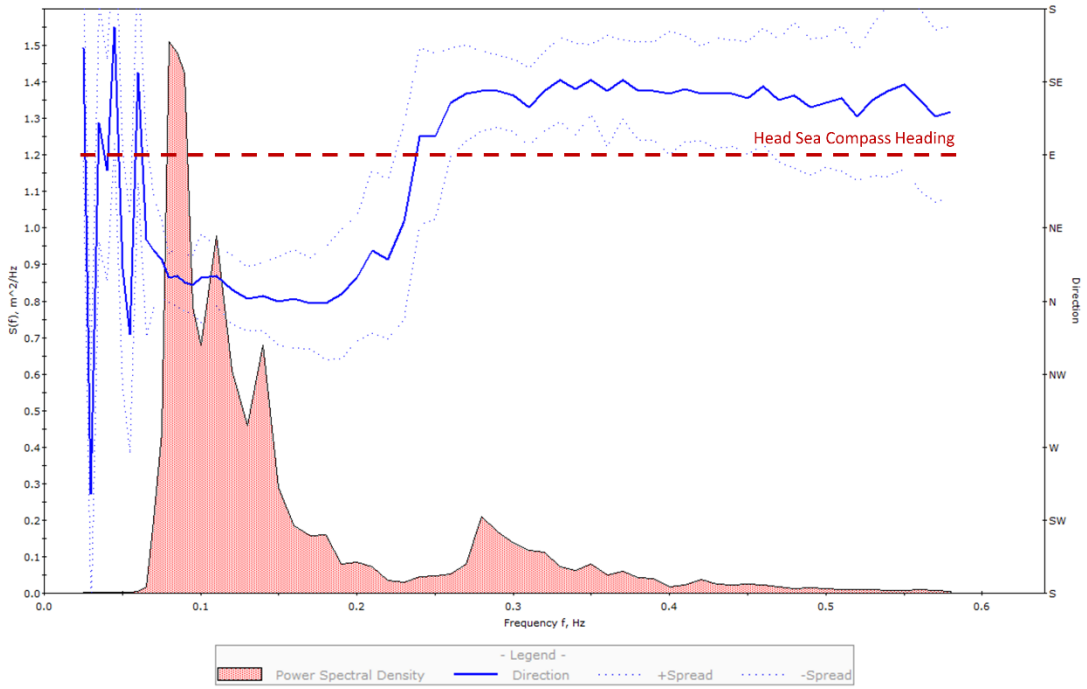

Figure 6.46. Estimated and actual wave direction. Trial at 25kts in Hs=1.3m.

6.9.4 Response at Different Headings

The effect of the heading on the VBM magnitude can be assessed from the polar plots in Figures 6.23-6.31, which confirm what would be reasonably expected.

At speeds up to 15kts the highest loads occur in head seas followed by bow quartering seas. Wave directions from abaft the beam generate appreciable smaller loads. At higher speeds, 20-25kts, the maxima still occur in head seas, but loads in seas from between directly astern and the stern quarter tend to approach those in seas from between the fore and the bow quarter.

6.9.5 Sagging-to-Hogging Ratio

The linear theory of ship motions predicts the same value of wave vertical bending moment for both sagging and hogging. There are, however, differences that arise from the hull form, which is not wall-sided. This is particularly the case for vessels with a small block coefficient, pronounced bow flare and/or high operating speeds. There are also hydrodynamic differences between the entry and exit of the hull at the waterplane, and between the crest and the trough of a non-sinusoidal wave (Hughes 1983). As a consequence, sagging bending moment can be significantly larger than hogging bending moment. This was also the case for the Severn, as shown in Figures 6.23-6.31. The only appreciable anomaly is in Figure 6.31 for the trial at V=25kts in Hs=1.5m, where the significant values of VBM in hogging exceed, at times, those in sagging. Since the sagging VBM is typically higher than the hogging VBM, data is often analysed in terms of 'sag-to-hog' ratio. Dependences are found with the vessel speed and with the wave height.

At speeds up to 15kts the highest sag-to-hog values occur in head seas, followed by bow quartering seas. Other headings generate small or negligible differences between sagging and hogging. At higher speeds, 20-25kts, appreciable values also occur, at times, in following and stern quartering seas.

The effect of the wave height is not straightforward to analyse, as the sag-to-hog ratio may be dependent also on the wave period and the two effects cannot be entirely separated out from the present set of data. An assessment can be made for the three trials at V=5kts in Hs=0.6, 1.6 and 3.0m, for which the wave peak periods are close to

those with the maximum probability of occurrence in the North Sea and waves have similar steepness (Section 6.9.2). If the significant values are considered, the sag-to-hog ratio near amidships (FR08) in head sea increases from 1.1 in Hs=0.6m, to 1.3 in Hs=1.6m and to 1.6 in Hs=3.0m. Similar conclusions can be drawn from the two trials at V=15kts in Hs=0.4 and 1.7m. These were conducted in seas with similar wave peak period, Tp=5.1 and 4.9s respectively. If the significant values are considered, the sag-to-hog ratio near amidships (FR08) in head sea increases from 1.2 in Hs=0.4 to 1.6 in Hs=1.7m. If the approximation of the comparisons is accepted, both examples suggest that the sag-to-hog ratio increases with the wave height. This relation suggests a departure from the assumptions of the linear theory, in particular the assumption of wall sidedness. Linear predictions become progressively less accurate as the wave height and, hence, the vessel motions increase.

6.9.6 Wave Load RAOs

Wave-induced vertical bending moment RAOs calculated from the sea trials are presented in Figures 6.32-6.40. Two data series are shown, for the first and the last head sea leg of each trial.

If all the results are considered at once, the two data series prove to be sensibly consistent. Differences should not be, in principle, attributable to changes of displacement, whose effects were attenuated by filtering out drift in the strain signals. Instead they are likely to highlight other factors, such as wave direction, current or wind, that, by changing during the trial, introduced some bias in the data. The most evident example is shown in Figure 6.39 for the trial at V=25kts in Hs=1.3m. The presence of two wave systems with different directions (Section 6.9.3), and whose energy changed during the trial, appears to be the main cause of significant differences in the VBM RAOs calculated for the two head sea legs. More sophisticated analysis techniques could improve the results.

The longitudinal distribution of VBM RAOs is what would be expected for a conventional hull form. One station forward of amidships (FR10) appears to sustain lower loads than expected if a curve was fitted through the experimental data points.

This could be either a feature of the vessel's structure or, more likely, an error in the estimation of the section modulus or the Young's modulus of the cross-section.

The consistency in the RAOs from trials carried out at the same speed, but in different wave heights, informs on the validity of linear theory, and therefore of the use of RAOs, for the analysis of the wave-induced vertical bending moment. This can be better appreciated from Figure 6.47, where the RAOs from the trials at V=5kts in Hs=0.6, 1.6 & 3.0m are superimposed. The similar RAOs in different wave heights suggest that at 5kts linear theory is accurate even in significant wave heights up to 3.0m. Similar results, with a greater scatter, are shown in Figure 6.48 for the trials at V=15kts in Hs=0.4 & 1.7m and similar conclusion can be drawn for speeds of 15kts in wave heights up to 1.7m.

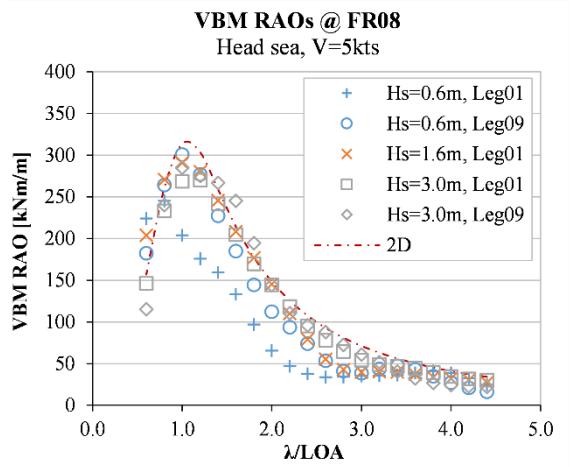

Figure 6.47. Wave-induced VBM RAOs near amidships (FR08). Head sea, 5kts, Hs=0.6, 1.6 & 3.0m.

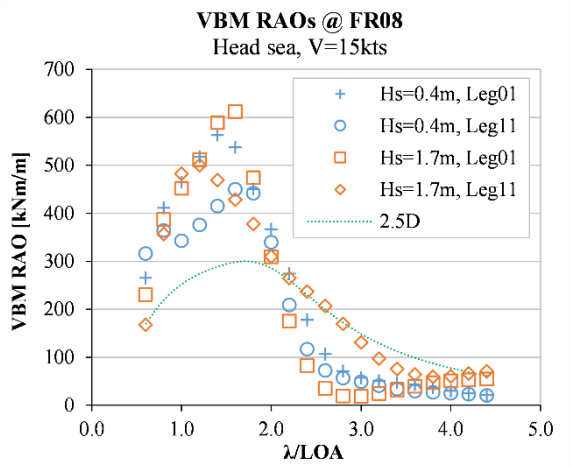

Figure 6.48. Wave-induced VBM RAOs near amidships (FR08). Head sea, 15kts, Hs=0.4 & 1.7m.

6.9.7 Comparison with Numerical Simulations

Numerical and experimental data series are co-plotted in Figures 6.32-6.40 for an assessment of the numerical model (Chapter 4) and to confirm the validity of the spectral analysis conducted on the sea trial data.

Figures 6.32-6.35 show the VBM RAOs at speeds up to 10kts and in significant wave heights up to 4.5m. The numerical RAOs well encompass the experimental values, with only one exception at V=10kts in Hs=4.5m near the fore (FR12 in Figure 6.35). If the longitudinal distribution of the load is considered, at this frame the load envelope has its steepest slope and what appears as a large gap between the two sets of data becomes

less of concern when considering the load distribution along the length of the vessel. It is still recognised that higher loads were measured, which might suggest a loss of accuracy of numerical model for that combination of speed and wave height. The agreement between the simulations and the sea trials is taken as outstanding near amidships (FR05 & FR08), which proves that the numerical simulations are accurate, at speeds up to 10kts, even in seas with a significant wave height up to 4.5m.

Figures 6.36-6.40 show the VBM RAOs at speeds from 15kts and in significant wave heights up to 3.1m. The same findings as for lower speeds are limited to wavelengths longer than twice the vessel length ($\lambda/LOA \geq 2$). At V=15kts only the trend of the RAOs is well captured, while the magnitude is clearly underestimated by the simulations. At V=20 & 25kts the numerical RAOs also miss to model a peak in the response at $\lambda/LOA \approx 1$.

The dependency with the vessel speed, and the loss of accuracy at V=10-15kts, seem to frame the predictive capability of the numerical model within the displacement regime. Of less relevance is the effect of the wave height.

6.10 Summary

The work described in this chapter is summarised in Figure 6.49. Dedicated seakeeping trials were conducted with an instrumented Severn lifeboat. Angular velocities and accelerations were measured at the centre of gravity of the vessel. Global and local structural responses induced by wave and slamming loads were measured with a system of strain gauges. The angular velocity and acceleration data collected was not analysed as part of this thesis. However, through the procedure presented for global wave loads, motion RAOs could be calculated and compared with those predicted numerically. Global sectional loads were found from strain measurements using the classical beam theory. Signal filtering was employed to isolate the wave-induced global loads from the whipping response of the hull girder to slamming impacts. The first term was used to validate CFD simulations through a direct comparison of the results, presented as RAOs. Signal filtering was employed to isolate local slamming-induced strains from global strains and local wave-induced strains. Local slamming pressures were estimated with a strain-to-pressure relation found through finite element analysis of the local structure.

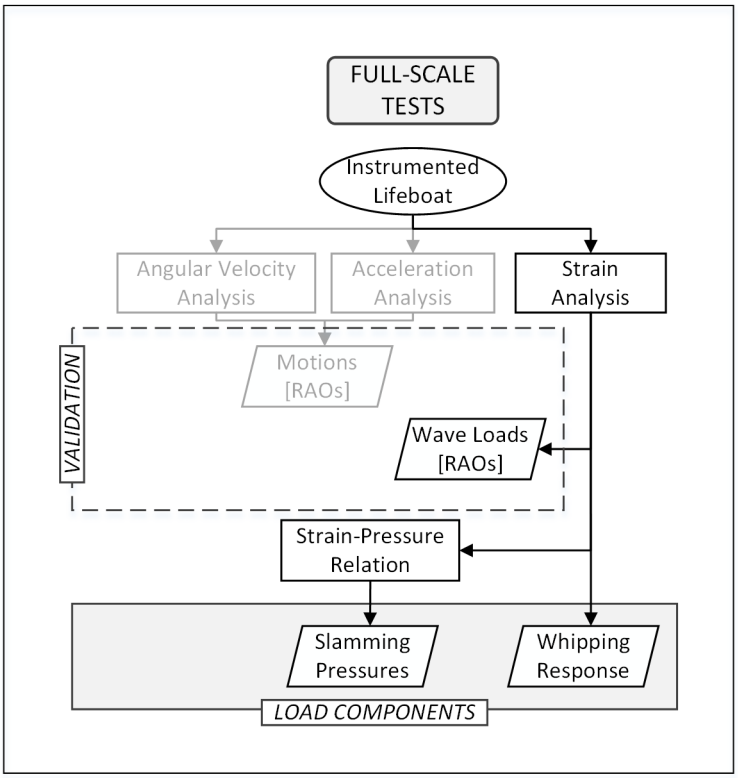

Figure 6.49. Direct calculation approach. Full-scale tests.

Chapter 7

Structural Response

7.1 Framework

The previous chapters concerned the prediction and measurement of seakeeping loads in given operating conditions. Numerical simulations, small-scale tests and sea trials produced results in terms of RAOs, and so for regular waves of unit amplitude. The sea trials also produced data on slamming loads that are directly related to the operating conditions and the duration of the trials. These results need to be extrapolated for conditions different from those tested. The procedure is based on probability and involves predicting extreme load values over a given period of exposure.

7.2 Definition of Extreme Loads

What is often of interest, especially for design purposes, is the response to loads that are experienced in waves, or sea states, that characterise the extreme environmental and operating conditions of the craft. Because of the stochastic nature of the sea and of the many possible operating conditions of a vessel, the prediction of these loads is inevitably related to the concept of probability. Short and long term statistical approaches have

been developed to predict extreme values of a ship response (Hughes 1983). The difference between the two lies in the statistical description of the sea state. A short-term description means that the significant wave height and the mean wave period are assumed constant during the time considered (Faltinsen 1990). This is the case for short periods, typically 1 to 4 hours, for which the sea can be considered to have remained nearly uniform and statistically stationary (Lewis 1988a). Short-term statistics is suitable to predict extremes over a limited period of time. In a long-term description of the sea, the significant wave height and the mean wave period will vary (Faltinsen 1990). Long-term statistics therefore accounts for the different sea conditions encountered by the vessel over longer periods of time.

Since for design purposes the loads of interest are the most severe ones sustained throughout the operational life of the vessel, periods of exposure of 20 to 25 years, with correction factors to account for the actual usage of the vessel, are common values for ship design. The use of these loads is well proven for design calculations, but not suitable to inform on the likely loads sustained during any voyage, which will be, in most cases, much lower. If the voyage is short enough that the sea state remains constant, then short-term statistics could be employed to predict the short-term maximum loads during the voyage. Yet, over the entire life of the vessel it can be expected that these short-term loads will be, at some point, exceeded.

This study makes use of short-term statistics to estimate the maximum seakeeping loads that are expected during any voyage. The period of exposure is set to 3 hours, a common value adopted by classification societies (e.g. American Bureau of Shipping (2011b) and Det Norske Veritas (2012a)). The results produced are intended to support the operation of small high-speed craft while their design would still rely on long-term predictions of the extreme loads sustained throughout their supposed operational file. Although only the short-term predictions are presented, the numerical and experimental data produced would allow estimation of extreme loads suitable for design calculations.

7.3 Construction of a Structural Response Curve

The conceptual operational envelope graph proposed by Riley and Marshall (Chapter 1) includes a structural limit curve plotted as a function of speed and sea state severity. The term 'structural limit' is intuitive but rather vague, since it largely depends on what is deemed to be a limit, on the probability level used to determine the extreme loads, and on the level of structural adequacy that is considered acceptable. The term 'structural response' is therefore preferred, as it leaves freedom in the determination of acceptable criteria for its assessment.

A method is proposed to determine a structural response curve as a function of speed and sea state severity. The method is based on the numerical and experimental results presented in the previous chapters. Speed on the abscissa is expressed as speed over ground (SOG), in knots, while the sea state on the ordinated as significant wave height (Hs), in metres. In order to work with two axes only, a number of parameters is fixed:

- Loading condition: full load departure of the Severn lifeboat used for the trials, as reported in Table 7.1.
- Heading: head sea.
- Spectral shape: JONSWAP (peak enhancement factor γ=3.3) for loads computed numerically and actual sea spectrum for slamming loads computed experimentally from sea trials.
- Wave period: range of peak wave periods as shown in Figure 7.1 (from Chapter 6).
- Return period: 3 hours.

Within the operational envelope plot, structural response curves can be constructed from specific grid points with coordinates: (SOG,Hs). Each point on the plot represents the structural response of the vessel to a load case consisting of the extreme loads that are likely to be experienced in that combination of speed (SOG) and sea state (Hs). The extreme loads are the maximum loads with a given return period, hence expected, in this case, to occur once within 3 hours.

Loading condition			Full load
Displacement	Δ	[kg]	42370
Centre of gravity (x)	LCG	[m]	6.42
Centre of gravity (z)	TCG	[m]	0.00
Centre of gravity (y)	VCG	[m]	2.28

Table 7.1. Loading condition for extreme load prediction.

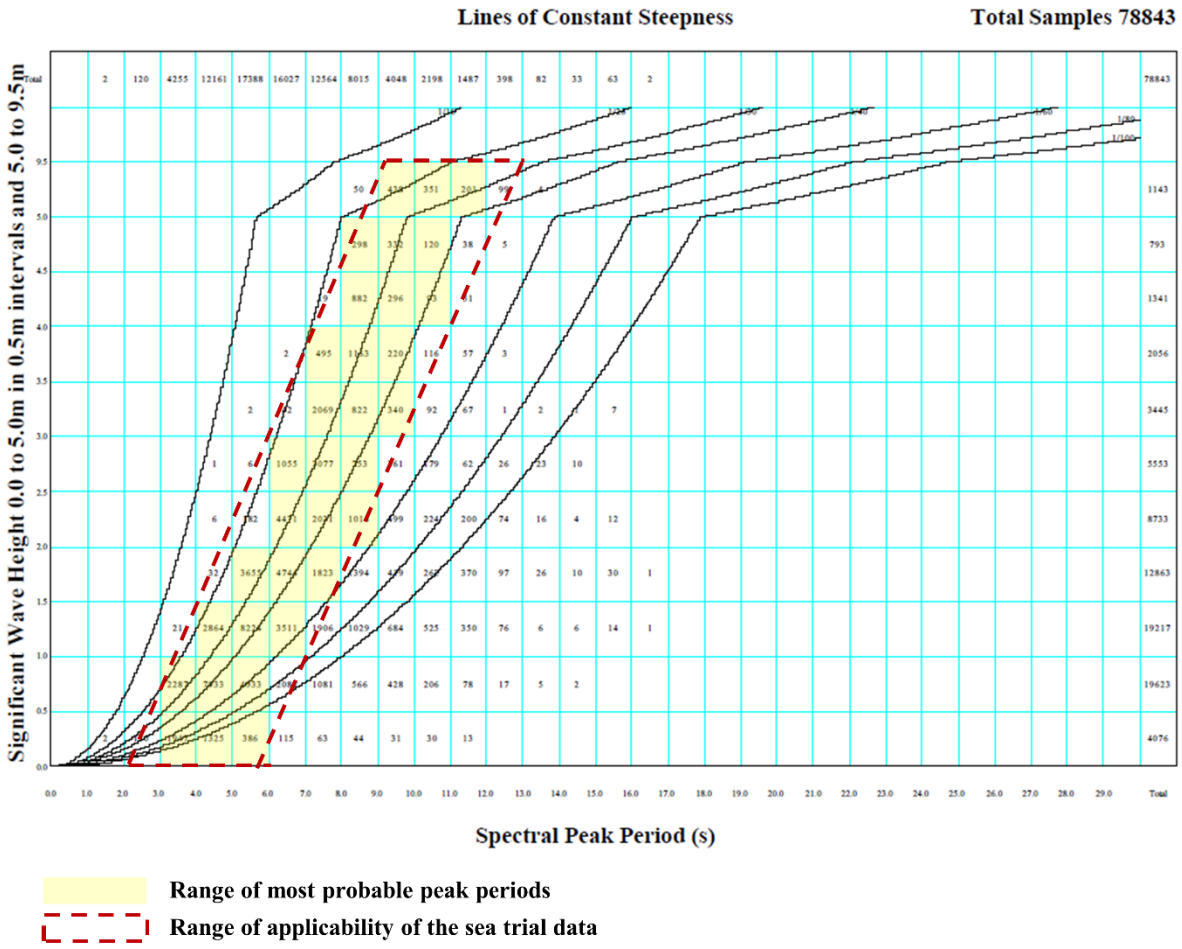

Figure 7.1. Wave scatter diagram for the North Sea showing the wave periods considered for the construction of the structural response curve (adapted from Southampton Oceanography Centre (2001))

7.4 Extreme Values of Linear Responses

Wave loads obtained from the hydrodynamic simulations have been treated, so far, in terms of their RAOs, hence for regular waves of unit amplitude. The estimation of extreme values with a given return period is based on the principles of linear theory detailed in Chapter 2. The global wave load RAOs and their related pressures are scaled linearly, according to the very notion of Response Amplitude Operator.

7.4.1 Prediction of Wave Loads

The extreme wave loads are found through the Extreme Load Analysis module embedded into MAESTRO (Chapter 4), by defining an equivalent wave through its amplitude, phase and length (the direction is already fixed by limiting the calculations to head sea). The VBM RAOs computed numerically are scanned to find the wave length that causes the response to reach its maximum. Found the wave length, the phase angle that corresponds to the maximum response is determined. The wave height is then estimated using a JONSWAP spectrum (ITTC 2002d) and a return period of 3 hours. An equivalent regular wave described by its heading, phase, length and amplitude, is therefore found. This is the wave that simulates the magnitude and location of an extreme VBM value, found by scaling the VBM RAO according to the height of the equivalent wave.

From every equivalent extreme wave, in fact two load cases with 180° phase shift are created: one for sagging and one for hogging. Because of the assumptions of the linear strip theories used for computing the wave loads, vertical bending moment and related pressures have the same and opposite value in sagging and hogging. An example of wave pressures applied to the structural model of the Severn is given in Figure 7.2.

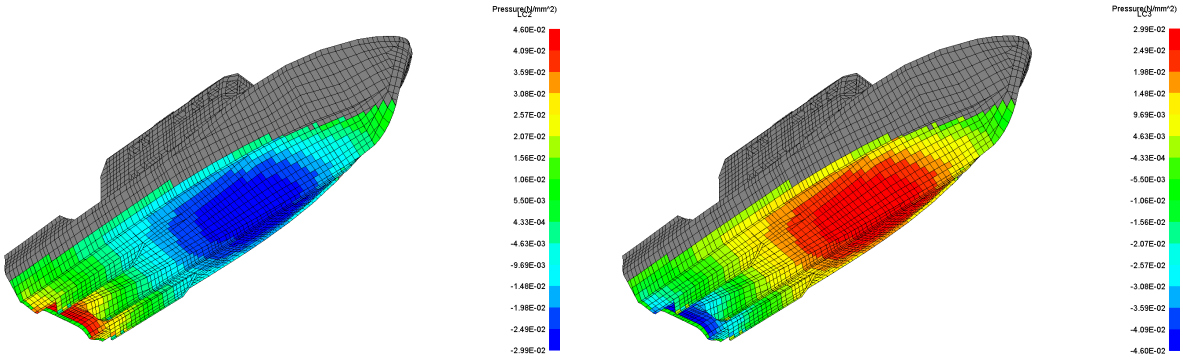

Figure 7.2. Extreme wave pressures in sagging (left) and hogging (right).

7.4.2 Prediction of Hydrostatic Loads

Once the extreme wave is defined, the hydrostatic pressure is computed through a static equilibrium balance (Chapter 4). An example of hydrostatic pressures applied to the structural model of the Severn is given in Figure 7.3. These are superimposed to the hydrodynamic pressures, forming the first two load components of each load case.

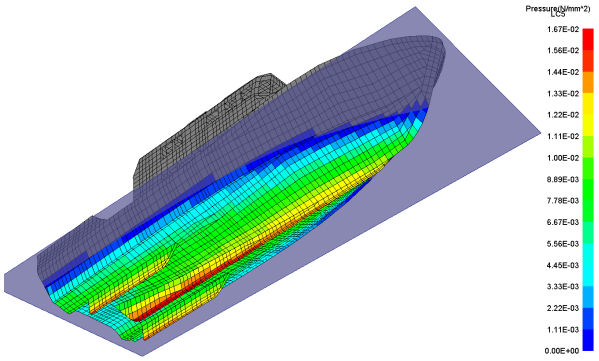

Figure 7.3. Hydrostatic pressures.

7.5 Extreme Values of Nonlinear Responses

The effects of slamming were measured during the sea trials and the data collected consists of a number of short-term data sets (Chapter 6). Extreme values are estimated by extrapolation of the measured data. The nonlinear nature of slamming implies that linear extrapolation by means of a transfer function is not be possible, but other statistical approaches can be applied (Ochi 1978, 1981, Hughes 1983).

The estimation of extreme values from observed short-term measurements relies on the asymptotic distribution developed by Gumbel (1954, 1958). The Gumbel distribution belongs to a family of continuous probability distributions, used in extreme value analysis, to assess, based on a sample of a given random variable, the probability of events that are more extreme than any previously observed. First used to predict extreme natural events, such as floods and wind gusts (Gumbel and Lieblein 1954, Palutikof *et al.* 1999), it has also been applied to predict extreme values of a ship response (Clarke 1986).

The cumulative distribution function of a real-valued random variable X is defined as:

$$F_X(x) = \text{Prob}(\text{X} \leq \text{x}) \tag{7.1}$$

where $F_X(x)$ represents the probability that X takes on a value less than or equal to x. The Gumbel distribution has the following cumulative distribution function:

$$F_X(x) = \exp[-\exp(-y)] \tag{7.2}$$

with y being the reduced variate, defined as:

$$y = \frac{x - \mu}{\sigma} \tag{7.3}$$

where μ is the location parameter and σ is the scale parameter. On a probability histogram, μ is a measure of where the distribution is centred on the horizontal axis (the real value axis) and σ is a measure of how dispersed is the distribution. Both μ and σ can be estimated from a sample of extreme values.

To assess how well the observations fit the theoretical distribution, data can be plotted on an extreme-value probability paper, or simply a 'Gumbel plot'. The procedure, detailed in Gumbel (1954, 1958) and Gumbel and Lieblein (1954), is reported here for the slamming data analysed.

Let us consider a signal representing a slamming-induced response recorded in head sea during a sea trial (Chapter 6). A maximum (peak) and a minimum (trough) value can be found for each minute of the record (Figures 7.4-7.5), hence two datasets are generated. For the vertical bending moment induced by slamming (whipping response), peaks and troughs represent the sagging and hogging bending moment respectively. For the response of single hull panels to slamming pressures, peaks and troughs represent positive and negative strains. Since troughs tend to have negative values and the Gumbel distribution is suitable to predict maxima, troughs are taken with opposite sign.

A Gumbel distribution is fitted to each of the datasets and values for μ and σ are estimated. An example is given in Figures 7.6-7.7, showing probability histograms of the actual data and the correspondent Gumbel distributions.

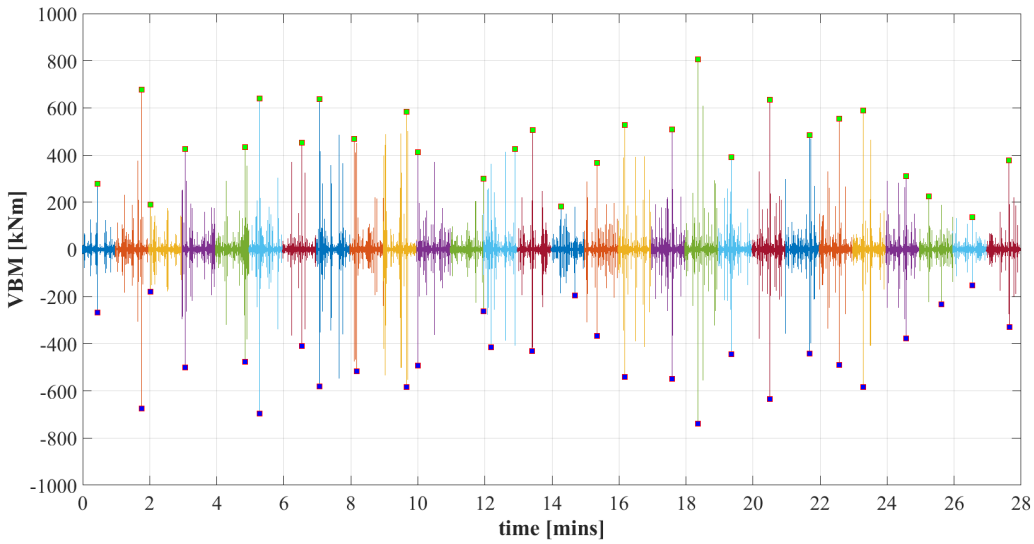

Figure 7.4. Sagging and hogging VBM maximum values for each minute of the record.

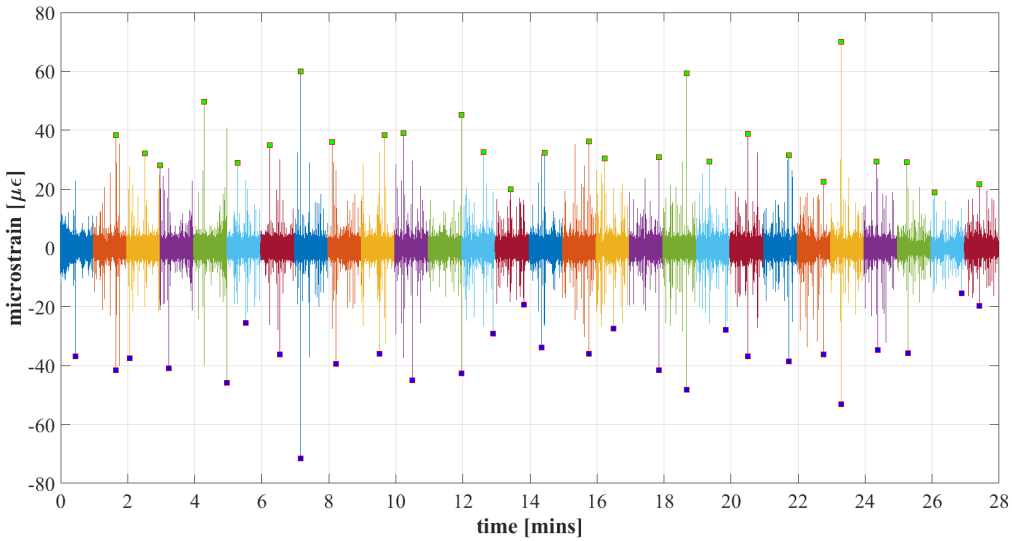

Figure 7.5. Positive and negative strain maximum values for each minute of the record.

Since probability histograms do not show how well extreme values are predicted by the 'ideal' distribution, Gumbel plots are produced. The two datasets of peaks and troughs (the latter with opposite sign) are sorted in ascending order and ranked from 1 to n. The cumulative frequency of the i^{th} term is obtained from:

$$P_i = \frac{i}{n+1} \tag{7.4}$$

where n is the number of observations, i is the order of the observations from the smallest, and P_i is the estimate of the cumulative frequency of the i^{th} term. These estimates are known as plotting positions.

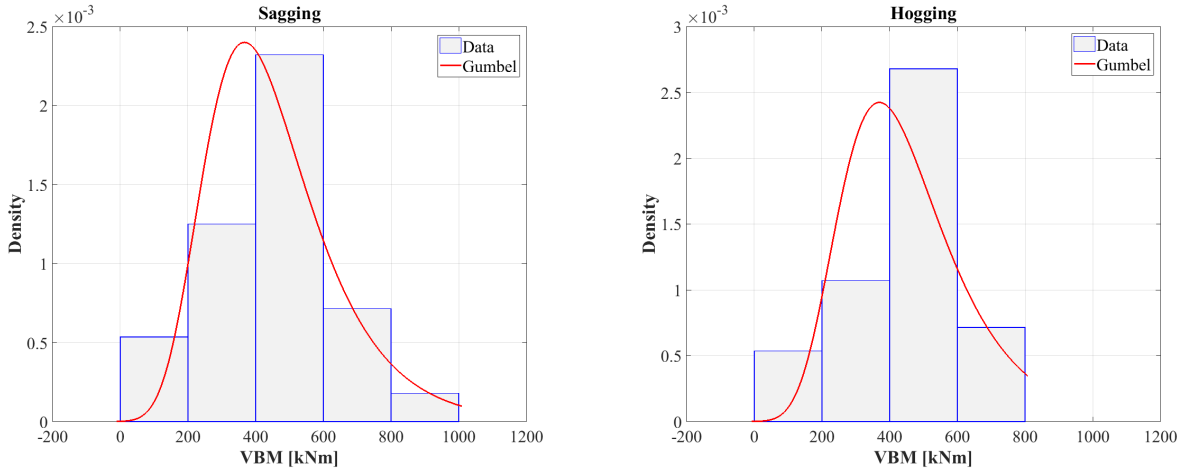

Figure 7.6. Probability histograms of sagging and hogging VBM values. Gumbel distribution superimposed to observations.

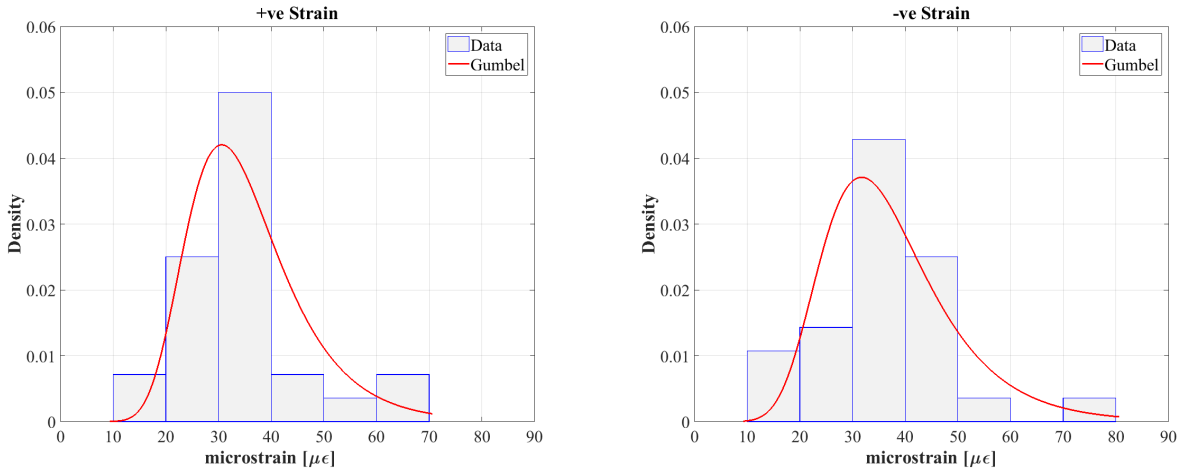

Figure 7.7. Probability histograms of positive and negative strain values. Gumbel distribution superimposed to observations.

The data is then plotted on a graph designed so that the Gumbel distribution shows exactly as a straight line. To achieve this, the reduced variate y is plotted on the abscissa while the ordinate is used for the magnitude of the observed values. The position of the observed values on the abscissa is determined by reversing Equation 7.2 and using the cumulative frequency of the observed values from Equation 7.4:

$$y_i = -\ln[-\ln(P_i)] \tag{7.5}$$

The Gumbel distribution fitted to the dataset can then be co-plotted as a straight line by reversing Equation 7.3, so that the observed values appear as a function of the reduced variate:

$$x = \sigma y + \mu \tag{7.6}$$

Then σ becomes the slope of the line and μ becomes the intercept.

A secondary x-axis showing the return period can also be added. The return period correspondent to a given value of the reduced variate can be computed from Equation 7.2, knowing that the cumulative distribution function is related to the return period by:

$$T = \frac{1}{1 - F_X(x)} \tag{7.7}$$

where T is the return period, in mins, and $F_X(x)$ is cumulative distribution function.

An example is shown in Figure 7.8. The closeness of the plotted points to the straight line is an indication of how well the data fits the theoretical distribution. If the fit is satisfactory, extreme values with a higher return period can be estimated. The figure shows the estimated extreme values with a return period of 3 hours. For this study, the theoretical distribution was considered satisfactory when the trend of the observed values had either a similar or a lower slope, hence when the extreme values predicted theoretically were either those expected or greater.

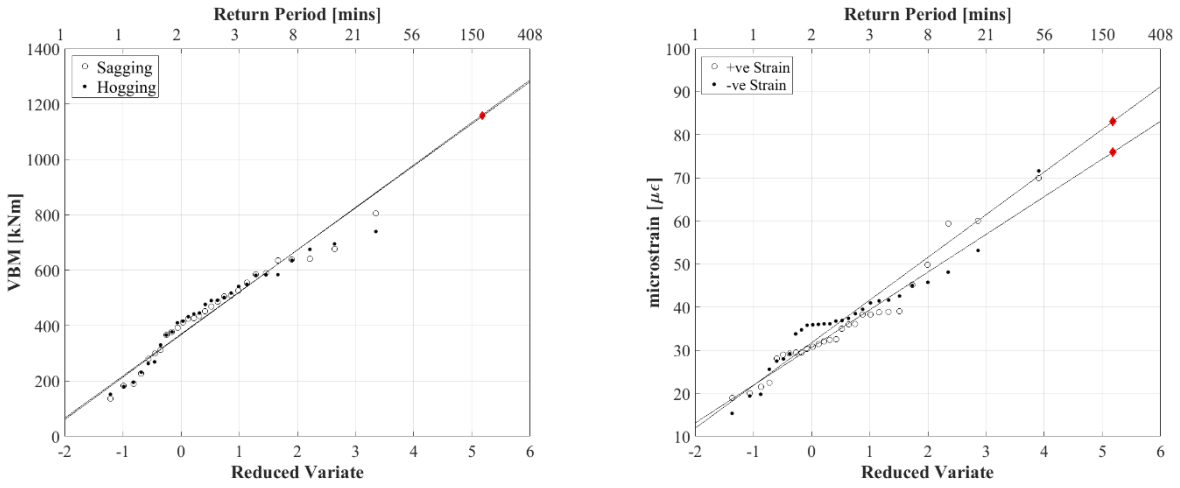

Figure 7.8. Gumbel plots of VBM (left) and panel strains (right). Extreme values with a return period of 180mins are estimated for each dataset.

7.5.1 Prediction of Global Slamming Loads

The whipping response of the hull girder to slamming impacts was measured with a system of strain gauges at five locations along the hull. The strain signals were filtered and converted to VBM signals (Chapter 6) and extreme values with a return period of 3 hours were estimated (Section 7.5). To account for the slamming-induced VBM in the in the structural response analysis, a load distribution needs to be extrapolated from the sagging and hogging extreme values estimated for the five instrumented frames along the hull.

A longitudinal load distribution is constructed from the data presented in Figure 7.9. The distribution consists of an envelope (Figure 7.10) that encompasses the measured values at five locations along the hull. The maximum vertical bending moment value is applied from 35% to 50%LOA. Aft of the plateau this value drops linearly to zero at the aft end, whilst forward of amidships it drops linearly to 0 at the forward perpendicular. The envelope is therefore entirely defined by the value taken at 35-50%LOA, which is to be determined for different combinations of SOG and Hs. This is achieved by considering the extreme values estimated near amidships for different trials (Figure 7.11). Two trials are omitted as conducted out of the range of wave periods considered (Section 8.3) and would appear as outliers. Trials conducted in similar wave heights are grouped into the same series and linear trend lines with zero intercept are fitted through each series. This implies that the effect of the speed on the slamming-induced VBM is assumed linear and that at 0 speed no slamming-induced loads occur.

The effect of the wave height is determined by entering the graph in Figure 7.11 with a set SOG, intercepting the trend lines and fitting a curve between the values found. This is shown in Figure 7.12 for SOG=25kts. Since the trend lines are linear, any other speed could have been chosen. By entering the graph in Figure 7.12 with a given Hs and intercepting the curve fitted through points, Figure 7.11 can be re-created with any chosen value of Hs as a parameter. This is shown in Figure 7.13 for Hs=1,2,...,5m. The figure reveals the combined effect of speed and wave height on the slamming-induced VBM near amidships. The longitudinal load envelope from Figure 7.10 can be scaled according to Figure 7.13 so that the extreme loads with a return period of 3 hours can be estimated for any combination of SOG and Hs.

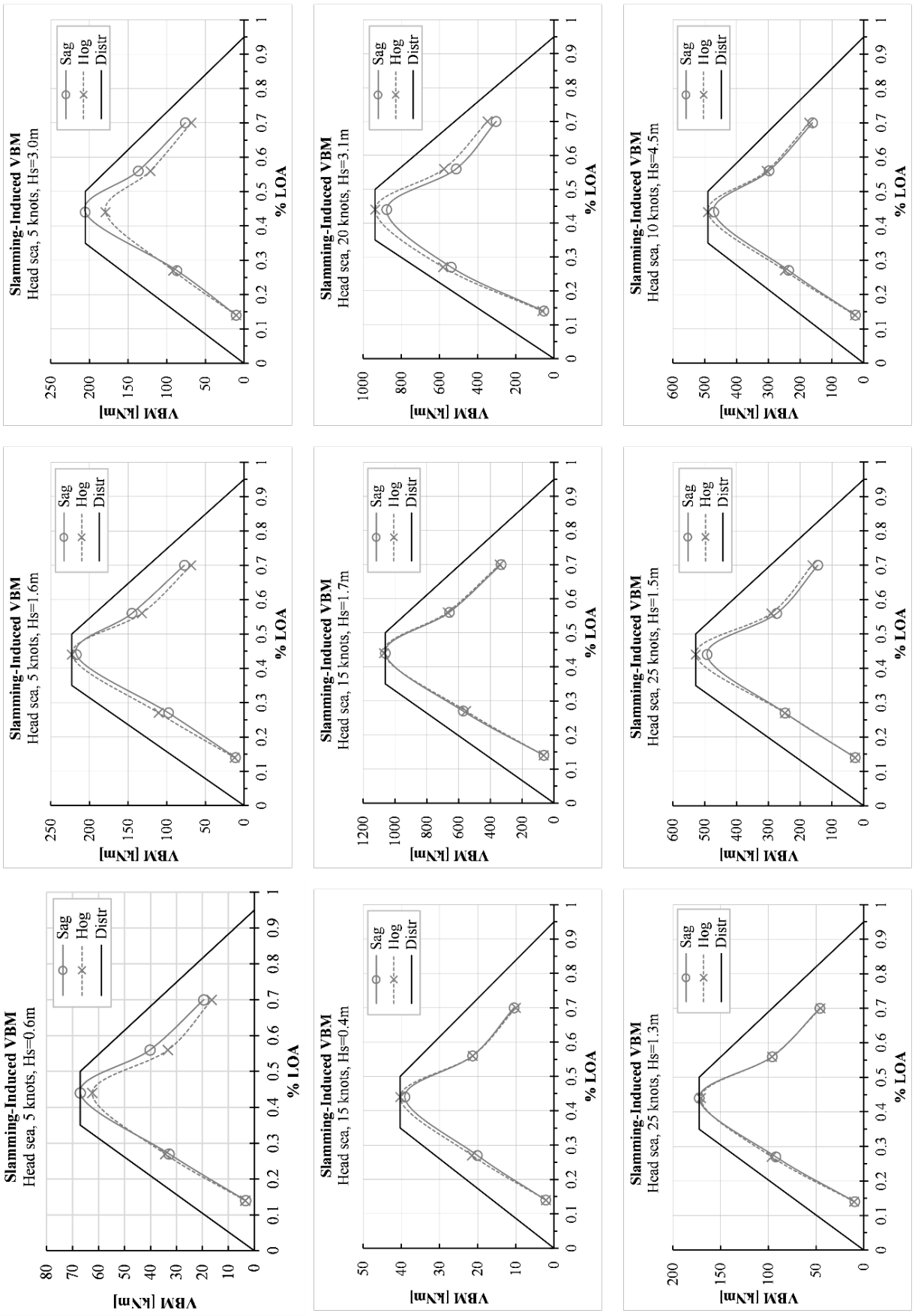

Figure 7.9. Slamming-induced VBM. Extreme values with a return period of 3 hours.

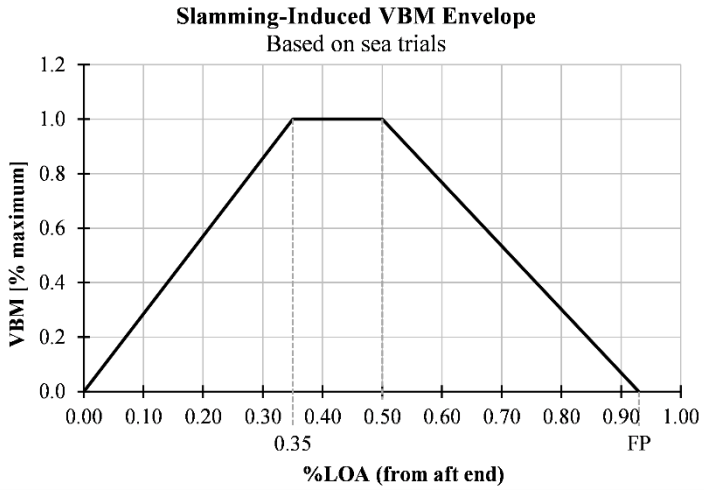

Figure 7.10. Longitudinal distribution of slamming-induced VBM. Constructed from sea trial data.

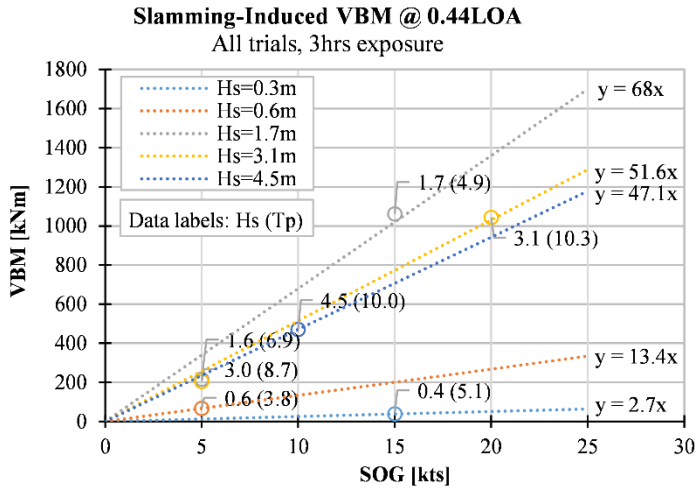

Figure 7.11. Speed effect on the slamming-induced VBM at 0.44LOA. Based on sea trials.

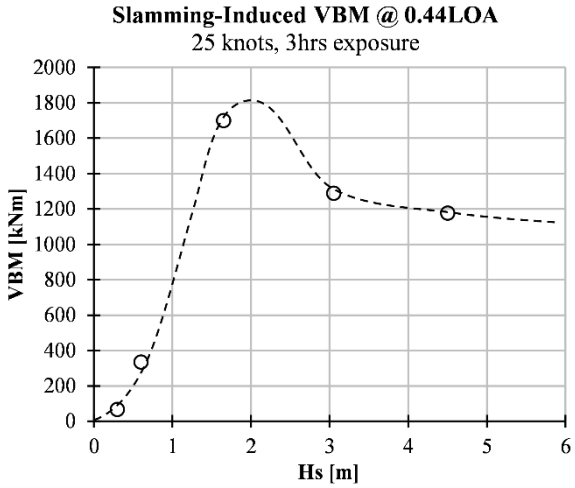

Figure 7.12. Wave height effect on the slamming-induced VBM at 0.44LOA. Based on sea trials.

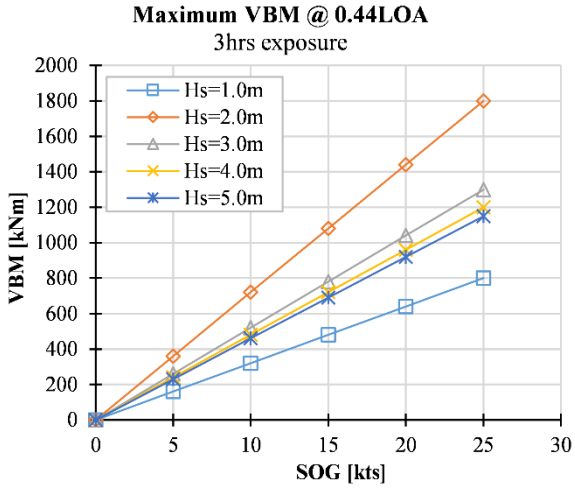

Figure 7.13. Speed and wave height effect on the slamming-induced VBM at 0.44LOA. Based on sea trials.

7.5.2 Prediction of Local Slamming Loads

The local slamming loads were measured with a system of strain gauges on six hull bottom panels and two bow panels. The strain signals were filtered and converted to equivalent static uniform panel pressures (Chapter 6) and extreme values with a return period of 3 hours were estimated (Section 7.5). Pressure values estimated from panels symmetric with respect to the centreline can be expected to be the same in head sea. Hence, from the eight panels instrumented, four pressure values were obtained by averaging the values from the port and the starboard side. To account for the slamming-induced pressures in the structural response analysis, a load distribution needs to be extrapolated from these values. This is achieved through the same procedure adopted for the global slamming loads.

Figure 7.16 shows that slamming pressures are small in seas with Hs<1m, for which the effect of slamming is considered negligible. The longitudinal trend of the pressures also varies with the vessel speed. Pressures on the bow are higher than those on the hull bottom at speeds up to 15kts and lower at speeds above 15kts. Two longitudinal distributions are therefore constructed: one for V≤15kts (Figure 7.14) and one for V>15kts (Figure 7.15).

At speeds up to 15kts (Figure 7.17) the maximum pressure value is applied between 85 and 100% LOA. Aft of the maximum pressure area the pressure drops linearly to zero at the aft end. The pressure distribution is therefore entirely defined by the value taken at 85-100%LOA, which is to be determined for different combinations of SOG and Hs. This is achieved by considering the extreme values estimated at the bow for different trials at V≤15kts (Figure 7.21). Since the pressure magnitude appears to depend on the vessel speed rather than on the wave height, a linear trend line is defined for all Hs (Figure 7.19). The longitudinal load envelope from Figure 7.17 can be scaled according to Figure 7.19 so that the extreme loads with a return period of 3 hours can be estimated for any combination of SOG and Hs.

At speeds above 15kts (Figure 7.20) the maximum pressure value is applied between 60 and 80% LOA. Aft of the plateau the pressure drops linearly to zero at the aft end, whilst forward it drops linearly to 0.5 of the maximum at the fore end. The pressure

distribution is entirely defined by the pressure value taken at 60-80%LOA, which is also to be determined for different combinations of SOG and Hs. This is achieved by considering the extreme values estimated at 67%LOA for all trials (Figure 7.21). The effect of the wave height (Figure 7.22) and the combined effect of wave height and speed (Figure 7.23) are found in the same way as outlined in the previous section for slamming-induced VBM. The longitudinal load envelope from Figure 7.20 can be scaled according to Figure 7.23 so that the extreme loads with a return period of 3 hours can be estimated for any combination of SOG and Hs.

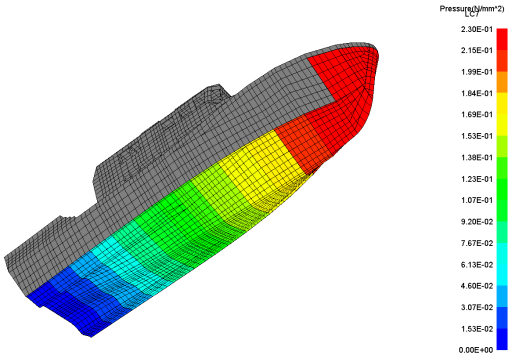

Figure 7.14. Slamming pressure distribution at V≤15kts.

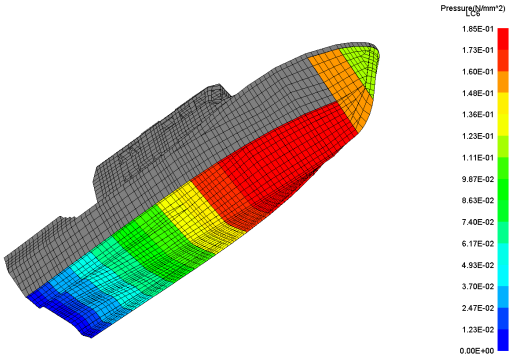

Figure 7.15. Slamming pressure distribution at V>15kts.

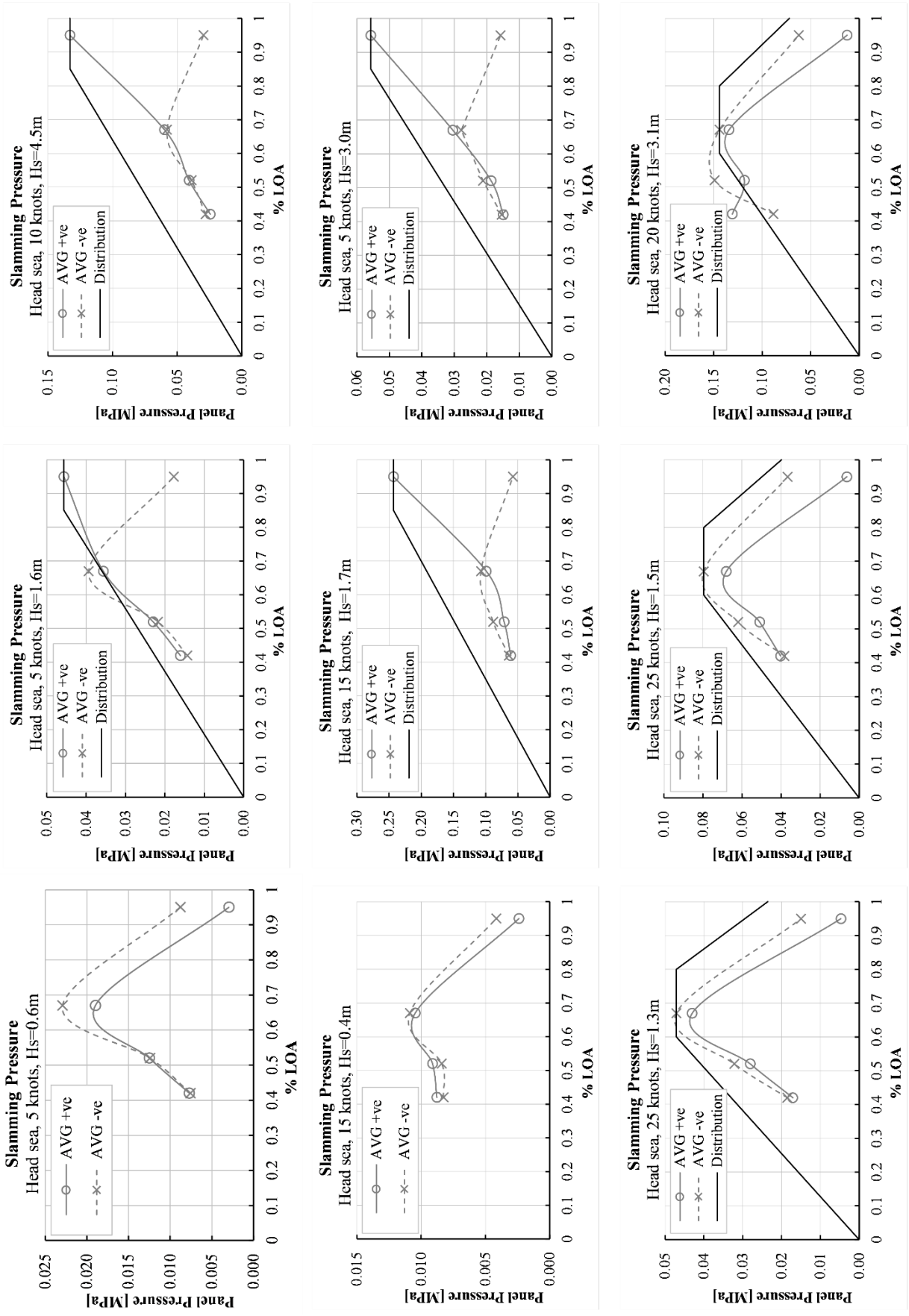

Figure 7.16. Slamming pressures. Extreme values with a return period of 3 hours.

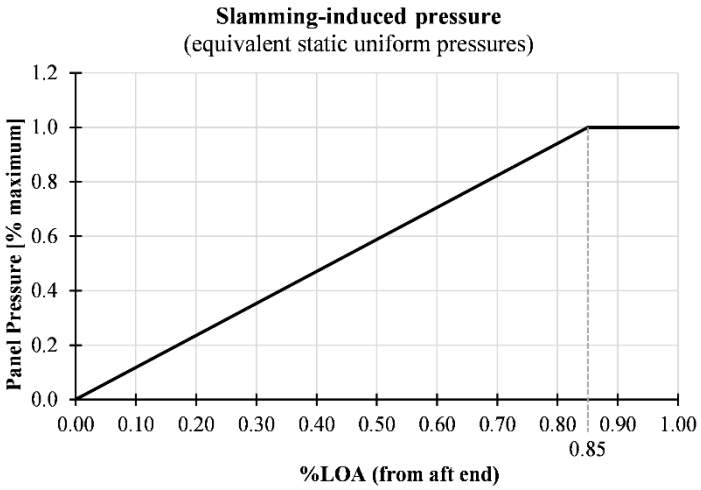

Figure 7.17. Longitudinal distribution of slamming pressures at V≤15kts. Constructed from sea trial data.

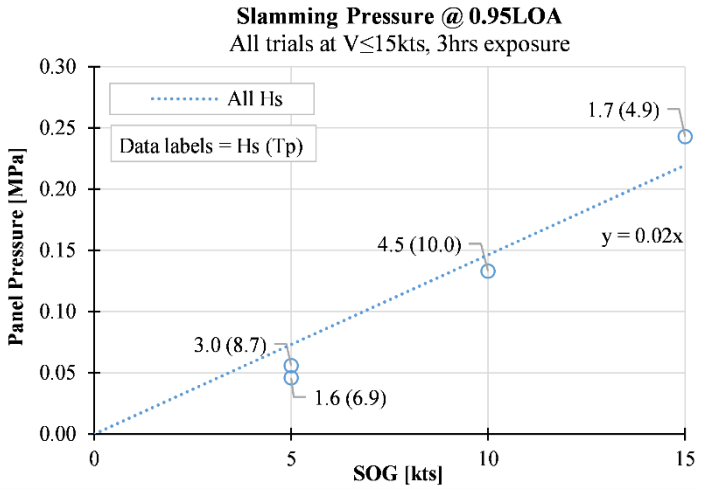

Figure 7.18. Speed effect on slamming pressures at 0.95LOA. Based on sea trials.

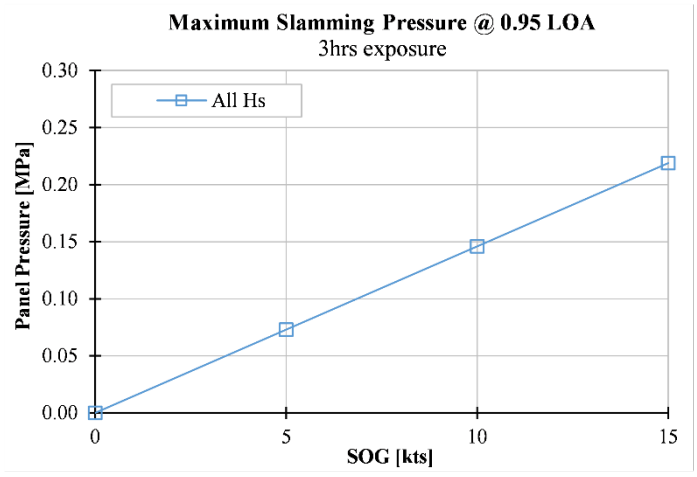

Figure 7.19. Speed and wave height effect on slamming pressures at 0.95LOA. Based on sea trials.

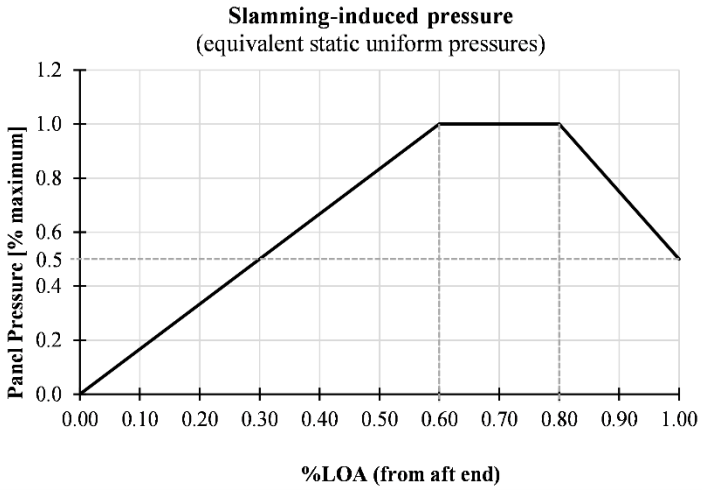

Figure 7.20. Longitudinal distribution of slamming pressures at V>15kts. Constructed from sea trial data.

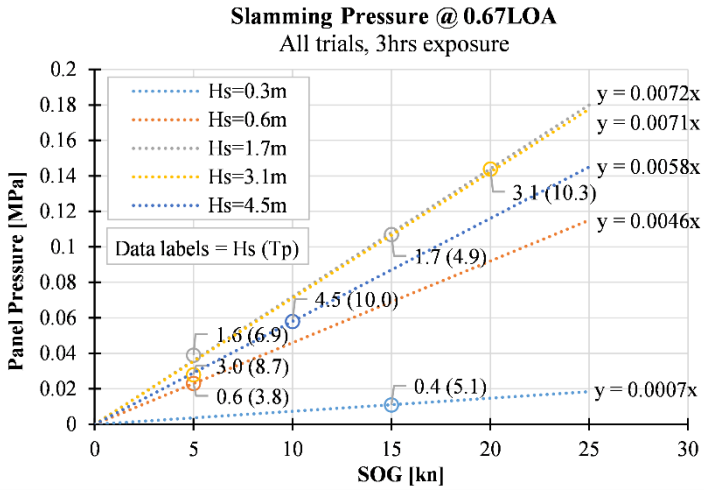

Figure 7.21. Speed effect on slamming pressures at 0.67LOA. Based on sea trials.

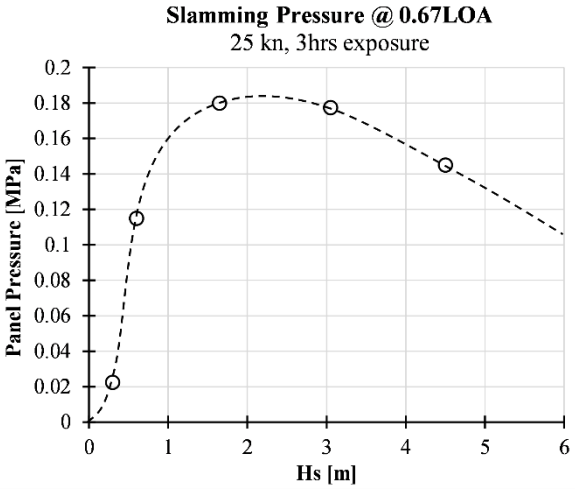

Figure 7.22. Wave height effect on slamming pressures at 0.67LOA. Based on sea trials.

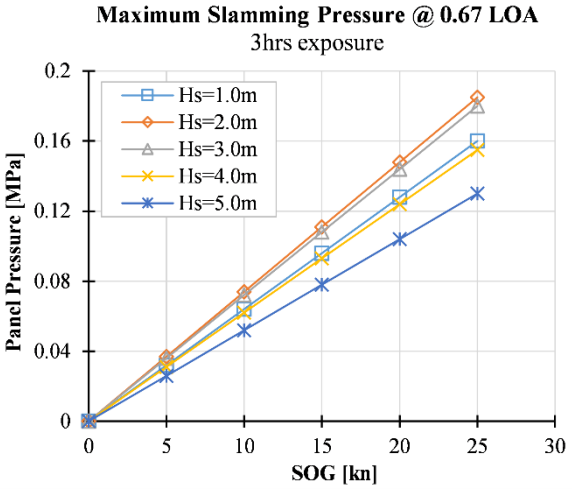

Figure 7.23. Speed and wave height effect on slamming pressures at 0.67LOA. Based on sea trials.

7.6 Load Case Definition

For the construction of a structural response graph, load cases are defined for each grid point with coordinates (SOG,Hs), where SOG=5,10,...,25kts and Hs=1,2,...,5m. The load components forming the load cases are hydrostatic, wave and slamming loads. This last term includes the whipping response of the hull girder and the slamming pressures acting at a local level on the hull panels. In principle all these load components would act simultaneously and should all be part of the same load case. The main limitation in achieving this was found in the simultaneous inclusion of the global and local slamming effects into the same load case. Because these are both a consequence of the same load nature, a slamming event, modelling the whipping response in addition to the local slamming pressures was found too conservative, as it somehow implies accounting twice for the same load. In addition, modelling slamming pressures as equivalent static panel pressures produces, at a global level, a vertical bending moment that is different from what would be caused by a real slamming event. The structural response analysis therefore followed the approach whereby global and local strength are treated, at first, in isolation. Different load cases are produced to assess the structural response to global and local loads.

The load components that have an effect at a global level are the hydrostatic, wave and whipping terms. Wave pressures obtained from the hydrodynamic simulations are scaled linearly according to the amplitude of the extreme wave. At speeds above 10kts, for which experimental measurements highlighted that the numerical simulations underestimate the wave load magnitudes, a correction is applied. This is defined as a scaling factor on the VBM RAOs, and related pressures, found from the sea trial VBM RAOs. The hydrostatic pressure is then computed through a static equilibrium balance and superimposed. The whipping response caused by slamming is considered as an addition to the vertical bending moment induced by the first two terms and modelled through a scaling factor. Since the hydrostatic, wave and slamming components are known, a final vertical bending moment load target that includes all terms can be defined. Hydrostatic and wave pressures are then scaled up until the load target is reached. Two load cases are in fact created, one for sagging and one for hogging.

The load components that have an effect at a local level are hydrostatic, wave and slamming pressures. The first two terms are modelled in the same way as for the global strength analysis. The last term is modelled through equivalent static pressures.

7.7 Structural Response Analysis

Once the load case is defined, the inertia relief method is applied to restrain the model (Chapter 4). The finite element analysis is performed as linear elastic, with stresses, strains and displacements output for evaluation. An example is shown in Figure 7.24.

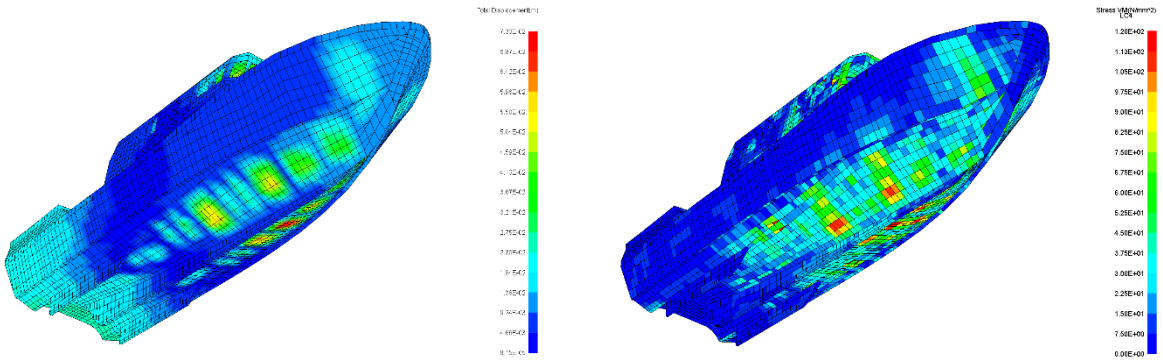

Figure 7.24. Structural analysis results. Total displacement (left) and Von Mises stress (right).

7.8 Results

Structural analyses were run for every combination of SOG=5,10,...,25kts and Hs=1,2,...,5m, for a total of 25 cases. Due to software limitations it was not possible to apply failure criteria for composite laminates, hence the Von Mises stress was considered for the evaluation of the structural response. Although Von Mises criterion would be applicable to ductile and isotropic materials, it still provides an indication of the stress level within the laminate and allows to compare different operating conditions in terms of stress developed within the structure.

Depending on the area of the structure considered, different speed versus sea state plots can be produced from the analyses. The maximum stress values can occur in areas of actual high stress as well as in areas with artificial stress concentrations. The assessment

of the structural response focused on clear areas of high stress, an example of which is shown in Figure 7.27. An example of artificial stress concentration is shown in Figure 7.28. In this case, the high stress values are attributed to the small area-to-thickness ratio and to the highly skewed shape of the shell elements. These high stress areas were disregarded.

Two plots are presented. Figure 7.27 shows the maximum Von Mises stress in the hull due to seakeeping loads that induce a global response (hydrostatic pressures, wave pressures and whipping). Figure 7.28 shows the maximum Von Mises stress in in the hull due to loads that induce a local response (hydrostatic, wave and slamming pressures). Both figures show the maximum stresses arising within the whole hull structure rather than specifying where the highest stresses occur, which can be found from an examination of the finite element model.

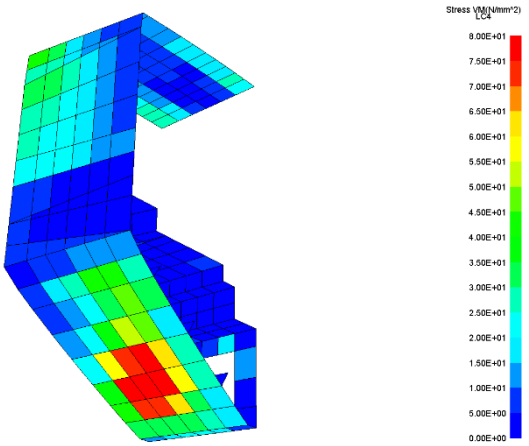

Figure 7.25. Example of a high stress area.

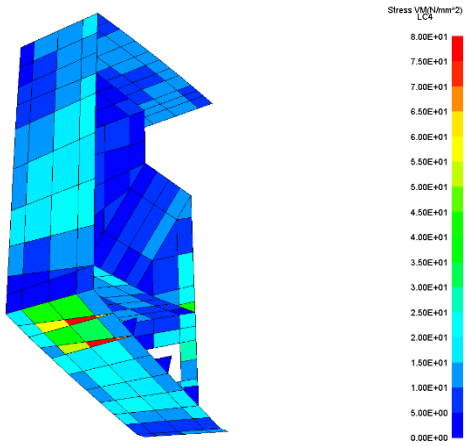

Figure 7.26. Example of an artificial stress area.

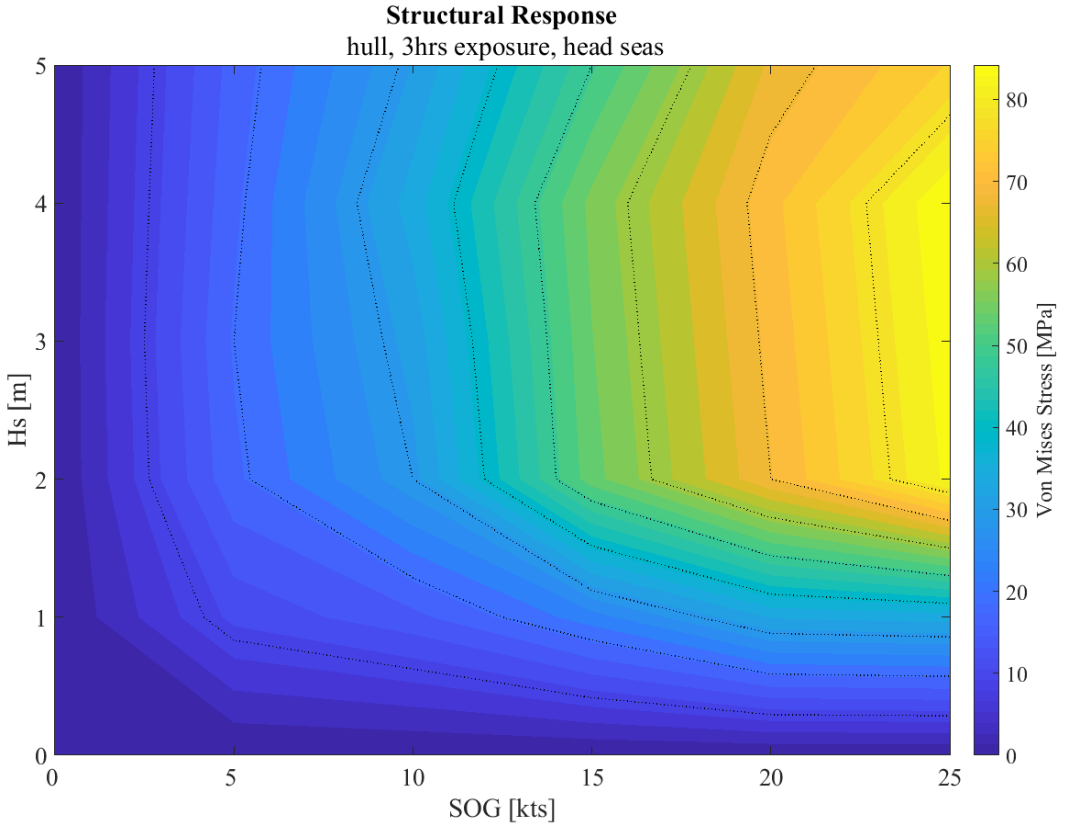

Figure 7.27. Structural response of the hull to global seakeeping loads.

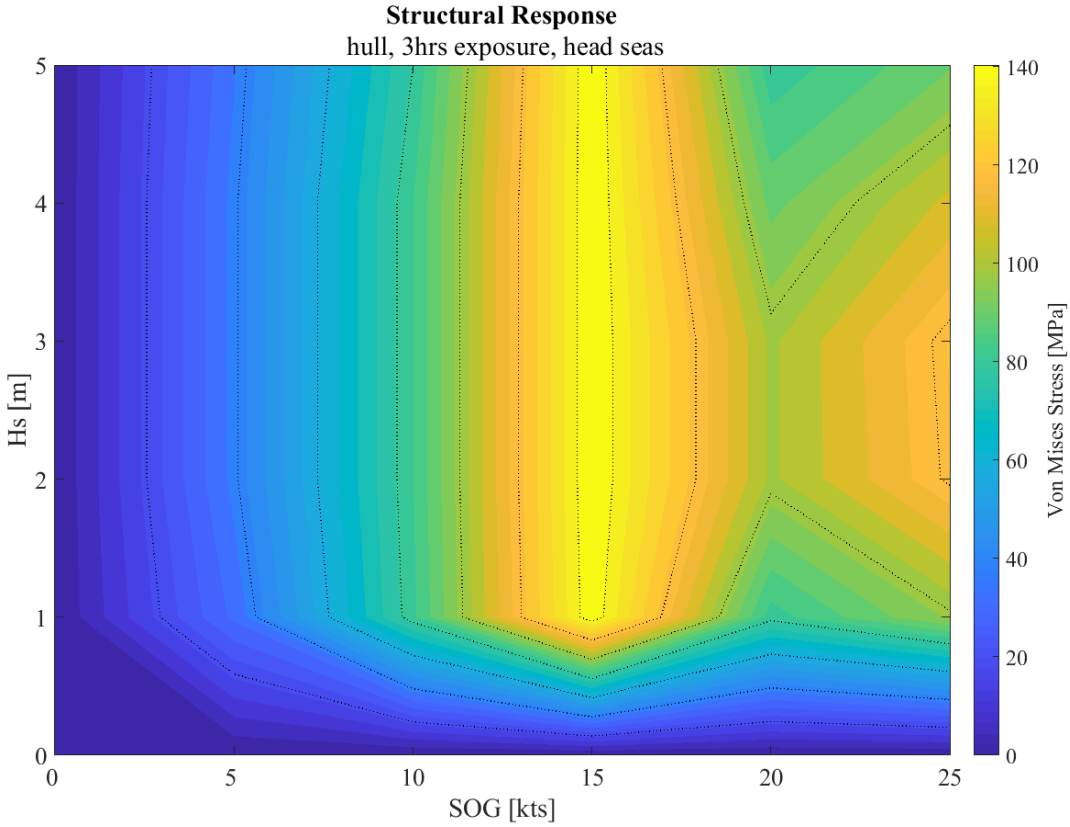

Figure 7.28. Structural response of the hull to local seakeeping loads.

7.9 Discussion

The inclusion of the whipping response and of the slamming pressures into different load cases implies that for each combination of SOG and Hs two sets of stress data are to be separately analysed. This is reflected in the results where two different structural response plots are produced.

Figure 7.27 shows the stresses that arise from global seakeeping loads sustained in different operating conditions. Loads and structural response are a function of both the vessel speed and the sea state severity. Structural stresses rise progressively as the operating speed increases. At any given speed, stresses initially rise as waves increase in height up to Hs=2-4m, to then reduce in higher waves. At 25kts the maximum stress values occur in seas with Hs≈4m. Although only the significant wave height is shown in the plot, the dependency of the structural response on the sea state should be attributed to the combined effect of wave height and period. Since the wave period of a seaway tends to increase together with its wave height, smaller and shorter waves can produce more extreme ship responses than higher and longer waves.

Figure 7.28 shows the stresses that arise from the local seakeeping loads sustained in different operating conditions. Although the stress values are only approximate, because global load effects are not completely accounted for, they confirm that slamming pressures dominate the loading scenario, causing stress magnitudes markedly higher than those produced by the superposition of hydrostatic pressures, wave pressures and the whipping response (Figure 7.27). Structural stresses are again dependent on the vessel speed, while, since the wave height was found to have little effect on the slamming pressures at speeds up to 15kts, the dependency of the stress magnitudes on the sea severity is less evident. Figure 7.28 also shows a high stress region at V=15kts, which is a direct consequence of the high slamming pressures measured during the sea trials at that speed. This high stress region could be the result of: an error in the estimation of the extreme slamming pressures and introduced by the small set of sea trials conducted; or the result of a transition from displacement to planing regime that causes real significant slamming loads. At speeds other than 15kts, the structural response is as described for Figure 7.27. At 25kts the maximum stress values occur in seas with Hs≈3m.

The global strength of the vessel can be assessed based on the load case used to produce Figure 7.27, which includes all those loads that cause a response of the hull girder. The local strength of the structure requires the modelling of all the loads that have a local effect. The consequence of treating whipping response and slamming pressures separately is that none of the load cases comprises all these loads, hence neither Figure 7.27 nor Figure 7.28 report exact local stress values. Moreover, the coarse mesh of the finite element model makes it impossible to determine the magnitude of local stress concentrations, which require a more detailed representation of the structure. These limitations are widely accepted in the design practice, where global and local strength assessments are carried out sequentially. From the structural response analyses conducted, it is possible to identify the areas of the structure carrying the highest stresses. For those areas, local and more detailed representations of the structure can be realised, either through local mesh refinement or with different finite element models. The effects of the global response can be included by imposing nodal displacements as boundary conditions to the local structural model, to account, at this stage, for both the global and local load effects.

The value of speed versus sea state plots lies in their intuitiveness and ease of understanding. Figures 7.27 & 7.28 are an effective representation of the response of the structure to the seakeeping loads sustained in different operating conditions. The inclusion of failure criteria into the assessment of the structural response, together with the identification of an acceptable level of structural adequacy, would enable the designer to determine the risk of structural damage associated with the different operating conditions of the craft. In Chapter 1, this was referred to as the 'structural limit', which contributes to identifying the safe operating envelope of a high-speed craft.

7.10 Summary

The work described in this chapter is summarised in Figure 7.29. The four load components found from Chapters 4-6 are superimposed into load cases that represent the extreme loads expected to be sustained in given operating conditions and within a given period of exposure. An extreme value analysis is therefore conducted to estimate extreme values of the load components. Wave pressures are estimated through an

equivalent wave approach and hydrostatic pressures are directly superimposed. Slamming loads are estimated by fitting Gumbel probability distributions to samples of maxima measured during the sea trials. Load envelopes are then generated to represent the load distribution along the hull. The structural response analysis is performed with a global structural model of the Severn developed with MAESTRO. The load components that form each of the load cases are applied to the model and the structure's response is computed through linear finite element analysis.

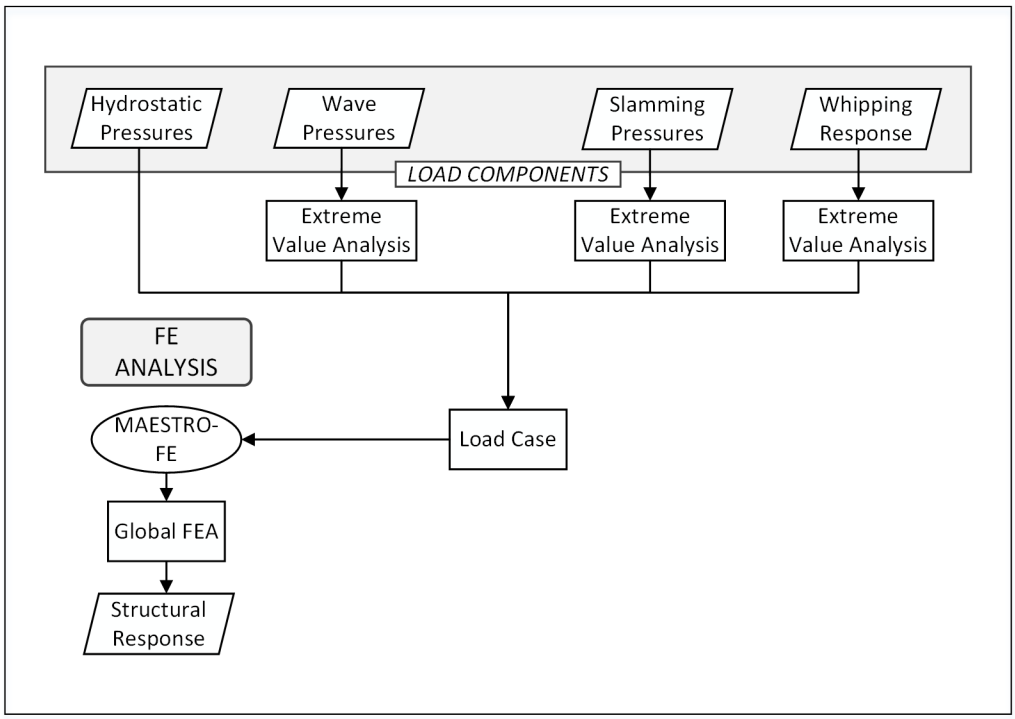

Figure 7.29. Direct calculation approach. Structural response.

Chapter 8

Conclusions

8.1 Direct Calculation of Seakeeping Loads and Structural Response

8.1.1 General View

Current design methods for small high-speed craft follow a relatively simplistic process that does not fully assess the margin of structural strength in the different operating conditions of the craft. To understand the seakeeping loads being sustained and the actual safety margins embedded into the structural design, both loads and structural response need to be explicitly analysed. This research developed a novel approach for the direct calculation of the loads sustained and the response of the structure for specific operating conditions. The schematic overview of the workflow (Chapter 3), expanded in the previous chapters (Chapters 4-7), is presented in its entirety in Figure 8.1.

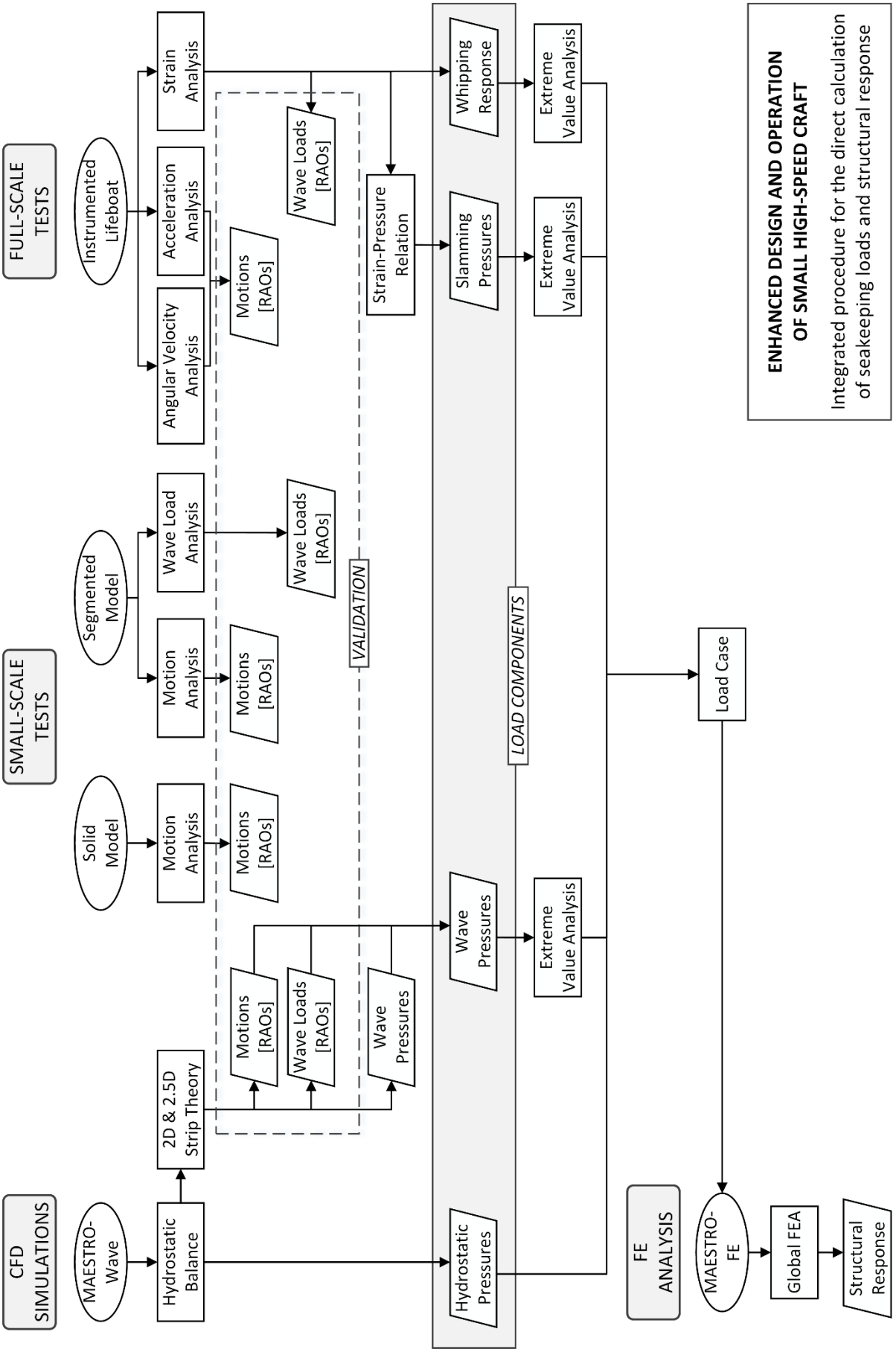

Figure 8.1. Direct calculation of seakeeping loads and structural response.

8.1.2 Numerical simulations

The linear strip theory methods used to predict hydrostatic and wave-induced loads confirm their computational efficiency and the advantages of outputting results that can be scaled linearly and assessed in terms of RAOs. Their application to the case of the Severn Class led to the following conclusions, extendable to comparable vessels:

- Numerical results confirmed that strip theory methods are more appropriate in head, bow quartering and beam seas than in following and stern quartering seas. With wave directions from abaft the beam, motion and load predictions were questionable at speeds higher than 5kts, for which the encounter frequency decreases significantly.
- Full-scale tests proved that accurate predictions of the load RAOs were made for seas with Hs up to 4.5m. Since the extreme load analysis showed that the highest seakeeping loads on the Severn are sustained in seas with Hs=2-4m, the wave height did not represent a practical constraint in the use of numerical results to predict extreme wave-induced loads.
- Small-scale and full-scale tests framed the range of applicability of the numerical simulations within the displacement regime. At semi-planing and planing speeds sectional global wave loads were significantly underestimated. To predict extreme wave load values a correction factor was applied to the numerical results; however, the use of more sophisticated nonlinear seakeeping codes would be more appropriate.
- The assumption of wall sidedness made by linear strip codes implies that the same value of vertical bending moment is predicted for bending in both sagging and hogging. The full-scale tests showed that there are in fact significant differences, even for small vessels. These differences should be included in the estimation of extreme load values. A simplistic but common method would be the application of a scaling factor to the loads predicted with linear codes.

8.1.3 Small-Scale Tests

A direct validation of the numerical simulations was obtained from the small-scale tests conducted with a solid and a segmented hull model. The tests highlighted the following aspects:

- Wave load results showed that it is possible to realise a segmented hull model without altering the seakeeping characteristics of the prototype hull and to measure sectional global wave loads on relatively small models (1.3m long). Adequate measurements of the wave-induced vertical bending moment were obtained from both stationary and forward speed tests.
- Important nonlinearities in the wave-induced loads appeared at semi-planing and planing speeds. Much less pronounced were the motion nonlinearities. This implies that the validation of numerical methods for seakeeping load prediction should be based on loads and not only on the vessel's motions.
- Tests were carried out in regular waves, which eased the data analysis and enabled direct comparison with numerical simulations in the frequency domain. This implies that any seakeeping nonlinearity arising in random seas was not captured.
- The major practical limitation of the tests was the towing of the model with a horizontal towing force. This is believed to have caused large discrepancies in the pitch motion results between experiments and simulations. The system used for the load data acquisition on the segmented model affected motion measurements during stationary tests. Practical advice for future tests was given in Chapter 5.

8.1.4 Full-Scale Tests

Validation of the numerical model and determination of slamming-induced loads relied on the sea trials, which remain an unequalled method to assess the seakeeping and structural response behaviour of a vessel. The two major challenges were the isolation of the different load components from raw signals and the conversion of the measured values to load quantities suitable for numerical structural analysis. Both these aspects were addressed, with the following conclusions:

- The data analysis showed how frequency-based filters can be employed to isolate wave and slamming induced loads without significant loss of frequency bands, which would result in the underestimation of the total loading.
- The conversion of strain values to hull girder vertical bending moment values was based on the classical beam theory. The comparison of the relative RAOs with those computed numerically proved that the method is successful even for small vessels of composite construction. Careful consideration should be given to the determination of the section modulus and the Young's modulus of the instrumented cross-sections.
- The wave-induced vertical bending moment was related to the sea state and RAOs were obtained through a spectral analysis, based on the assumption of long crested unimodal seas. The analysis proved suitable for fairly unidirectional seas but limited for data collected in more confused conditions. Analysis techniques modelling multimodal and short crested seas would be more appropriate for data collected in multiple wave systems and with significant wave spread.
- The determination of slamming-induced pressures was based on the principle of measuring strains. With a focus on the structure rather than on the loading, these have scientific and practical advantages compared to pressure measurements. The structural response of the vessel is measured directly and loads that have generated it are found by reverse calculation. This inherently supersedes the need to model pressures accurately enough to reproduce a realistic structural response. Data sampling rates adequate for capturing a transient response of the structure are typically lower than those required for modelling transient pressure loads. Strain gauges have practical advantages compared to pressure transducers, which can be subject to temperature shocks, sensitivity to changes of medium and dependency of the pressure measurements on the sensor used. Strain gauges are also relatively easy to install and do not require drilling of the hull.
- The conversion of slamming strains to pressures was based on the principle that a transient non-uniform pressure distribution can be modelled as static and uniform. A strain-to-pressure conversion factor was found for each of the instrumented panels through linear static finite element method. The major challenge was the identification of suitable boundary conditions for the finite element model. It is believed that the structural arrangement of the Severn Class and the construction

materials employed are the cause of a more complex structural behaviour than what could be expected for an aluminium alloy counterpart with a conventional hierarchical structural layout. In one case, this led to questioning the strain-to-pressure conversion found, which was corrected based on expert judgement.

8.1.5 Structural Response Analysis

The behaviour of the vessel's structure in different operating conditions was assessed by analysing its response to extreme loads expected to occur once within a given period or exposure. Concluding remarks on the statistical methods adopted to predict extreme values of linear and nonlinear loads, on the generation of load cases by superposition of single load components and on the structural finite element analysis are as follows:

- Extreme wave-induced loads were estimated from their RAOs, computed numerically. The task confirmed the significant advantages of linear theory, which enables determination of loads in an irregular sea from loads in regular elementary waves and a statistical description of the sea.
- Extreme slamming-induced loads were estimated experimentally. It should be recognised that this task was based on a relatively small, although carefully selected, set of sea trials, which makes the load estimates susceptible to bias and error. Further sea trials and in-service monitoring would add value to this work. The statistical extrapolation methods employed will also require further evaluation on other vessels in order to determine their general applicability.
- The extreme value analysis of nonlinear loads and responses was based on Gumbel probability distributions. The fitness of the Gumbel distribution should be evaluated on a case-by-case basis and other distributions (e.g. Weibull) could prove more appropriate for different data sets.
- Loads and responses of transient nature, such as those induced by slamming, were modelled as static, which greatly simplifies the structural response analysis. The major consequence is that the bending moment produced by a static slamming pressure envelope is different from what would be produced by a slamming impact. The global and local responses of the hull structure to slamming loads need to be analysed separately, through different load cases. The combined response should be

determined, at a later stage, from local structural models, where the global response can be superimposed, by applying boundary conditions, to the local loads.

- Evaluation of the structural response, computed through linear finite element method, relied on Von Mises stress. Von Mises criterion was a practical solution to compare different operating conditions in terms of stresses developed within the structure; however, a thorough strength assessment would require inclusion of failure criteria for composite laminates.
- The explicit load calculation procedure was exploited to investigate the structure's response, demonstrating how this method enables assessment of the level of structural adequacy in the different operating scenarios of the craft.
- Structural analysis results were presented in graphs showing the structural response as a function of the vessel speed and the sea state severity. These graphs are an effective means of presenting the risk of structural damage associated with different operating conditions. This could be simply referred to as the 'structural limit', which contributes to identifying the safe operating envelope of a high-speed craft.

8.2 Applicability of the Research

The data and the results produced are directly applicable to the Severn Class and can be extrapolated for vessels with comparable hull form type, length and operating speed. The approach developed for the explicit calculation of loads and structural response (Figure 8.1) has a much broader applicability. In general, it is deemed valid for high-speed craft whose structural design has to consider both global and local aspects, and significant slamming-induced loads. The framework of the research should be set within limits defined by the following two types of vessel:

- Smaller vessels for which hull girder loads become insignificant and local slamming loads dominate. This is the case of small planing hulls, in particular those not in continuous contact with the water. The modelling of hydrostatic, wave-induced loads and global slamming effects becomes superfluous, since the structural design is entirely dominated by local slamming loads. The structural analysis is likely to require a more sophisticated treatment of the slamming pressures to account for

their transient nature. This aspect becomes even more important for hulls of composite sandwich construction (Chapter 2).

- Larger vessels for which the global strength becomes of primary importance, requiring consideration of hull girder loads not assessed as part of this research, such as: shear forces, torsion, horizontal bending moment and dynamic vertical bending moment due to springing. Some of these loads could be embedded into the research approach without major difficulties; others may require different methods, such as hull girder natural frequency calculations or hydroelastic analyses.

8.3 Guidance for Practical Design

8.3.1 General Remarks

This work is addressed to designers who seek an enhanced approach to the design of small high-speed craft. Streamlined design methods already exist (e.g. classification societies' basic standards) and have proved successful. Their main limitation is that they are not suitable for direct calculations of loads and structural response, which makes it impossible to tailor the structural design to the intended use of the craft.

This research overcomes the limitations of simplistic design methods by combining numerical and experimental tasks into a procedure that analyses loads and response for a specific vessel. When adopted for practical design, this procedure results in an improved understanding of the actual loads experienced and of the response behaviour of the structure. The designer obtains more control over the structural design and over the level of structural adequacy required, producing solutions optimised for the operational profile of the vessel and the expected loads sustained during operation. The 'structural limit' can be considered together with the other factors that determine how a craft should be operated. This implies designing according to the required operational envelope of the craft, by treating the different operational limits together rather than in isolation, a requirement for a cohesive design that considers all of the design space.

The workflow schematically represented in Figure 8.1 can be partitioned into a hydrodynamic problem, which uses numerical and experimental methods to explicitly calculate seakeeping loads, and a structural problem, which uses a numerical (the finite

element) method to determine the structural behaviour of the vessel under the computed loads.

Numerical seakeeping and structural simulations require input information that is typically determined through the design process. Analyses can be executed with initial design values or with more accurate information that becomes available towards the final design stages. The flexibility of these methods makes them well suited for practical design.

Model-scale seakeeping tests, although require the development of a hull model, which makes them less versatile than numerical simulations, are also standard practice for design purposes. Due to the moderate resource requirements, model tests can be conducted with approximate values to drive the design process or with final values to confirm the performance of the vessel. Testing of different hulls to select the optimum hull form, for example, is relatively common.

Full-scale seakeeping tests are a rarity for practical design. They require conspicuous resources and a prototype vessel. If full-scale tests were omitted from the proposed approach (Figure 8.1), the workflow would miss validation of the numerical simulations against full-scale data and determination of the slamming-induced loads, therefore requiring adjustment. In general, higher fidelity numerical simulations and towing tank tests with an experimental setup capable of modelling the full-scale elastic behaviour of the vessel will be required.

8.3.2 Validation of Numerical Simulations without Full-Scale Tests

Validation of the numerical simulations has been achieved at a simulation output level, where the motions and sectional global wave loads computed numerically have been compared against those measured at scale with model tests. To enhance the reliability of the validation task, small-scale tests can involve:

- Tests with a self-propelled model to eliminate the inaccuracies introduced by towing.
- Tests in irregular seas to account for nonlinearities not captured in regular waves and improve the confidence in the prediction of extreme loads. Extreme load values

can be predicted from either the load RAOs, based the principle of superposition, or with Extreme Value Analysis, based on probability distributions.

Without real-scale data, the range of applicability of the selected numerical tool has to be assessed entirely through model tests. Recognising the challenge of modelling numerically the seakeeping of a vessel at high-speed regimes, it is fundamental that experiments include tests at semi-planing and planing speeds.

8.3.3 Determination of Slamming Loads without Full-Scale Tests

Excluding the estimation of slamming loads from sea trial measurements, alternative methods are required that account for the nonlinear nature of slamming for estimating extreme load values. Different solutions can be adopted to determine the whipping response of the hull girder and local slamming pressures.

The whipping response can be determined from small-scale tests. These will have to be conducted with a flexible segmented hull model as opposed to a rigid one. By scaling the stiffness of the hull girder and its vibratory characteristics it will be possible to evaluate the transient global response of the hull to slamming impacts. A suitable test matrix to enable estimation of extreme load values will be required.

Slamming pressures can be determined with advanced numerical simulations capable of including slamming and predicting its locally induced pressures. It should be accepted that computations become considerably more demanding. To minimise the effort, use of advanced numerical tools can be restricted to investigation of some cases of interest, identified through simulations based on simpler and more efficient codes. The nonlinear character of slamming-induced loads implies that simulations will have to be run in the time domain and in random seas. The simulation time should also be long enough to allow estimation of extreme load values from datasets of load maxima. In addition, numerical and/or experimental drop tests of hull sections (Chapter 2), are an option to complement the seakeeping simulations and increase the confidence over their predictions.

8.4 Guidance for Future Work

This research proposes a versatile method that can be expanded and modified to suit different applications. The following implementations would be valuable advances:

- While linear potential flow codes are well suited for displacement speeds, nonlinear codes are the appropriate tool at higher speeds. Where nonlinearities are weak, wave loads can still be produced in terms of RAOs, which simplifies the estimation of extreme values. Where nonlinearities are important, different statistical methods are required. Extreme load analysis based on Gumbel distribution or similar would be an option to explore. Validation of nonlinear numerical methods is suggested through comparison against the extreme load values estimated from sea trial data with the same statistical means.
- Extension to headings other than head sea would be valuable. While this work could be easily extended to the case of bow quartering and beam seas, more appropriate numerical methods than the strip theory are likely to be required in stern quartering and following seas. Moreover, on headings abaft the beam the computation of motion and load RAOs from on-board measurements becomes considerably more complex. Since up to three wave systems can be encountered at the same frequency, the computation of the response spectrum from its encounter spectrum becomes a triple value problem. For craft travelling at high speeds, this aspect will become a concrete limitation.
- Long-term structural response monitoring would add great value to the extreme value analysis conducted, as it would enable measurements to be compared against long-term predictions, therefore validating the proposed method.
- Extreme values and envelopes of slamming-induced pressures relied on a relatively small set of sea trials. An established experimental method to investigate slamming pressures consists of drop tests of hull sections. These tests would complement the sea trial data and provide an alternative means to construct pressure envelopes.
- The scope of the research was limited to the case of a naked hull, without active trim-control devices (e.g. stern flaps, interceptors). These are customarily mounted on small high-speed craft and have a great influence on the running attitude. Their effect on the structural loads is less clear and should be investigated. It is expected

that the contribution of trim-control devices to the seakeeping loads could be modelled as an addition to the naked hull reference case.

- Global structural response analysis is more established for metal alloy than composites structures. Several failure criteria have been developed to predict failure of composite laminates (see Hinton *et al.* (2004)), with the most popular now implemented into general purpose finite element programs. Inclusion of suitable failure criteria for the strength assessment of ship structures into naval architecture design packages is needed.
- With the possibility to determine the level of structural adequacy for different operating scenarios, it is now necessary to define what is acceptable and, most important, where the structural 'limit' should lie with respect to the other operational limits of the craft. Even recognising that safe operating envelopes are vessel specific, there seem to be different viewpoints on which limit should have the highest risk of being reached first and how much before the others. Also, optimisation of the craft structure does not imply that a high risk of structural damage should be taken together with a high risk of other catastrophic events occurring - 'better to roll down a hill than to fall off a cliff'.

8.5 Original Contribution to Knowledge

The main research contribution is the fusion of numerical and experimental methods into a methodology to enhance the structural design and support the operation of small high-speed craft. The following features represent the key contributions to knowledge:

- Review of the current state-of-the-art methods for the prediction of hull loads and response with regard to small high-speed craft. The review has highlighted the limitations of the different methods and shown how structural design can be enhanced through their systematic integration into a single workflow.
- Development of a procedure for the prediction of the seakeeping loads sustained, which produces results in a form suitable for analysing the consequential response of the structure.
- Systematic integration of numerical and experimental methods and validation of numerical seakeeping models through comparison against experimental data.

- Development of practical guidance for the conduct of seakeeping experiments with measurement of motions and loads. The viability to measure global wave loads at scale, even with relatively small hull models has been proved.
- Elaboration and application of a method to estimate extreme loads from numerical and experimental datasets. A technique for the treatment of slamming pressures based on full-scale strain measurements has been proposed, providing an alternative to pressure measurements.
- Investigation of the concept of 'structural limit' and its implications at the design stage and during operation. It has been shown how the procedure developed can be employed to determine the structural limit of a craft.

8.6 Potential Beneficiaries

A wide range of possibilities is available to implement the research results. Potential beneficiaries are:

- **RNLI.** The results of this research are already been exploited to support the 'Severn Life Extension Programme' undertaken by the RNLI to lengthen the service life of the Severn Class lifeboats. They are also well suited to be extended to other RNLI's all-weather lifeboat classes with comparable features and operational requirements. Looking forward, this research is likely to be coupled with separate work undertaken by the RNLI to improve the crew safety without compromising the vessels' structural integrity. This will ensure a cohesive design approach in line with the new design philosophies. It is expected that this approach to the design and operation of lifeboats will result in improved performance, an optimised response to emergency call-outs and increased safety for the on-board crews.
- **Classification Organisations.** Practical design follows, in most cases, standards provided by classification organisations. The proposed approach has the potential to be implemented into these organisations' standards and lead to an upgrade of their design rules and guidelines.
- **Research Community.** A substantial amount of numerical and experimental data has been produced, with the added value that all datasets are relative to one vessel (the Severn Class lifeboat). This feature should ease further comparison of the results

obtained through different means and validation of numerical and experimental methods. It is hoped that the data generated will be further exploited, in a wider research context, by the marine community.

For practical work, the following user categories are expected to benefit directly from the proposed method for an enhanced structural design and operation of small high-speed craft:

- **Designers** through a better control over the structural design that enables optimisation of the structure according to the vessel's operational profile.
- **Maintainers** through a vessel-specific understanding of the load patterns and of the structural behaviour, hence by providing an aid to targeted inspections.
- **Operators** through an increased insight into the actual loads experienced and the strength of the structure, which will enable coxswains and shipmasters to make informed decisions on the risks being taken.
- **Trainers and trainees** through an increased awareness of the implications of high speed to the structural integrity of the vessel.

8.7 Conclusions and Future Directions

A functional approach to improve the structural design and operation of small high-speed craft has been proposed and validated. The originality of this work is in the systematic integration of numerical and experimental methods to explicitly calculate the seakeeping loads sustained and the structural response of the craft. A vast amount of data has been produced, with potential for further exploitation and a wide range of possibilities to implement the research results, with effect on design, operation, maintenance and training practice.

This research will lead to a more advanced structural design approach, improved performance of small high-speed craft and a superior assessment and understanding of the risk and consequences of structural damage. The beneficiaries of this work are all those designers, regulatory bodies and researchers who seek an enhanced approach to the structural design and operation of small high-speed craft.

References

Allen, R.G. and Jones, R.R., 1972. A Semiempirical Computerized Method for Predicting Three-Dimensional Hull-Water Impact Pressure Distributions and Forces on High-Performance Hulls. Bethesda, MD, USA: Naval Ship Research and Development Center, R&D Report No. 4005.

Allen, R.G., Jones, R.R., and Taylor, D.W., 1978. A Simplified Method for Determining Structural Design-Limit Pressures on High Performance Marine Vehicles. Presented at the Advanced Marine Vehicles Conference, San Diego, CA, USA.

American Bureau of Shipping (ABS), 2011a. Guidance Notes on Structural Direct Analysis for High-Speed Craft.

American Bureau of Shipping (ABS), 2011b. Guide for Slamming Loads and Strength Assessment for Vessels.

American Bureau of Shipping (ABS), 2014. Rules for Building and Classing High-Speed Craft.

American Bureau of Shipping (ABS), 2015. Guide for Hull Condition Monitoring Systems.

Bales, S.L., Lee, W.T., and Voelker, J.M., 1981. Standardized Wave and Wind Environments for NATO Operational Areas. David W. Taylor Naval Ship R&D Center, No. DTNSRDC/SPD-0919-01.

Bertram, V., 2012. Practical Ship Hydrodynamics. Second Edition. Butterworth-Heinemann.

Bhattacharyya, R., 1978. Dynamics of Marine Vehicles. John Wiley & Sons Inc.

Blount, D.L. and Codega, L.T., 1992. Dynamic Stability of Planing Boats. Marine Technology, 29 (1), 4–12.

Boller, C., Fou-Kuo, C., and Yozo, F., 2009. Encyclopedia of Structural Health Monitoring. John Wiley & Sons Ltd.

Chuang, S.-L., 1966. Slamming of Rigid Shaped Bodies with Various Deadrise Angles. Washington, DC, USA: David Taylor Model Basin, R&D Report No. 2268.

Clark, S.D., Shenoi, R.A., Allen, H.G., Hicks, I.A., and Cripps, R.M., 1997. Fatigue Assessment of High Performance Small Craft Incorporating FRP Sandwich Materials. Presented at the 4th International Conference on Fast Sea Transportation (FAST'97), Sidney, AU, 263–268.

Clarke, J.D., 1986. Wave Loading in Warships. Presented at the Advances in Marine Structures Conference, Dunfermline, UK: Elsevier Applied Science, 1–25.

Codega, L. and Lewis, J., 1987. A Case Study of Dynamic Instability in a Planing Hull. Marine Technology, 24 (2), 143–163.

Cook, R.D., Malkus, D.S., Plesha, M.E., and Witt, R.J., 2002. Concepts and Applications of Finite Element Analysis. Fourth Edition. John Wiley & Sons Inc.

Cripps, R.M., 2005. Design and Development of Lifeboats - Damage Evaluation and Repair of Composite Structures. Applied Mechanics and Materials, 3–4, 3–8.

Cripps, R.M., Cain, C.F., Phillips, H.J., Rees, S., and Richards, D., 2004. Development of a New Crew Seat for All Weather Lifeboats. Presented at the SURV 6 Conference: Surveillance, Pilot & Rescue Craft, London, UK: The Royal Institution of Naval Architects, 69–75.

Cripps, R.M., Phillips, H.J., and Cain, C.F., 2004. Development of Integrated Design Procedures for Lifeboats. Presented at the SURV 6 Conference: Surveillance, Pilot & Rescue Craft, London, UK: The Royal Institution of Naval Architects, 9–15.

Cripps, R.M., Phillips, H.J., and Cain, C.F., 2005. Development of Integrated Design Procedures for Lifeboats. International Journal of Small Craft Technology, 147 (B1), 1–8.

Daidola, J.C. and Mishkevich, V., 1995. Hydrodynamic Impact on Displacement Ship Hulls. Ship Structure Committee, Technical Report No. SSC 385.

Datawell B.V., 2014. Datawell Waverider Reference Manual for DWR-MkIII and DWR-G.

Det Norske Veritas (DNV), 2012a. Rules for Classification of High Speed, Light Craft and Naval Surface Craft.

Det Norske Veritas (DNV), 2012b. Rules for Classification of High Speed, Light Craft and Naval Surface Craft - Direct Calculation Methods.

Diab Group, 2018. Divinycell H - Technical Data and Technical Characteristics.

Drouet, C., Cellier, N., Raymond, J., and Martigny, D., 2013. Sea State Estimation Based on Ship Motions Measurements and Data Fusion. Presented at the 32nd International Conference on Ocean, Offshore and Arctic Engineering (OMAE2013), Nantes, FR: The Society of Naval Architects and Marine Engineers.

Faltinsen, O.M., 1990. Sea Loads on Ships and Offshore Structures. Cambridge University Press.

Faltinsen, O.M., 2006. Hydrodynamics of High-Speed Marine Vehicles. Cambridge University Press.

Grassman, M.J. and Hildstrom, G.A., 2003. Structural Trials of the RV Triton - a Status Update and Quick-Look Report.

Gumbel, E.J., 1954. Statistical Theory of Extreme Values and Some Practical Applications. Washington, DC, USA: US Government Printing Office.

Gumbel, E.J., 1958. Statistics of Extremes. Columbia University Press.

Gumbel, E.J. and Lieblein, J., 1954. Some Applications of Extreme-Value Methods. The American Statistician, 8 (5), 14–17.

Gupta, M., McCain, M., and Eisele, A., 2003. A Route or Mission-Dependent Approach for the Calculation of Rational Structural Dynamic Loads for High-Speed Multihulls. Transactions of The Society of Naval Architects and Marine Engineers, 111, 535–556.

Hayman, B., Haug, T., and Valsgard, S., 1991. Response of Fast Craft Hull Structures to Slamming Loads. Presented at the 1st International Conference on Fast Sea Transportation (FAST'91), Trondheim, NO, 381.

Heller, S.R. and Jasper, N.H., 1960. On The Structural Design of Planing Craft. Quarterly Transactions of The Royal Institution of Naval Architects, 49–65.

Hinton, M.J., Kaddour, A.S., and Soden, P.D., 2004. Failure Criteria in Fibre Reinforced Polymer Composites: The World-Wide Failure Exercise. Elsevier.

Hoffmann, K., 1989. An Introduction to Measurements using Strain Gages. Hottinger Baldwin Messtechnik GmbH.

Hudson, F.D., Hicks, I.A., and Cripps, R.M., 1993. The Design and Development of Modern Lifeboats. Proceedings of the Institution of Mechanical Engineers, Part A: Journal of Power and Energy, 207 (1), 3–22.

Hughes, O.F., 1983. Ship Structural Design: a Rationally-Based, Computer-Aided, Optimization Approach. Wiley-Interscience.

Hughes, O.F. and Kee Paik, J., 2010. Ship Structural Analysis and Design. The Society of Naval Architects and Marine Engineers.

IMO, 2000. International Code of Safety for High Speed Craft 2000 (2008 Edition).

ITTC, 1999a. Recommended Procedures and Guidelines: Testing and Extrapolation Methods. High Speed Marine Vehicles. Sea Keeping Tests. International Towing Tank Conference, No. 7.5-02-05–04.

ITTC, 1999b. Recommended Procedures and Guidelines: Testing and Extrapolation Methods. High Speed Marine Vehicles. Structural Loads. International Towing Tank Conference, No. 7.5-02-05–06.

ITTC, 2002a. Recommended Procedures and Guidelines: Model Manufacture & Ship Models. International Towing Tank Conference, No. 7.5-01-01–01.

ITTC, 2002b. Recommended Procedures and Guidelines: Testing and Extrapolation Methods. High Speed Marine Vehicles. Resistance Test. International Towing Tank Conference, No. 7.5-02-05–01.

ITTC, 2002c. Recommended Procedures and Guidelines: Testing and Extrapolation Methods. Loads and Responses, Sea Keeping. Sea Keeping Experiments. International Towing Tank Conference, No. 7.5-02-07–02.1.

ITTC, 2002d. The Specialist Committee on Waves. Final Report and Recommendations to the 23rd ITTC. Venice, IT.

ITTC, 2011. Recommended Procedures and Guidelines: Global Loads Seakeeping Procedure. International Towing Tank Conference, No. 7.5-02-07–02.6.

ITTC, 2017. Recommended Procedures and Guidelines: Sloshing Model Tests. International Towing Tank Conference, No. 7.5-02-07–02.7.

Jacobi, G., Thomas, G., Davis, M.R., and Davidson, G., 2014. An Insight into the Slamming Behaviour of Large High-Speed Catamarans through Full-Scale Measurements. Journal of Marine Science and Technology, 19 (1), 15–32.

Jasper, N.H., 1949. Dynamic Loading of a Motor Torpedo Boat (YP110) During High-Speed Operation in Rough Water. David Taylor Model Basin, R&D Report No. C–175.

Jeans, G., Bellamy, I., Jan de Vries, J., and van Weert, P., 2003. Sea Trial of the New Datawell GPS Directional Waverider. Presented at the 7th Working Conference on Current Measurement Technology, San Diego, CA, USA, 145–147.

Johns, S., 2018. Understanding Engine Power Characteristics and their Effects on Boat Performance and Engine Reliability in Low Hour, High Load, RNLI SAR Lifeboat Applications. Presented at the SURV 9 Conference: Surveillance, Pilot & Rescue Craft, London, UK: The Royal Institution of Naval Architects, 81–92.

Johnson, M.C., 2004. Improvements in the Conduct and Interpretation of Ship Seakeeping Trials. PhD Thesis. University of Southampton, Southampton, UK.

Kapsenberg, G.K., 2011. Slamming of Ships: Where Are We Now? Philosophical Transactions of The Royal Society A: Mathematical, Physical and Engineering Sciences, 369 (1947), 2892–2919.

Kim, S.-Y., Kim, K.-H., and Kim, Y., 2015. Comparative Study on Pressure Sensors for Sloshing Experiment. Ocean Engineering, 94, 199–212.

Lang, E.J. and Chou, T.-W., 1998. The Effect of Strain Gage Size on Measurement Errors in Textile Composite Materials. Composites Science and Technology, 58 (3), 539–548.

Lee, W.T., 1995. Global Wave Statistics for Structural Design Assessments. Bethesda, MD, USA: Naval Surface Warfare Center, R&D Report No. NSWCCD-HD-1048-01.

Lee, W.T. and Bales, S.L., 1984. Environmental Data for Design of Marine Vehicles. Presented at the Ship Structure Symposium '84, New York, NY, USA: The Society of Naval Architects and Marine Engineers.

Lewis, E.V., 1988a. Principles of Naval Architecture. Volume 1 - Stability and Strength. The Society of Naval Architects and Marine Engineers.

Lewis, E.V., 1988b. Principles of Naval Architecture. Volume 3 - Motions in Waves and Controllability. The Society of Naval Architects and Marine Engineers.

Lim, S., Turkmen, S., Rostami, A.B., Prini, F., Kurniawati, V.R., Carchen, A., Gibson, M., Benson, S., Birmingham, R., Dow, R.S., Murphy, A.J., and Pazouki, K., 2018. Ship Performance – Using the Real World as a Laboratory. Presented at the Full Scale Ship Performance Conference, London, UK: The Royal Institution of Naval Architects, 1–14.

Lloyd, A.R.J.M., 1989. Seakeeping: Ship Behaviour in Rough Weather. Ellis Horwood Ltd.

Lloyd's Register (LR), 2014. Rules and Regulations for the Classification of Special Service Craft.

Ma, M., Zhao, C., and Danese, N., 2012. A Method of Applying Linear Seakeeping Panel Pressure to Full Ship Structural Models. Presented at the 11th International Conference on Computer Applications and Information Technology in the Maritime Industries, Liege, BE, 50–61.

Ma, M., Zhao, C., and Hughes, O., 2014. A Practical Method to Apply Hull Girder Sectional Loads to Full-Ship 3D Finite-Element Models Using Quadratic Programming. Ships and Offshore Structures, 9 (3), 257–265.

MAESTRO Version 11.5.0, 2017. MAESTRO User Manual.

Manganelli, P., Wagemakers, B., and Wilson, P.A., 2003. Investigation of Slamming Loads Using Slam Patches on a Scale Model of an Open60' Class Yacht. The International Journal of Small Craft Technology, 145 (B1), 47–62.

Marón, A. and Kapsenberg, G., 2014. Design of a Ship Model for Hydro-Elastic Experiments in Waves. International Journal of Naval Architecture and Ocean Engineering, 6 (4), 1130–1147.

Met Office, 2010. Fact Sheet 6 - The Beaufort Scale.

Müller-Graf, B., 1997. Dynamic Stability of High Speed Small Craft. Presented at the 25th WEGEMT School on Small Craft Technology, Athens, GR: WEGEMT Association.

National Oceanic and Atmospheric Administration, 1987. Sea State Photographs for Determining Wind Speed.

Nielsen, U.D., 2006. Estimations of On-Site Directional Wave Spectra from Measured Ship Responses. Marine Structures, 19 (1), 33–69.

Ochi, M.K., 1978. Generalization of Rayleigh Probability Distribution and Its Application. Journal of Ship Research, 22 (4), 259–265.

Ochi, M.K., 1981. Principles of Extreme Value Statistics and Their Application. Presented at the Extreme Load Response Symposium, Arlington, VA, USA: The Society of Naval Architects and Marine Engineers, 15–30.

Ojeda, R., Gangadhara Prusty, B., and Salas, M., 2004. Finite Element Investigation on the Static Response of a Composite Catamaran under Slamming Loads. Ocean Engineering, 31 (7), 901–929.

Palutikof, J.P., Brabson, B.B., Lister, D.H., and Adcock, S.T., 1999. A Review of Methods to Calculate Extreme Wind Speeds. Meteorological Applications, 6 (2), 119–132.

Phelps, B. and Morris, B., 2013. Review of Hull Structural Monitoring Systems for Navy Ships. Melbourne, AU: Maritime Platforms Division, DSTO Defence Science and Technology Organisation, Technical Report No. DSTO-TR-2818.

Phelps, B.P., 1997. Determination of Wave Loads for Ship Structural Analysis. Melbourne, AU: Aeronautical and Maritime Research Laboratory, No. DSTO-RR-0116.

Phillips, H.J., Sheppard, P.J., Venning, G., Austen, S.J., and Houchen, S., 2009. Theoretical and Practical Aspects of Conducting a Major Composite Repair. Presented at the SURV 7 Conference: Surveillance, Pilot & Rescue Craft, Poole, UK: The Royal Institution of Naval Architects, 117–124.

Prini, F., Benson, S., Birmingham, R.W., Dow, R.S., Ferguson, L.J., Sheppard, P.J., Phillips, H.J., Johnson, M.C., Mediavilla Varas, J., and Hirdaris, S., 2018. Full-Scale Seakeeping Trials of an All-Weather Lifeboat. Presented at the SURV 9 Conference: Surveillance, Pilot & Rescue Craft, London, UK: The Royal Institution of Naval Architects, 25–36.

Prini, F., Benson, S., Birmingham, R.W., Dow, R.S., Phillips, H.J., Sheppard, P.J., and Mediavilla Varas, J., 2015. Seakeeping Analysis of a High-Speed Search and Rescue Craft by Linear Potential Theory. Presented at the International Conference on Lightweight Design of Marine Structures (LIMAS2015), Glasgow, UK, 87–96.

Prini, F., Birmingham, R.W., Benson, S., Dow, R.S., Sheppard, P.J., Phillips, H.J., Johnson, M.C., Mediavilla Varas, J., and Hirdaris, S., 2018. Enhanced Structural Design and Operation of Search and Rescue Craft. Presented at the 13th IMDC International Marine Design Conference, Helsinki, FI: Taylor & Francis Group, 439–452.

Prini, F., Birmingham, R.W., Benson, S., Phillips, H.J., Sheppard, P.J., Mediavilla Varas, J., Johnson, M., and Dow, R.S., 2016. Motions and Loads of a High-Speed Craft in Regular Waves: Prediction and Analysis. Presented at the 24th International HISWA Symposium on Yacht Design and Yacht Construction, Amsterdam, NL, 1–14.

Qualisys Motion Capture Systems [online], 2018. Available from: https://www.qualisys.com/ [Accessed 17 Jul 2018].

Razola, M., 2013. On Structural Design of High-Speed Craft. Licentiate Thesis. KTH Royal Institute of Technology, Stockholm, SE.

Razola, M., Rosén, A., and Garme, K., 2014a. Allen and Jones Revisited. Ocean Engineering, 89, 119–133.

Razola, M., Rosén, A., and Garme, K., 2014b. Experimental Evaluation of Slamming Pressure Models Used in Structural Design of High-Speed Craft. International Shipbuilding Progress, 61, 17–39.

Renilson, M., Scrace, R., Johnson, M., and Richardson, C., 2004. Trials to Measure the Hydrodynamic Performance of RV Triton. Presented at the International Conference on Design & Operation of Trimaran Ships, London, UK: The Royal Institution of Naval Architects, 5–18.

Riley, M.R. and Marshall, J., 2013. Empirical Equations for Developing Ride Severity Envelopes for Planing Craft Less Than 55 Feet in Length. Bethesda, MD, USA: Naval Surface Warfare Center Carderock Division, Technical Report No. NSWCCD-83-TM-2013/36.

Roark, R.J., 1965. Formulas for Stress and Stain. Fourth Edition. McGraw-Hill Inc.

Roberton, D.M.V., 2015. Residual Life Assessment of Composite Structures: With Application to All Weather Lifeboats. PhD Thesis. University of Southampton, Southampton, UK.

Rosén, A., 2001. Impact Pressure Analysis on High-Speed Craft in Waves through FE-analysis on Measurement Data. Presented at the 8th International Symposium on Practical Design of Ships and Other Floating Structures (PRADS2001), Shanghai, China: Elsevier Science Ltd., 629–635.

Rosén, A., 2005. Impact Pressure Distribution Reconstruction from Discrete Point Measurements. International Shipbuilding Progress, 52 (1), 91–107.

Rosén, A. and Garme, K., 1999. Slamming Studies on High-Speed Planing Craft through Full-Scale Trials and Simulations. Presented at the 5th International Conference on Fast Sea Transportation (FAST'99), Seattle, WA, USA.

Rosén, A. and Garme, K., 2004. Model Experiment Addressing the Impact Pressure Distribution on Planing Craft in Waves. The International Journal of Small Craft Technology, 146 (B1).

Royal National Lifeboat Institution [online], 2018. Available from: https://rnli.org/ [Accessed 23 Jul 2018].

Salvesen, N., Tuck, E.O., and Faltinsen, O., 1970. Ship Motions and Sea Loads. Presented at the SNAME Annual Meeting, New York, NY, USA: The Society of Naval Architects and Marine Engineers, 1–30.

Salvino, L.W. and Collette, M.D., 2009. Monitoring Marine Structures. In: Encyclopedia of Structural Health Monitoring. John Wiley & Sons Ltd.

Savitsky, D., 2003. On the Subject of High-Speed Monohulls. In: Greek Section of The Society of Naval Architects and Marine Engineers. Athens, GR.

Savitsky, D. and Brown, P.W., 1976. Procedures for Hydrodynamic Evaluation of Planing Hulls in Smooth and Rough Water. Marine Technology, 13 (4), 381–400.

Schellin, T.E., Shigunov, V., Troesch, A.W., Kim, D.-H., and Maki, K., 2015. Prediction of Loads for Ship Structural Design. Naval Engineers Journal, 127 (1), 103–134.

Slaughter, S.B., Cheung, M.C., Sucharski, D., and Cowper, B., 1997. State of the Art in Hull Response Monitoring Systems. Ship Structure Committee, Technical Report No. SSC-401.

Southampton Oceanography Centre, 2001. Wind and Wave Frequency Distributions for Sites around the British Isles. Southampton, UK.

St. Denis, M. and Pierson, W.J., 1953. On the Motions of Ships in Confused Seas. Presented at the SNAME Annual Meeting, New York, NY, USA: The Society of Naval Architects and Marine Engineers, 280–357.

Stone, K.F., 2005. Comparative Structural Requirements for High Speed Craft. Ship Structure Committee, Technical Report No. SSC-439.

Tannuri, E.A., Sparano, J.V., Simos, A.N., and Da Cruz, J.J., 2003. Estimating Directional Wave Spectrum Based on Stationary Ship Motion Measurements. Applied Ocean Research, 25 (5), 243–261.

Temarel, P., Bai, W., Bruns, A., Derbanne, Q., Dessi, D., Dhavalikar, S., Fonseca, N., Fukasawa, T., Gu, X., Nestegård, A., Papanikolaou, A., Parunov, J., Song, K.H., and Wang, S., 2016. Prediction of Wave-Induced Loads on Ships: Progress and Challenges. Ocean Engineering, 119, 274–308.

Topper, M.B.R., 2013. Semantics of Spectral Density for Ocean Waves. The University of Edinburgh, Technical Report.

Vishay Precision Group, 2014. Strain Gage Selection: Criteria, Procedures, Recommendations. Vishay Precision Group – Micro-Measurements, Technical Note No. TN-505-4.

Von Kármán, T., 1929. The Impact on Seaplane Floats during Landing. Washington, DC, USA: National Advisory Committee for Aeronautics, Technical Note No. 321.

de Vries, J.J., Waldron, J., and Cunningham, V., 2003. Field Tests of the New Datawell DWR-G GPS Wave Buoy. Sea Technology, (44), 50–55.

Wagner, H., 1932. Loading of Seaplanes. Washington, DC, USA: National Advisory Committee for Aeronautics, Technical Memorandum No. 622.

Zhao, C. and Ma, M., 2016. A Hybrid 2.5-Dimensional High-Speed Strip Theory Method and Its Application to Apply Pressure Loads to 3-Dimensional Full Ship Finite Element Models. Journal of Ship Production and Design, 32 (4), 216–225.

Zhao, C., Ma, M., and Hughes, O., 2013. Applying Strip Theory Based Linear Seakeeping Loads to 3D Full Ship Finite Element Models. Presented at the 32nd International Conference on Ocean, Offshore and Arctic Engineering (OMAE2013), Nantes, FR: The American Society of Mechanical Engineers.

Zhao, R. and Faltinsen, O., 1993. Water Entry of Two-Dimensional Bodies. Journal of Fluid Mechanics, 246, 593–612.

Zhao, R., Faltinsen, O., and Aarsnes, J., 1997. Water Entry of Arbitrary Two-Dimensional Sections with and without Flow Separation. Presented at the 21st Symposium on Naval Hydrodynamics, Washington, DC, USA: National Academy Press, 408–423.

Appendices

The appendix contains the following information:

Appendix 1	Publications and other outputs
Appendix 2	Small-scale tests. Specifications for the construction of the Severn Class hull models
Appendix 3	Small-scale tests. Calibration of the strength bar used on the segmented hull model
Appendix 4	Full-scale tests. Trial trajectories
Appendix 5	Full-scale tests. Instrumentation plan for sea trials
Appendix 6	Full-scale tests. Record sheet for manually recorded values
Appendix 7	Full-scale tests. Finite element study for conversion of strain values to equivalent pressure values

Appendix 1

Publications and other Outputs

Publications produced as part of the research:

- Prini, F., Benson, S., Birmingham, R., Dow, R.S., Phillips, H.J., Sheppard, P.J., and Mediavilla Varas, J., 2015. Seakeeping Analysis of a High-Speed Search and Rescue Craft by Linear Potential Theory. Presented at the LIMAS2015 International Conference on Lightweight Design of Marine Structures, Glasgow, UK, 87–96.
- Prini, F., Birmingham, R.W., Benson, S., Phillips, H.J., Sheppard, P.J., Mediavilla Varas, J., Johnson, M., and Dow, R.S., 2016. Motions and Loads of a High-Speed Craft in Regular Waves: Prediction and Analysis. Presented at the 24th International HISWA Symposium on Yacht Design and Yacht Construction, Amsterdam, NL, 1–14.
- Prini, F., Benson, S., Birmingham, R.W., Dow, R.S., Ferguson, L.J., Sheppard, P.J., Phillips, H.J., Johnson, M.C., Mediavilla Varas, J., and Hirdaris, S., 2018. Full-Scale Seakeeping Trials of an All-Weather Lifeboat. Presented at the SURV 9 Conference: Surveillance, Pilot & Rescue Craft, London, UK: The Royal Institution of Naval Architects, 25–36.
- Prini, F., Birmingham, R.W., Benson, S., Dow, R.S., Sheppard, P.J., Phillips, H.J., Johnson, M.C., Mediavilla Varas, J., and Hirdaris, S., 2018. Enhanced Structural Design and Operation of Search and Rescue Craft. Presented at the 13th IMDC International Marine Design Conference, Helsinki, FI: Taylor & Francis Group, 439–452.

Other Outputs

- Severn Class scaled hull models
  These models belong to the RNLI. Under an agreement between the RNLI and Newcastle University, as of March 2019 the models are stored at Newcastle University and may be viewed by appointment with the hydrodynamics laboratory.

Appendix 2

Specifications for the Construction of the Severn Class Hull Models

NOTES

The report attached was originally produced for the RNLI. It was amended for release as part of this thesis.

RNLI NEWCASTLE UNIVERSITY LLOYD'S REGISTER

Enhanced Design of Search and Rescue Craft

Specifications for the Construction of the Severn Class Hull Models

Task 2.2.2 Report

[AMENDED FOR RELEASE]

1 INTRODUCTION

A series of experiments at model scale will be conducted, as part of the project 'Enhanced Design of Search and Rescue Craft', to study the seakeeping behaviour of the Severn Class. The data obtained will be used to validate and tune the numerical model for the prediction of the wave-induced loads sustained by the craft during operation. This document outlines the requirements and specifications for the design and construction of the scaled hull models.

2 OBJECTIVES

- Calculate the motion and global load RAOs for a range of headings, speeds and wave frequencies
- Validate numerical predictions obtained with MAESTRO-Wave code
- Provide data for comparison against full-scale tests

3 SCOPE OF THE EXPERIMENTS

- Deep water only
- Towed model (no self-propelled model)
- One displacement condition
- Model in the naked condition with centre and bilge keels (no trim tabs, rudders, shafts, A-brackets or propellers and no bow thruster opening or fairing)

4 RECOMMENDED PROCEDURES AND GUIDELINES

The ITTC provides established procedures and guidelines for performance prediction and evaluation of designs by either experimental or computational methods. The following ITTC Recommended Procedures address resistance, seakeeping and structural load model tests with conventional displacement vessels:

- 7.5-01-01-01 Model Manufacture – Ship Models
- 7.5-02-02-01 Testing and Extrapolation Methods - Resistance Test
- 7.5-02-07-02.1 Testing and Extrapolation Methods - Seakeeping Experiments
- 7.5-02-07-02.6 Testing and Extrapolation Methods - Global Loads Seakeeping Procedure

The following ITTC Recommended Procedures address resistance, seakeeping and structural load model tests with High Speed Marine Vehicles (HSMV):

- 7.5-02-05-01 High Speed Marine Vehicles – Resistance Test
- 7.5-02-05-04 High Speed Marine Vehicles – Sea Keeping Test
- 7.5-02-05-06 High Speed Marine Vehicles – Structural Loads

HSMV are defined as vessels with any of the following characteristics:

- Froude Number Fn>0.45
- Speed $V > 3.7\,\nabla^{1/6}$ (m/s)
- Dynamically supported vessels with high trim angles

For this purpose, the Severn Class should be treated as a HSMV, since:

- It reaches Fn≈1.0
- It reaches V≈12.9 m/s >> $V = 3.7\nabla^{1/6} \approx 6.9$ m/s

Relevant aspects for the design of the hull models, as stated in the ITTC Recommended Procedures, are reviewed in the following sections.

4.1 RESISTANCE TESTS

[From 7.5-02-02-01 & 7.5-02-05-01]

Resistance tests are performed to collect data from which the resistance of a model hull for a given speed can be determined. During each run, the following quantities are measured and recorded continuously:

- Resistance
- Speed
- Running attitude (sinkage fore and aft or running trim and sinkage)

Resistance tests for conventional displacement ships and HSMV are performed in a similar manner. The main differences in the testing of HSMVs are:

- Dynamic lift and trim are more important
- Air resistance is more important and may affect the dynamic trim
- Scale effects on lifting surfaces and appendages can be challenging to account for
- Special attention must be given to minimising the model weight

4.1.1 Superstructure

When testing conventional displacement ships, the superstructure is not generally included and only the hull shell is manufactured. However, due to the more important role that air resistance plays in the hydrodynamics of a high-speed craft, it is recommended to test with a superstructure of basic shape and main dimensions representative of the full-scale prototype. The alternatives to the use of a superstructure are presented in detail in 7.5-02-05-01.

4.1.2 Turbulence Stimulators

For tests conducted at Reynolds numbers based on hull length of less than $5x10^6$, boundary layer turbulence stimulation is recommended. A description of different means of turbulence stimulation is given in 7.5-01-01-01.

For HSMVs, the use of wires for turbulence stimulation is not recommended due to the risk of air suction. Extra care must be taken in the placement of the turbulence stimulators when the craft's running attitude changes significantly with the speed.
Turbulence stimulation is also recommended for any appendage subject to laminar flow. This is likely to include:

- Appendages penetrating through the boundary layer of the model
- Appendages of HSMVs which are often too small to obtain Reynolds numbers larger than $5x10^6$

4.1.3 Towing Point

The towing system should be designed to avoid artificial trim effects due to the towing force. Hence, the application of the towing force should represent as closely as possible the direction of the propulsion force. The preferred way of achieving this is to tow in line and in the direction of the propeller shaft. Alternatively, the tow force should be in line of the propeller shaft and at the vertical passing through the LCG. Where this is not possible, a correction in the position of the LCG should be introduced in order to account for the artificial trim moments introduced by the towing system.

4.1.4 Model Size

The model should be as large as possible for the size of the facility, with respect to:

- Blockage
- Shallow water
- Model mass
- Maximum speed of the towing carriage

4.1.5 Blockage

The dimensions of the towing tank should be large enough to avoid blockage effects. However, formulae are given for including blockage corrections when necessary.

For conventional displacement ships, 7.5-02-02-01 outlines different formulae based on mean-flow theory for both blockage and shallow water corrections. Generally, their range of applicability is: model size 3.5m<L<9m; tanks of approximately 2:1 breadth to water depth ratio; and speed range 0.08<Fn<0.4. Out of this range of applicability guidance given by Graff (1969) is recommended.

For HSMVs, limitations due to blockage effects are addressed for different types of craft:

- *Planing hulls*
  According to Savitsky the tank width should be at least seven times the model beam:

$$B_T \geq 7B_M$$

- *Semi-displacement hulls and hydrofoils*
  According to Muller-Graf the tank depth should be greater than 0.8 times the model length and the tank width should be greater than twice the model length

$$h_T > 0.8L_M$$
$$B_T > 2L_M$$

For all types of HSMV, it is recommended to avoid those situations where the hump speed of the model approaches or coincides with the critical depth speed of the tank. This occurs for depth Froude numbers:

$$Fn_h = V/\sqrt{(gh)} = 1.0$$

4.2 SEAKEEPING TESTS

[From 7.5-02-07-02.1 & 7.5-02-05-04]

The main purpose of seakeeping tests on conventional displacement ships is to obtain the linear response functions in waves. The seakeeping behaviour of high-speed craft is characterised by high accelerations and can be nonlinear, with a degree of nonlinearity that increases with the craft speed. Semi-planing craft, which operate at lower speeds, have typically less complex responses.

At Froude numbers above 1.0, it is considered that the response of the craft is strongly nonlinear and the principle of linear superposition is no longer acceptable for analysing measurements. Tests in regular waves can still be performed to obtain the response amplitude operators (RAOs) and, hence, interesting information on the response of the craft to different exciting frequencies. However, they are not recommended for predicting the response of the craft in a random seaway.

4.2.1 Model Size

The lower limit to the model size is given by the required displacement to carry the model structural weight, the measurement equipment and the propulsion unit. Viscous effects can generally be neglected for seakeeping studies, as they play a minor role. Hence there are no minimum requirements for the model size based on Reynolds numbers as there are for resistance tests. However, it is noted that viscous effects do play a non-negligible role for roll damping and forces on stabilising fins or rudders. The upper limit for the model size is given by the constraints of the experimental facility:

- Tank size, hence tank wall interference
- Speed of the towing carriage
- Wave maker capabilities

4.2.2 Tank Wall Interference

For seakeeping experiments on displacement vessels, recommendations are made on the maximum allowable size of the model in order to avoid interference with the tank walls. The maximum frequency at which tank wall interference occurs in head waves is given in Figure 1 as a function of the model length L_M, the tank breadth B_T and the Froude number Fn.

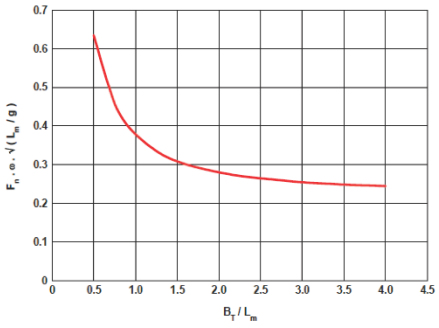

Figure 1 Maximum frequency at which tank wall interference occurs in head waves.

A comprehensive theory for predicting the effects of tank wall interference on the hydrodynamics of a ship advancing in waves was presented by Kashiwagi and Ohkusu (1989). The diagrams for assessing presence of interference were later confirmed by experimental tests (Kashiwagi and Ohkusu, 1990). These diagrams shown in Figure 2, were included in the 19th ITTC Seakeeping Committee Report as they make clear the degree of tank wall interference. However, their range of applicability is up to approximately Fn =0.3.

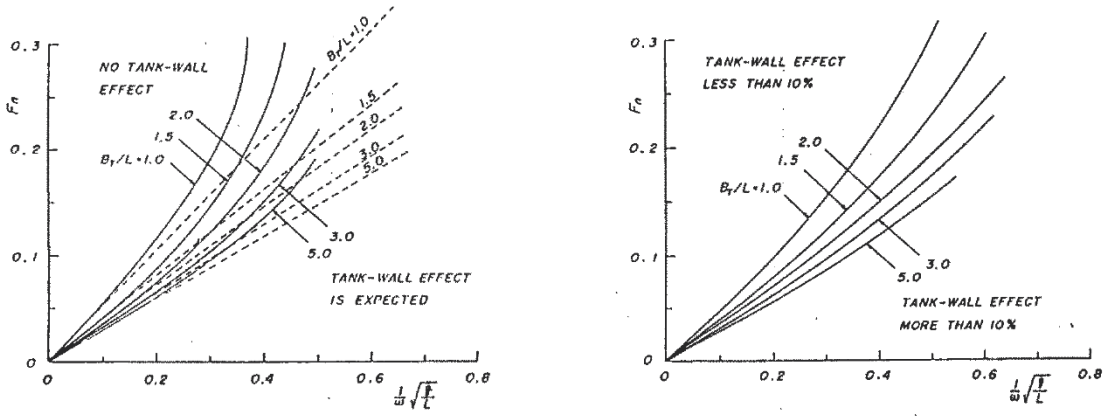

Figure 2. (Left) Occurrence of tank wall interference. (Right) Zones for a given level of tank wall interference.

A more generally applicable theory is presented by Lloyd (1989). Two equations are formulated defining the critical speed at which tank wall interference begins in head and following seas. These equations are based on the wave encounter frequency and the radiated wave celerity for deep water. Figure 3, based on these equations, shows the conditions for which tank wall interference occurs in head and following seas.

In head seas the Froude number Fn must be greater that the critical Froude number Fn_{crit} to avoid tank wall interference. Differently, in following seas the Froude number must lie within a specific range of values. This range decreases as the model length increases, up to when the model length equals one quarter of the tank width, for which there is only one Froude number, for each wave frequency, that will yield to results not affected by interference. As a consequence, the maximum allowable model length for seakeeping tests in following seas is one quarter of the tank width. Larger models will always experience interference for any value of Froude number or wave frequency.

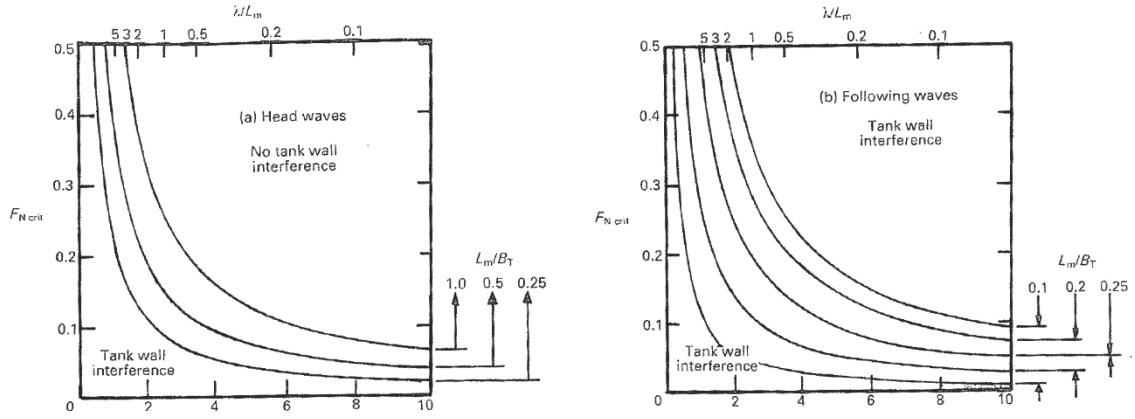

Figure 3. Tank wall interference in head and following waves (from Lloyd (1989)).

4.2.3 Weight Distribution

Careful consideration must be given to the weight distribution, especially when small size hull models are employed. The risk is the inertia of the model being too high to be representative of the inertia of the prototype. Another factor to consider is the hull stiffness, which is an important characteristic if rigid body motions are to be measured. Therefore, the model should be of light and stiff construction.

In order to measure bending moments, shears and torsion experienced by the hull girder in waves, both the longitudinal and transverse weight distribution must be correctly reproduced at scale. In other cases, only the radii of gyration are to be simulated. For tests in head or following seas, the model can be restrained in roll motion. If this is the case, it is not necessary to reproduce the transverse weight distribution.

4.2.4 Towing Point

The towing system should be designed to impose minimum restraint on the motions of the model. In the case of planing monohulls, most often the towing point lies at the intersection of the LCG and the propulsor's thrust line. The effects of appendages and propeller forces on the pitching moment should be estimated and accounted for separately. A non-varying towing thrust angle is usually adopted to tow models in waves.

4.2.5 Ride Control Systems

The ITTC recommends that any ride control system that improves the seakeeping characteristics of the vessel is included in the model for tests in waves. For fins and lifting surfaces, a turbulence stimulator should be applied. The actual fin angle of the fin of lifting surface should be measured to check on the accuracy of the actuator system.

For seakeeping tests with a free model, the ITTC considers necessary to test the model complete of foil systems and actively controlled flaps, if these are fitted to the full-scale prototype.

4.2.6 Superstructure

Planing craft models are usually tested with a sealed deck to avoid water entering. In many cases, simplified superstructures are built to evaluate spray and water impact.

4.2.7 Headings

- *Head seas*
  Tests in head seas can be carried out with a towed model.

  Lateral motions can be completely restrained. Surge motions can be restrained or the model can be towed with a spring system. For the latter, a spring with an appropriate resonance frequency, which is different from the wave encounter frequency, should be selected.

- *Following seas*
  Tests in following seas should be performed with the model free to surge. Large surge motions should be allowed in order to assess correctly if the model is predisposed to nose diving or green water over the bow. It is difficult to allow large surge motion with a spring system, which therefore does not represent an optimum solution. A self-propelled model is a good solution for tests in following waves. Alternatively, a constant tension winch can be used.

- *Quartering seas*
  If a towed model is used for seakeeping test in quartering sea, the model is to be kept on course. A system to keep the model on course should compensate for the hydrodynamic mean loads experienced by the model and for tests at high speed this system needs to be rather stiff. This would have a significant influence on the ship motions. Therefore, for performing seakeeping tests in quartering seas, a self-propelled model is recommended.

4.2.8 Typical Model Tests for HSMV

Seakeeping model tests on HSMVs are typically conducted in head or following seas. The model is let free to pitch and heave, whilst surge, sway, roll and yaw are restrained.

Fridsma (1971) performed an extensive series of test on planing hulls. He showed that in head seas, for Froude numbers Fn>1.0 the motions and added resistance of a model free to surge and propelled with constant thrust are the same as those measured with constant speed tests, hence with the model restrained in surge.

4.2.9 Wave Environment

Regular Waves

For conventional hull forms, tests in regular waves are run to obtain the linear response functions of the vessel. Tests should be carried out at a range of speeds and wavelengths. The minimum range of wavelengths to consider is 0.5Lpp to 2.0Lpp. Either the ratio wave height-to-Lpp or the ratio wave height-to-wavelength should be kept constant. The advised value of the ratio of wave height to wavelength is 1/50.

For high-speed craft the motion responses can be nonlinear. As a consequence, the motion RAOs are not unique and cannot be used to predict the performance of the craft in irregular seas with confidence. In this case, the craft performance in irregular seas is to be assessed.

Irregular Waves

Tests in irregular seas are required for conventional displacement ships to study extreme effects (e.g. slamming, green water, nose diving, broaching). For HSMV these tests are also required due to the nonlinear behaviour of the craft – when motions and accelerations are not linearly dependent to the wave amplitude. In this case, tests in irregular waves are carried out also to check the normal operation limits. Several wave energy spectra are available and the choice depends on the focus of the test:

- *Normal operating conditions*
  For tests aimed at determining the operational limits not in extreme conditions, the two-parameter ITTC Standard Spectrum is recommended as a description of the wave energy distribution over the frequency range. This spectrum describes a fully developed sea state which is believed relevant for normal operating conditions.

- *Extreme conditions*
  For tests aimed at assessing the craft responses in extreme seas, the JONSWAP Spectrum is recommended. Since an extreme weather is usually of short duration, the sea state cannot be expected to be fully developed, hence a peak enhancement factor $\gamma>>1$ should be used to generate the JONSWAP spectra.

For HSMVs travelling in local wind generated waves, the encounter frequency is usually high. This does not result in any significant motion. Differently, the effect of the swell are of more importance to the operability and safety aspects of these craft. Local wave information for operability studies on HSMVs is recommended.

Wave Encounters

Based on review of data from different facilities, a minimum of 100 wave encounters is recommended for tests in head seas. The total run time required to record 100 encounters can be estimated from the modal frequency of the employed wave spectrum.

Due to the high speeds involved in the testing of planing craft, the size of the facility may limit the run time to a few seconds only. If this is the case, many runs are necessary to reach 100 wave encounters. It is standard practice to put together the measurement time records and analyse the whole set of data as if it was a single run.

4.3 STRUCTURAL LOAD TESTS

[From 7.5-02-07-02.6 & 7.5-02-05-06]

The purpose of these tests is to measure global wave loads through seakeeping experiments. Possible areas of interest that can be investigated are:

- *Primary Design Loads*
  Require a relatively low degree of complexity.

- *Slamming, Whipping and Springing Loads*
  Require a higher degree of complexity. Scaling issues for the modelling of the local hydrodynamic pressure and hydroelasticity arise.

- *Validation of Computational Methods*
  Require greater accuracy in the measurement of control forces which affect the resultant global loads, as these will need to be compared against those from numerical methods.

- *Frequency Domain Application to Lifetime Designs*
  Aim at deriving the frequency response of global loads for a sea state of concern. The measured load response functions can also be compared against those from numerical methods.

- *Application to Extreme Loads – Stochastic Analysis*
  Require appropriate seaway modelling techniques to ensure proper representation of the extreme sea. Care must be given to the wave making capabilities of the facility.

- *Fatigue Analysis and Design*
  Different and distinct seaways and operational sectors need to be verified. Results are combined with numerical methods to determine the cumulative lifetime global loading.

- *Safe Operating Envelope*
  Aim at assessing limiting environmental loads, operational aspects and structural strength.

4.3.1 Hydroelasticity

The structural loading problem can be treated as hydroelastic or non-hydroelastic. The hydroelastic approach requires the structural dynamics to be modelled correctly, which means scaling both the weight distribution and the hull stiffness.

Whilst in some cases hydroelasticity plays an important role, it is negligible in others. As an example, for bottom slamming, hydroelasticity must be considered for determining the magnitude of slamming loads. For bow slamming where the deadrise angle is typically more than 15deg, hydroelastic effects have been proved to be less important.

4.3.2 Local and Global Loads

Structural loads can be divided into local and global loads:

- *Local loads*
  When the measurement of local loads is the objective of seakeeping tests, the global response of the ship can be assessed to identify the relative speed and orientation of a local area of interest with respect to waves.

  In those cases where hydroelasticity plays an important role, the dynamic behaviour of the area of interest must be correctly modelled if the magnitude of the slamming loads is the objective. Otherwise the tests can still be conducted, but results can only be used to document the occurrence of slamming and not to measure the magnitude of the slamming forces. Whenever hydroelasticity can be neglected, slamming forces can be measured on a structure stiff enough to avoid artificial hydroelastic effects.

- *Global loads*
  For monohull vessels, hull girder bending moments are the most important global loads. These can be measured with a number of model types, described in the following section.

4.3.3 Model Types

Two types of model can be employed for measuring structural global loads during seakeeping tests: hydro-structural or segmented.

Hydro-Structural Model

A hydro-structural model is representative of the full-scale prototype down to the local structural level. Geometric, hydrodynamic and structural similarities, for what concerns global bending moments and shear forces, are satisfied. Hence, the measurement of bending moments and shear forces can be taken at any cross-section along the hull length.

A hydro-structural model is rather complex, costly and time consuming to realise. Experiments with this approach have only been performed on a limited basis. Moreover, structural loads are to be found from strain measurements. Establishing a reliable relation between measured strains and global or local forces on a hydro-structural scaled model is difficult.

Segmented Model

In a segmented model, the hull is divided into several independent segments. Global loads can be investigated through force transducers (typically strain gauges) at the segmentations, by means of a structure independent from the external hull shell and connecting the hull segments. A segmented model is easier to calibrate than a hydro-structural model and results can be more readily analysed. This makes segmented models the most common option for practical testing.

Two types of segmented model exist, depending on the type of interface connecting the segments:

- *Rigid Segmented Model*
  Segments are rigidly connected so that the stiffness of the hull girder is much higher than that of the prototype vessel. The model's shape does not change when run in a seaway and the natural frequency of the structure is much greater than the wave frequencies.

- *Elastic Segmented Model*
  This type of model requires some knowledge of the hull girder strength and stiffness along its length because the stiffness of the structure should represent, as closely as possible, the stiffness of full-scale prototype, at least in correspondence of the segmentation cuts.

  The natural frequency of the hull girder should also be scaled correctly. If the model is realised by means of an elastic beam made of the same material as the full-scale prototype, theoretically the scaling law is the fifth power of the scaling factor used to realise the hull model. However, the correct scaled natural frequency is difficult to achieve in practice, hence a value estimated either numerically or from full-scale data should be used to adjust the model's natural frequency.

4.3.4 Structure for Segmented Models

Both rigid and elastic segmented models can incorporate:

- *Backbone beam or internal truss*
  In correspondence of the segmentation cuts the beam is fitted with strain gauges to measure forces a moments. Ideally, the neutral axis of the backbone beam or the internal truss should match as closely as possible the neutral axis of the full-scale hull girder. Examples of segmented models fitted with a backbone beam and an internal truss are shown in Figures 4 & 5 respectively.

  The backbone beam is typically made of aluminium due to weight and ease of manufacture, although other materials can be employed. For rigid segmented models the backbone should be stiff. For elastic segmented models the backbone or the internal truss usually have a varying cross-section that represents the actual hull girder's stiffness. This can be done by altering the flange thickness of the backbone beam or by tapering the internal truss.

- *Instrumented joint connections (force transducers)*
  Forces and moments can also be measured with force transducers at the interface between two segments. For rigid segmented models, the connection between the segments should to be stiff. For elastic segmented model, the connection between the segments should be flexible and have the same structural damping as the full-scale prototype at the location of the joint. An example of segmented model fitted with force transducer is shown in Figure 6.

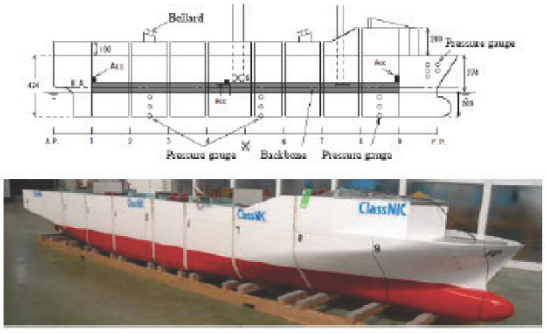

Figure 4 Elastic segmented model with backbone beam (from 7.5-02-07-02.6).

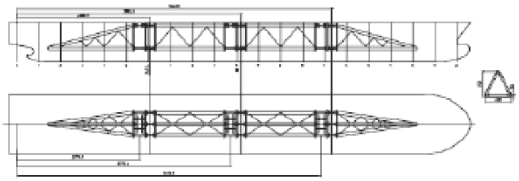

Figure 5 Elastic segmented model with internal truss (from 7.5-02-07-02.6).

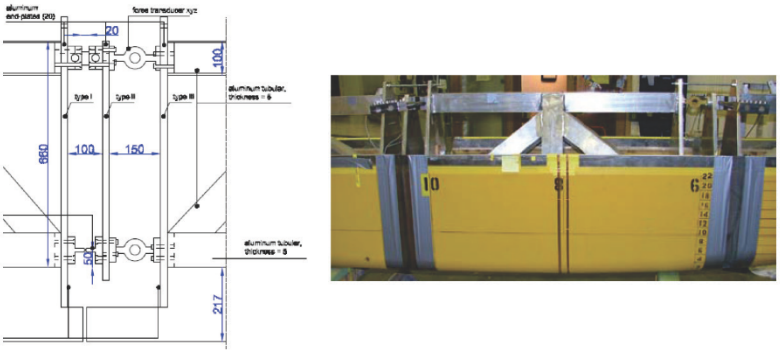

Figure 6 Segmented model with force transducers (from 7.5-02-07-02.6).

4.3.5 Weight Distribution

The correct weight distribution and inertial properties should be represented in the model at both a global and a segment level, that is:

- Each segment must have the same weight and inertial characteristics as the corresponding segment on the full-scale prototype
- The overall hull weight and inertia must be correctly represented at the model scale

4.3.6 Model Size

Froude's similitude should be used for global loads experiments. The scaling factor should be determined according to the features of the facility, as for conventional seakeeping tests, and according to the restrictions that the structural similarity implies (e.g. weight and inertia at a segment level, stiffness of the hull girder).

4.3.7 Model Segmentation

For segmented models, the number and location of cuts are selected based on the objectives of the tests and on the primary modes of structural deformation to be studied, for example:

- Mid-ship bending moment - amidships cut
- Maximum shear - three/four cuts along the ship length
- Load longitudinal distribution - five or more cuts along the ship length

For elastic segmented models, the segmentation should be such that the most important eigenmodes can be represented. Hence, the location and number of cuts can be determined when the primary eigenmodes of the full-scale prototype are known. It is advised to perform a comparison between the mode shapes of the segmented model and the estimated mode shapes of the full-scale prototype. This should be done to check the validity of the results obtained with the model tests.

When elastic segmented models are employed to assess the ship response to specific modes, it is mandatory to identify the structural damping of the model structure. Structural damping is important when observing a succession of impacts and plays a major role in the assessment of whipping and springing responses.

The gap between segments is typically 5-10mm in width for conventional ship models. Watertightness is ensured by sealing the gaps along the segmentation cuts. Use of a dental quality latex (Figure 7), slightly indented towards the hull so that the external hull shape is minimally affected, is recommended for this purpose.

Figure 7. Example of segment sealant.

5 THE FACILITY

The experiments will be performed at Newcastle University's towing tank, with principal particulars:.

TOWING TANK SPECIFICATIONS	
Length	37 m
Width	3.7 m
Maximum Water Depth	1.25 m
Maximum Carriage Speed	3.5 m/s
WAVEMAKER CAPABILITIES	
Wave Period	0.5-2.0 s
Wave Height (period dependent)	0.02-0.12 m

6 THE SEVERN CLASS

The main particulars of the Severn Class lifeboat are:

Length Overall	LOA	17.00	[m]
Length Waterline	LWL	15.57	[m]
Beam Overall	BOA	5.62	[m]
Beam Waterline	BWL	5.00	[m]
Draught (at amidships)	T	1.46	[m]
LCG (aft of amidships)	LCG	1.30	[m]
LCG (from transom)	LCG	6.45	[m]
Displacement	Δ	43170	[kg]
Speed max	V	25	[kts]
Speed max	V	12.86	[m/s]
Wet Surface Area	WSA	94.73	[m^2]

7 MODEL SIZE

The model size is determined to the largest possible with respect to the size of the facility and the scope of the tests. The scaling ratio $\boldsymbol{\lambda}$ is selected based on the following constraints.

7.1.1 Blockage

From Savitsky's formula (planing craft):

$$B_T \geq 7B_M$$

Light Load	Full Load
$B_M \leq 0.53\ m$	$B_M \leq 0.53\ m$
$\boldsymbol{\lambda \geq 9.13}$	$\boldsymbol{\lambda \geq 9.32}$

From Muller-Graf's formula (semi-planing craft):

$$h_T \geq 0.8L_M$$

Light Load	Full Load
$L_M \leq 1.56\ m$	$L_M \leq 1.56\ m$
$\boldsymbol{\lambda \geq 9.92}$	$\boldsymbol{\lambda \geq 9.97}$

7.1.2 Shallow Water

$$\frac{V_M}{\sqrt{gh_T}} < 1$$
$$V_M < 3.50\ m/s$$

$\boldsymbol{\lambda > 13.48}$	@ 25 kts
$\boldsymbol{\lambda > 16.90}$	@ 28 kts
$\boldsymbol{\lambda > 19.41}$	@ 30 kts

7.1.3 Carriage speed

$$V_{carriage} = \frac{V_{Smax}}{\sqrt{\lambda}} = V_{Mmax}$$
$$\lambda > \left(\frac{V_{Smax}}{V_{carriage}}\right)^2$$

$V_{carriage} = 3.5\ m/s$	$\boldsymbol{\lambda > 13.48}$	@ 25 kts
	$\boldsymbol{\lambda > 16.90}$	@ 28 kts
	$\boldsymbol{\lambda > 19.41}$	@ 30 kts

7.1.4 Tank Wall Interference

From the hydrodynamic analysis with MAESTRO-Wave a suitable range of wave frequencies was identified as

$$0.90 < \omega < 3.01\ rad/s\ (2.08 < T < 6.98\ s)$$

It is assumed a scale factor $\lambda > 13.48$ that, as shown above, represents the upper limit for the model size. This calls for:

- Model length $L_M = 1.15\ m$, hence $\frac{L_M}{B_T} = 0.31\ m$
- Range of wave frequencies at model scale $3.30 < \omega\sqrt{\frac{L_M}{g}} < 11.05\ rad/s$, which can be made non-dimensional as

  $1.13 < \omega\sqrt{\frac{L_M}{g}} < 3.78$

From the following diagrams, showing the occurrence of tank wall interfere in head seas and following seas (after Lloyd (1989)):

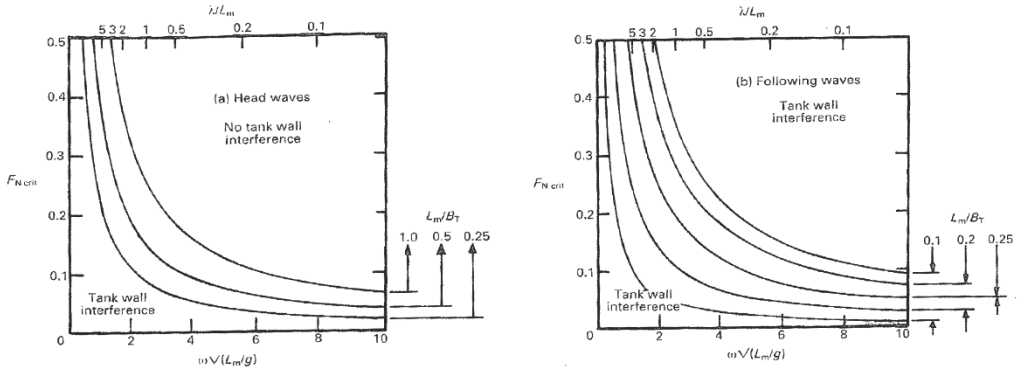

- In head seas, tank wall interference is not expected to occur.
- In following seas, tank wall interference would occur for all wave frequencies and speeds since: $L_M/B_T = 0.31\ m$. This limits the scope of the tests to head seas only. Following seas tests would still be possible in the proposed facility, although good correlation with the full-scale behaviour should not be expected.

7.1.5 Wave Maker Capabilities

A suitable range of wave periods was identified as: $2.08 < T < 6.98\ s$.

	Required wave period	Wave maker period
$@\ \lambda = 13.48$	$0.57 < T < 1.90\ s$	$0.50 < T < 2.0\ s$

NOTE: according to Lloyd (1989), the water depth should be at least half the longest wave length envisaged to avoid unwanted shallow water effects on the waves.

7.1.6 Design Scaling Factor

$$\lambda = 13.5$$

SEVERN CLASS PARTICULAR			REAL SCALE	MODEL SCALE
Scale Factor			1	13.50
Length Overall	LOA	[m]	17.00	1.259
Length Waterline	LWL	[m]	15.57	1.153
Beam Overall	BOA	[m]	5.62	0.416
Beam Waterline	BWL	[m]	5.00	0.370
Draught (at amidships)	T	[m]	1.46	0.108
LCG (aft of amidships)	LCG	[m]	1.30	0.096
LCG (from transom)	LCG	[m]	6.45	0.478
Displacement	Δ	[kg]	43170	17.12
Speed max	V	[kts]	25	6.80
Speed max	V	[m/s]	12.86	3.50
Wet Surface Area	WSA	[m^2]	94.73	0.520

8 BIBLIOGRAPHY

- Bhattacharyya, Rameswar. 1978. *Dynamics of Marine Vehicles*. John Wiley & Sons Inc.
- Lloyd, A R J M. 1989. *Seakeeping: Ship Behaviour in Rough Weather*. Ellis Horwood.
- ITTC. 1990. 'ITTC Seakeeping Committee Report 1990.' Proceedings of the 19th ITTC.
- 'Global Loads Seakeeping Procedure'. 2011. 7.5-02-07-02.6. ITTC Recommended Procedures and Guidelines.
- 'Model Manufacture & Ship Models'. 2002. 7.5-01-01–01. ITTC Recommended Procedures and Guidelines.
- 'Testing and Extrapolation Methods. High Speed Marine Vehicles. Dynamic Instability Tests'. 1999. 7.5-02-05–07. ITTC Recommended Procedures and Guidelines.
- 'Testing and Extrapolation Methods. High Speed Marine Vehicles. Resistance Test'. 2002. 7.5-02-05–01. ITTC Recommended Procedures and Guidelines.
- 'Testing and Extrapolation Methods. High Speed Marine Vehicles. Sea Keeping Tests'. 1999. 7.5-02-05–04. ITTC Recommended Procedures and Guidelines.
- 'Testing and Extrapolation Methods. High Speed Marine Vehicles. Structural Loads'. 1999. 7.5-02-05–06. ITTC Recommended Procedures and Guidelines.
- 'Testing and Extrapolation Methods. Loads and Responses, Sea Keeping. Sea Keeping Experiments'. 2002. 7.5-02-07-02.1. ITTC Recommended Procedures and Guidelines.
- 'Testing and Extrapolation Methods. Resistance. Resistance Test'. 2002. 7.5-02-02–01. ITTC Recommended Procedures and Guidelines.

Appendix 3

Strength Bar Calibration

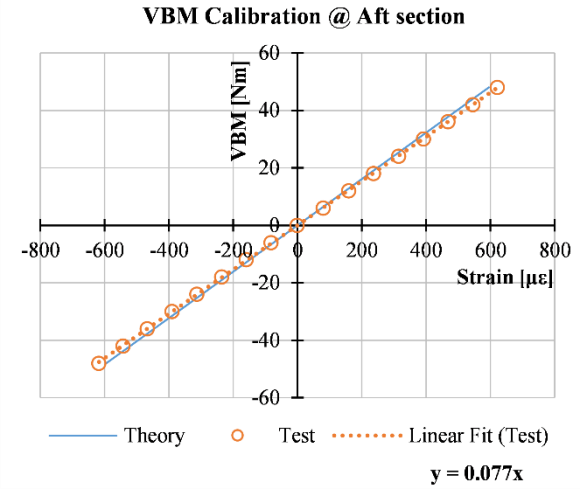

Figure Apx.1.1. Calibration of the strain gauges measuring vertical bending moment at 0.25LWL.

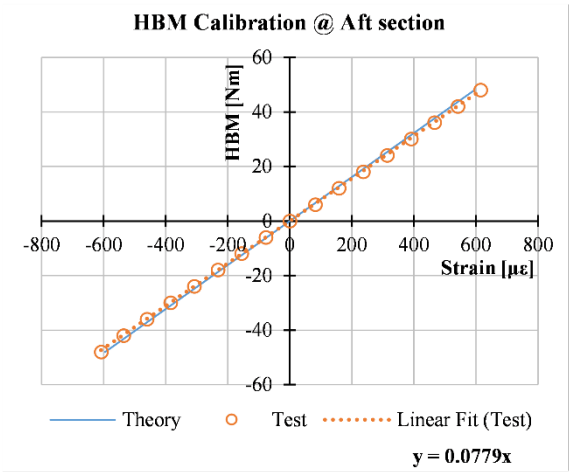

Figure Apx.1.2. Calibration of the strain gauges measuring horizontal bending moment at 0.25LWL.

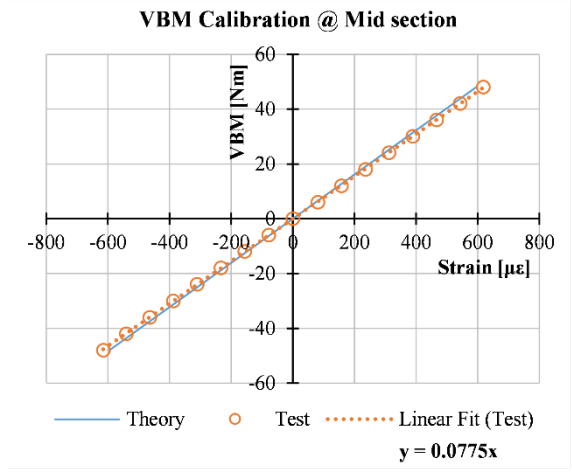

Figure Apx.1.3. Calibration of the strain gauges measuring vertical bending moment at 0.50LWL.

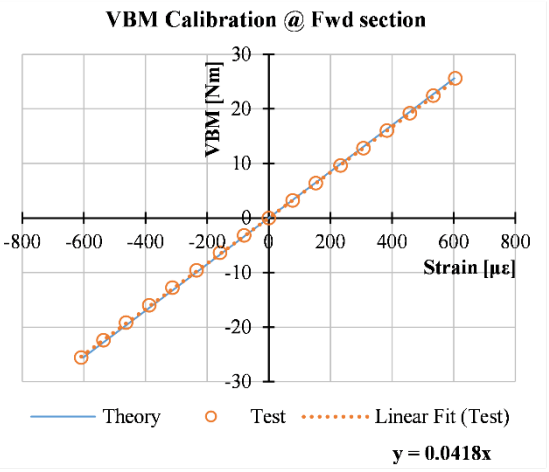

Figure Apx.1.4. Calibration of the strain gauges measuring horizontal bending moment at 0.50LWL.

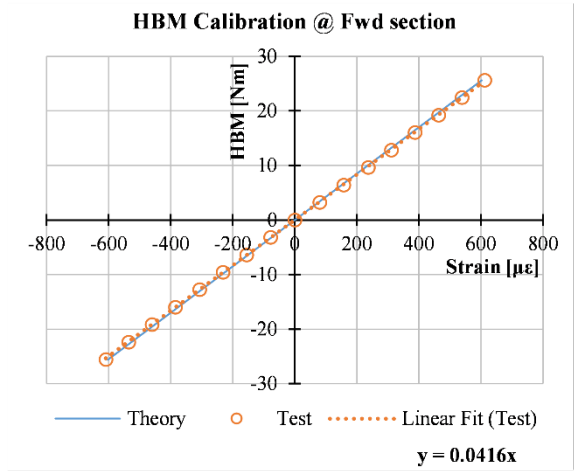

Figure Apx.1.5. Calibration of the strain gauges measuring vertical bending moment at 0.75LWL.

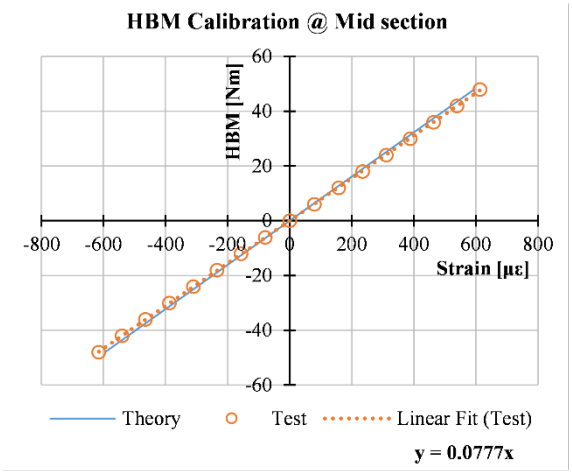

Figure Apx.1.6. Calibration of the strain gauges measuring vertical bending moment at 0.75L_{WL}.

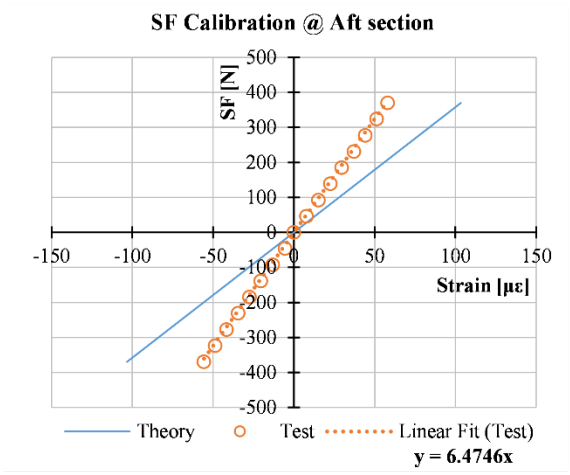

Figure Apx.1.7. Calibration of the strain gauges measuring vertical shear force at 0.25LWL. The readings are affected by bending strain sensed by the shear gauges.

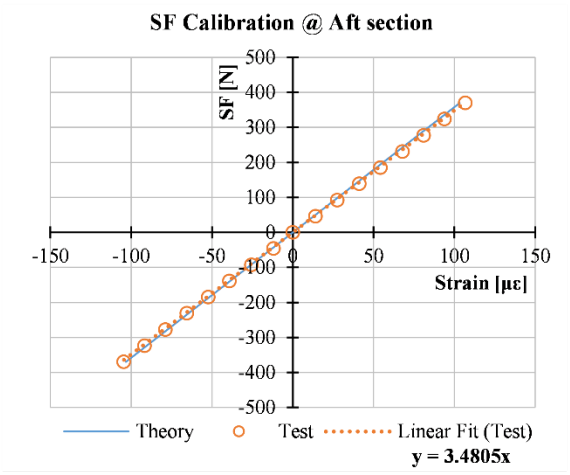

Figure Apx.1.8. Calibration of the strain gauges measuring vertical shear force at 0.25LWL. A correction factor is applied to account for the parasitic bending strain.

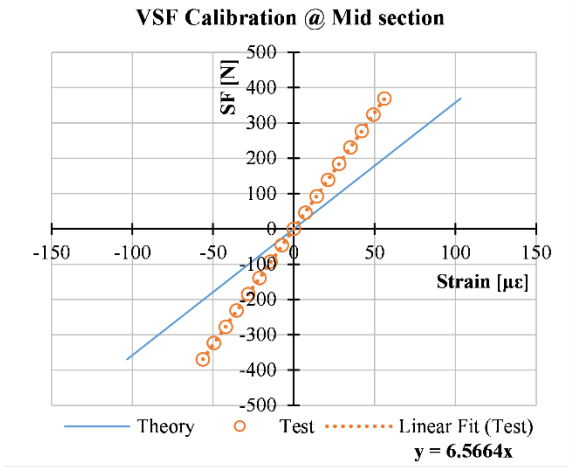

Figure Apx.1.9. Calibration of the strain gauges measuring vertical shear force at 0.50LWL. The readings are affected by bending strain sensed by the shear gauges.

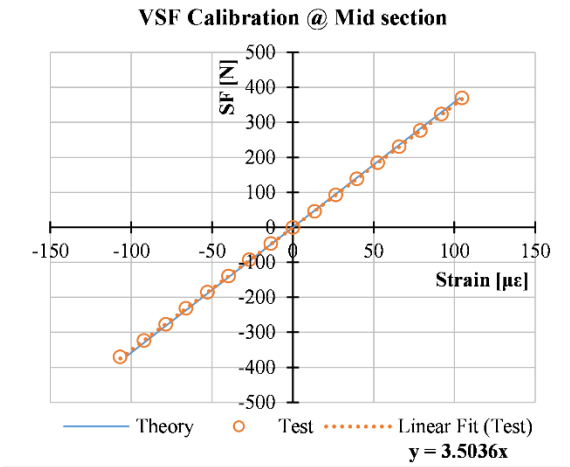

Figure Apx.1.10. Calibration of the strain gauges measuring vertical shear force at 0.50LWL. A correction factor is applied to account for the parasitic bending strain.

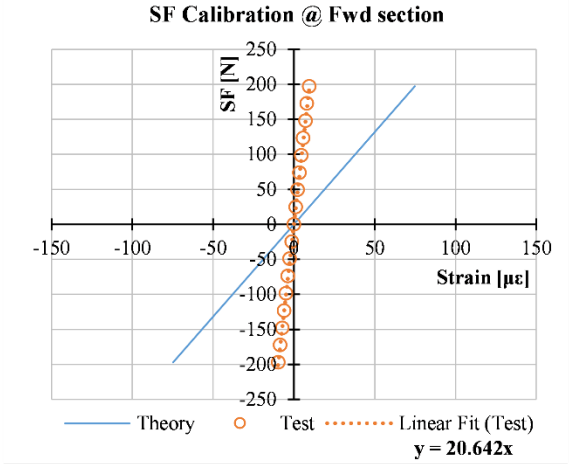

Figure Apx.1.11. Calibration of the strain gauges measuring vertical shear force at 0.75LWL. The readings are affected by bending strain sensed by the shear gauges.

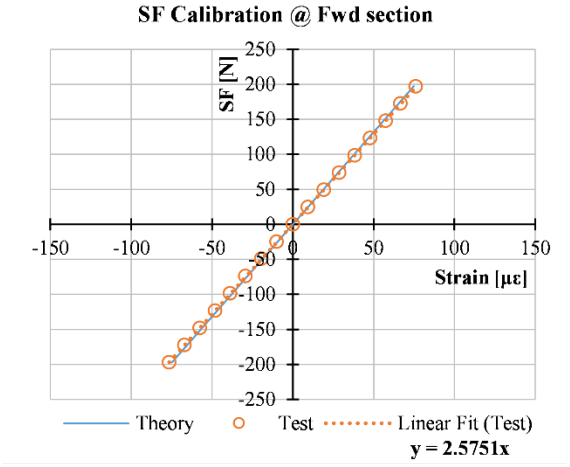

Figure Apx.1.12. Calibration of the strain gauges measuring vertical shear force at 0.75LWL. A correction factor is applied to account for the parasitic bending strain.

Appendix 4

Trial Trajectories

NOTES

Drawings not at scale.

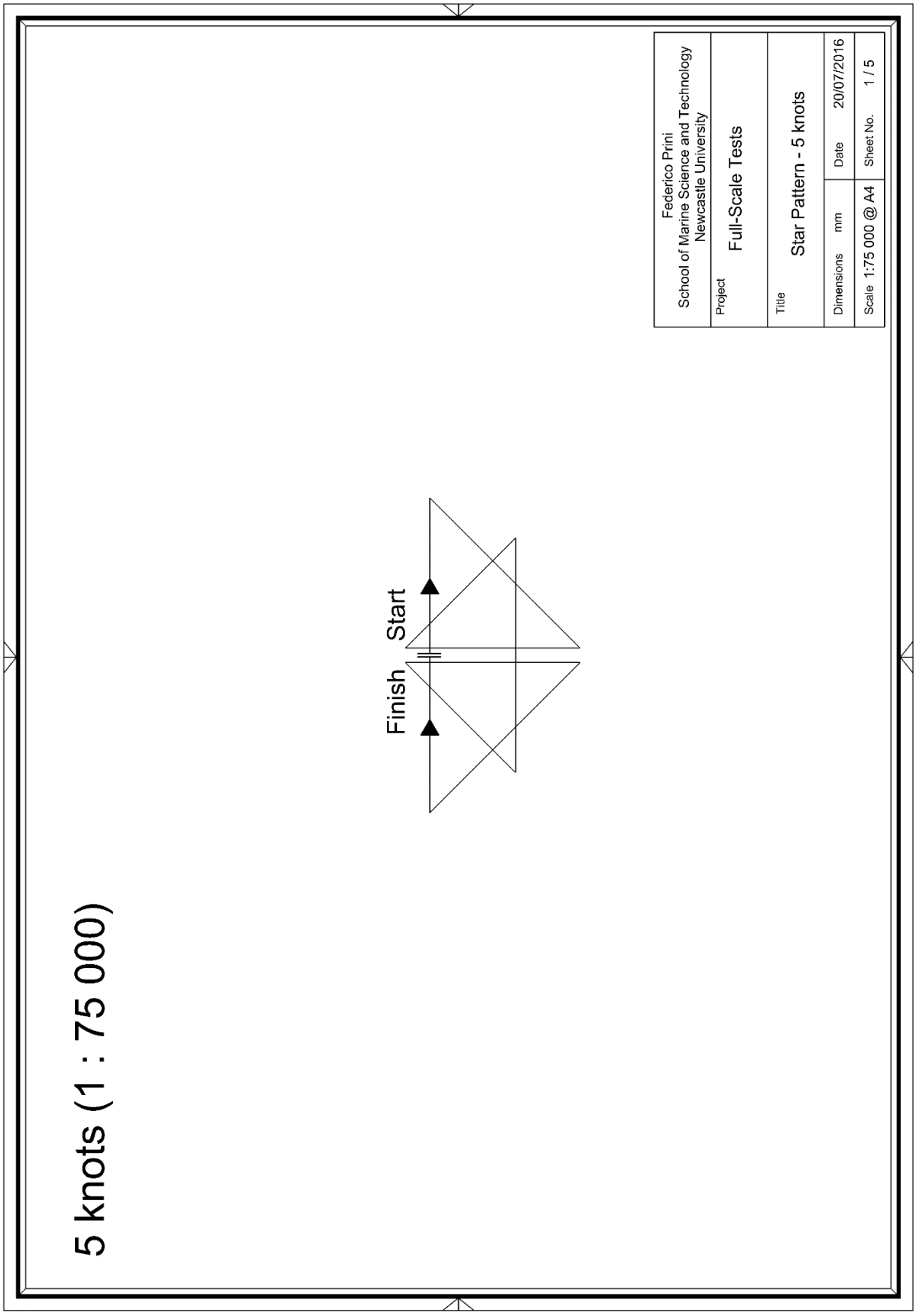
5 knots (1 : 75 000)
Start
Finish
Federico Prini
School of Marine Science and Technology
Newcastle University
Project
Full-Scale Tests
Title
Star Pattern - 5 knots
Dimensions mm
Date 20/07/2016
Scale 1:75 000 @ A4
Sheet No. 1 / 5

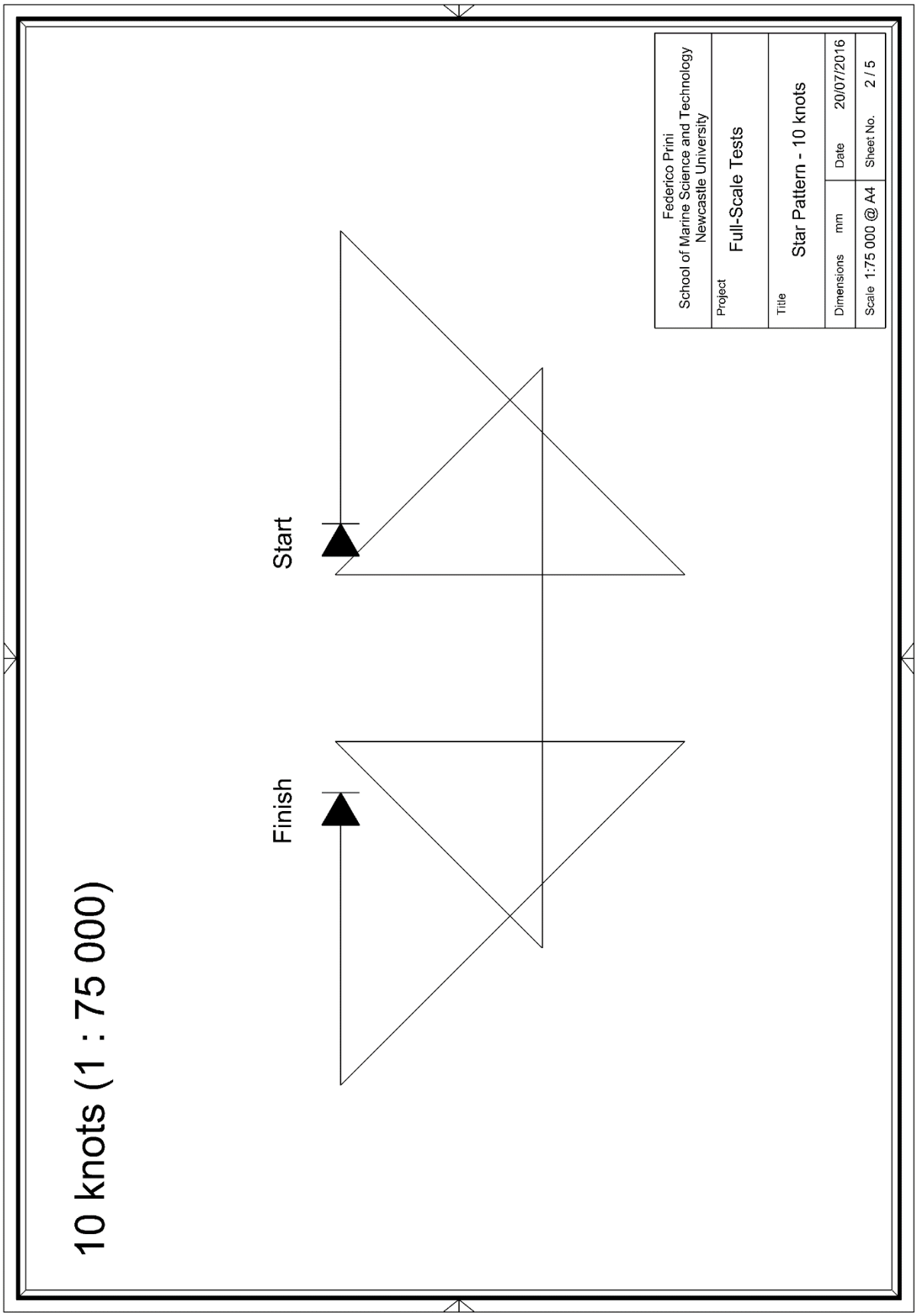
10 knots (1 : 75 000)
Start
Finish
Federico Prini
School of Marine Science and Technology
Newcastle University
Project
Full-Scale Tests
Title
Star Pattern - 10 knots
Dimensions mm
Date 20/07/2016
Scale 1:75 000 @ A4
Sheet No. 2 / 5

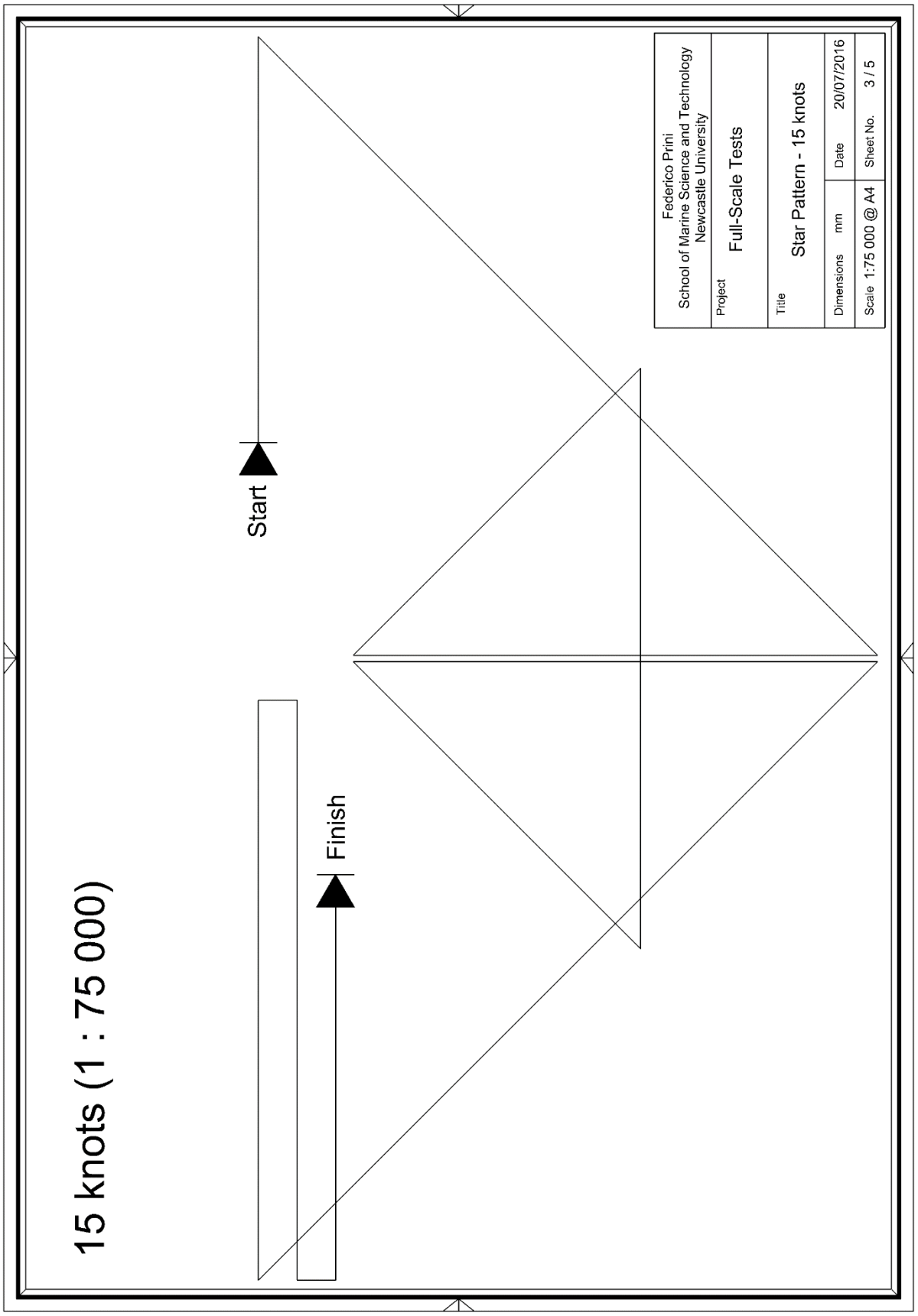
15 knots (1 : 75 000)
Start
Finish
Federico Prini
School of Marine Science and Technology
Newcastle University
Project
Full-Scale Tests
Title
Star Pattern - 15 knots
Dimensions mm
Date 20/07/2016
Scale 1:75 000 @ A4
Sheet No. 3 / 5

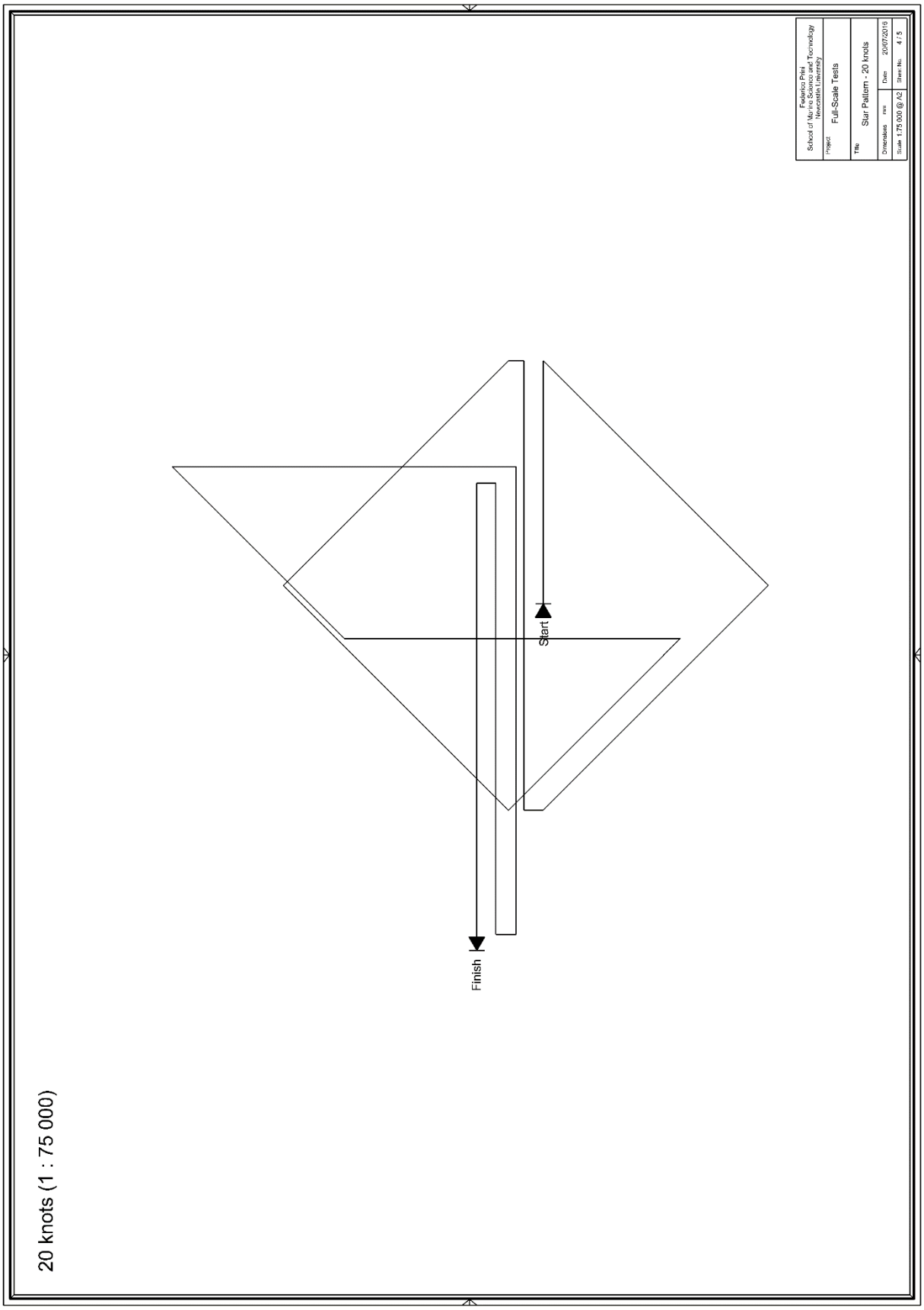
Federico Prini
School of Marine Science and Technology
Newcastle University
Project:
Full-Scale Tests
Title:
Star Pattern - 20 knots
Dimension: mm
Date: 20/07/2016
Scale: 1:75 000 @ A2
Sheet No.: 4 / 5
Start
Finish
20 knots (1 : 75 000)

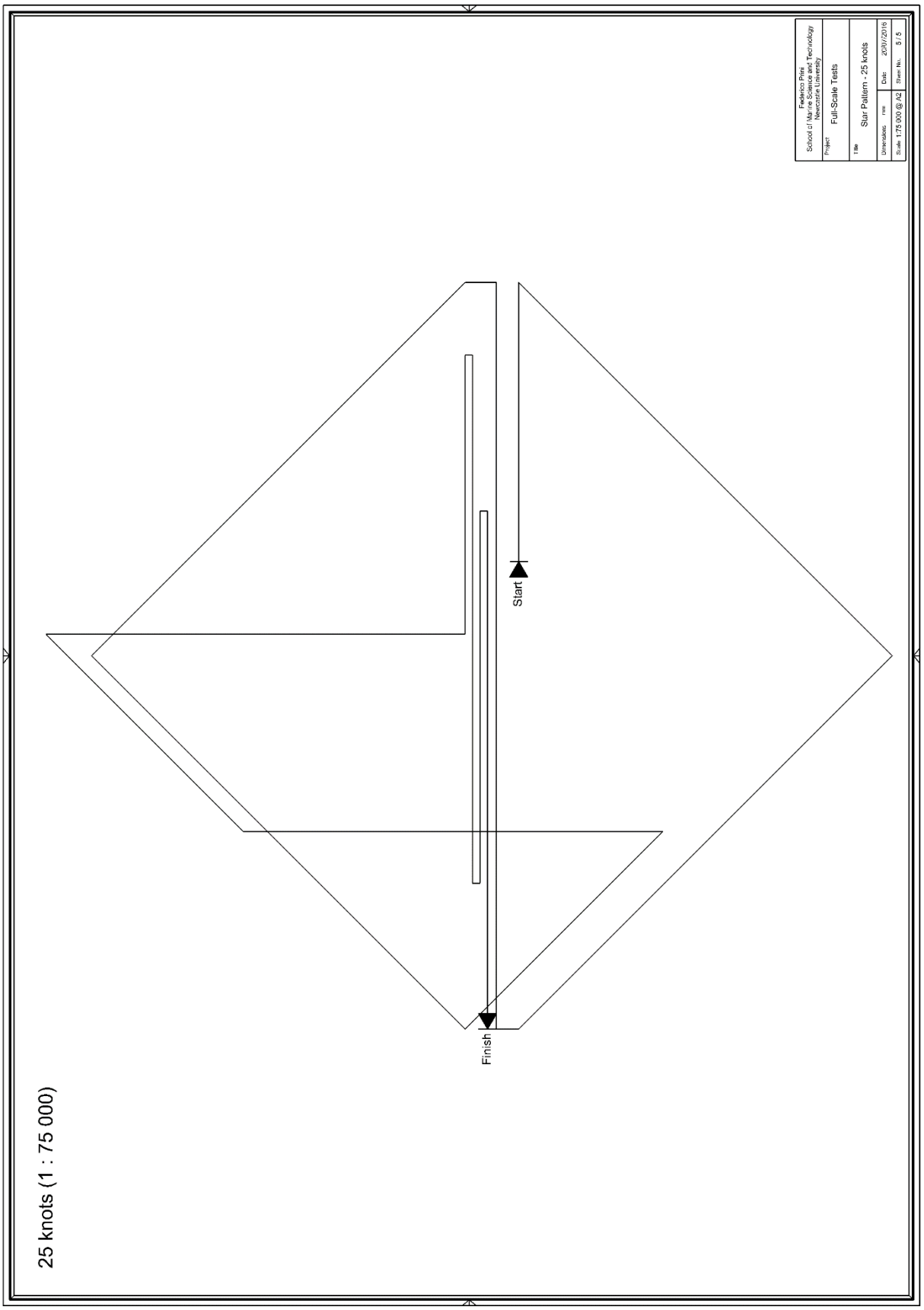
Fabrice Pinel
School of Marine Science and Technology
Newcastle University
Project
Full-Scale Tests
Title
Star Pattern - 25 knots
Dimensions mm
Date: 20/9/2016
Scale 1:75 000 @ A2
Sheet No.: 5 / 5
Start
Finish
25 knots (1 : 75 000)

Appendix 5

Instrumentation Plan

NOTES

Drawings not at scale.

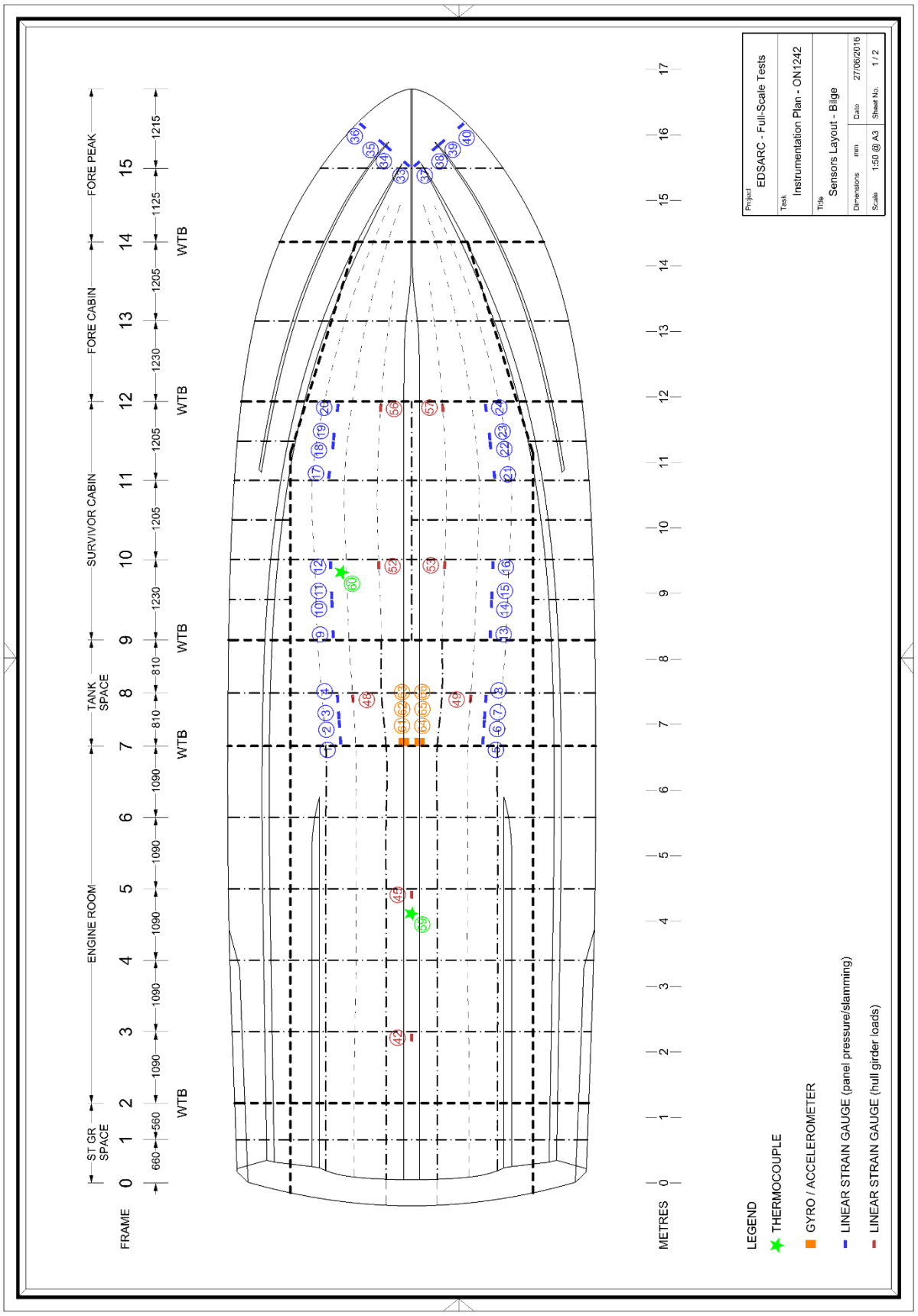
Project
EDSARC - Full-Scale Tests
Task
Instrumentation Plan - ON1242
Title
Sensors Layout - Bilge
Dimensions mm
Date 27/06/2016
Scale 1:50 @ A3
Sheet No. 1 / 2
ST GR SPACE
ENGINE ROOM
TANK SPACE
SURVIVOR CABIN
FORE CABIN
FORE PEAK
WTB
FRAME
METRES
LEGEND
THERMOCOUPLE
GYRO / ACCELEROMETER
LINEAR STRAIN GAUGE (panel pressure/slamming)
LINEAR STRAIN GAUGE (hull girder loads)

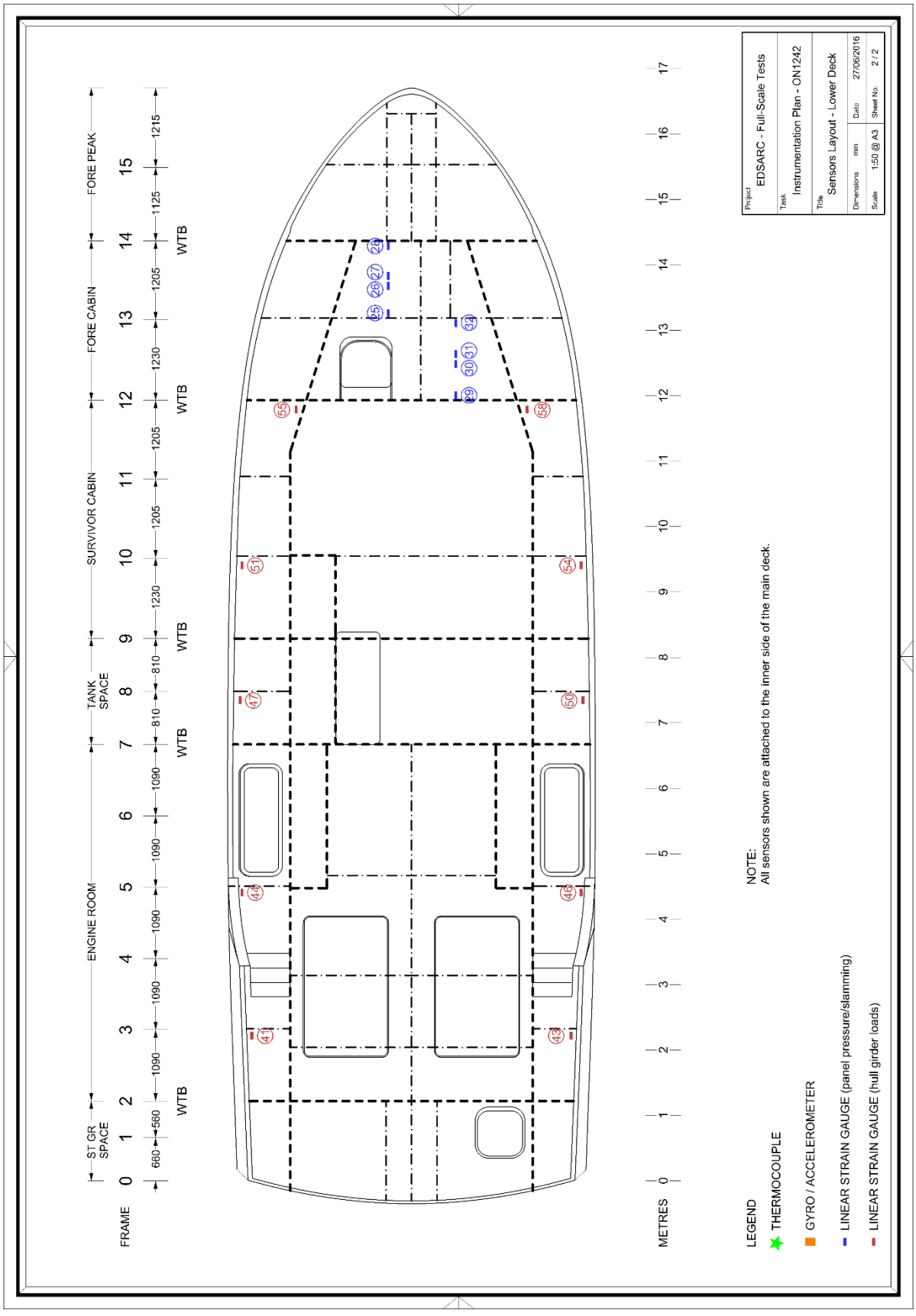
FRAME
0
1
2
3
4
5
6
7
8
9
10
11
12
13
14
15
ST GR SPACE
ENGINE ROOM
TANK SPACE
SURVIVOR CABIN
FORE CABIN
FORE PEAK
660
560
1090
1090
1090
1090
810
810
1230
1205
1205
1230
1205
1125
1215
WTB
METRES
0
1
2
3
4
5
6
7
8
9
10
11
12
13
14
15
16
17
NOTE:
All sensors shown are attached to the inner side of the main deck.
LEGEND
THERMOCOUPLE
GYRO / ACCELEROMETER
LINEAR STRAIN GAUGE (panel pressure/slamming)
LINEAR STRAIN GAUGE (hull girder loads)
Project
EDSARC - Full-Scale Tests
Task
Instrumentation Plan - ON1242
Title
Sensors Layout - Lower Deck
Dimensions
mm
Date
27/06/2016
Scale
1:50 @ A3
Sheet No.
2 / 2

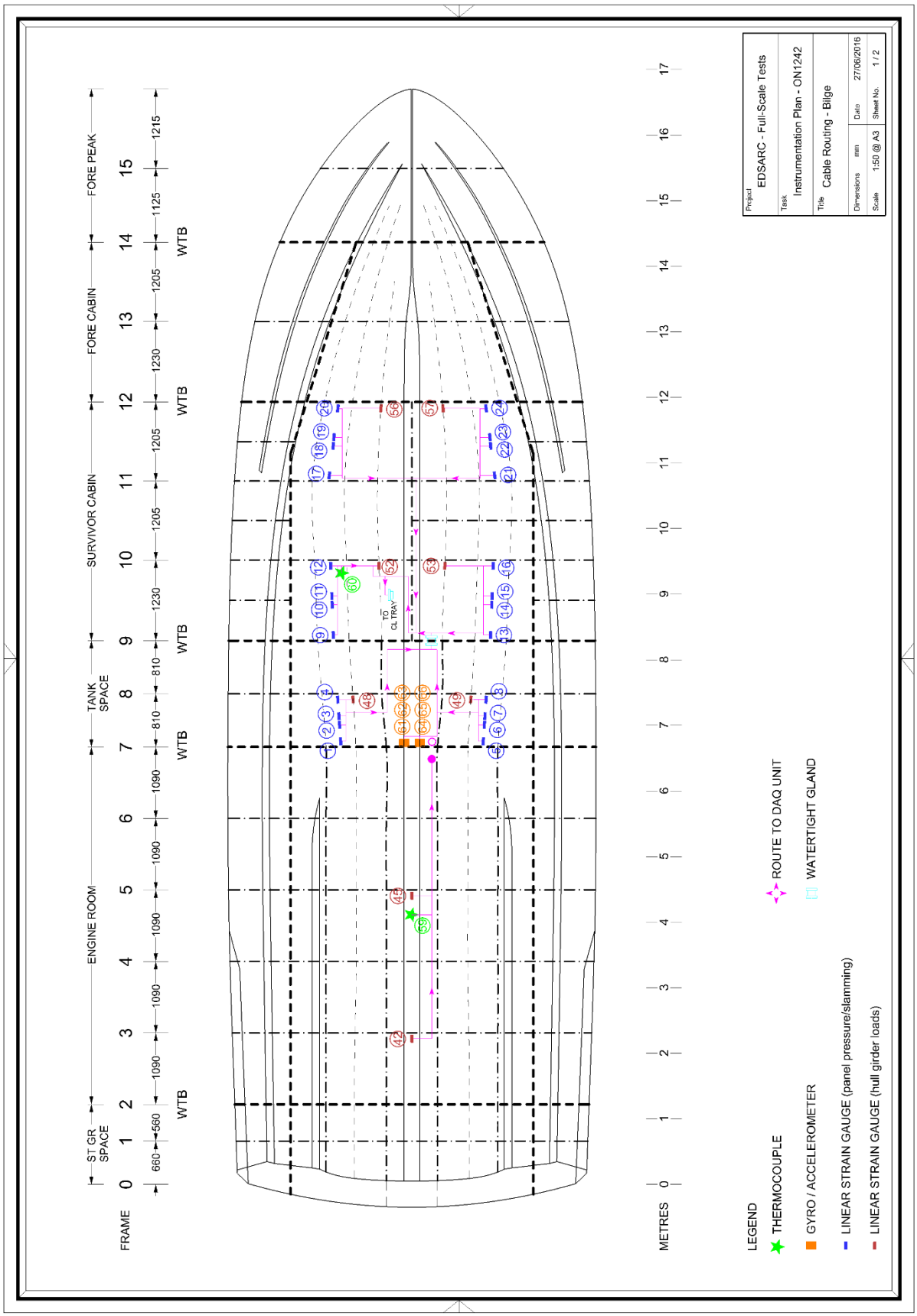
Project
EDSARC - Full-Scale Tests
Task
Instrumentation Plan - ON1242
Title
Cable Routing - Bilge
Dimensions
mm
Date
27/06/2016
Scale
1:50 @ A3
Sheet No.
1 / 2
ST GR SPACE
ENGINE ROOM
TANK SPACE
SURVIVOR CABIN
FORE CABIN
FORE PEAK
WTB
FRAME
METRES
TO CL TRAY
LEGEND
THERMOCOUPLE
GYRO / ACCELEROMETER
LINEAR STRAIN GAUGE (panel pressure/slamming)
LINEAR STRAIN GAUGE (hull girder loads)
ROUTE TO DAQ UNIT
WATERTIGHT GLAND

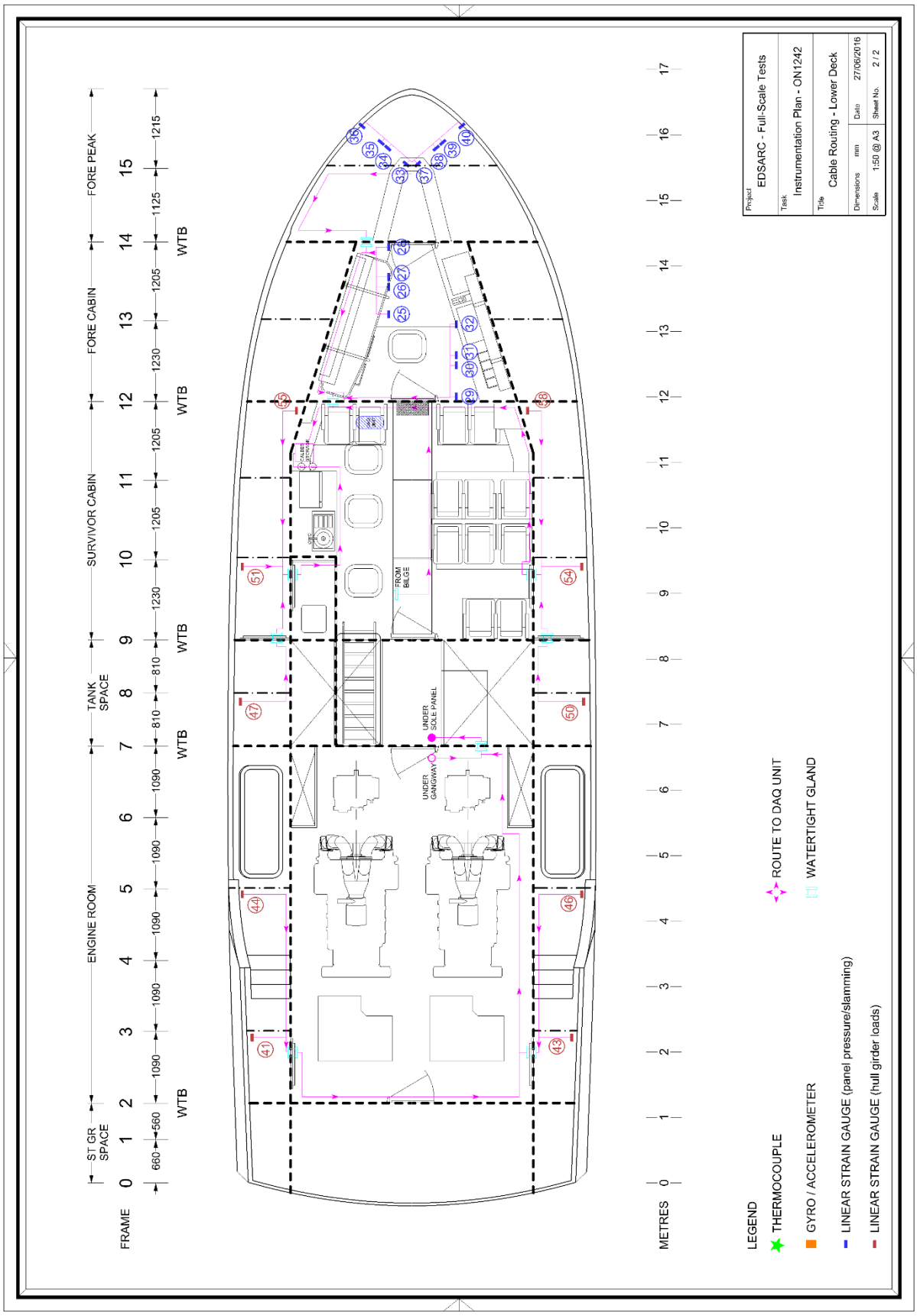
Project
EDSARC - Full-Scale Tests
Task
Instrumentation Plan - ON1242
Title
Cable Routing - Lower Deck
Dimensions
mm
Date
27/06/2016
Scale
1:50 @ A3
Sheet No.
2 / 2
FRAME
ST GR SPACE
ENGINE ROOM
TANK SPACE
SURVIVOR CABIN
FORE CABIN
FORE PEAK
WTB
METRES
FROM BILGE
UNDER SOLE PANEL
UNDER GANGWAY
LEGEND
THERMOCOUPLE
ROUTE TO DAQ UNIT
GYRO / ACCELEROMETER
WATERTIGHT GLAND
LINEAR STRAIN GAUGE (panel pressure/slamming)
LINEAR STRAIN GAUGE (hull girder loads)

Appendix 6

Trial Record Sheet

Seakeeping Trial Record Sheet

Trial Name		Boat ON		Carried out by	
Date		Time		Location		High Water	

Loading Condition

No of Crew		Approx Crew Weight [kg]	

Draught Aft [m] before trial		Draught Fwd [m] before trial		Water Sg before trial		Fuel Reading Pt [lt] before trial		Fuel Reading Stb [lt] before trial		Fuel Consumed [lt]
Draught Aft [m] after trial		Draught Fwd [m] after trial		Water Sg after trial		Fuel Reading Pt [lt] after trial		Fuel Reading Stb [lt] after trial		

Frame 15 Inspection

Visual Inspection before trial		Tap Test before trial		NOTES
Visual Inspection after trial		Tap Test after trial		

Conditions at Start

Time		Wind [kts]		Wave Length [m]		Sea State [Douglas]		Water Depth [m]
Location	N W	Wind Direction [deg]		Wave Height [m]		Wave Direction [deg]		

Conditions at End

Time		Wind [kts]		Wave Length [m]		Sea State [Douglas]		Water Depth [m]
Location	N W	Wind Direction [deg]		Wave Height [m]		Wave Direction [deg]		

Sea State Visual Assessment	

Wave Buoy

Switched On		Switched Off	

Deployment Location	N W	Deployment Time	
Pick-up Location	N W	Pick-up Time	

Position Update	N W	Time Received	
Position Update	N W	Time Received	
Position Update	N W	Time Received	
Position Update	N W	Time Received	
Position Update	N W	Time Received	
Position Update	N W	Time Received	
Position Update	N W	Time Received	
Position Update	N W	Time Received	
Position Update	N W	Time Received	
Position Update	N W	Time Received	
Position Update	N W	Time Received	
Position Update	N W	Time Received	
Position Update	N W	Time Received	
Position Update	N W	Time Received	

Leg Record

Leg Number	Position		Time		Direction to sea	Compass Heading	SOG [kts]	STW [kts]	Running Trim	Trim Tab Angle	Propeller RPM	
	Start	End	Start	End							Pt	Stb
1												
2												
3												
4												
5												
6												
7												
8												
9												
10												
11												
12												
13												
14												

NOTES

Appendix 7

Strain to Pressure Conversion

Introduction

A review of the seakeeping trials conducted with the Severn Class lifeboat was given in Chapter 6. The estimation of slamming pressures from the trials data relies on a relation between the pressure load acting on a structural member and the consequential strain measured on it. This strain-to-pressure conversion was found from a local finite element model of the instrumented structure through linear static structural analysis. The details of the analysis are given hereunder.

Model details

Calculation of the slamming pressures on the hull was based on the strain readings from six panels on the hull bottom and two at the bow. All the panels were instrumented with the same strain gauge layout (Chapter 6). The strain gauges used for calculating slamming pressures were the two gauges located at the midspan of each panel, whose signals were averaged to obtain one strain signal. The strain attributable to slamming pressure loads was isolated by high-pass filtering the strain signals (Chapter 6).

All the instrumented panels on the Severn were symmetric with respect to the vessel centreline, hence finite element models were constructed for the starboard side only, resulting in four distinct models, as shown in Figure 1. The hull bottom panels have a similar structural layout. The plating is a single skin laminate supported by top-hat longitudinals and transverse frames. Whilst the aspect ratio varies, all panels are of quasi rectangular shape. Preliminary simulations revealed that the plating was not entirely supported by the longitudinal stiffeners, as it would be expected for a hierarchical structural layout, but rather that plating and stiffeners act as a grillage. The part of the hull structure modelled was therefore extended to a whole hull transverse section. Supporting members were identified as the centreline joint, the chine and the transverse frames. The bow panels are of sandwich construction and unstiffened. The supporting members were identified as the stem, the hull-to-deck joint and a ring frame, which makes the panels quasi triangular.

Figure 1. Highlight of the hull part modelled.

The shape and dimensions of the hull structure modelled were determined from technical drawings and construction sheets of the Severn, backed by measurements taken aboard during the sensor installation. The same material properties as those used for the global finite element model (Chapter 4) were used.

The geometrical models were discretised with 4-node quadrilateral shell elements. The average element size was 15mm for the hull bottom structure and 100mm for the bow structure, values determined from the thickness of laminates in order to satisfy the typical requirements of shell elements in terms of area-to-thickness ratio. The material properties of the laminates were assigned ply by ply, using the shell layered definition. The geometrical and meshed models are shown in Figures 2–9.

The following solutions were adopted for modelling of the actual structure and discretising it with finite elements. The foam infill of the longitudinals was not modelled, assuming that this does not contribute to the bending stiffness of the relative structural members. The assumption is not atypical and further supported by the low stiffness of the foam used for the realisation of the stiffeners. The stiffeners' webs would stretch over the plating with a tapered end, as per conventional construction practice. The tapered areas were modelled with a constant thickness covering over half of the tapered width.

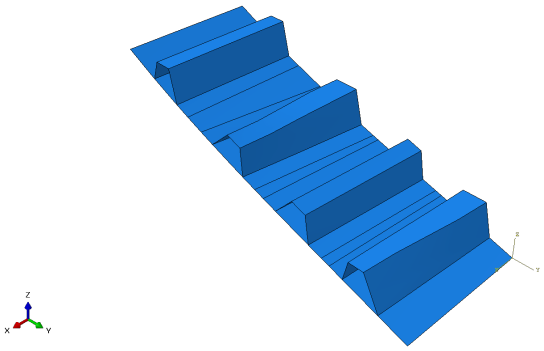

Figure 2. FE model 1 geometry.

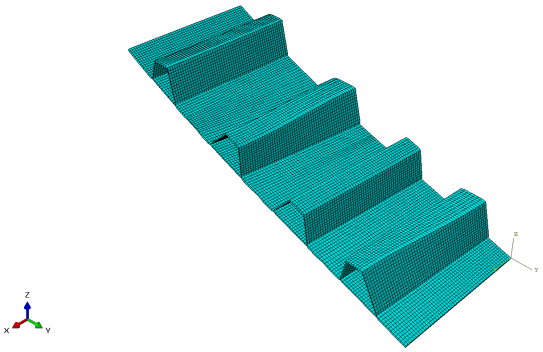

Figure 3. FE model 1 mesh.

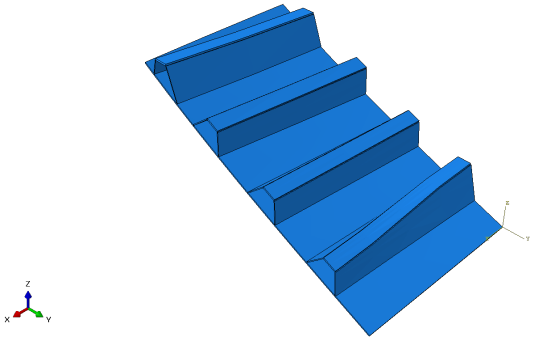

Figure 4. FE model 2 geometry.

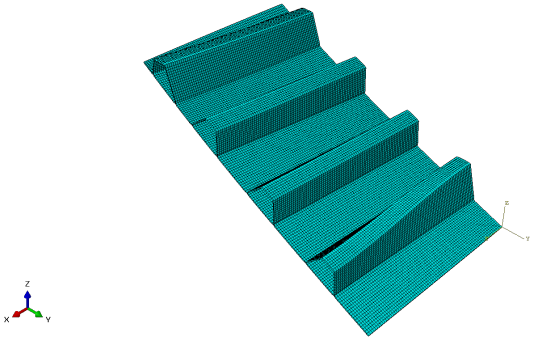

Figure 5. FE model 2 mesh.

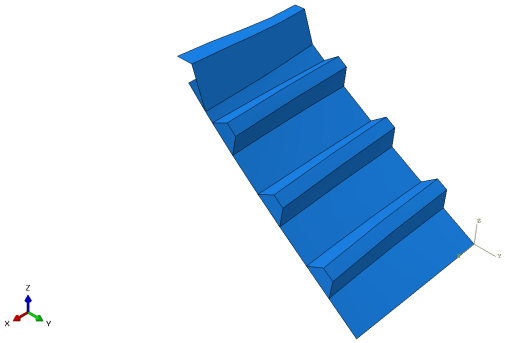

Figure 6. FE model 3 geometry.

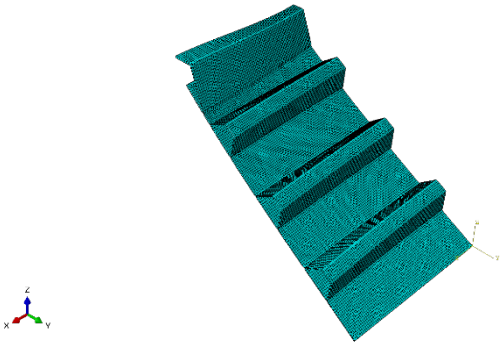

Figure 7. FE model 3 mesh.

Figure 8. FE model 4 geometry.

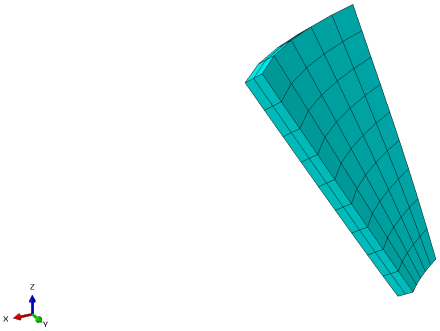

Figure 9. FE model 4 mesh.

Boundary Conditions

Rigid restraints were applied in lieu of the surrounding structure, also preventing rigid body motions. Rotations and displacements were constrained on all the edges supported by transverse frames, transverse bulkheads, centreline joint, chine and stem. Additional restraints were applied to the longitudinal bulkhead receiving stiffeners. A uniformly distributed static pressure of 1 MPa was applied to the outer side of the plating, acting inwards. The position of the restraints and the loads applied on the four distinct models are shown in Figures 10–13.

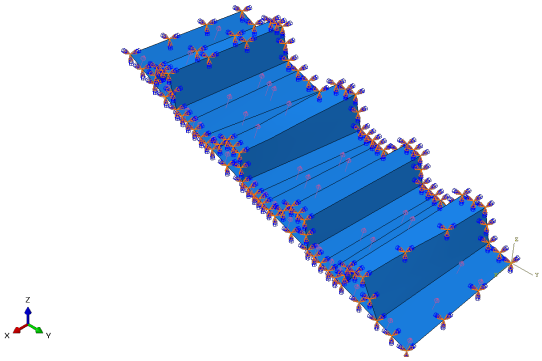

Figure 10. FE model 1 boundary conditions.

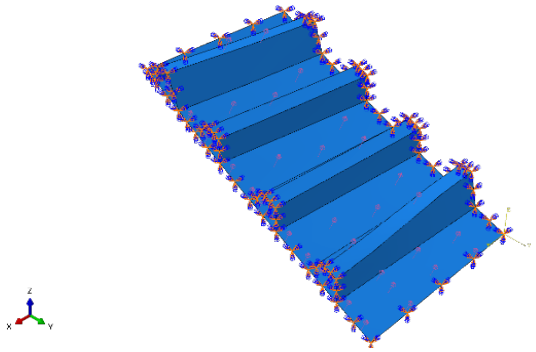

Figure 11. Section 2 boundary conditions

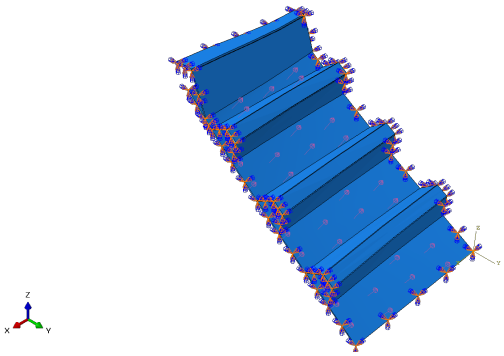

Figure 12. FE model 3 boundary conditions.

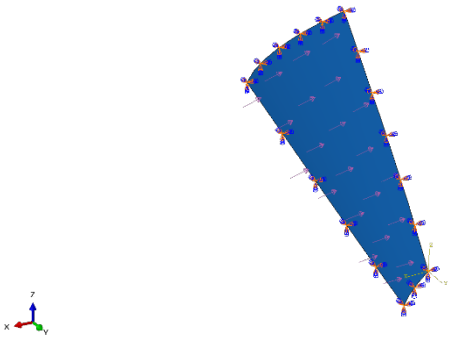

Figure 13. FE model 4 boundary conditions.

Analysis

The structural analysis was performed as linear and static, with stresses, strains and displacements output for evaluation. Stresses and strains were computed for three integration points within each ply of the laminate and plotted in the 'active' strain gauges direction, that is, the direction along which the strain gauges measuring grids are oriented. Since the strain readings were taken on the internal surface of the plating,

the first integration point of the innermost ply was considered for the strain to pressure conversion. An example of displacement result is shown in Figures 14–15 for one of the hull bottom section (Model 3). For the same model, Figures 16–17 show the surface stress and strain along the strain gauges' active direction.

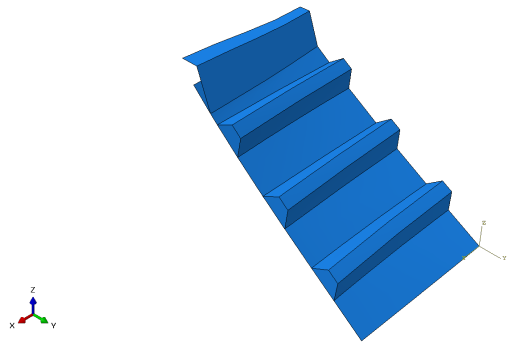

Figure 14. Model 3 un-deformed model.

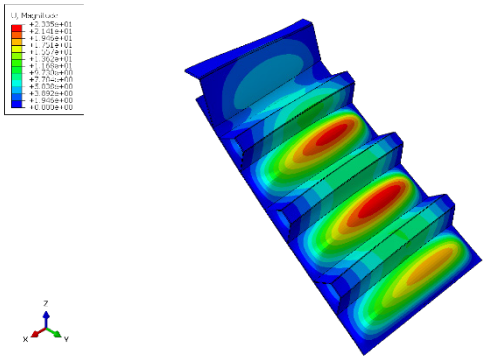

Figure 15. Model 3 displacement magnitude (x8 magnification).

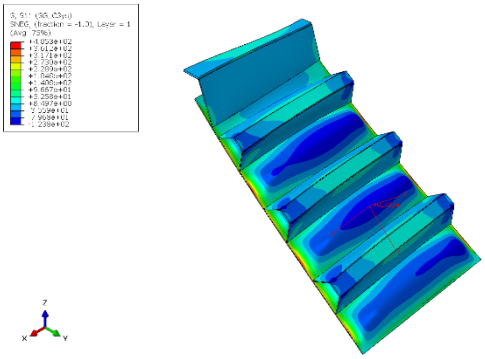

Figure 16. Model 3 surface stress in the strain gauges' active direction (x8 magnification)

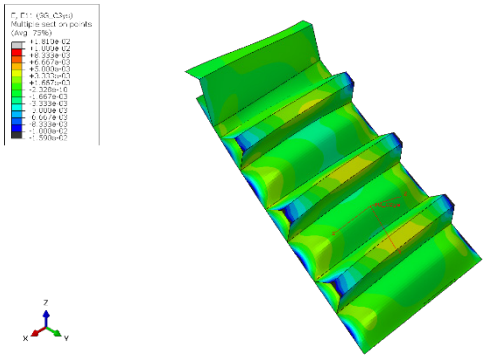

Figure 17. Model 3 surface strain in the strain gauges' active direction (x8 magnification).

Results

From the structural analysis, conversion factors were produced for each of the instrumented panels. The first panel from the stern (Model 1) is significantly shorter than the other hull bottom panels and a different conversion factor would be expected. The value computed was found, however, unrealistic because it would produce slamming pressures that are significantly higher at amidships than on the forward portion of the hull. The results from Model 1 were therefore misbelieved. The cause is likely attributable to the presence of the fuel tanks above that panel or to a more complex structural response that was not appropriately captured by limiting the modelled area to a transverse section of the hull bottom.

The conversion factor computed for the other two hull bottom panels was similar, which would be expected because of the same size and laminate layup of the panels and the surrounding structural members. The conversion factor was therefore used for both panels and extended to the whole hull bottom, including Model 1. The final conversion factors adopted are reported in Table 1.

Table 1. Strain to pressure conversion.

Model	Panel position	Distance from aft end [m]	Pressure [MPa]	Strain [με]
Model 1	Hull bottom	7.14	1	866
Model 2	Hull bottom	8.84	1	866
Model 3	Hull bottom	11.39	1	866
Model 4	Bow	16.15	1	2440